FINAL REPORT | NOVEMBER 2019

Museum of the Bible Dead Sea Scroll Collection Scientific Research and Analysis

ARTFRAUDINSIGHTS

Table of Contents

Executive Summary (Colette Loll) 1

Advisory Team Approach 4

Summary of Analyses 5

Summary Physical Characteristics (Abigail Quandt) 6

Summary of Elemental and Molecular Analysis (Jennifer Mass) 15

Fragment Detail (Surface, Ink, Anomalies) 29

- MOTB.SCR.000120 30
- MOTB.SCR.000121 33
- MOTB.SCR.000122 38
- MOTB.SCR.000123 43
- MOTB.SCR.000124 46
- MOTB.SCR.003170 51
- MOTB.SCR.003171 56
- MOTB.SCR.003172 61
- MOTB.SCR.003173 66
- MOTB.SCR.003174 73
- MOTB.SCR.003175 79
- MOTB.SCR.003183 83
- SIG.SCR.004742 90
- SCR.0004768 & SCR.004741 96
- SCR.004769 101

Results of Molecular, Elemental and Chemical Analysis 107

- FTIR Report (SAFA) 108
- XRF Report (Aaron Shugar) 168
- SEM Report (Aaron Shugar) 188
- Microchemical Test Summary (SAFA) 207

Advisory Team Bios 210

Executive Summary

Since 2002, many previously unknown textual fragments inscribed in Hebrew or Aramaic have surfaced on the antiquities market. Believed to be newly discovered biblical artifacts belonging to the canon of the Dead Sea Scroll Discovery, dozens have been acquired, publicly exhibited, and published by private and institutional collectors.

The Museum of the Bible curates 16 of these fragments. These textual artifacts were purchased on behalf of Mr. Steven Green in four lots from four separate private collectors. Thirteen of these fragments were published by a team of scholars in *Dead Sea Scrolls Fragments in the Museum Collection* (Publications of Museum of the Bible 1; Leiden: Brill, 2016). The volume was a collection of editions whose purpose was to provide a comprehensive physical and textual description of the fragments, and to situate them contextually within discussions of biblical texts, the Dead Sea Scrolls, and early Jewish history. At the time of publication, no scientific examination of the Museum's scroll fragments had been carried out.

Since publication, scholars have expressed growing concern about the authenticity of these fragments. Exhaustive appraisals of the scribal features that grounded authenticity claims revealed inconsistencies with the original Dead Sea Scrolls. Additionally, suspicious physical anomalies observed on six of the fragments prompted further investigation into their provenance and led the Museum to sponsor scientific testing.

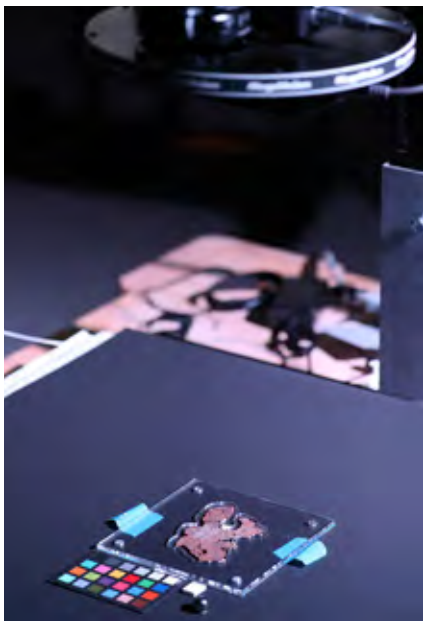

In April 2017 the Museum requested scientific testing of five fragments by the Bundesanstalt für Materialforschung und -prüfung (BAM). While awaiting results, and prior to being put on display, the Museum's provenance research indicated further uncertainty of their origin. When the Museum opened, the fragments were labeled as "problematic" to reflect this uncertainty. The preliminary scientific study of the Museum's fragments, received in October 2018, led to the suggestion that the mineral deposits and the writing support material were inconsistent with being authentic. It was concluded that all five studied fragments exhibited characteristics "inconsistent with ancient origins" and they were removed from view pending further study.

As a result of the concerns raised by this initial study, a more detailed materials investigation of the entire Museum of the Bible fragment collection was sought. In February 2019 the Museum contracted Art Fraud Insights, LLC to recruit and manage an independent Advisory Team for the purpose of designing and conducting a rigorous scientific protocol for the imaging and materials analysis of the fragment collection. The goal of the research effort was to gather enough information that would allow for an evidence-based conclusion that would either confirm or refute the authenticity of each fragment.

To that end, comprehensive imaging and scientific analysis were conducted on the collection between May and October 2019. In addition to multispectral and reflectance transformation imaging (MSI/RTI) imaging and multiple physical examinations with both traditional and 3D microscopy, a subset of the collection was selected and sampled for a full elemental and molecular profile. The specific tools used for this analysis included Fourier transform infrared spectroscopy (FTIR), macro x-ray fluorescence imaging (MA-XRF), scanning electron microscopy – energy dispersive x-ray analysis (SEM-EDS), micro-Raman spectroscopy (Raman), and microchemical testing.

After an exhaustive review of all the imaging and scientific analysis results, it is the unanimous conclusion of the Advisory Team that none of the textual fragments in the Museum of the Bible's Dead Sea Scroll collection are authentic. Moreover, each exhibits characteristics that suggest they are deliberate forgeries created in the twentieth century with the intent to mimic authentic Dead Sea Scroll fragments.

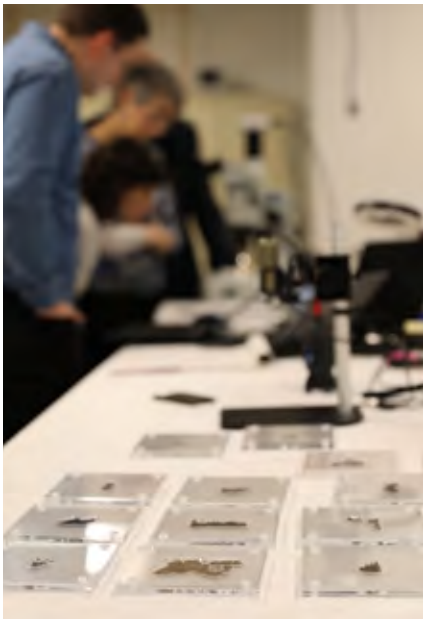

Once this determination was made, the Advisory Team became focused on *how* they were constructed to deceive. Through physical examination, we determined that, with one exception, the substrate of the Museum's scroll fragments appears to be leather rather than the surface tanned and untanned parchment that is characteristic of the authentic Dead Sea Scrolls. The degraded condition of the fragments reinforces our theory that modern writing was applied to small scraps taken from archeological deposits of leather. Through elemental and molecular analysis, we further found that the raw skins of the leather substrates for the MOTB fragments appear to have been lime-depilated, a technology that postdates the original Dead Sea Scrolls.

All of the MOTB fragments, despite being purchased from different sources, were remarkably similar in that they were all heavily coated with a shiny amber material that was identified by FTIR analysis as a protein, most likely animal skin glue. It is likely that the glue was applied primarily as a means of reinforcing the fractured and torn substrates before writing. At the same time, coating the surfaces with animal glue would simulate the gelatinization seen in many authentic Dead Sea Scroll fragments, where hydrolysis has permanently converted the collagen fiber network to a hard, glue-like mass. We concluded the fragments have been further manipulated with a coating selected to simulate the surface appearance of many of the originals.

Many physical anomalies observed in the application of the ink reinforce the theory that degraded fragments of archeological leather, most likely ancient and already covered with a variety of mineral deposits from the environment, were used as substrates for writing. In all of the fragments that contained writing, we observed examples where modern ink was applied atop preexisting surface deposits and across cracks and areas of delamination already present on the repurposed material.

We were able to confirm the mineralogy of the surface deposits is consistent with the Dead Sea region, and with other geological sites in the Middle East. In some cases, a variety of loose mineral deposits were also scattered over the forgeries after writing, and while the ink was still wet, in order to give the impression that these were authentic Dead Sea Scroll fragments that had come from the Qumran caves. It is our opinion that all of these methods were utilized with an express intent to deceive.

The extensive research sponsored by the Museum of the Bible has resulted in the creation of a rigorous and reproducable protocol for the scientific interrogation of questioned ancient textual artifacts. The field will benefit from the release of the complete research results, which will facilitate comparisons with other questioned fragments. Further, the release of all associated images and datasets will considerably aid the identification and removal of texts that may have contaminated important literary, paleographic and linguistic datasets.

Please direct any questions regarding this report to:

Colette Loll
Art Fraud Insights, LLC
colette@artfraudinsights.com
(703) 395-4672

Advisory Team Approach

The Advisory Team conducted its research according to standard and internationally accepted protocols recognized by museums and scholars and in a manner consistent with respect to similar artifacts—texts of similar age and potential scholarly, historical and cultural significance. The team approached the project with a singular vision of developing and utilizing the most appropriate imaging and research technologies, methodologies, and practices to produce the most unimpeachable reproducible results that will stand up to a rigorous peer-review process. The team observed documentation, image, and data management best practices throughout the project. All raw files, data, images, and associated documentation were filed and maintained on a secure, independent FTP site. Where appropriate, photographic and video records of testing were captured.

Access to prior research, reports, photography, and the fragments themselves was facilitated by MOTB staff members, however, the Advisory Team conducted its investigation and drew its conclusions independent of any Museum input. Throughout the project, the Advisory Team maintained its objectivity and independence and ensured that the research methodology and technical implementation offered valid empirical results. After careful review of all the imaging and testing results, and through ongoing discussion and collaboration, a consensus opinion regarding the authenticity of each of the fragments was reached.

The Advisory Team members include (in alphabetical order):

Thomas Kupiec, Ph.D. (Independent Forensic Scientific and Technical Advisor)
Founder of The Kupiec Group and CEO of ARL Bio Pharma and DNA Solutions

Colette Loll (Project Manager)
Founder and Director of Art Fraud Insights, Doctoral candidate at Georgetown University

Jennifer Mass, Ph.D.
SAFA President, Andrew W. Mellon Professor of Cultural Heritage Science, Bard Graduate Center for Decorative Arts, Design History, and Material Culture

Rebecca Pollak
SAFA Senior Research Conservator

Abigail Quandt
Abigail Quandt, Head of Book and Paper Conservation and Senior Conservator of Manuscripts and Rare Books, the Walters Art Museum

Aaron Shugar, Ph.D.
Andrew W. Mellon Professor of Conservation Science in the Art Conservation Department, SUNY – Buffalo State. Adjunct Professor in the Anthropology Departments of both the University of Toronto and the University of Buffalo, SUNY. Adjunct Professor in the Chemistry Department, SUNY - Buffalo State

A professional biography of each Advisory Team member is provided on page 209.

Summary of Analyses

	Physical Examination and Imaging			Chemical and Molecular Analysis			
Fragment	**Imaging MSI/RTI**	**Microscopic Examination**	**Hirox**	**FTIR**	**XRF**	**SEM**	**Chemical Testing**
MOTB.SCR.000120 (Exodus)	X	X	X				
MOTB.SCR.000121 (Psalms)	X	X	X	X	X	X	X
MOTB.SCR.000122 (Leviticus?)	X	X	X				
MOTB.SCR.000123 (Instruction)	X	X	X				
MOTB.SCR.000124 (Genesis)	X	X	X	X	X		X
MOTB.SCR.003170 (Daniel)	X	X	X				
MOTB.SCR.003171 (Jonah)	X	X	X				
MOTB.SCR.003172 (Jeremiah)	X	X	X				
MOTB.SCR.003173 (Numbers)	X	X	X	X	X		
MOTB.SCR.003174 (Ezekiel)	X	X	X				
MOTB.SCR.003175 (Nehemiah)	X	X	X				
MOTB.SCR.003183 (Micah)	X	X	X	X			
SIG.SCR.004742 (Leviticus)	X	X	X	X	X		X
SCR.004741 (No writing)	X	X	X	X			
SCR.004768* (*previously connected to 4741)	X	X	X				
SCR.004769 (No writing)	X	X	X				X

Summary of Physical Characteristics

Methodology

Microscopic examination

Micrographs were acquired and analyzed utilizing a Unitron Z12 Stereo Microscope with a Fiber Optic Illuminator – 150w (Dolan Jenner) and captured with a Lumenera 3-6URC Color CCD Camera. Images were taken utilizing INFINITY Analyze software from Lumenera.

Hirox images were acquired and analyzed with a HIROX RH-2000 microscope with a MXB-2500REZ (35x-2500x turret zoom lens) to capture 3D surface topography. A MXB-5040RZ (50x-400x) with AD-5040RVS (variable angle adapter: 25,35,45 and 55 degree angle view with 360 degree rotation) was used to capture video. KH-8700_3D-Viewer_1.2.0 viewing software was utilized to view captured images and movies.

Imaging

The MegaVision system used for Multispectral Imaging (MSI) and Reflectance Transmission Imaging (RTI) capture included:

- EV camera with 51 Mpixel E7 Monochrome digital back
- 120mm Macro UV-IR ApoChromat lens
- Dual filter Wheel with R, G, B, UVblock, O22, and UVpass filters for fluorescence signature analysis
- Multispectral lights including the following wavebands: 365, 385, 420, 450, 470, 500, 520, 590, 615, 630, 650, 730, 850, and 940 nm.
- RTI Arc with 56 image captures with 4500K illuminants distributed over uniform hemisphere of 1.2 meter radius.
- Each image includes in the scene a calibrated color target and spectralon reference target with measured spectral values. Additionally, a spherical RTI target is in each scene to aid in the derivation of RTI image files.
- 81 image captures of each fragment individually positioned in the scene. No change in object, MSI illuminant, or camera position was made during the image capture sequence.
- Imaging setup was constrained by the individualized fragment plexiglass housings. The top covers were removed so that nothing was between the fragment surface and the lens, but to minimize risk of damage, the fragments were imaged inside the plexi housing base.
- Raw, Flattened (calibrated) and rendered image files in 16-bit dng and 16-bit TIFF format were supplied. CIE L*a*b images derived directly from 9 visible bands were supplied. The values of the color image data are spectrophotometric-equivalent color measurements.
- All MS image data is referenced to spectral reflectance standards (included in the scene of each image so that spectral reflectance data may be derived directly from the images. Also, curated, high-quality JPG images derived from the TIFF images were supplied. RTI images were also curated and Light Direction Reference file was derived.

Discussion

Substrate

In order to discuss the physical properties of the MOTB DSS fragments it is important to first point out the essential differences between parchment and leather. While the initial stages of parchment and leather production are identical the end products are very different from each other. In the case of leather many of the properties of raw skin, including flexibility and resilience, are preserved by tanning agents that permanently fix the collagen fibers in their original interwoven state. Once the hair and flesh are removed the skins are immersed in a vat of tanning liquors that permeate the fiber matrix through its thickness. When traditional vegetable tannins are used the skin takes on a characteristic yellow or reddish-brown color. The outer grain layer of leather, where the hair follicles are located, has a textured surface that is often very three dimensional, with low and high areas. The appearance of the grain can vary according to the animal species and to the area of the skin from which a piece of leather has been cut. Inscribing text on leather can be difficult because of its raised grain and slightly spongy texture, and this is why it was rarely used as a writing support, especially after the production of parchment for books in codex format increased around the fourth century, ACE. The flesh side of leather is exceedingly fibrous and uneven and therefore unsuitable for writing.

Parchment is made by stretching a dehaired and de-fleshed animal skin on a wooden frame or board until dry. The extreme tension put on the collagen fibers during drying causes them to become permanently aligned parallel to each other and this is what gives parchment its slightly stiff, sheet-like quality. While the skin is still on the frame it is scraped with a lunar knife to create a smooth, even surface on both sides, making them equally suitable for writing. Depending on the extent of scraping, the pattern created by the empty hair follicles is retained in the finished parchment. However, unlike with leather, the hair follicles have a flattened and distorted appearance due to the stretching of the skin. The superficial application of a tannin solution was most likely done by the DSS scribes before writing, so as to permanently fix their water-soluble carbon black writing inks to the parchment support. While the tannins would slightly darken the surface, they would not penetrate through to the center of the parchment or alter its unique characteristics, allowing the smooth texture and slight stiffness of the material to be preserved and the inner core of the skin to retain its natural creamy white color.

In all but one case, which is discussed below, the substrate of the MOTB scroll fragments appears to be leather rather than the lightly tanned or untanned parchment that is characteristic of the authentic Dead Sea Scrolls. This determination is based on the following observations: the material is thick and uneven and extremely fibrous on its verso or flesh side, the grain is often very pronounced, with high and low points that impede the writing, and the medium to dark brown color of the substrate is consistent throughout its thickness. The following examples of ancient parchment and leather from Qumran that are in the Schøyen collection are compared with a representative MOTB DSS fragment that exhibits leather-like properties. (**Figure 1** on page 10)

Several fragments in the Schøyen collection also appear to have been written on leather rather than on parchment and share many other similarities with the MOTB fragments. Samples of the writing support from two Schøyen fragments, MS2713, and MS2861, were analyzed at the NSF-Arizona AMS Facility, University of Arizona, Tucson in 1999 and 2000 respectively. The date ranges that were obtained (118 BCE-73 ACE for MS2713, and 338 BCE-54 ACE for MS2861) indicates that ancient material was used in their production. Although these two fragments have not been examined or analyzed by the team, or to this point suspected of being forgeries, they bear a striking resemblance to the MOTB fragments, suggesting that the writing supports of the latter may be of ancient origin. To the best of our knowledge no further analysis has been conducted beyond Ira Rabin's published results in 2016, in which she describes MS2713 as one of two fragments in The

Figure 1

Schøyen MS 5905/7 Fragment of authentic DSS scroll

Schøyen MS 5905/6 Degraded leather strap

MOTB.SCR.000123 Thick support with raised grain (recto); fibrous uneven flesh side (verso)

Schøyen Collection identified as "definitively" leather. The degraded condition of the two dated Schøyen fragments and the MOTB fragments, indicated by blackening of the grain surface, multiple cracks through the thickness, delamination, and loss of the grain layer, compression of the collagen fibers, loss of flexibility, and extreme embrittlement in some cases, reinforces the theory that the writing in both cases was applied to small scraps taken from archeological deposits of ancient leather. A comparison of a fragment from each collection can be seen in **Figure 2** on page 11.

Figure 2

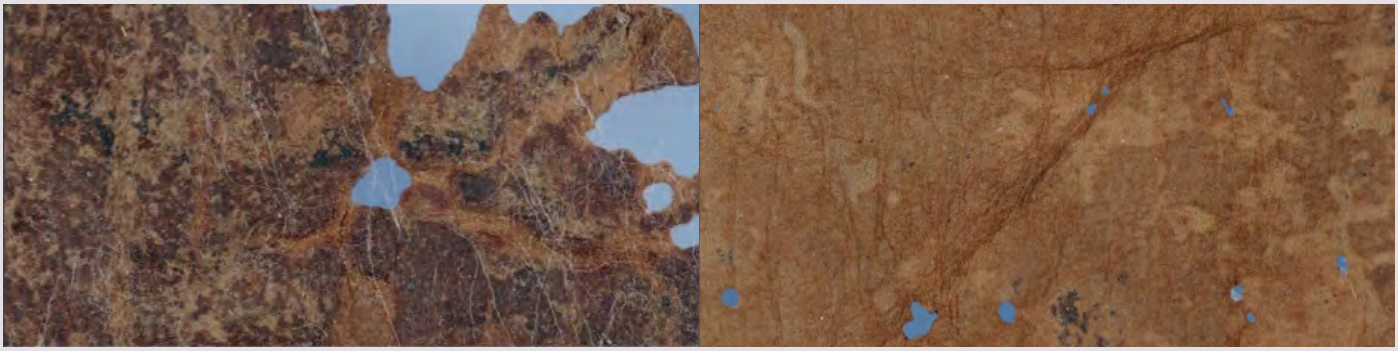

Schøyen MS2713 Details (recto/verso) of one of two dated fragments on ancient material

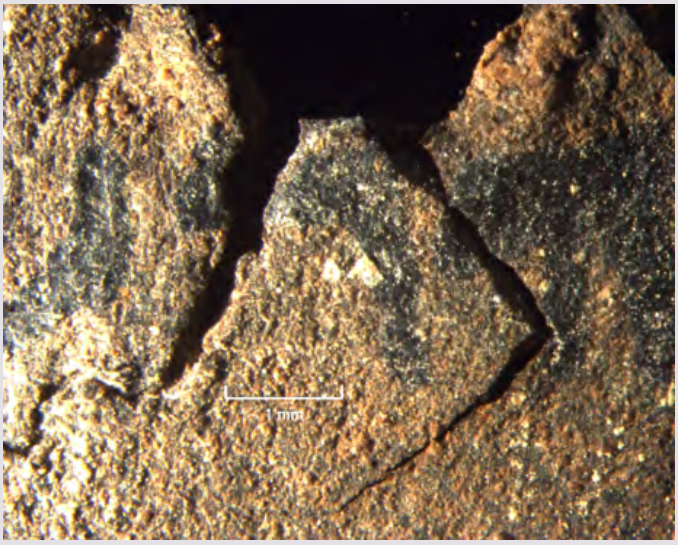

MOTB.SCR.000121 Cracks in brittle substrate

MOTB.SCR.004741 Grain black from oxidation

MOTB.SCR.004742 (Leviticus) is quite thin compared to all the other MOTB fragments and does not appear to have a raised grain layer or a rough flesh side, suggesting that the substrate could be parchment rather than leather. However, the support appears to have been thoroughly coated with an amber material (most likely animal skin glue) and, as a result, has developed a very hard, smooth surface on both sides that completely obscures the original texture of the skin. The pronounced distortion of the fragment, which can often be useful for distinguishing parchment from leather, is probably due to the glue impregnation that has caused the thin substrate to curl inwards towards the flesh side. (**Figure 3**)

Figure 3

MOTB.SCR.004742 Leviticus fragment

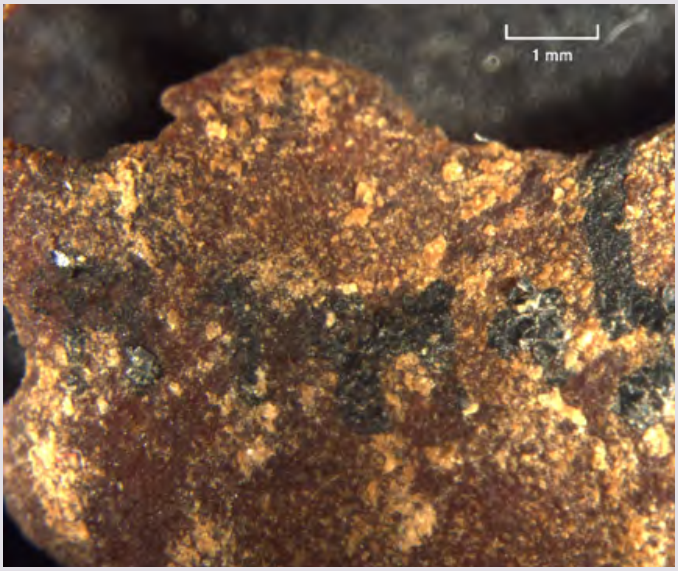

MOTB.SCR.004742 Detail of amber coating

The origin of the substrate material and work of the forgers

Fragments of deteriorated leather could have been obtained by the forgers from a number of known sites, including the Qumran caves where the authentic DSS were found or farther afield. One interesting possibility is that pieces of Roman-era leather shoes, which have been found at a number of archeological sites from this period, might have served as the substrate for some of the forgeries. Many of the MOTB fragments have small round holes in random locations that were likely caused by boring insects. Other larger holes, however, have a different shape and are aligned with one another, giving the distinct impression that they were manmade. As observed by Kipp Davis (personal communication, 7/24/2019), there is a striking resemblance between the lacing holes found in the remains of ancient shoes from Vindolanda (a Roman site in the UK) and in the Schøyen collection, and the holes found in one of the suspected Schøyen DSS forgeries (**Figure 4**). At least one of the MOTB fragments (MOTB.SCR.003183) exhibits a very similar pattern of holes. While the shapes are not identical, probably due to different patterns of wear and stretching of the leather in the original shoe, the holes in the Schoyen and MOTB fragments line up in a similar way. (**Figure 5** on page 13)

Figure 4

Schøyen MS 1655/5 Leather shoe fragment

Intact leather shoe from Roman site Vindolanda. Image from Vindolanda Trust.

Figure 5

Schøyen MS5426 Possible line of manmade holes at right

MOTB.SCR.003183 Possible line of manmade holes at right

All of the MOTB fragments were found to be heavily coated with a shiny amber material that was identified by FTIR analysis as a protein, with the best reference match being animal skin glue. (**Figure 6**) Comparisons with known samples of animal skin glue reinforce this identification. Given the number of tears, deep cracks, and areas of embrittlement, it is likely that the glue was applied primarily as a means of reinforcing the fractured and torn substrates before writing. At the same time, coating the surfaces with animal glue would simulate the gelatinization seen in many authentic DSS fragments, where hydrolysis has permanently converted the collagen fiber network to a hard, glue-like mass. The possibility that the black layer below the writing is a coating was considered, yet no pigmented materials were identified during analysis with FTIR. This suggests instead that the blackening is a discoloration phenomenon, caused by oxidation of the collagen fibers at the surface, that is commonly seen on deteriorated leather artifacts. It is possible that some of the clear pressure-sensitive tapes seen on several MOTB fragments were applied by the forgers, to join broken and detaching pieces together before writing. (**Figure 7**) Although these tapes are obviously modern, they would also have simulated the appearance of authentic fragments that were joined with tape by DSS scholars in the late 1940's and early 1950's.

Figure 6

MOTB.SCR.003174 Fibers saturated with glue

Figure 7

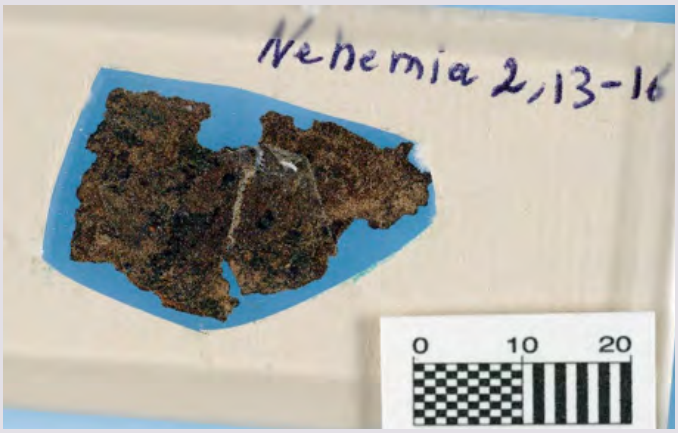

MOTB.SCR.003175 Verso with piece of tape

The inks of the MOTB fragments that were sampled have been identified as carbon black bound with a vegetable gum and/or animal skin glue. Compared to the carbon inks of the authentic DSS, which are thinly applied and relatively matte in appearance, the inks of the forgeries are very thick and shiny, suggesting that there is a higher ratio of binder to carbon black in the mixture. While this result may have been accidental, given the hydrophilic nature of many carbon black pigments that can make them difficult to disperse in an aqueous medium, it is also possible that the forgers intentionally prepared a more viscous and sticky ink that would adhere well to the irregular and fragmented surfaces of their supports. **Many anomalies observed in the application of the ink reinforce the theory that degraded fragments of archeological leather, most likely ancient and already covered with a variety of mineral deposits from the environment, were used as substrates for writing.** Some of these anomalies include ink going across and into deep cracks in the substrate, ink skipping over the high points of the grain layer and

waterfalling off the edges of the fragments, ink extending beyond the intact grain layer to adjacent areas of delamination and lying on top of thick, granular mineral deposits. (**Figure 8** on page 15) In some cases, a variety of loose mineral deposits were then scattered over the forgeries after writing, perhaps even before the ink had dried, in order to give the impression that these were authentic DSS fragments that had come from the Qumran caves and had been buried there for centuries.

The scholars have observed that the characters within single lines of text on the MOTB fragments do not often line up as they should, and that the writing appears in many cases to conform to the ragged and irregular profiles of the substrates. In addition to confirming these observations we have documented the presence of incised ruling lines on two fragments (MOTB.SCR.3171 and MOTB.SCR.3183) that were made using a narrow point and a straight edge. (**Figure 9**) However, this artificial ruling was carelessly executed, sometimes creating a double line where there should be only one, and the writing rarely follows the lines. In two other examples (MOTB.SCR.003173 and MOTB.SCR.3175) the ruling lines, instead of being incised, were created with a white waxy-looking material that was probably applied with a pen or a grease pencil. The scholars also observed an unusual feathering of the ink on several of the fragments. This feature can be explained by the challenge of writing on such uneven leather surfaces that were already covered with mineral deposits.

Figure 8

MOTB.SCR.003173 Viscous ink across and into a crack

MOTB.SCR.003172 Ink flows over torn edge

Figure 9

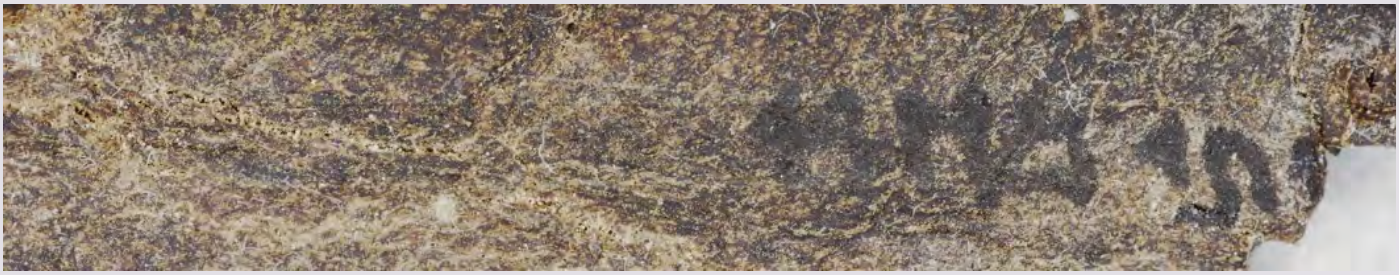

MOTB.SCR.003171 Detail showing faint inscribed line and text that is misaligned at the end

These irregularities would have caused the ink to flow beyond the boundaries of the letters and into the rivulets created by the raised grain and the granular deposits. Sometimes the scholars noted an apparent bleeding of the ink through to the verso of certain fragments, or possible offset of the ink that might have occurred when the scrolls were rolled. These areas of the reverse were examined by the team and were found not to be ink, but instead black stains that were likely already present on the substrates at the time that the forgeries were created.

Restoration and remounting of the fragments prior to their sale

Most, if not all, of the MOTB fragments appear to have been remounted prior to sale and this has been established by comparing the natural light images taken by the West Semitic Research Project photographers with the current appearance of the fragments. It is possible that some of the remounting was done at a firm in Eppstein, Germany, Antiques Analytics GmbH, that is known to have been used by the dealer Lee Biondi. Information about this company was provided by Lee Biondi to Abigail Quandt, who was contacted on two occasions about the possibility of providing private conservation services for DSS fragments in his collection. However, the legitimacy of Antiques Analytics has not been confirmed. The remounting consisted of the removal of some of the paper hinges on the reverse and the encapsulation of the fragments in clear acrylic sandwiches. Attempts to further reinforce the fragile substrates, and provide better joins for fragments in one or more pieces, may have been done at the same time. This restoration work included the use of thin, fibrous tissue papers and paper-based pressure-sensitive tapes on the reverse of several fragments, and the application to the front of acrylic and cellulose-based coatings that were identified on some of the forgeries analyzed with FTIR. (**Figure 10**)

Figure 10

MOTB.SCR.003174 Restoration materials on verso

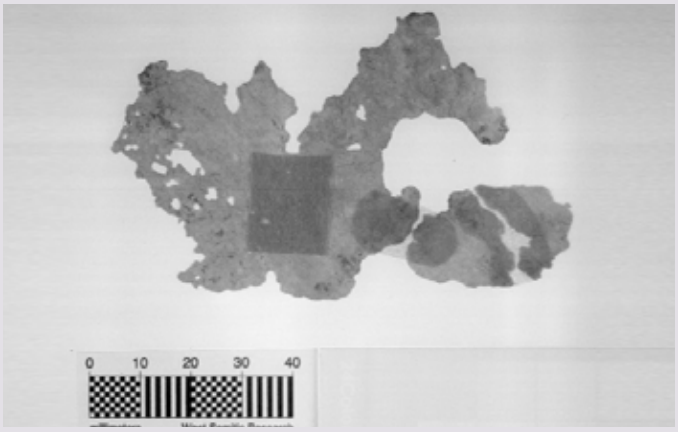

MOTB-SCR.000124 Tissue joins on verso

Summary of Elemental and Molecular Analysis

I. Introduction

The Dead Sea Scrolls, dating from the 3rd century BCE to the 1st century, CE, are a cache of Jewish manuscripts, predominantly written on parchment, from the Qumran caves in Israel that provide an exceptionally early source for the texts that make up the Old Testament. The Scrolls also provide invaluable information about the shape of early Judaism and contextual religious and cultural background information about Roman Palestine and the emergence of Christianity. The Museum of the Bible owns sixteen fragments of these ancient Jewish texts. However, at the time of the publication of the Museum of the Bible Dead Sea Scroll fragments, no scientific examination of the scroll fragments had been carried out, as has been done with other finds from Qumran caves. A preliminary study of the mineral deposits on the Museum of the Bible fragments, published in 2018, led to the suggestion that these deposits were inconsistent with the fragments being authentic Dead Sea Scrolls. Physical features of the fragments, such as the relationship between the inscriptions and the damaged portions of the fragments, suggested that the substrates were ancient but that the writing was added later. As a result of the concerns raised by this initial study, a more detailed materials investigation of the Museum of the Bible fragments was sought.

We now know that there is much information to be gained from the direct study of the Museum of the Bible Dead Sea Scroll collection. This includes studying the fragments under different wavelengths of light, studying them under high magnification, identifying the materials from which they were made, and identifying the materials deposited on their surfaces. Our in-depth study involved six fragments, selected as representatives of the sixteen fragments that naturally divide into six groups by their different visual appearances. Our study included making an overall map of their elemental compositions and doing spot molecular analysis of the mineral deposits, inks, coatings, and restoration materials. We also conducted microchemical testing for evidence of vegetable tannins. We combined our elemental and molecular data to obtain comprehensive information on the fragments' mineral deposits in a minimally invasive manner. Finally, we imaged a cross-section of a previously detached section from one of the fragments under the electron microscope to more fully address the nature of the animal hide substrate. **We found that the substrates for the Museum of the Bible fragments are leather rather than parchment (except in one case), that the raw skins when originally processed appear to have been lime-depilated[1] (a technology that postdates the Dead Sea Scrolls), and that the ink was applied to already aged pieces of leather rather than when the material was newly made and intact. The mineralogy of the surface deposits is consistent with the Dead Sea region, and with other geological sites in the Middle East, but the fragments are forgeries with modern ink being applied to repurpose archeological leather scraps. These fragments have been additionally treated with a protein coating that appears to be animal hide glue, selected to simulate the appearance of the more degraded original Dead Seas Scrolls.**

The specific tools used for chemical analysis and imaging in this study included Fourier transform infrared spectroscopy (FTIR), macro x-ray fluorescence imaging (MA-XRF), scanning electron microscopy – energy dispersive x-ray analysis (SEM-EDS), micro-Raman spectroscopy (Raman), and microchemical testing (a more sensitive method of determining tannins than FTIR, which cannot resolve minor phases of a mixture below 10% of the total). Chemical compounds that are not detectable with the molecular analysis techniques (not selected for microsampling because they were visually indistinguishable from other phases present) can be inferred using the elemental analysis data. This

is accomplished by examining the data for positive correlations, places where the concentration of one element rises together with the concentration of another element. For example, chloride salts cannot be identified with FTIR and are rarely observed with Raman spectroscopy (because of their weak light scattering properties). However, the positive correlation of calcium and chlorine for scroll fragment SCR.000124 (Genesis) suggests that calcium chloride is present. Another example of this in the elemental data is the positive correlation of the iron and titanium concentrations for SCR.003173 (Numbers). This allows us to infer the presence of iron and titanium compounds such as ilmenite (an iron and titanium oxide). In short, FTIR is a point analysis technique, while the MA-XRF data covers the entire scroll fragment. As a result, the elemental data allows us to propose compounds in the scroll fragments that the FTIR point analysis may have missed.

II. Molecular Analysis – micro-FTIR

A. Mineral Deposits

The most common minerals that we identified on the scroll fragments included chalk, clay minerals, talc, and quartz[2] (see **Figure 1**). Other rarer minerals that we definitively identified included gypsum, ankerite, and aragonite (see **Figures 2** and **3**). **These mineralogical findings from the FTIR data are consistent with the known compositions of mineral evaporites at the Dead Sea, the mineral deposits in the caves at Qumran, and the literature on the mineralogy of other studied DSS fragments.**[3] Clay minerals associated with the Dead Sea region include smectite, kaolinite, illite, and small amounts of palygorskite[4].

The mineral phases identified are shown in **Table 1**.

Table 1. Mineral Phases Identified on the Museum of the Bible Dead Sea Scrolls*

Phase Name	Chemical Formula	Description
Chalk	$CaCO_3$	Terrestrial form of calcium carbonate
Aragonite	$CaCO_3$	Marine form of calcium carbonate
Gypsum	$CaSO_4.2H_2O$	Hydrated calcium sulfate
Quartz	SiO_2	Framework silicate – major component of sand
Kaolinite clay	$Al_2Si_2O_5(OH)_4$	a bentonite-group clay [bentonites are aluminosilicate clay
minerals that can be sodium, potassium, or calcium rich		
Talc	$Mg_3Si_4O10(OH)_2$	A magnesium silicate
Attapulgite	$[(Mg,Al)_2Si_4O_{10}(OH)$	A clay mineral
Montmorillonite	$(Na,Ca)_{0.33}(Al,Mg)_2(Si_4O10)(OH)_2 \cdot nH_2O$	A clay mineral
Ankerite	$Ca(Fe,Mg,Mn)(CO_3)_2$	Similar to dolomite but with small amounts of iron and manganese replacing magnesium.

*Different classifications of clay minerals are highly chemically and physically similar to one another, and as a result they can be broadly classified by FTIR, but not always definitively identified. X-ray diffraction is required for a definitive identification. The clays that best match the FTIR data are shown here.

The mineral deposits on the six different Dead Sea Scroll fragments studied are listed in **Table 2** below. Direct spectral evidence for representative major mineral deposits on the Museum of the Bible scroll fragments using molecular analysis is shown in the data following the table. One of the most important features to note in the data from the Museum of the Bible fragments is that calcium minerals were exceedingly prevalent, occurring on all of the six fragments studied. Chalk was identified in five of the six fragments. **This suggests that the substrates of the Museum of the Bible fragments may have been lime-depilated and not enzymatically depilated, as would be the predominant method for skins dating from the 3rd century BC – 1st century AD.**[5] Calcium can also be deposited onto animal skins from a lime bath used to dehair them and as chalk applied for degreasing, whitening and/or smoothing.[6] However, the deep intrusion of the calcium into the skin substrate observed here is suggestive of a lime depilation.

What follows below is a summary of the data collected on the materials that make up the Museum of the Bible Dead Sea Scrolls.

Table 2. Sediments - Summary of inorganic phases identified in the sediment samples of the studied fragments.[7]

Fragment	SEDIMENT – inorganic phases identified		Clay mineral best match(es)
000121	cream	• calcium carbonate • phyllosilicate clay • quartz	illite
	tan	• calcium carbonate • phyllosilicate clay	kaolinite
	black	• calcium carbonate • phyllosilicate clay • quartz	montmorillonite
000124	cream	• calcium carbonate • calcium oxalate • calcium stearate • gypsum • phyllosilicate clay	attapulgite, montmorillonite
003173	cream	• calcium carbonate • gypsum • phyllosilicate clay • quartz	kaolinite, montmorillonite
003183	tan	• calcium carbonate • dolomite • gypsum • phyllosilicate clay • quartz	kaolinite, montmorillonite
004741	cream	• calcium carbonate • cerussite • phyllosilicate clay • quartz	illite
004742	cream	• calcium carbonate • phyllosilicate clay	kaolinite, montmorillonite
	tan	• ankerite • phyllosilicate clay • calcium silicate	kaolinite, montmorillonite

Figure 1. Sample 121, region 6. A tan-hued deposit is identified here as a mixture of clay minerals and chalk.

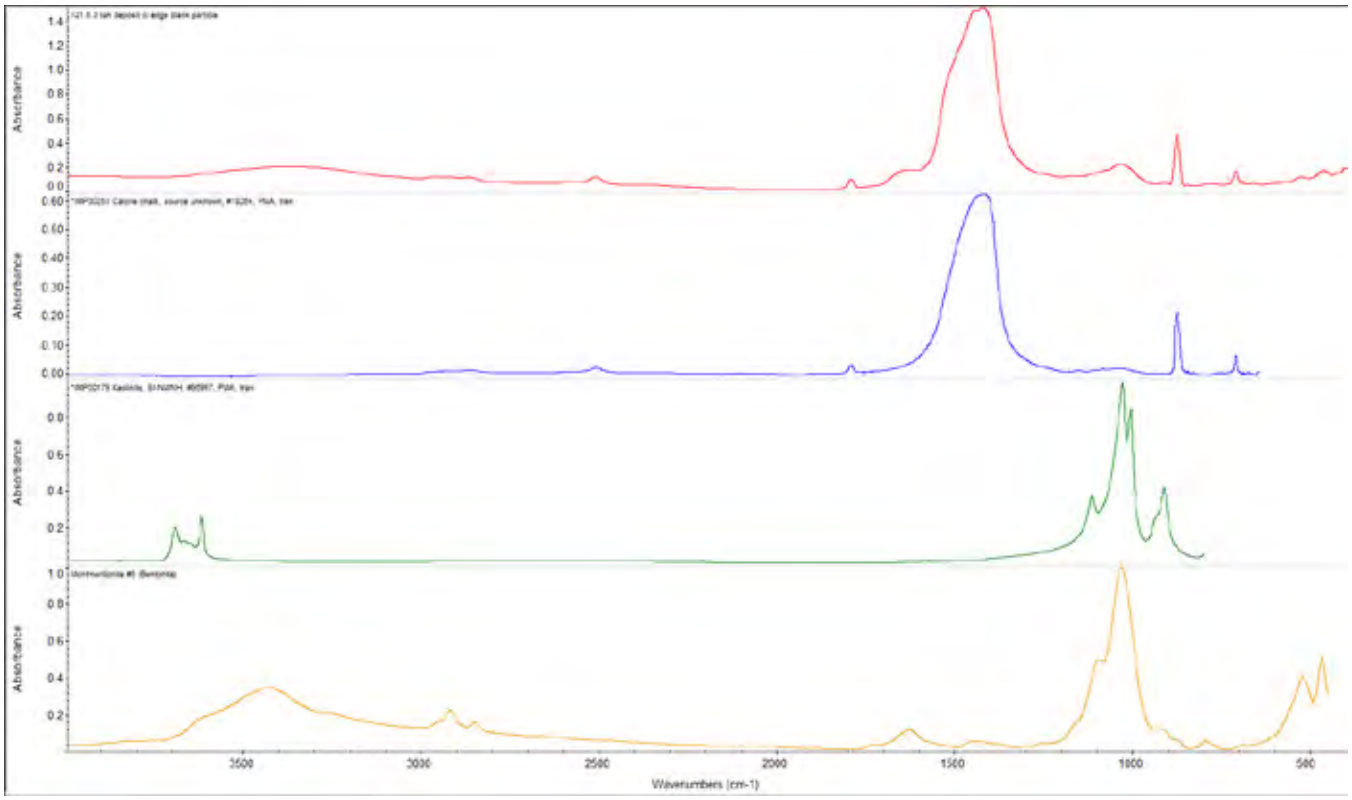

Figure 2. Fragment 3173, region 1. A cream-colored deposit on this fragment is identified here as comprised of chalk, quartz, gypsum, and clay minerals.

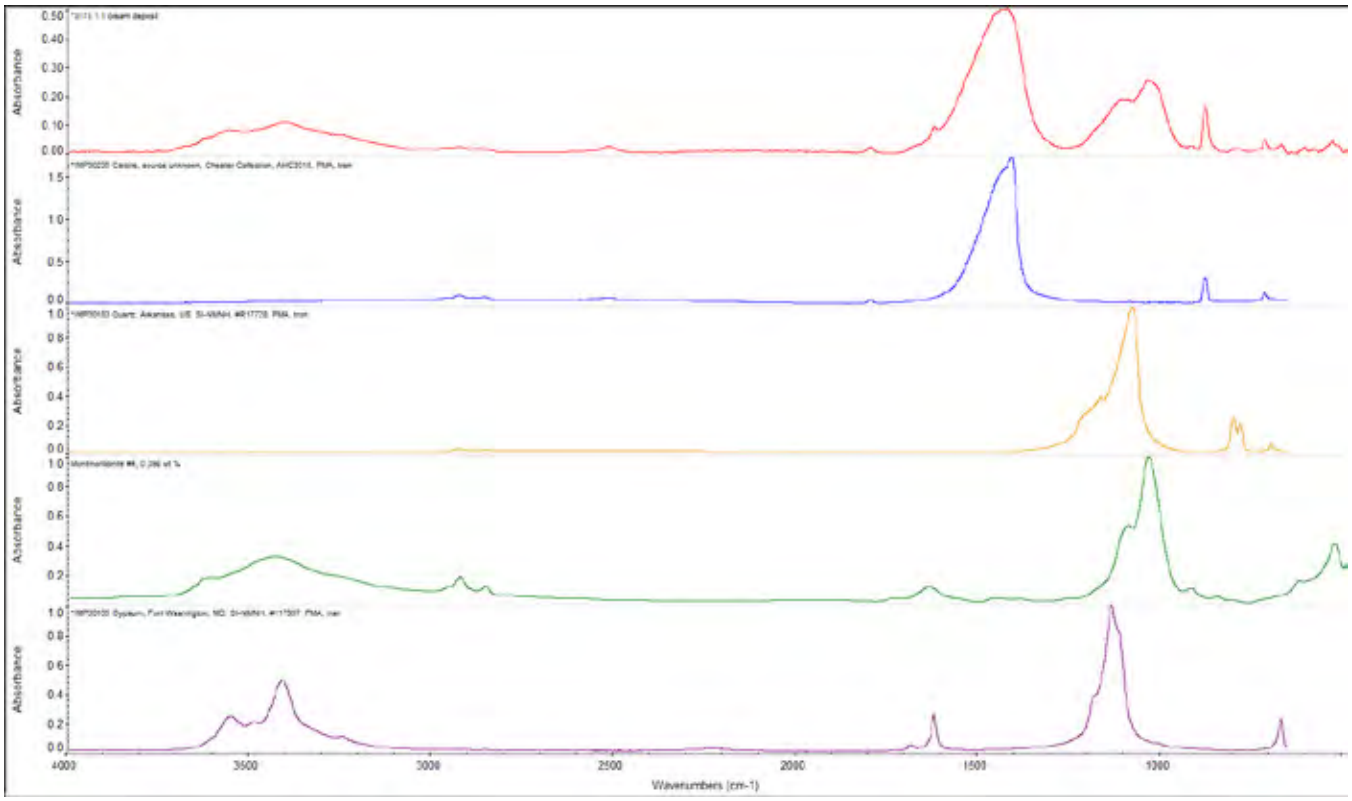

Figure 3. Fragment 3183, region 3. Sediment on the verso of the fragment is revealed to be dolomite and clay.

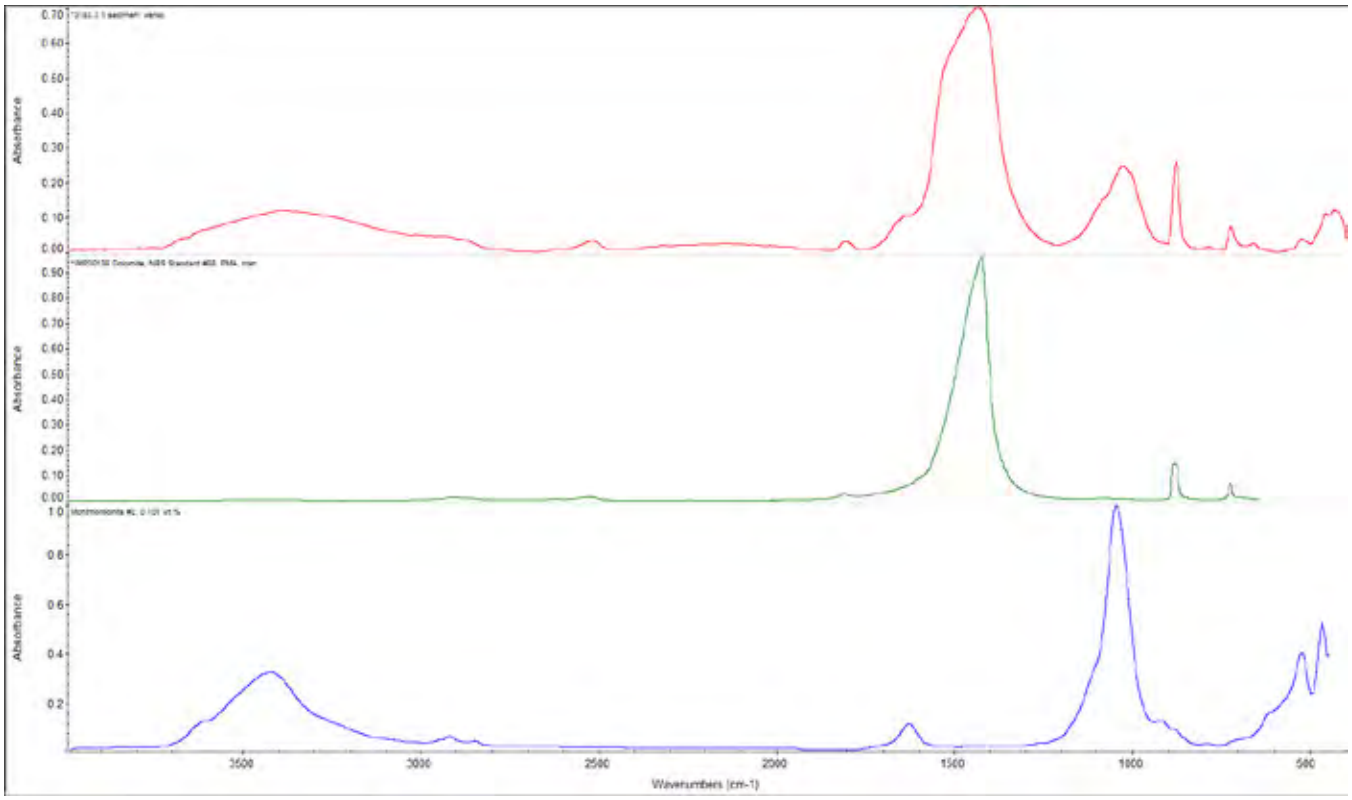

Figure 4. Fragment 124, region 1. Cream-colored deposit analysis reveals the presence of both calcium oxalate and calcium stearate [Note the instrumental noise is due to using an infrared (FTIR) microscope onsite in an air path (rather than nitrogen), and so signal from water and carbon dioxide is observed].

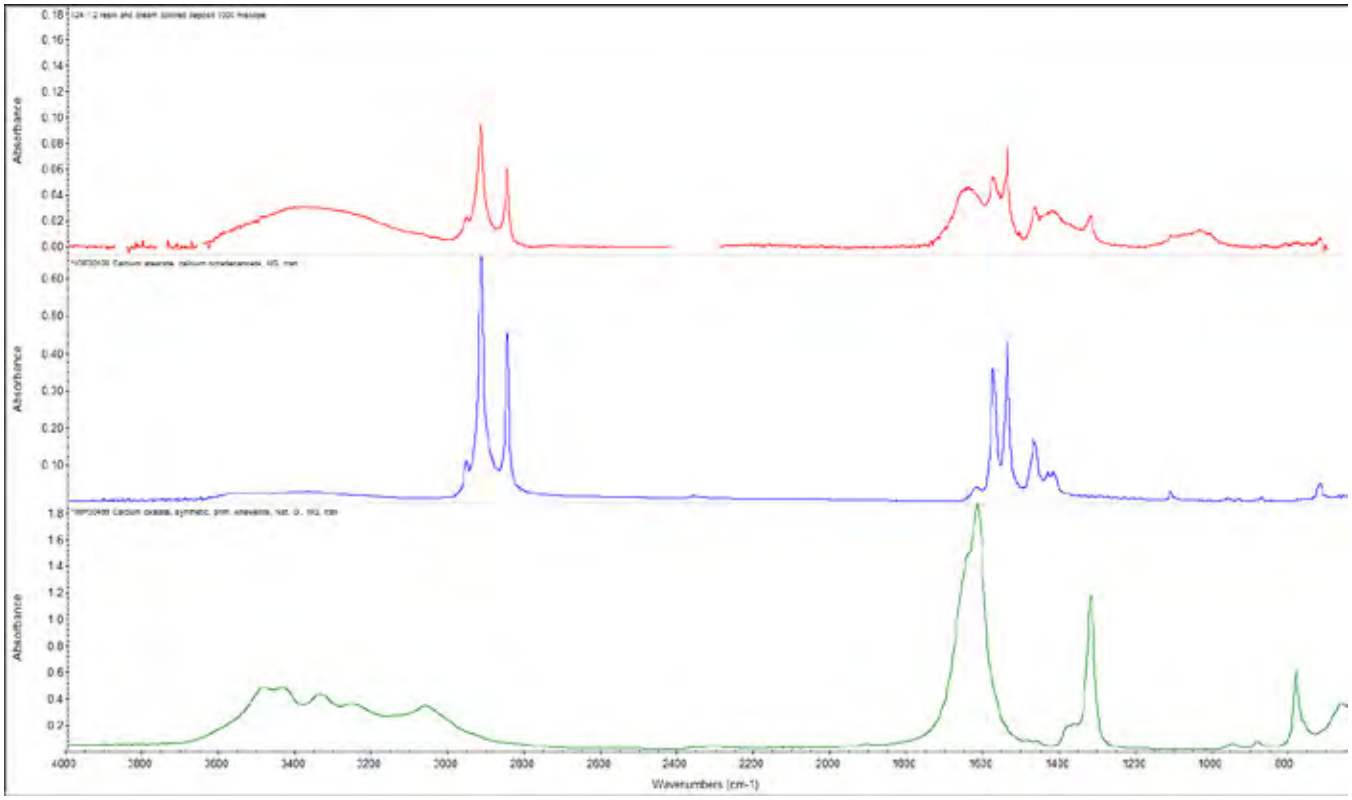

B. Degradation Phenomena

The calcium minerals (gypsum, chalk, and calcium silicate) were found to have reacted with fats from the animal skin substrate (and possibly an applied oil suggested by cross-section staining), producing two degradation products - calcium stearate and calcium oxalate. Calcium oxalate is formed as a result of bacterial and fungal attack of chalk-containing leather fragments. Calcium oxalates [CaC2O4.H2Ox], also identified by Rabin et al, are commonly occurring organic degradation products resulting from the formation of oxalic acid in reaction with calcium-rich minerals such as chalk or limestone. In animal hide, oxalates can also be due to the use of urine or plant extracts in the depilation process. [8] They further occur as degradation products observed in the breakdown of organic coatings such as oils. Another metal carboxylate, calcium stearate, was identified in a sediment sample (SCR 000124) and coating (SCR 004741). This calcium soap formation would similarly form from reaction of the calcium in the chalk deposits (and calcium sulfate present as gypsum, identified in SCR 000124, SCR 003173, and SCR 003183) with fatty acids from an oil introduced into the support through handling or treatment.[9] It could also form as a result of the reaction of the calcium salts with residual fats (stearic acid) remaining in the skin.

The reaction/degradation products which observed calcium stearate and calcium oxalate are shown below in **Figure 5**.

Figure 5. Fragment 124, region 1. Cream-colored deposit analysis reveals the presence of both calcium oxalate and calcium stearate [Note the instrumental noise is due to using an infrared

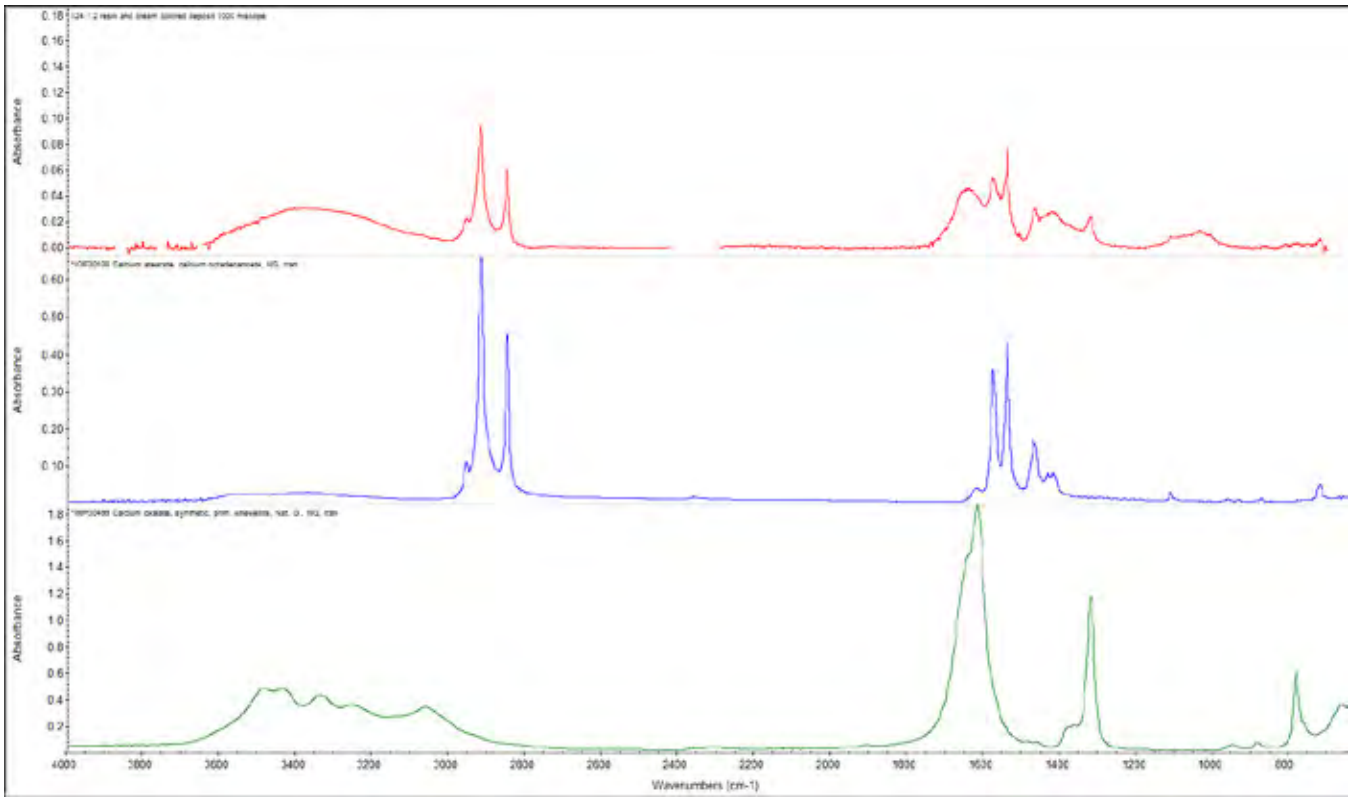

The data shown above (and additional data available in our full report) are consistent with animal skin fragments that have all undergone lime depilation, and so they are not consistent with the well-documented finds from the Qumran region.

C. Inks

The black inks on all of the Dead Sea Scroll fragments are carbon based and are predominantly bound with tree gums such as gum Arabic. The use of a carbon black ink was confirmed by Raman spectroscopy (data not shown). The materials identified in the inks by FTIR are shown in **Table 3**.

Table 3. Inks - Summary of organic phases identified in the ink samples of the studied fragments.

Fragment	INK – organic phases identified	best match(es)
000121	• animal skin glue • cellulosic material	hemicellulose
000124	• animal skin glue • tree gum • cellulosic material	gum Arabic, cellulose
003173	• animal skin glue • tree gum • calcium oxalate	gum Arabic
003183	NA	
004741	• animal skin glue • polysaccharide	sturgeon glue with honey
004742	• animal skin glue	hide glue

Two examples of the relevant data (**Figure 6** and **Figure 7**) are shown below and on the next page.

Figure 6. Sample 121, region 3. Black ink sample revealing a plant gum binder and a protein.

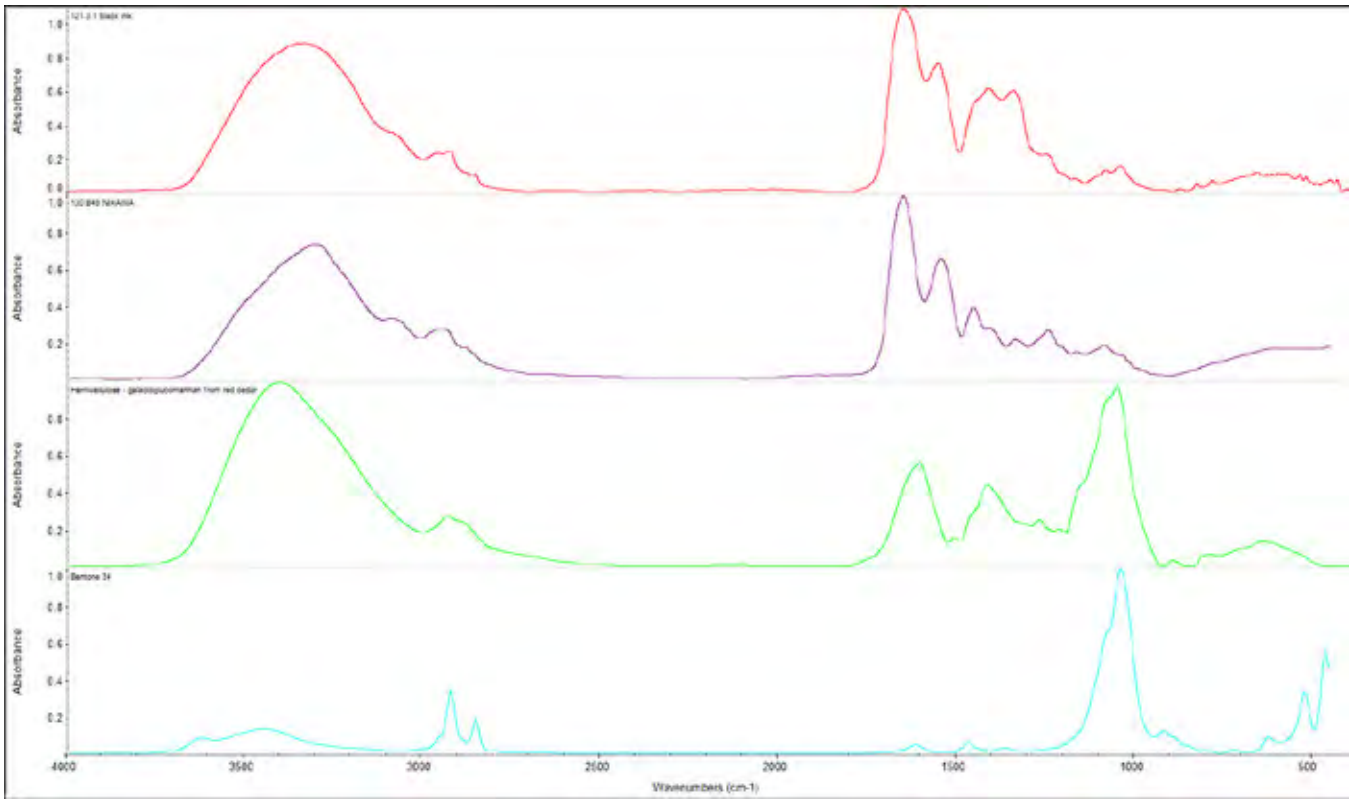

Figure 7. Sample 3173, region 2, spectrum 1. Black ink.

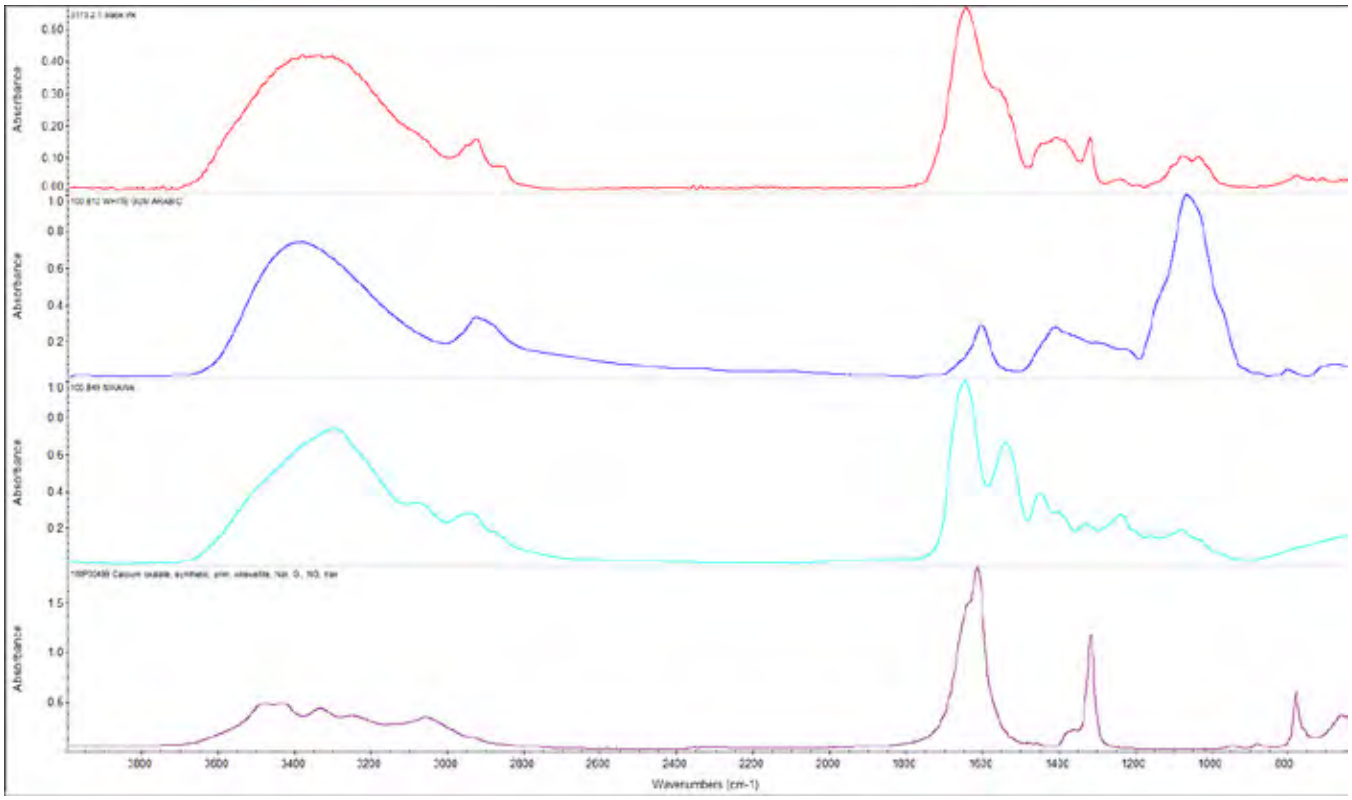

D. Coatings and Conservation Materials

All findings for the transparent amber-hued coating on the fragments point to an animal skin glue (best reference match and visual appearance). This coating was likely applied to contribute to the 'aged' appearance of the fragments and to provide a smooth surface for the added inscription by reinforcing the torn and cracked substrates that were already deteriorated before writing. A similar coating should form naturally from the degradation of the leather (gelatinized surface). It is important to note that infrared spectroscopy alone cannot distinguish among specific types of applied protein coatings.

The conservation adhesives identified on the fragments include an acrylic polymer, an alkyd resin (a type of synthetic drying oil), and, primarily, cellulose-based materials such as cellulose gum(s) and wheat starch. Repairs on the reverse of the fragments indicate that they have undergone previous conservation treatments, but no conservation records are available. A biocidal material added to preserve the fragments, isothiasolinone, was also suggested by the data. The table below summarizes the coatings and surface treatments identified on the Museum of the Bible fragments.

Table 4. Coatings - Summary of organic phases identified in the coatings and other surface materials sampled from the studied fragments.

Fragment	COATING – organic phases identified		best match(es)
000121	saturated fibrils	• animal skin glue • cellulosic material • bromine compound	• hemicellulose • 2,5-dibromonitrobenzene
	pink accretion	• alkyd polymer	Aralon 970
000124	fibrils	• cellulosic material	cellulose
003173	cream	• calcium carbonate • gypsum • phyllosilicate clay • quartz	hemicellulose
	fibrils	• acrylic copolymer	methyl methacrylate n-butyl acrylate
	glossy material over ruled lines	• cellulosic material	wheat starch
003183	amber material	• animal skin glue	
004741	coating	• cellulosic material • calcium stearate	jute fiber, Kayocel 10-NC-50 [cellulose fiber with inorganic filler]
004742	orange resinous material	• animal skin glue • poss. biocide	isothiasolinone
	Leather substrate [diffuse reflectance]	• cellulosic material	cellulose [microscope reflection], viscose rayon

Two examples of the data this table is derived from are shown in **Figure 8** and **Figure 9** below and on the next page.

Figure 8. Sample 3173, region 6. The glossy material over the ruled lines is an acrylic resin.

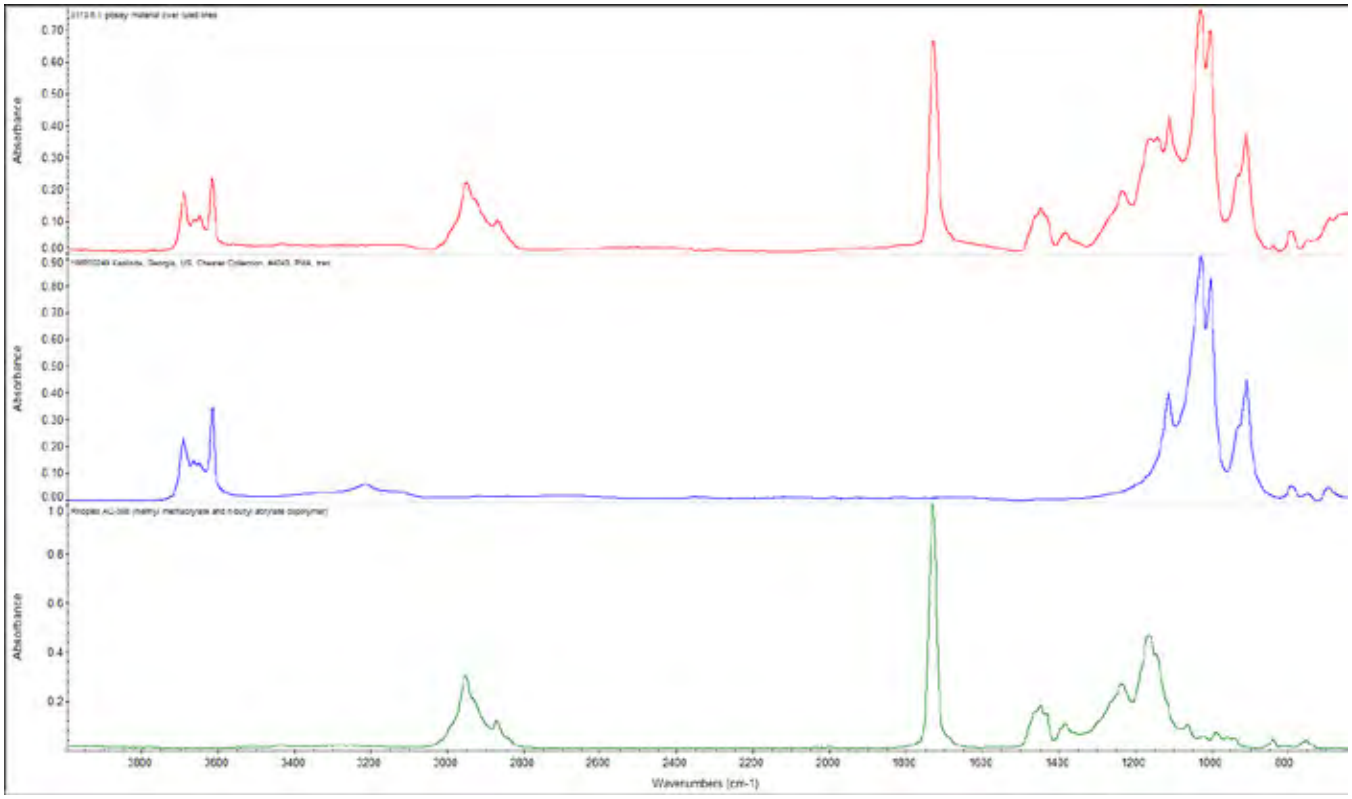

Figure 9. Sample 3183, region 2. Amber-colored coating material, darker brown recto.

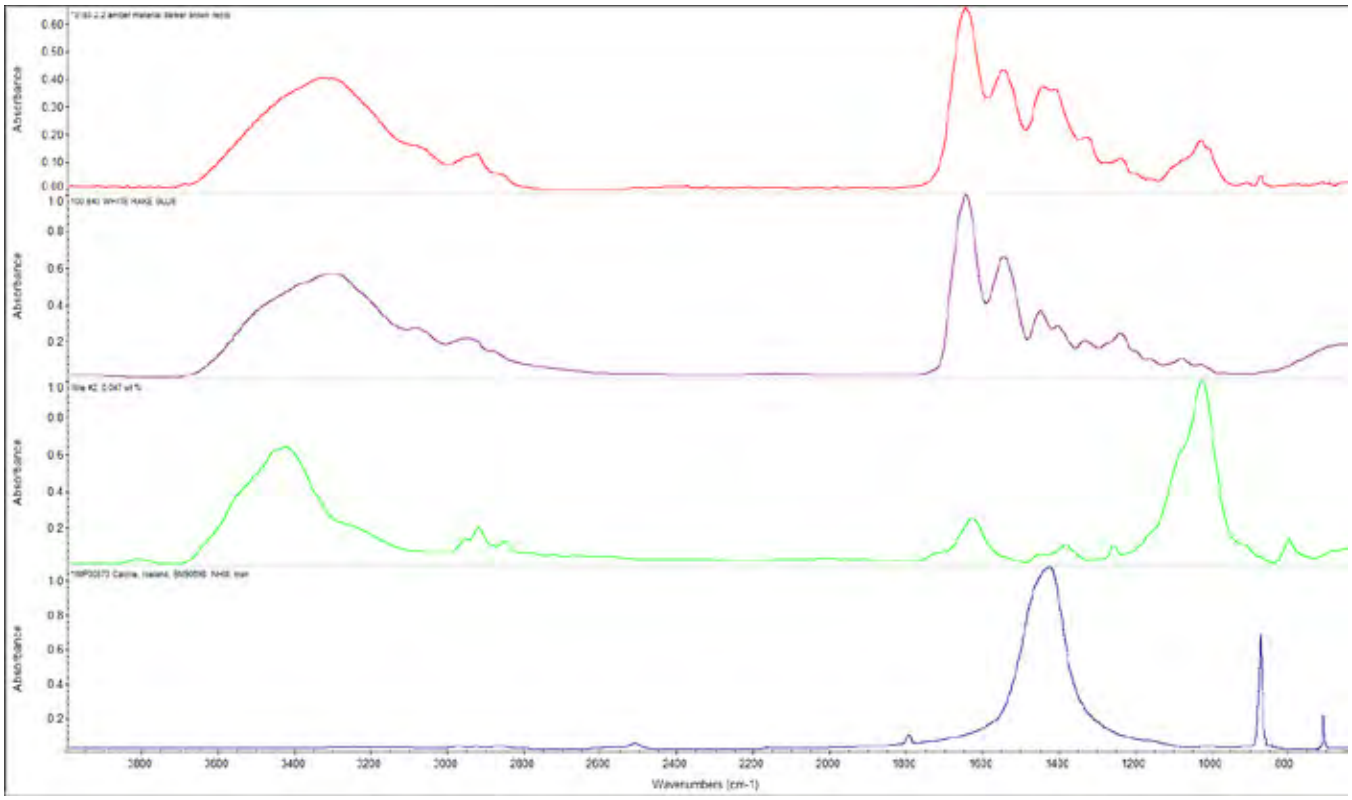

III. Elemental Imaging – MA-XRF

The major elements identified in the fragments are calcium, potassium, iron, chlorine, sulphur, silicon, and phosphorus. Minor elements included sodium, manganese, aluminum, nickel, bromine, titanium, strontium, and magnesium. More unusual elements, suggestive of an external or man-made origin, included traces of selenium, zinc, and lead and more substantial amounts of copper. In addition to the mineral deposits identified previously, a number of minerals and evaporites/salts are suggested by the elemental data.[10]

Overall, the minerals and evaporites (salt deposits from sea spray) suggested by the data include calcium bromide, potassium chloride, sodium chloride, potassium bromide, and calcium chloride. The elemental data further suggest the presence of calcium phosphates, dolomite, alum, talc, palygorskite/attapulgite clays, and ilmenite. Ilmenite is commonly found in association with clay minerals. Alum treatment is identified by Rabin et al. in a Temple Scroll fragment. [11] The elemental correlations for the four fragments studied are explained in more detail on the following page.

Figure 10. Selected elemental maps from SCR000121.

Elemental Correlations

The fragment SCR000121 correlations (**Figure 10** above) suggest the presence of aluminosilicate minerals including clay minerals[12]. The presence of gypsum is suggested by the positive correlation between calcium and sulfur. The presence of potassium chloride, potassium bromide, and sodium chloride are also suggested by the elemental correlations. The correlation of calcium and magnesium is characteristic of their geological relationship. The presence of ilmenite (FeTiO3) is suggested by the correlation between iron and titanium (this is an accessory mineral found in many clays). The presence of talc is suggested by a correlation between magnesium and silicon. Magnesium and silicon correlations are also suggestive of palygorskite/attapulgite clays [(Mg,Al)2Si4O10(OH) ·4(H2O)].

The elemental correlation data for fragment SCR000124 are strongly suggestive of gypsum, aluminosilicate clay minerals, potassium bromide, calcium bromide, calcium chloride, talc, ilmenite (FeTiO3, one of many iron and titanium containing accessory minerals in clays and sands). The correlation of aluminum, potassium, and sulfur is suggestive of the presence of alum. The correlation of calcium and phosphorus observed here is suggestive of a calcium phosphate mineral evaporite such as apatite. Phosphates are known to occur in the Dead Sea region (phosphate mining occurs within 50 miles of the coast), and apatite [Ca5(PO4)3(OH,F,Cl)] makes up 1-5% of environmental dust deposited over the Dead Sea[13]. The correlation of magnesium and calcium is suggestive of their geological relationship, including the possible presence of dolomite.

Fragment SCR 003173 shows correlations that are suggestive of aluminosilicate clay minerals, gypsum, ilmenite (FeTiO3), or other iron and titanium containing clay accessory mineral, and potassium chloride. The manganese and sulfur correlation is likely related to black manganese deposits along the Dead Sea coastline, although these have been found to be predominately manganese oxides. The manganese is consistent with poorly crystalline manganese oxide/hydroxide crusts that have been observed on the shores of the Dead Sea[14].

Fragment SCR 004742 demonstrates correlations that are suggestive of aluminosilicate clay minerals and potassium chloride. One example of the raw data (elemental maps) used to generate these correlations is shown below. The lighter the color, the higher the concentration of the element being mapped. High calcium and chlorine contents are revealed by the data below.

IV. Elemental Imaging – Scanning Electron Microscopy

Two small samples from SCR000121 were examined in cross-section, and are referred to here as Sample A and Sample B. Both samples show evidence of the application of an oil (see **Figure 11** below). **This may be what is responsible for the darkening of the fragments as a whole.** The fiber structures of the samples are highly compressed at the base and show some more flowing fibers at the top. Determining directionality is difficult, most likely due to the degradation of the leather that has occurred over time. High calcium contents are present as observed in the MA-XRF images. X-ray mapping in the SEM shows the clear distribution of elements throughout the structures and shows the higher atomic number elements associated with the accretions on the surface of the fragments. Possible mineralization/mineral deposits inferred from these data include: calcium carbonates (i.e. calcite CaCO3), gypsum ($CaSO_4 \cdot 2H_2O$), calcium phosphates (apatite (Ca10(PO4)6(OH)2) and derivatives thereof), clays, iron calcium aluminosilicates (i.e. omphacite (Ca, Na)(Mg, Fe2+, Al)Si2O6), quartz and possibly rutiled quartz, calcium silicates (Ca2SiO4) and variable salts (Na, Mg, and K based). FTIR and MA-XRF analysis confirms these findings. Elemental distribution maps of the cross-section 121A in **Figure 12** on page 26 demonstrate the relationships and likely mineral deposits discussed above.

Sample A

Figure 11. Images of sample 121A. The images above are taken under UV irradiation using DAPI illumination on the left and FITC illumination on the right (these are immunological stains). The images show the fibrous structure of the leather towards the top of the images. There does not appear to be significant elongation of the fibers. The lower region fluorescence is indicative of an oil impregnation.

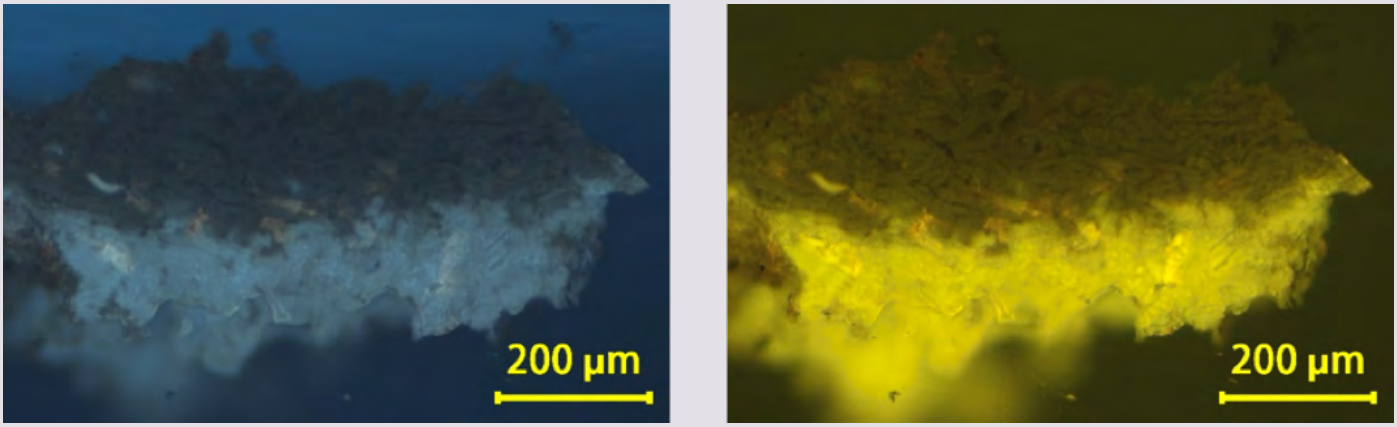

Figure 12. Elemental distribution map from Figure 10 showing a wide distribution of calcium and the relationship of the elements to each other. (Note that Al and Br overlap one another and are difficult to differentiate.)

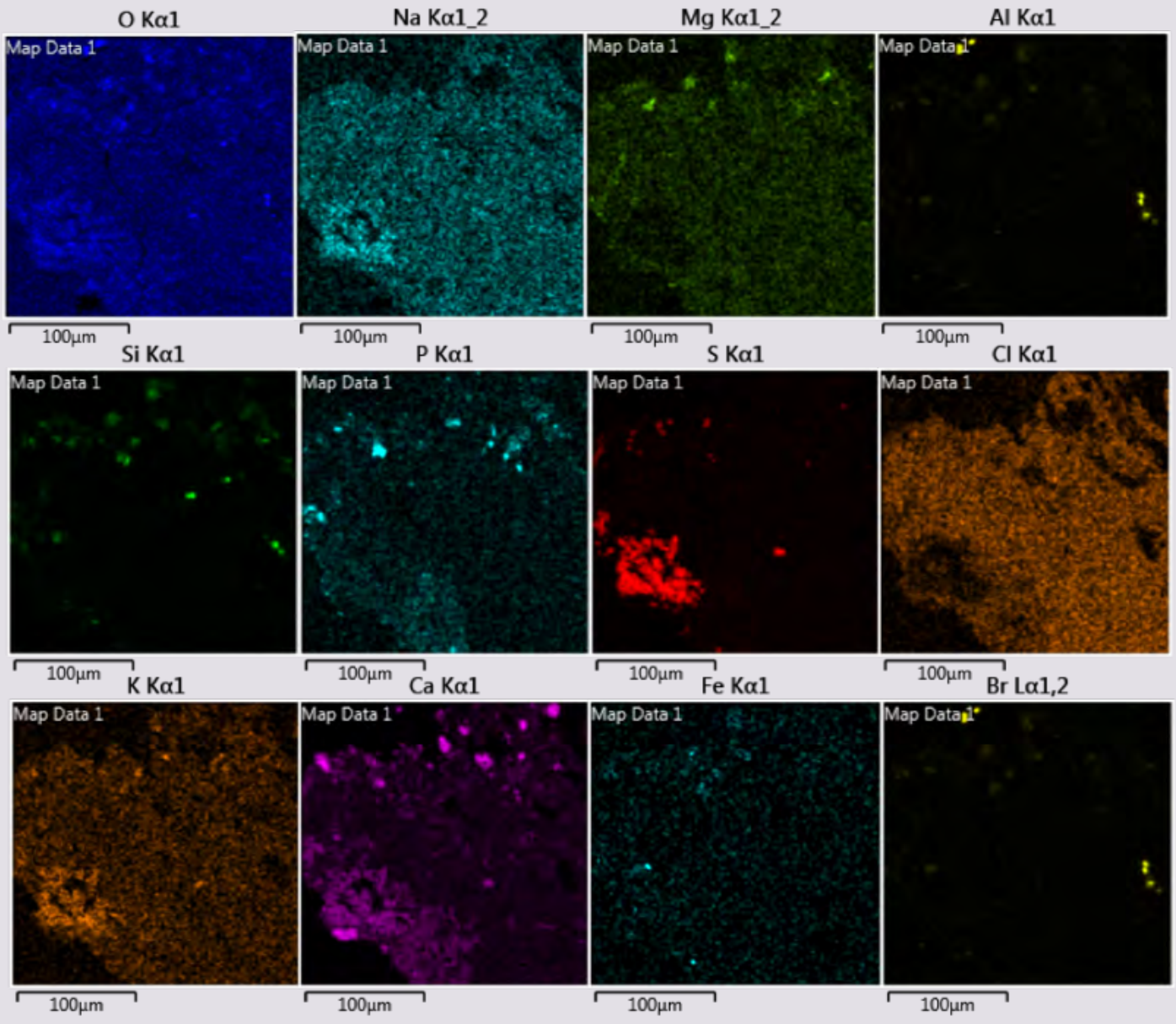

References:

[1] See Section IIA for a full discussion of this conclusion – the Ca in the fragments can come from many different sources related to the preparation and storage of the skins, but its distribution points to a lime depilation.

[2] All minerals detected by FTIR unless otherwise noted.

[3] Derrick, M. R. "Evaluation of the State of Degradation of Dead Sea Scroll Samples Using FT-IR-Spectroscopy." *Book and Paper Group Annual 10* (1991): 49-65; Arieh Singer, Eliezer Ganor, Stefan Dultz, and Walter Fischer, "Dust Deposition over the Dead Sea", *Journal of Arid Environments* (2003), 53:41-59.

[4] Arieh Singer, Eliezer Ganor, Stefan Dultz, and Walter Fischer, "Dust Deposition over the Dead Sea", *Journal of Arid Environments* (2003), 53:41-59.

[5] Poole, J. B, and R. Reed. "The Preparation of Leather and Parchment by the Dead Sea Scrolls Community." *Technology and Culture 3,* no. 1 (1962): 1-26.

[6] Maor, Y., Shor, P., and Aizenshtat, Z., "White Halos Surrounding the Dead Sea Scrolls", *Journal of Cultural Heritage,* 28 (2017) 90 – 98.

[7] Note that infrared spectroscopy does not distinguish between all phyllosilicate clays, and so best database matches are provided here (Infrared and Raman User's Group database). X-ray diffraction is required for definitive confirmation of clay mineral mixtures.

[8] Bicchieri, M., et al. "Microscopic Observations of Paper and Parchment: The Archaeology of Small Objects." *Heritage Science 7,* no. 1 (2019): 1-12; Pinzari, F., G. Pinar and Cialei, V. "A case study of ancient parchment biodeterioration using variable pressure and high vacuum scanning electron microscopy," in Meeks, Nigel, and British Museum. *Conservation Research Section. Historical Technology, Materials and Conservation : SEM and Microanalysis.* London: Archetype Publications, in Association with the British Museum, 2012.

[9] Vichi, A., et al. "Study of the Degradation and Conservation of Historical Leather Book Covers with Macro Attenuated Total Reflection-Fourier Transform Infrared Spectroscopic Imaging." *Acs Omega 3,* no. 7 (2018): 7150-157. 2018; Y. Maor, et al., White halos surrounding the Dead Sea scrolls, Journal of Cultural Heritage (2017), http://dx.doi.org/10.1016/j.culher.2017.06.003 (accessed August 29, 2019).

[10] MA-XRF data unless otherwise noted.

[11] Rabin, I., and O. Hahn. "Characterization of the Dead Sea Scrolls by Advanced Analytical Techniques." *Analytical Methods 5,* no. 18 (2013): 4648-654.

[12] In which aluminum, silicon, calcium, magnesium, iron, potassium, and sodium will all have positive correlations.

[13] Arieh Singer, Eliezer Ganor, Stefan Dultz, and Walter Fischer, "Dust Deposition over the Dead Sea", *Journal of Arid Environments* (2003), 53:41-59.

[14] R. A. Garber, A. Nishri, A. Nissenbaum, G.M. Friedman, "Modern deposition of manganese along the Dead Sea shore", *Sedimentary Geology,* 30(4), December 1981, 267 – 274.

Fragment Detail (Surface, Ink, Anomalies)

MOTB.SCR.000120 30
MOTB.SCR.000121 33
MOTB.SCR.000122 38
MOTB.SCR.000123 43
MOTB.SCR.000124 46
MOTB.SCR.003170 51
MOTB.SCR.003171 56
MOTB.SCR.003172 61
MOTB.SCR.003173 66
MOTB.SCR.003174 73
MOTB.SCR.003175 79
MOTB.SCR.003183 83
SIG.SCR.004742 90
SCR.0004741 & SCR.004768 96
SCR.004769 101

MOTB.SCR.000120 (Exodus)

Fragment No.	MOTB.SCR.000120
Text	Exodus
Inv Group	1
Notes	Biondi Exo 17

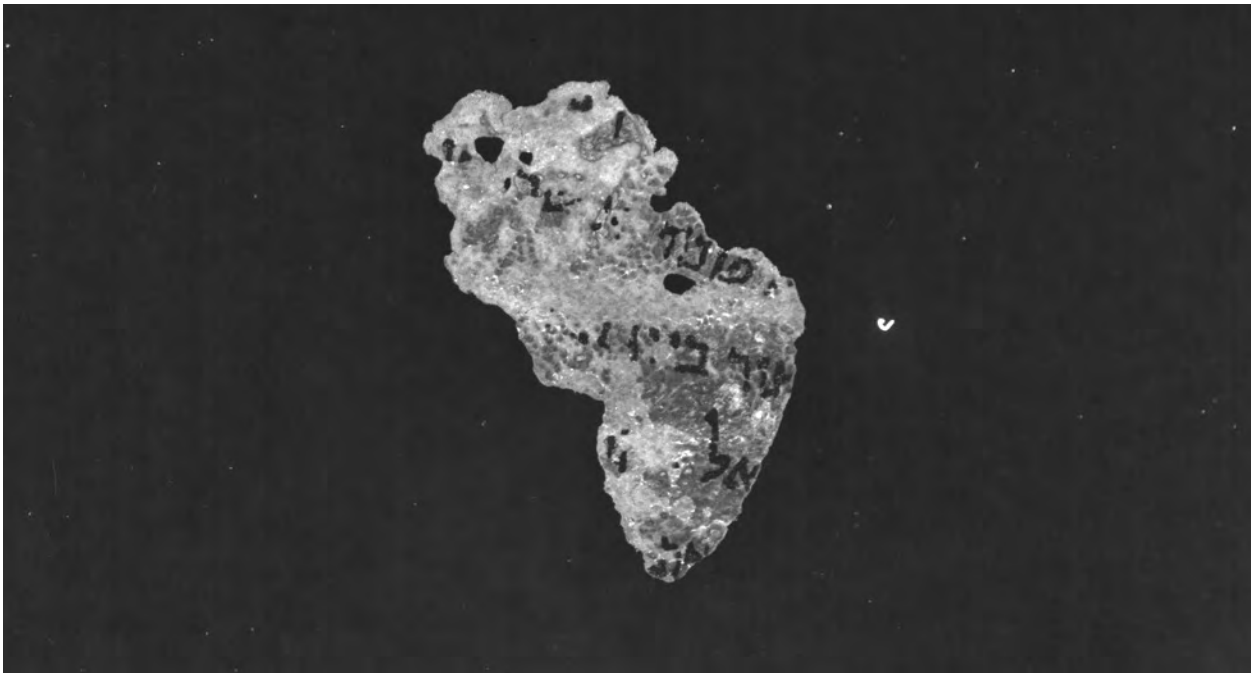

File Name:	MOTB.SCR.000120_001_PM_RL_20190424.tif (Micrograph) 1
Description:	Detail of top right section with very bumpy surface (raised grain); writing conforms to irregular edge of fragment and to areas where the grain layer is still intact.

File Name:	MOTB.SCR.000120_002_PM_RL_20190424.tif (Micrograph) 2
Description:	Detail of bottom edge, ink conforms to irregular shape of fragment, flows over edge, accretions also go over edge

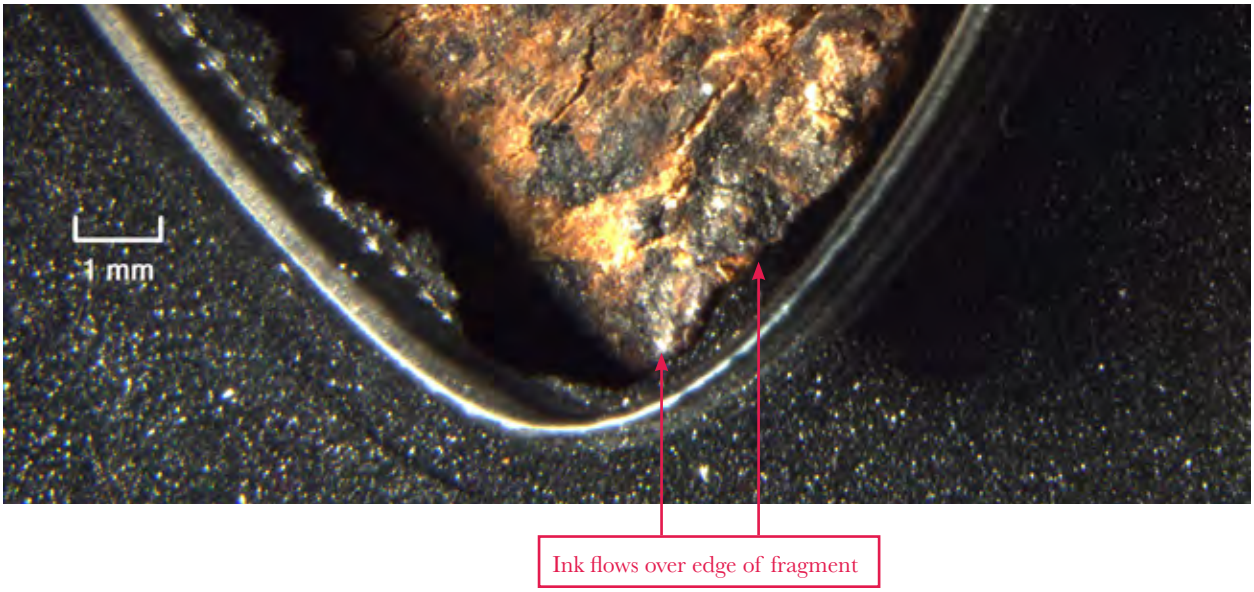

File Name:	MOTB.SCR.000120_002_PM_RL_20190424.tif (Micrograph) 3
Description:	Detail of right edge, just below center, long crack runs parallel to edge, ink and surface deposits flow across and into the crack at second and third lines of text

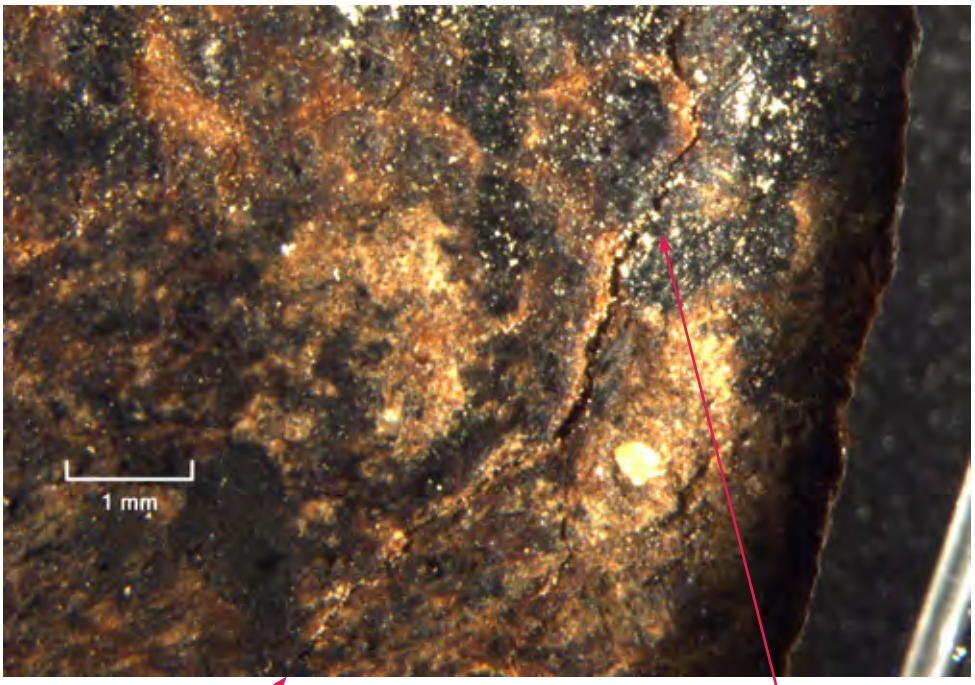

Long stroke of ink in third line of text extends across and into long crack

Ink flows across and into deep vertical crack

File Name:	MOTB.SCR.000120005.jpg (Hirox) 4
Description:	Ink applied on top of large, bulbous cream-colored accretion that projects out on the right

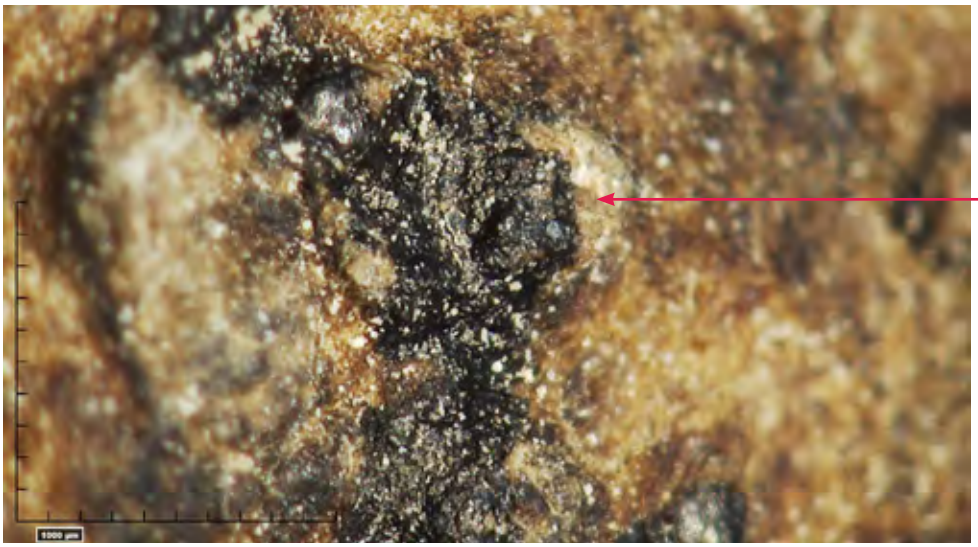

Bulbous cream-colored deposit is mostly covered by the ink

MOTB.SCR.000121 (Psalms)

Fragment No.	MOTB.SCR.000121
Text	Psalms
Inv Group	1
Notes	Biondi Psalm 11 Sampled

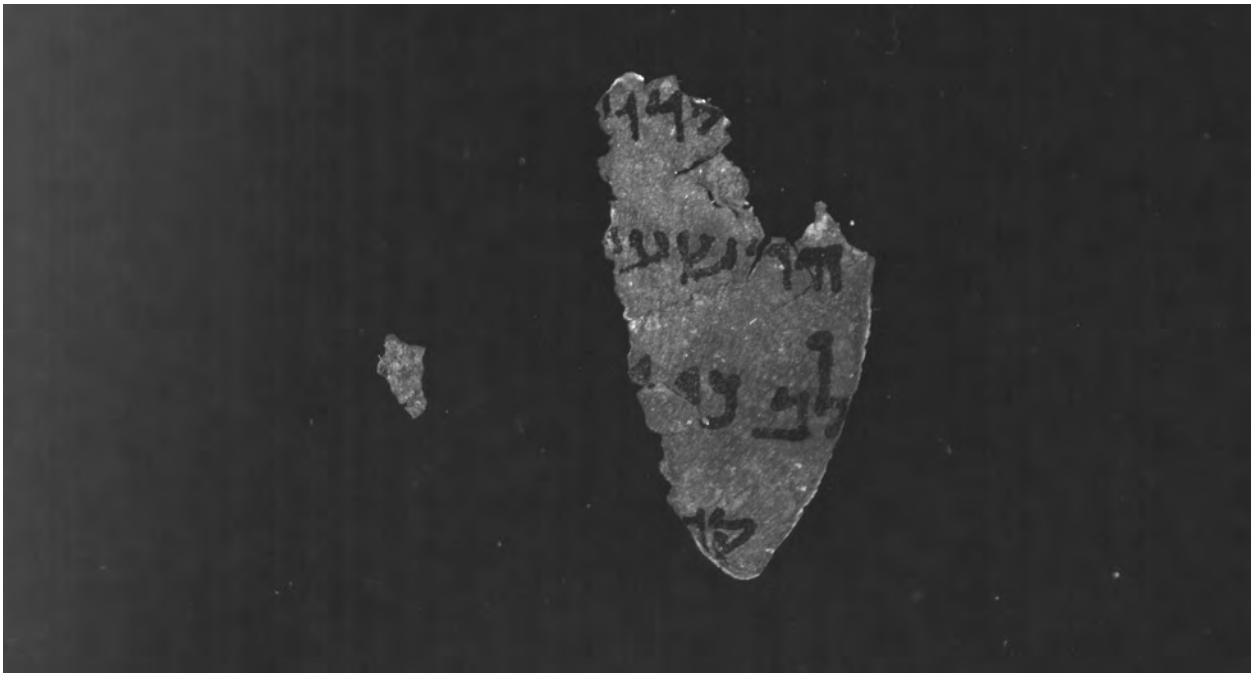

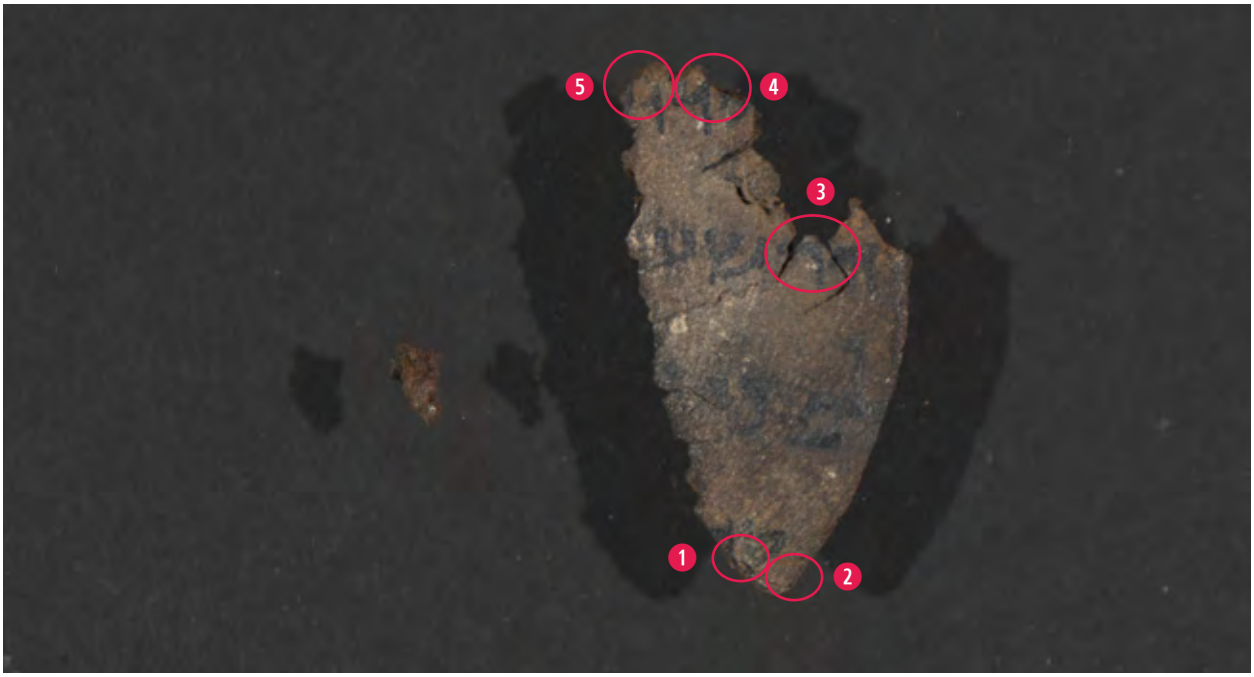

File Name:	MOTB.SCR.000121_001_PM_NL_20190424.tif (Micrograph)
Description:	Detail of bottom edge, ink flows across surface crack and over the edge

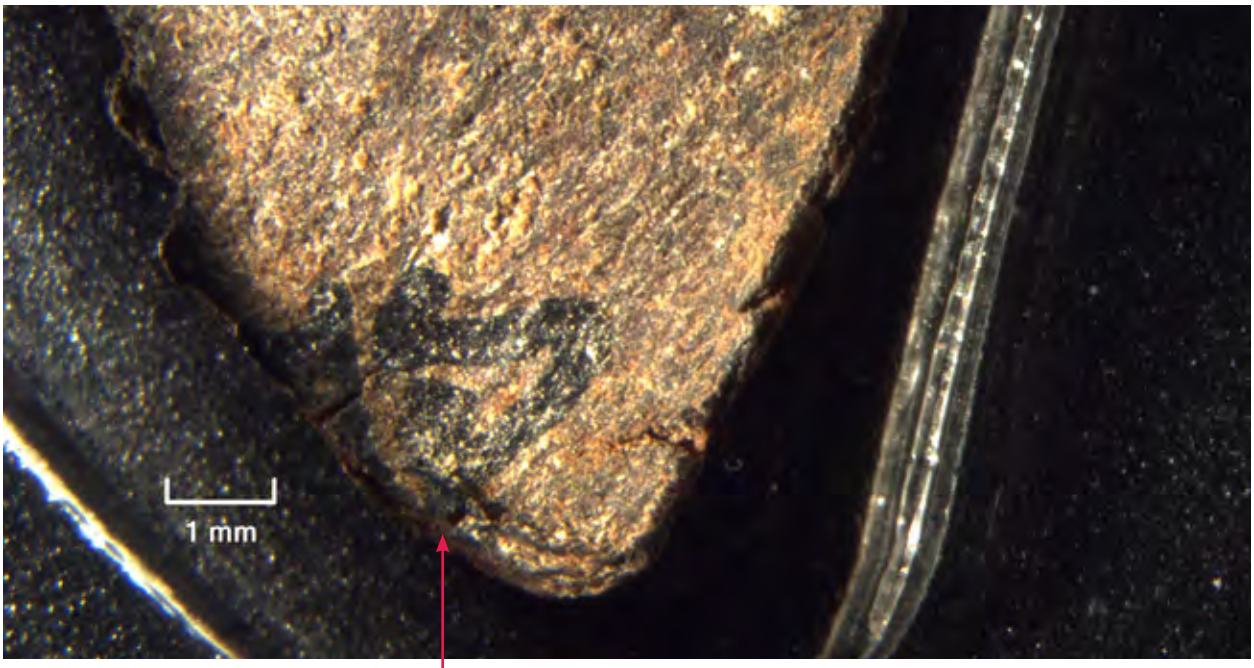

Ink flows over cracks and delaminated substrate at tip of fragment

File Name:	MOTB.SCR.000121005.jpg (Hirox) 1
Description:	Bottom edge with delamination of substrate and curling of thin grain layer, possibly due to heat exposure; fibers impregnated with amber-colored animal glue

Thin grain layer curled back, possibly due to heat exposure

Compacted fibers impregnated with amber glue

File Name:	MOTB.SCR.000121003.jpg (Hirox) 2
Description:	Ink on bottom tip of substrate goes across deep crack; shiny, transparent coating on top of ink, grain layer overhangs rest of substrate, which is very brittle and has broken off

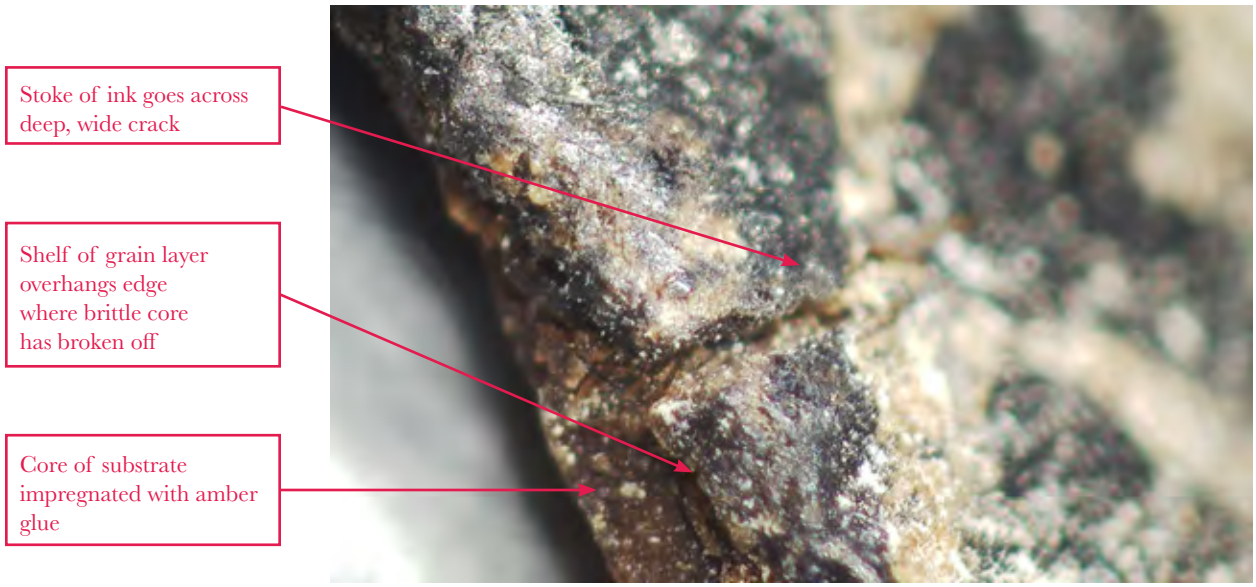

File Name:	MOTB.SCR.000121021.jpg (Hirox) 3
Description:	Top right edge, second line of text with deep cracks and hard edges indicating embrittlement of substrate. Letter in the center extends across and into crack at left. (Note: large L-shaped crack formed and pieces broke off top right corner after WSRP photos were taken.)

File Name:	MOTB.SCR.000121013.jpg (Hirox) 4
Description:	Top edge, left half, with ink flowing over broken/torn edge of substrate in center. Sharp edge of grain layer along break indicates extreme embrittlement of substrate. (Note: several pieces broke off right corner after WSRP photos were taken, with resulting loss of ink.)

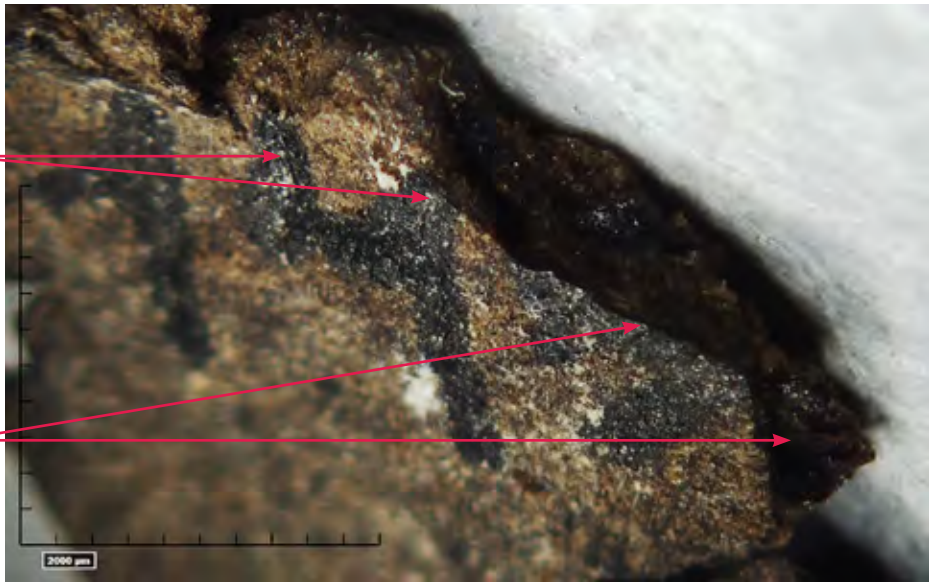

File Name:	MOTB.SCR.000121027.jpg (Hirox) 4
Description:	Ink waterfalling off broken, torn upper edge; white deposits on top of ink

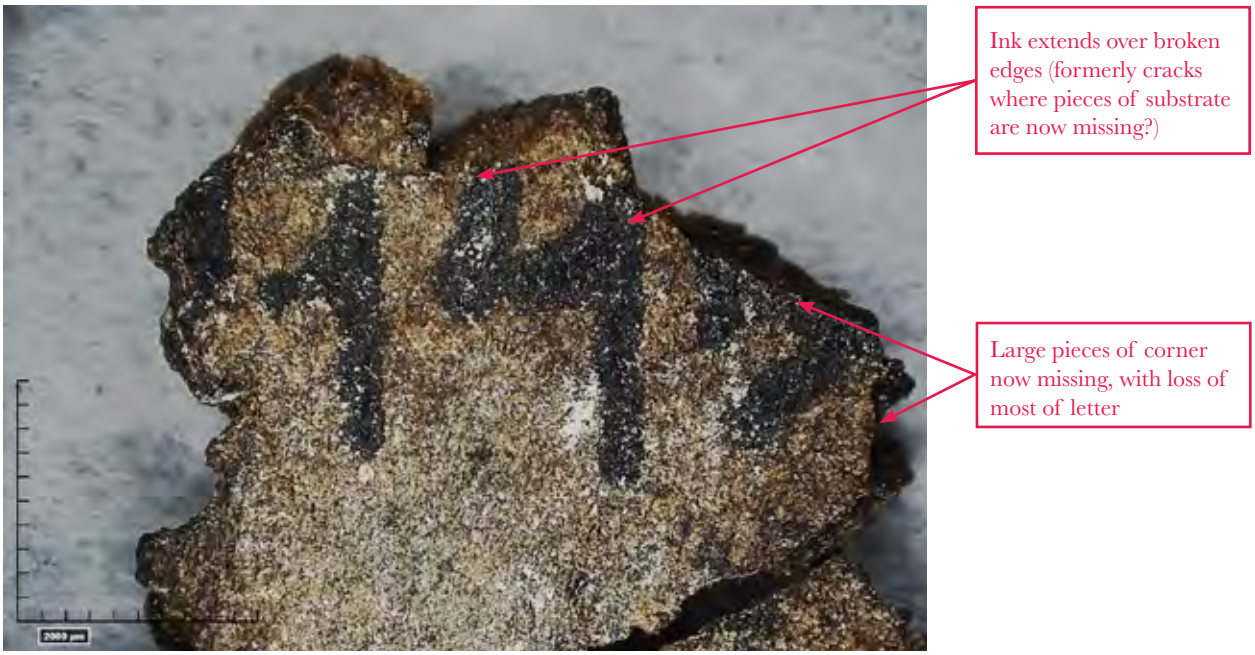

File Name:	MOTB.SCR.000121015.jpg (Hirox) 5
Description:	Top edge, left side, with sharp edge of grain layer along break, torn shelf of fibers below impregnated with thick, shiny animal glue

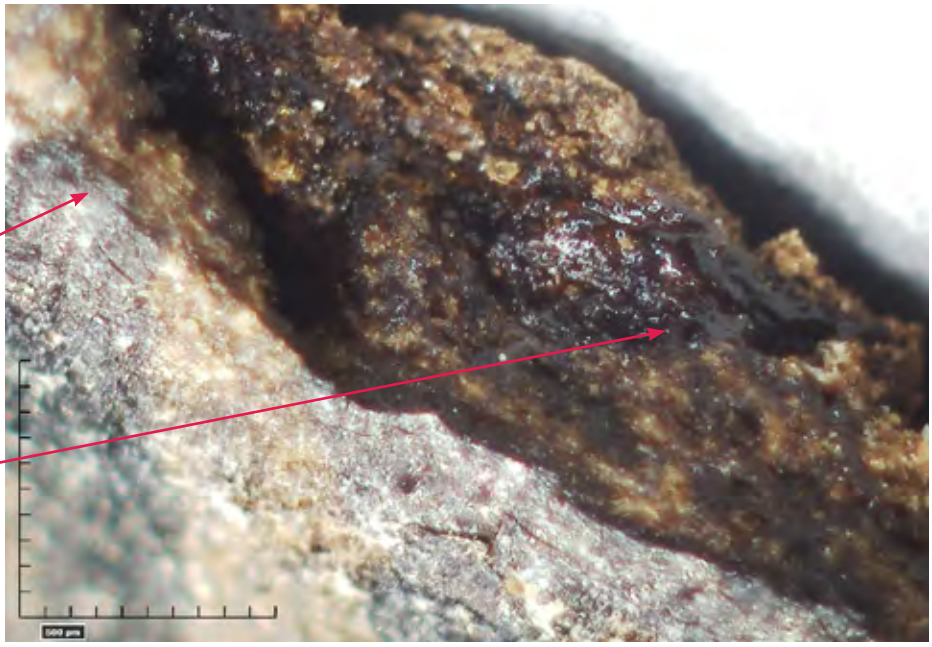

File Name:	MOTB.SCR.000121030.jpg (Hirox) 5
Description:	Top edge, left side, thick cream-colored deposit lies on top of ink at right

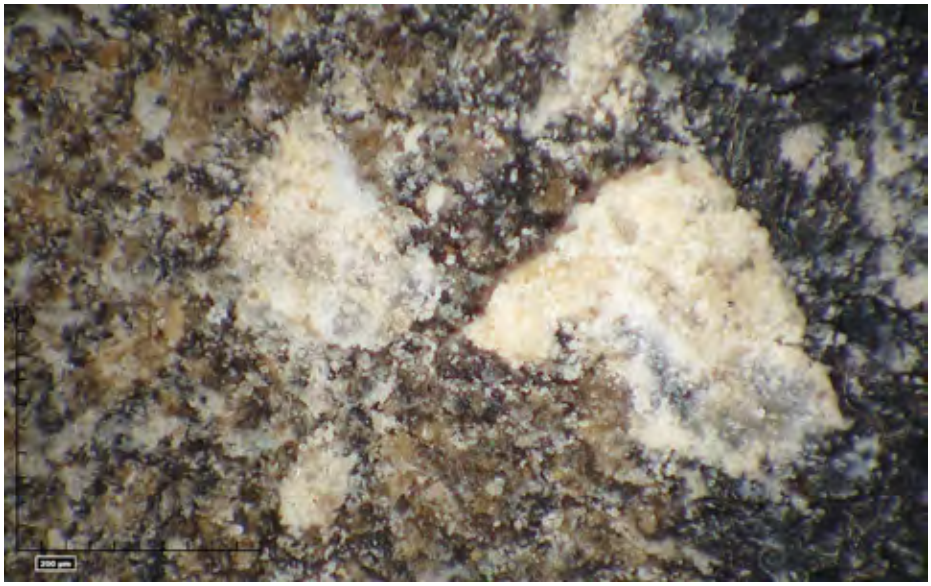

MOTB.SCR.000122 (Leviticus?)

Fragment No.	MOTB.SCR.000122
Text	Leviticus?
Inv Group	1
Notes	Biondi Q4418

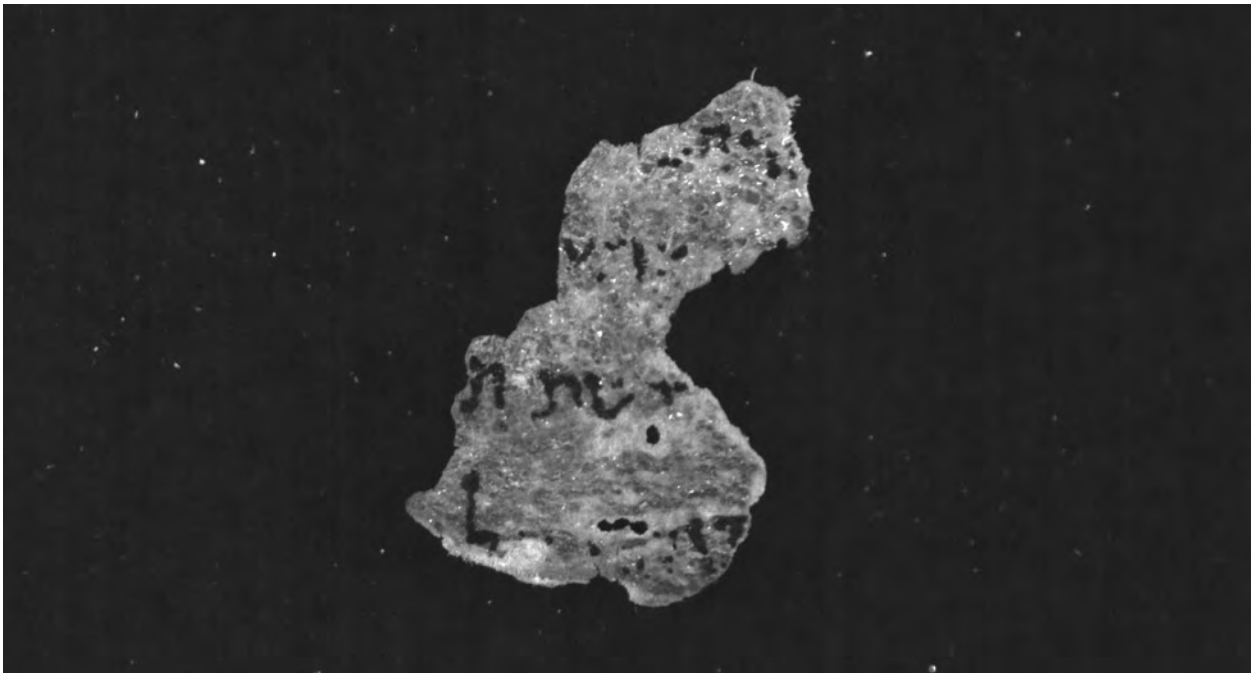

File Name:	MOTB.SCR.000122_002_PM_RL_20190424.tif (Micrograph) 1
Description:	Detail of top right edge, ink appears to skip across high points of grain layer as scribe attempted to write first line of text

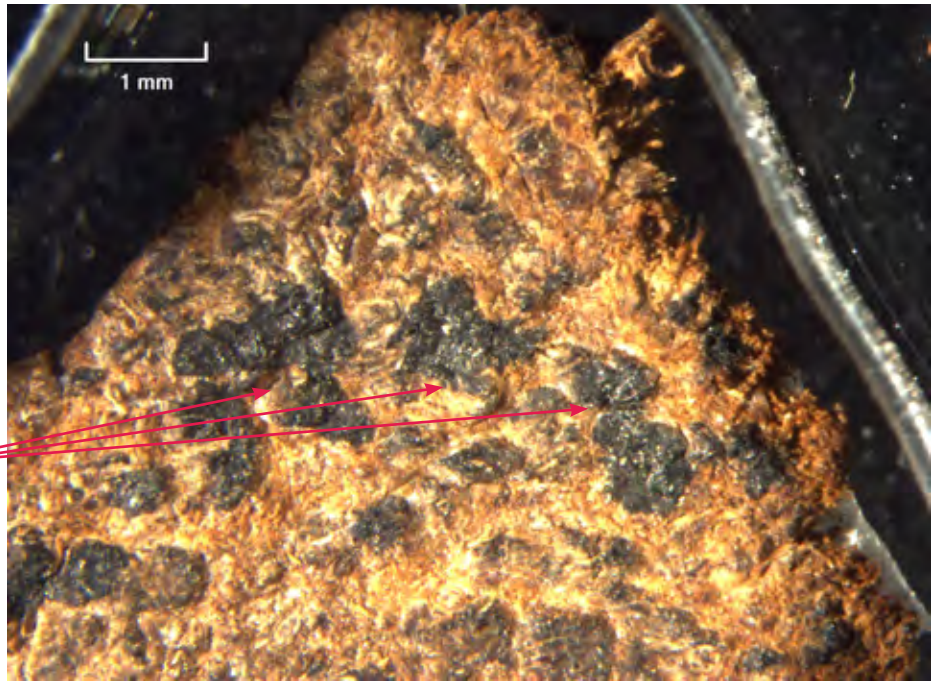

Ink of first line of text deposited only on high points of very textured grain layer

File Name:	MOTB.SCR.000122_003_PM_RL_20190424.tif (Micrograph) 2
Description:	Detail of bottom left edge, left of center, detail of fibers at torn, frayed edge saturated with resinous amber material (animal glue)

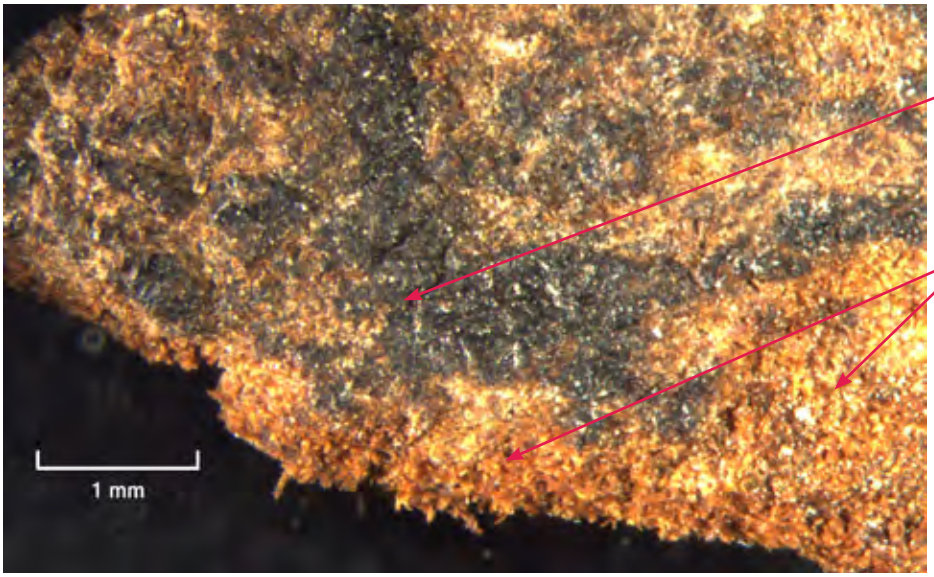

"Lamed" extends to edge of intact grain layer

Fibrous core of skin exposed in area of grain loss is impregnated with amber glue

File Name:	MOTB.SCR.000122001.jpg (Hirox) 2
Description:	Larger view of bottom left edge, loss of grain layer to right of center has exposed fibrous core of skin impregnated and compacted with amber glue

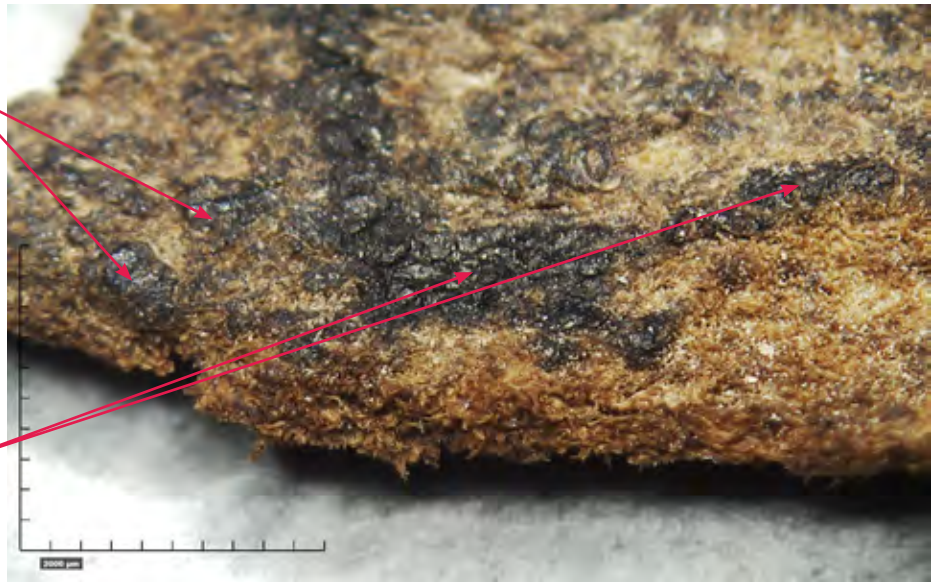

File Name:	MOTB.SCR.000122_001_PM_NL_20190424.tif (Micrograph) 3
Description:	Third line of text at left edge; ink flows across and into vertical crack; left edge of island coated with dark amber glue

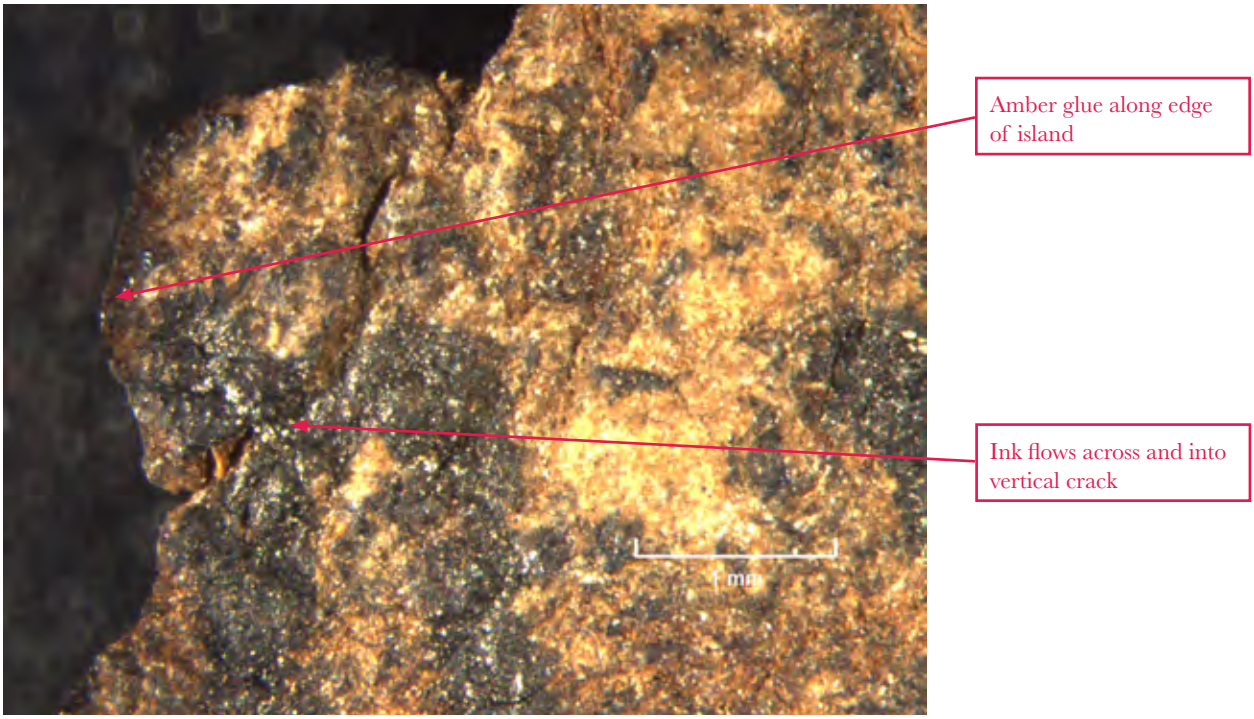

File Name:	MOTB.SCR.000122010.jpg (Hirox) 3
Description:	Detail of left edge with vertical crack (third line of text), ink flows across and into deep crack, mineral deposits scattered over ink and into crack

File Name:	MOTB.SCR.000122/3dimage_0011.jpg (3D Hirox) 3
Description:	3D image of vertical crack at left edge (third line of text) showing ink falling into deep crack

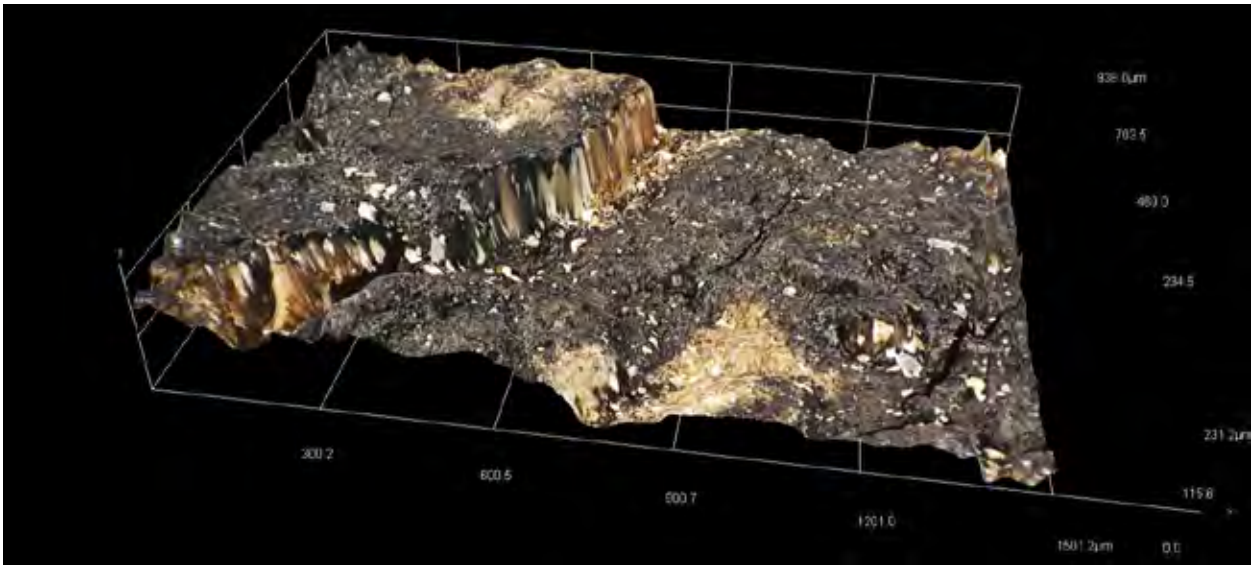

File Name:	MOTB.SCR.000122006.jpg (Hirox) 4
Description:	Ink of second line of text falls over left edge of fragment; shiny, thick black ink contrasts with highly textured grain layer which is dark from oxidation

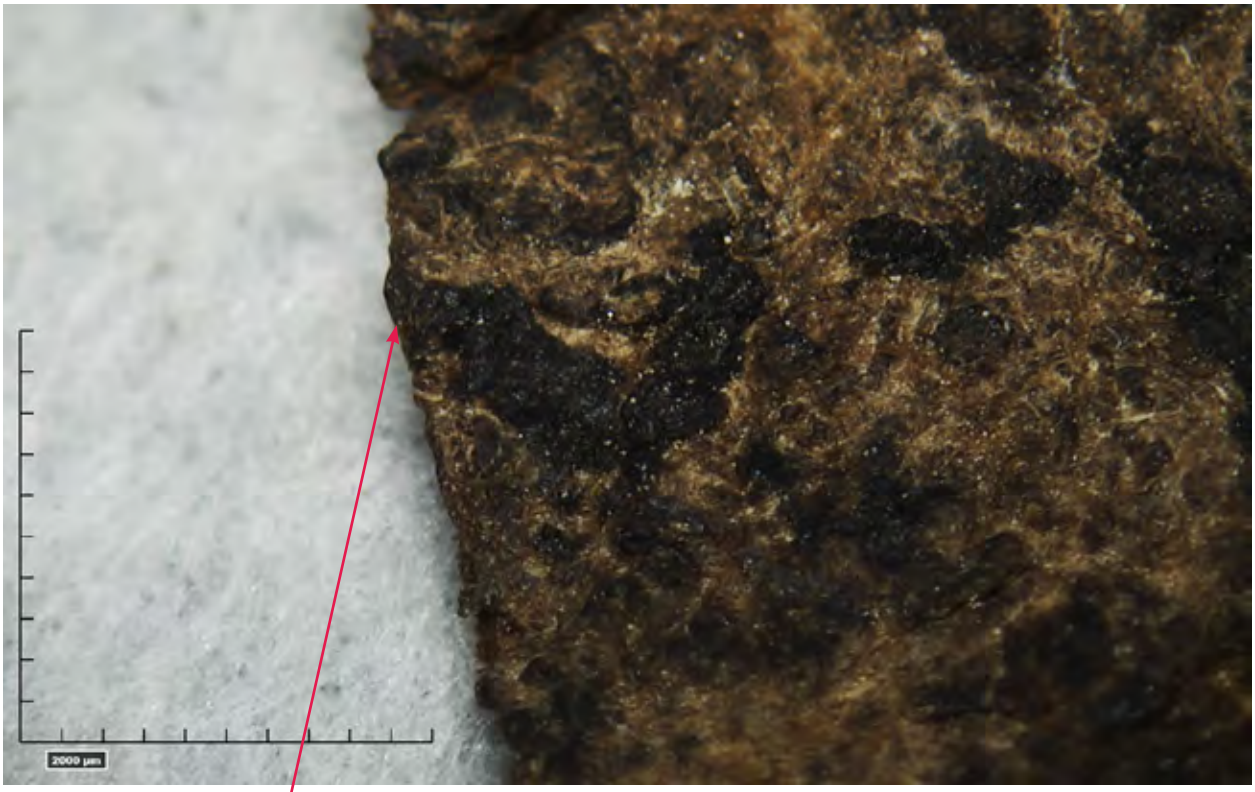

MOTB.SCR.000123 (Instruction)

Fragment No.	MOTB.SCR.000123
Text	Instruction
Inv Group	1
Notes	

File Name:	MOTB.SCR.000123_001_PM_RL_20190424.tif (Micrograph) 1
Description:	Detail of left side, faint diagonal striations seen in raking light may be from a brush-applied acrylic coating (the latter was identified with FITR)

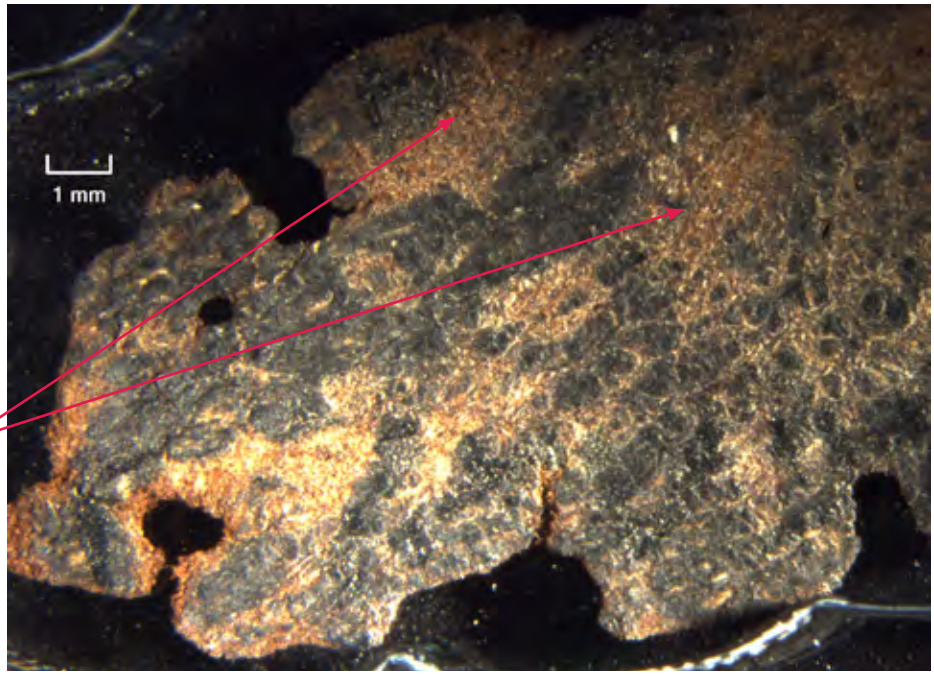

Diagonal striations across surface may be from application of a transparent coating

File Name:	MOTB.SCR.000123010.jpg (Hirox) 1
Description:	Top edge, left side, showing grain layer blackened from oxidation; lighter areas at far left are where grain is missing; perimeter of hole impregnated with dark amber glue

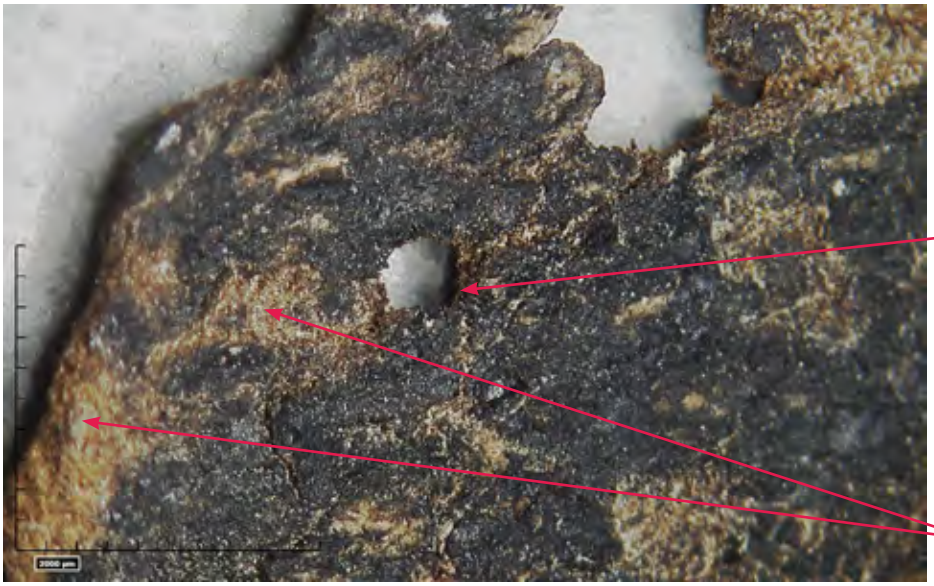

Fibers around perimeter of hole impregnated with amber glue

Lighter brown areas are core of skin where grain is missing

File Name:	MOTB.SCR.000123_002_PM_NL_20190424.tif (Micrograph) 2
Description:	Detail of top left edge, left of center, ink on top of surface deposits, edge saturated with resinous amber material

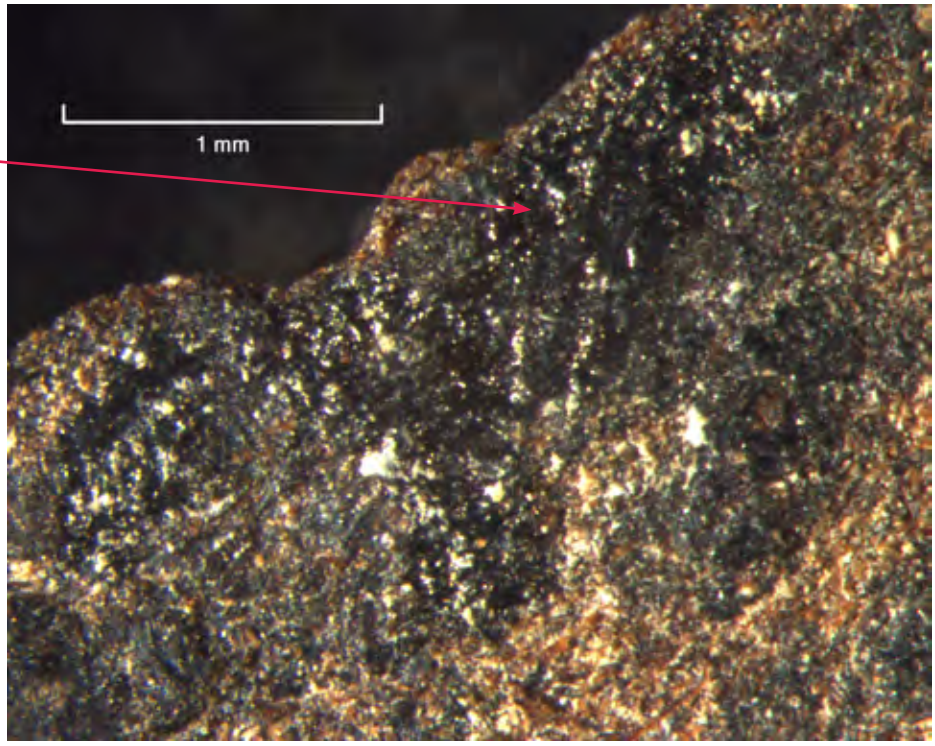

File Name:	MOTB.SCR.000123002.jpg (Hirox) 2
Description:	Shiny, viscous ink sits proud of surface because it lies on top of granular deposits

MOTB.SCR.000124 (Genesis)

Fragment No.	MOTB.SCR.000124
Text	Genesis
Inv Group	2
Notes	Included in BAM Report Sampled

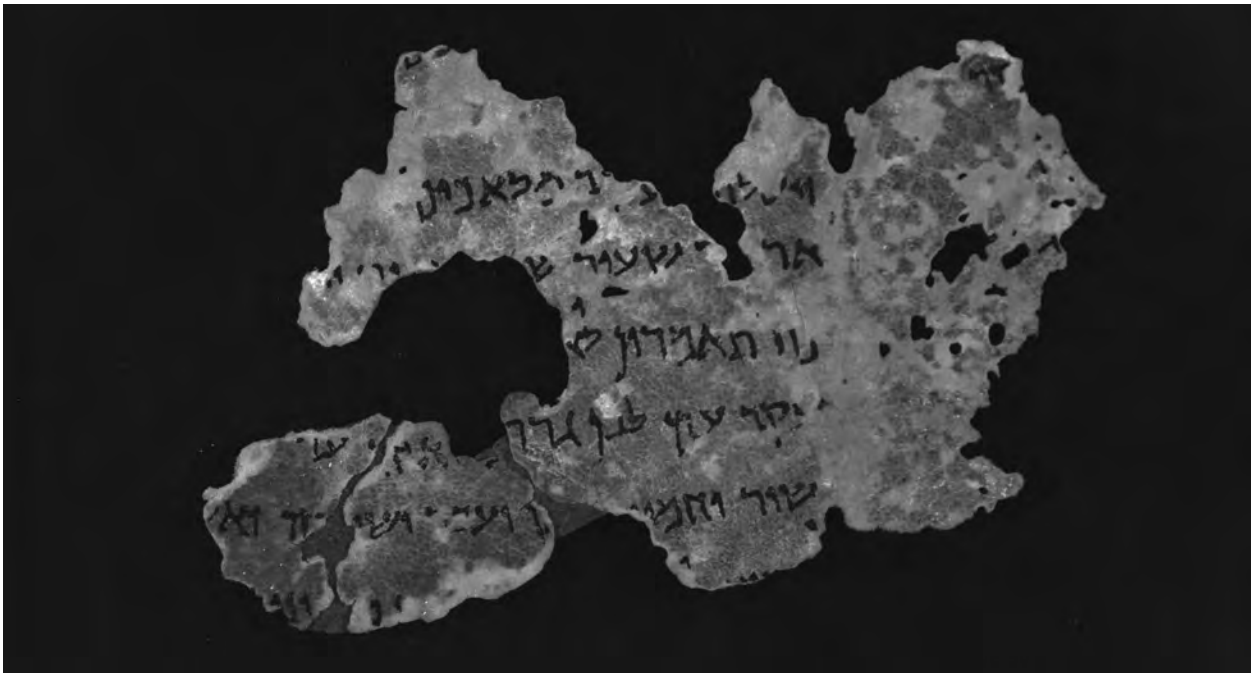

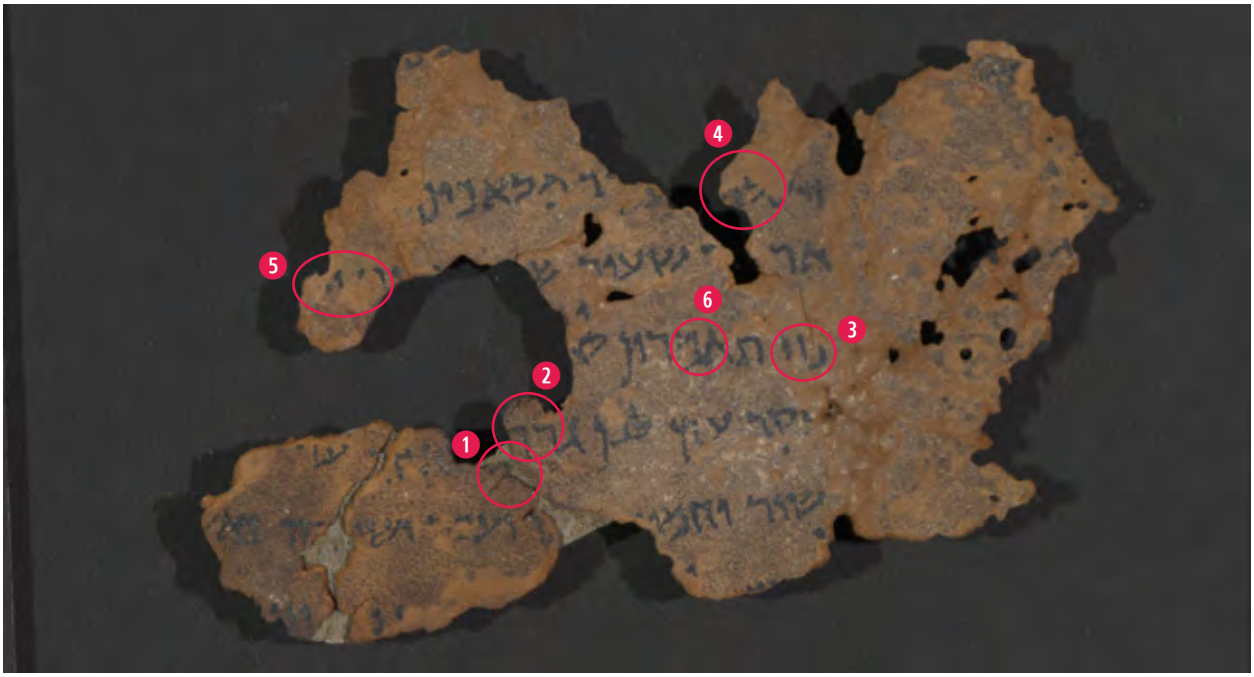

File Name:	MOTB.SCR.000124_001_PM_NL_20190424.tif (Micrograph) 1
Description:	Detail of tissue paper repair connecting two fragment pieces, shiny amber glue pooling in deep surface crack; thicker, darker glue deposits along the edge of lower piece.

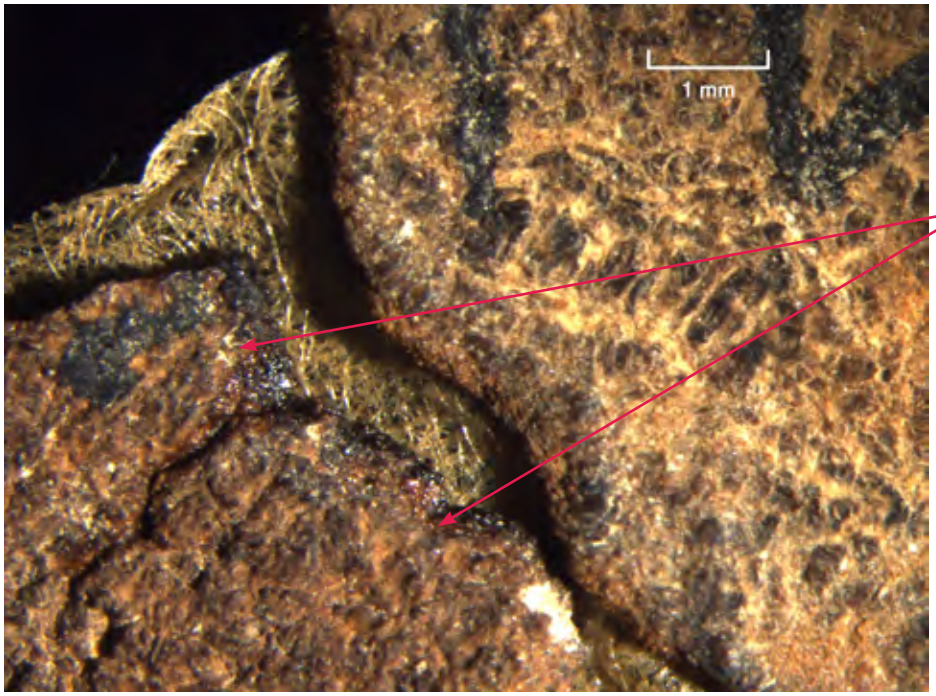

File Name:	MOTB.SCR.000124_002_PM_NL_20190424.tif (Micrograph) 2
Description:	Detail of center section, left edge, just below center, where ink flows across crack; to the right, large loss in grain layer is continuous with the crack at the left.

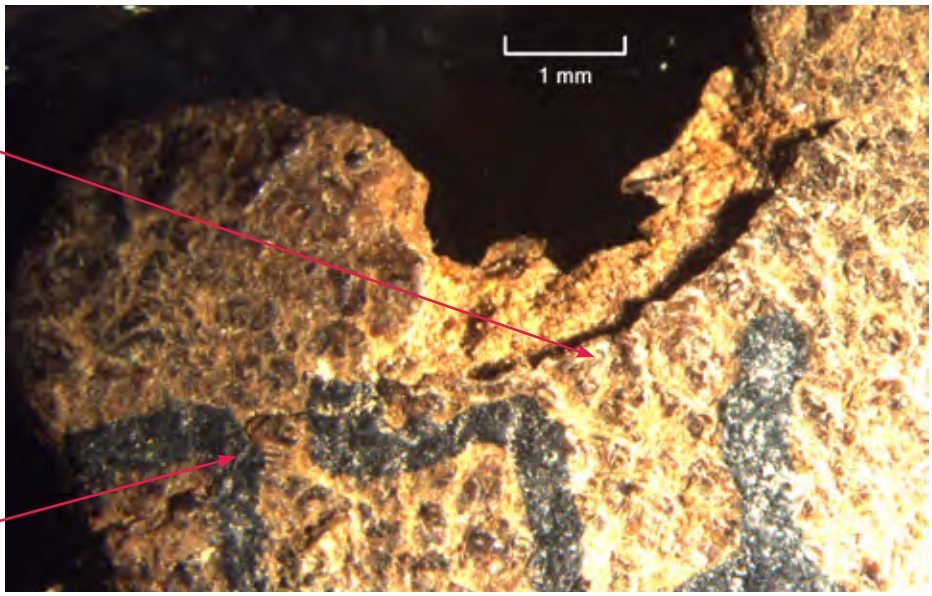

File Name:	MOTB.SCR.000124_005_PM_RL_20190424.tif (Micrograph) 3
Description:	Detail of middle of center section, ink at the right flows across flap in leather on to areas of grain loss

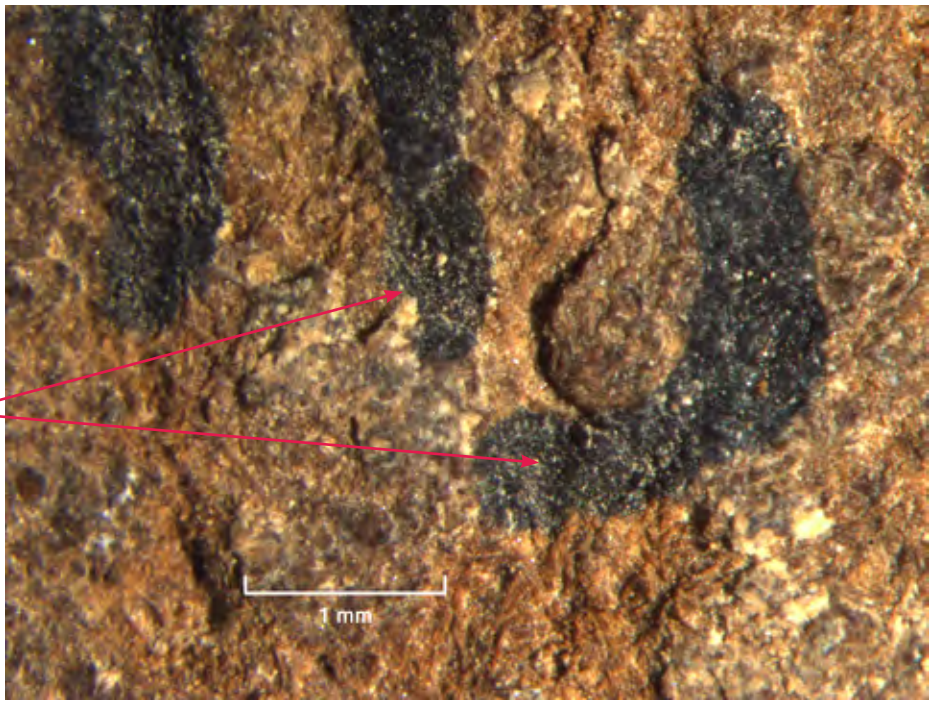

File Name:	MOTB.SCR.000124/MOTB.SCR.000124013.jpg (Hirox) 1
Description:	Ink passes over the abraded and torn edge that is coated with glue, powdery white deposits on top of ink and in grain recesses

File Name:	MOTB.SCR.000124/MOTB.SCR.000124010.jpg (Hirox) 4
Description:	Upper portion of the largest piece, to right of center, where some ink on darker intact grain layer extends on to delaminated areas, which are lower than the grain layer and more fibrous and uniform in appearance

File Name:	MOTB.SCR.000124008.jpg (Hirox) 4
Description:	Detail of image 5a, showing ink extending to the right over edge of grain layer and on to an area of delamination (ink appears thinner and slightly translucent here)

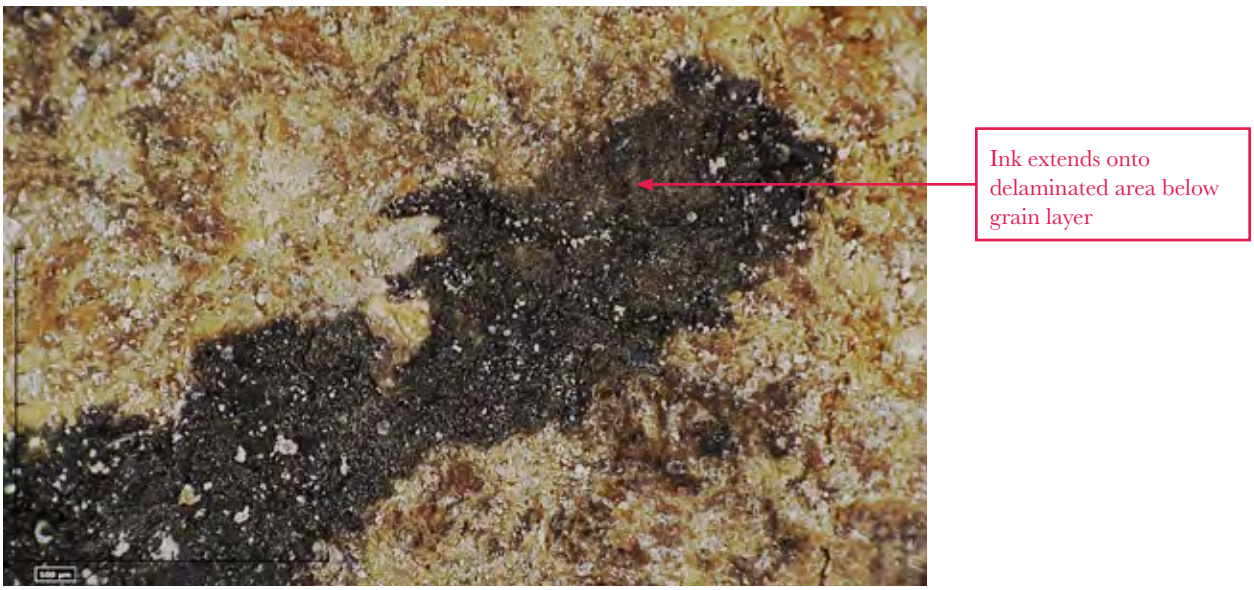

File Name:	MOTB.SCR.000124/MOTB.SCR.000124007.jpg (Hirox) 5
Description:	Upper portion of largest piece to left of center. Stroke of ink extends to the right on to an area where darker brown grain layer is missing.

File Name:	MOTB.SCR.000124/MOTB.SCR.000124028.jpg (Hirox) 6
Description:	Detail of thick, shiny ink that appears lumpy due to having been applied over granular deposits.

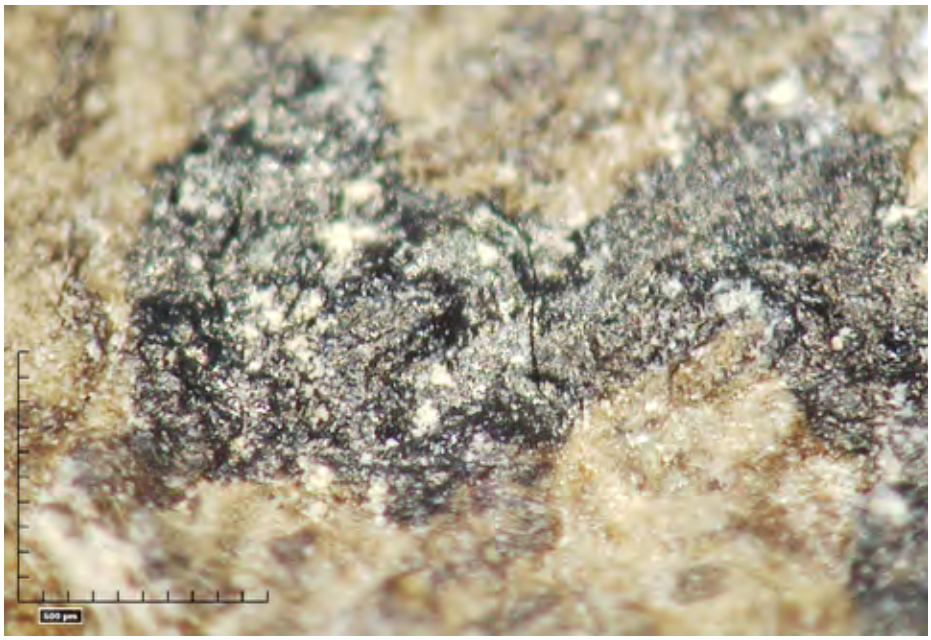

MOTB.SCR.003170 (Daniel)

Fragment No.	MOTB.SCR.003170
Text	Daniel
Inv Group	3
Notes	New MSI images forthcoming

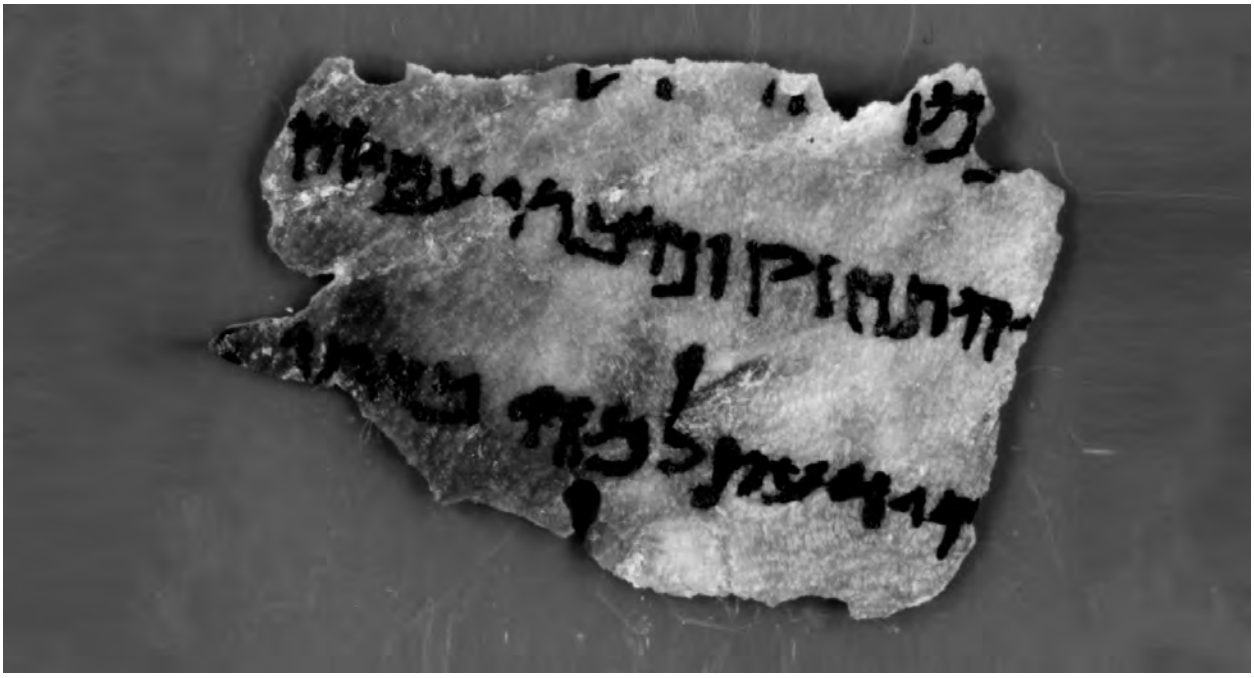

File Name:	MOTB.SCR.003170_002_PM_NL.tif (Micrograph) 1
Description:	Detail of top edge, right of center, where the ink passes over an area of damage. Blackened deteriorated grain layer has worn away along the upper edge.

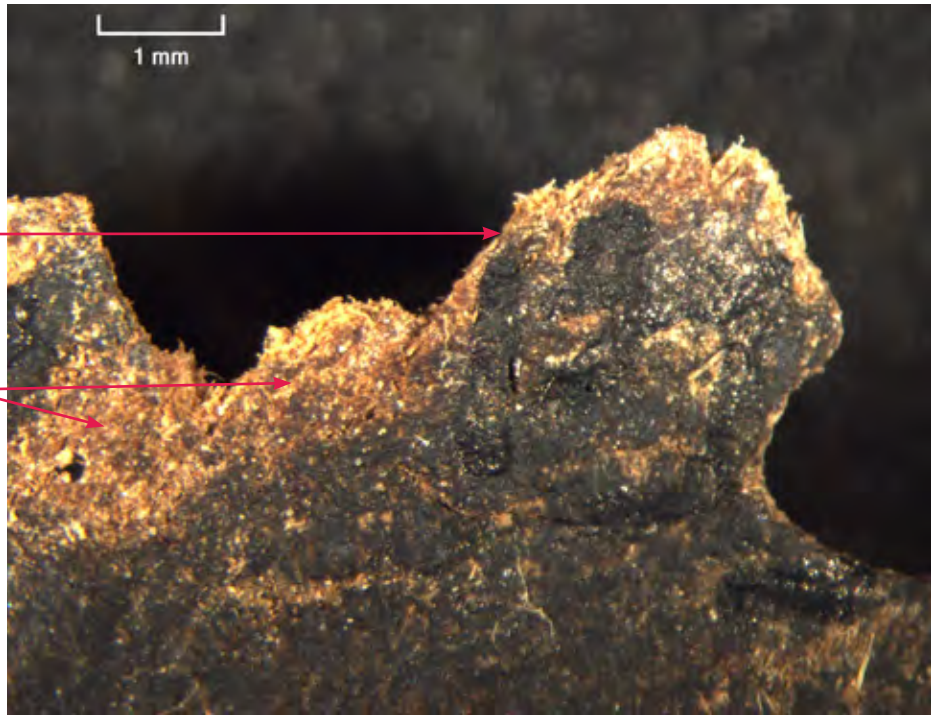

File Name:	MOTB.SCR.003170006 (MOTB.SCR.000124029).jpg
Description:	Detail of right edge of the fragment, with a series of deep, irregular cracks and ink at far right that falls over worn edge

File Name:	MOTB.SCR.003170/MOTB.SCR.003170004.jpg (Hirox) 2
Description:	Detail of right edge where ink goes across a diagonal crack and falls over worn edge; thick cream deposits on top of ink.

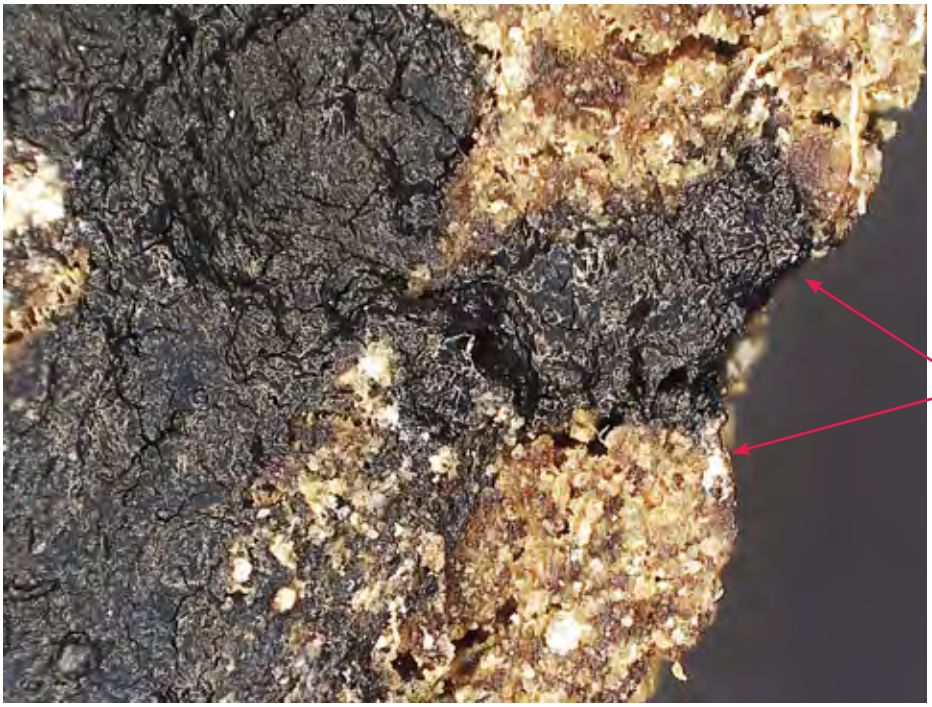

File Name:	MOTB.SCR.003170011 (MOTB.SCR.000124034).jpg 3
Description:	Bottom edge to the left of a large hole, showing sharp edge of brittle grain layer that has broken off

File Name:	MOTB.SCR.003170010 (MOTB.SCR.000124033).jpg (Hirox) 3
Description:	Closer detail of broken bottom edge to left of center, showing shelf of dark glue-impregnated fibers projecting out beyond missing grain layer.

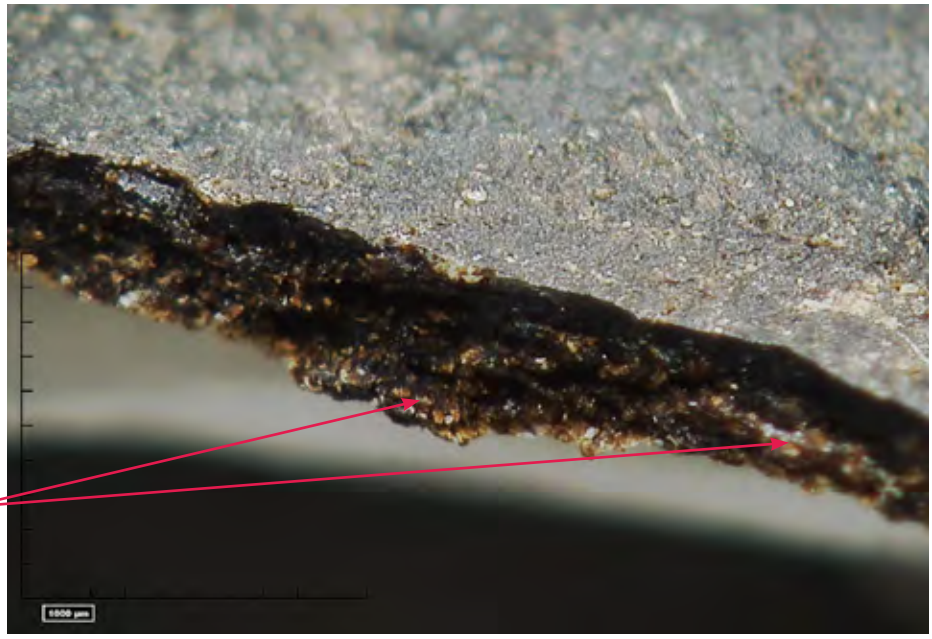

File Name:	MOTB.SCR.003170019 (MOTB.SCR.000124042).jpg (Hirox) 4
Description:	Second line of text at center (letter "qof) showing ink applied over deteriorated grain surface that is full of wide parallel cracks

File Name:	MOTB.SCR.003170/3dimage_0015.jpg (3D Hirox) 4
Description:	3D image of 5b showing very rough surface of substrate to which ink was applied

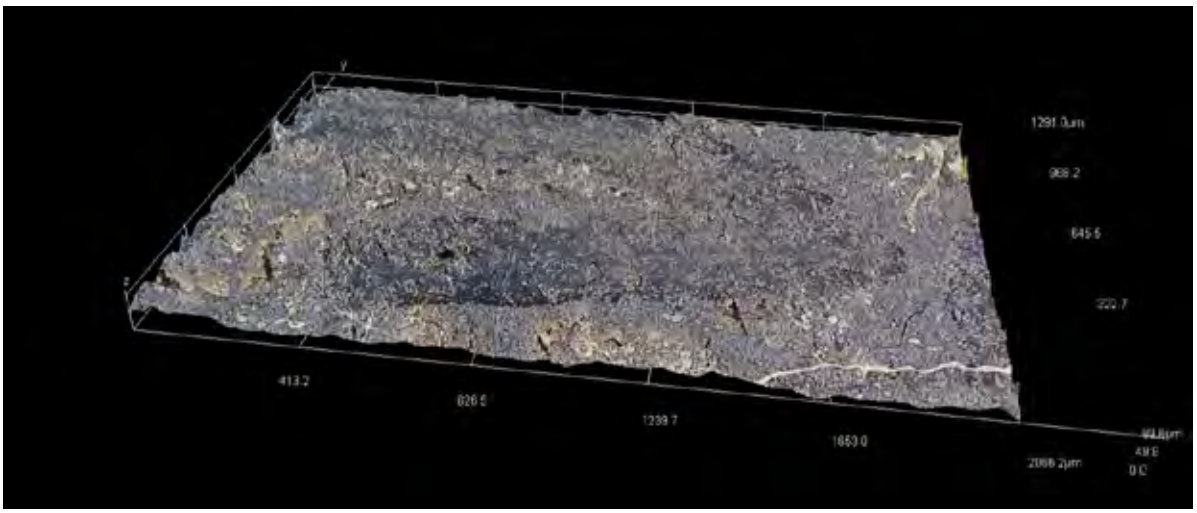

File Name:	MOTB.SCR.003170/3dimage_0006.jpg (3D Hirox) 5
Description:	3D map at end of second line of text, where ink extends to the left across grain loss

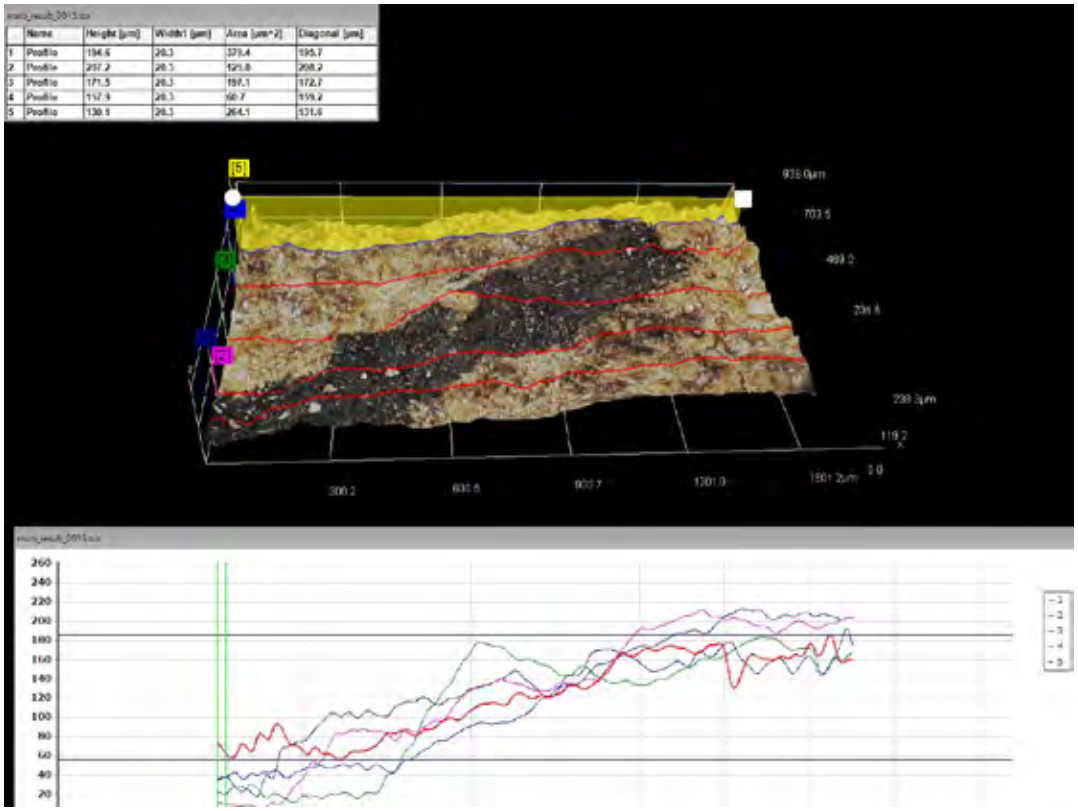

MOTB.SCR.003171 (Jonah)

Fragment No.	MOTB.SCR.003171
Text	Jonah
Inv Group	3
Notes	Included in BAM Report

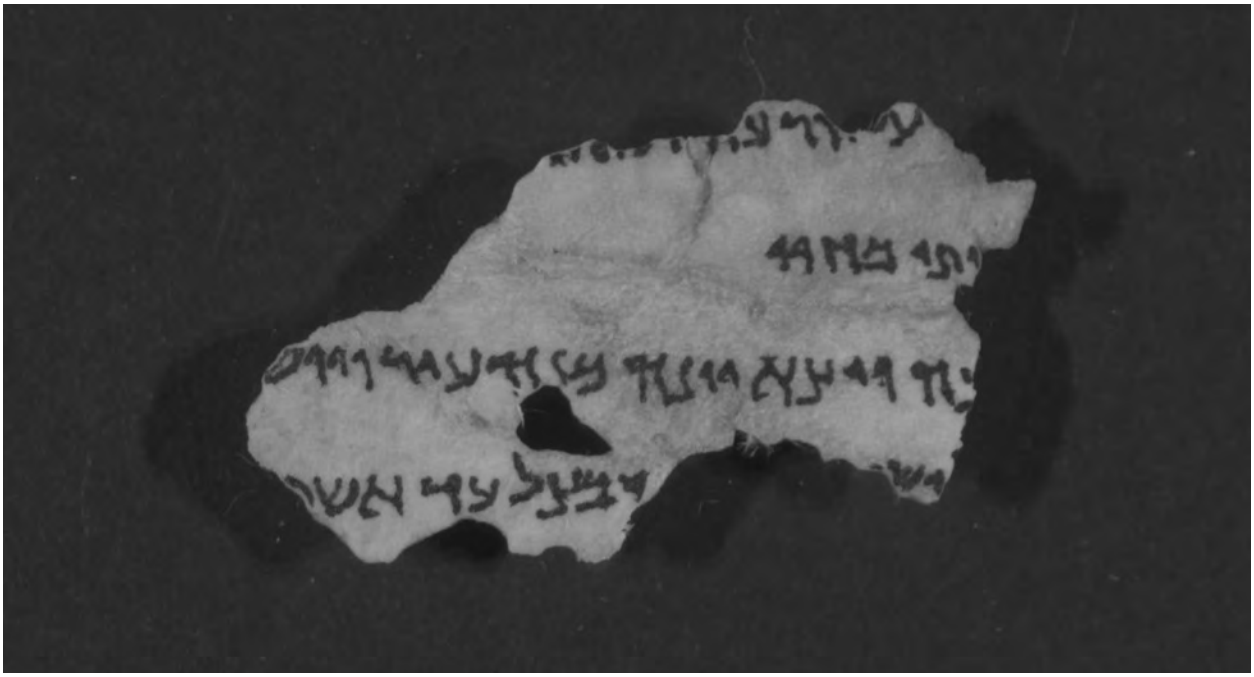

File Name:	MOTB.SCR.003171_001_PM_NL_20190424.tif (Micrograph) 1
Description:	Detail of upper right edge, ink falling over stepped down edge

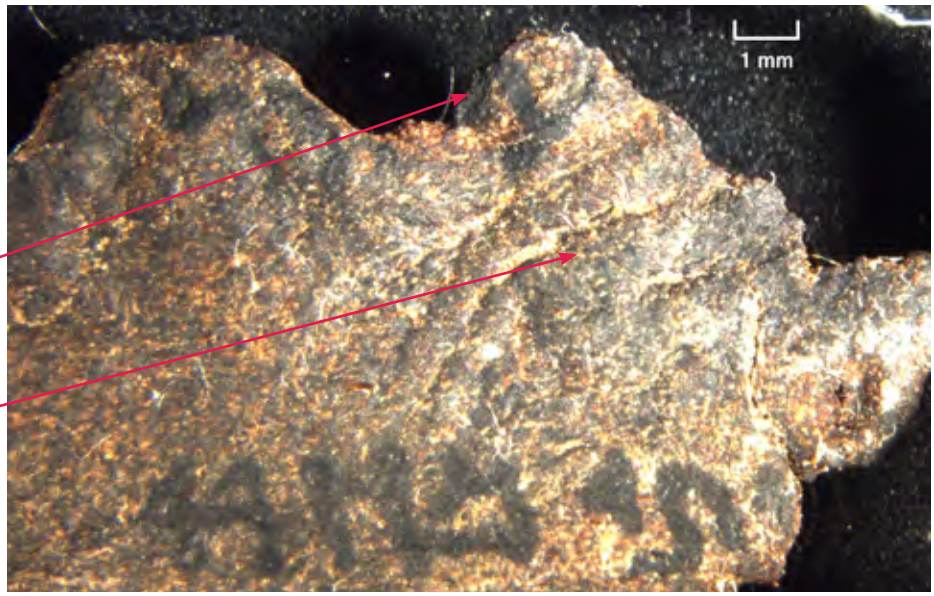

File Name:	MOTB.SCR.003171_003_PM_NL_20190424.tif (Micrograph) 2
Description:	Detail of feathering of ink, lower quadrant, left of center

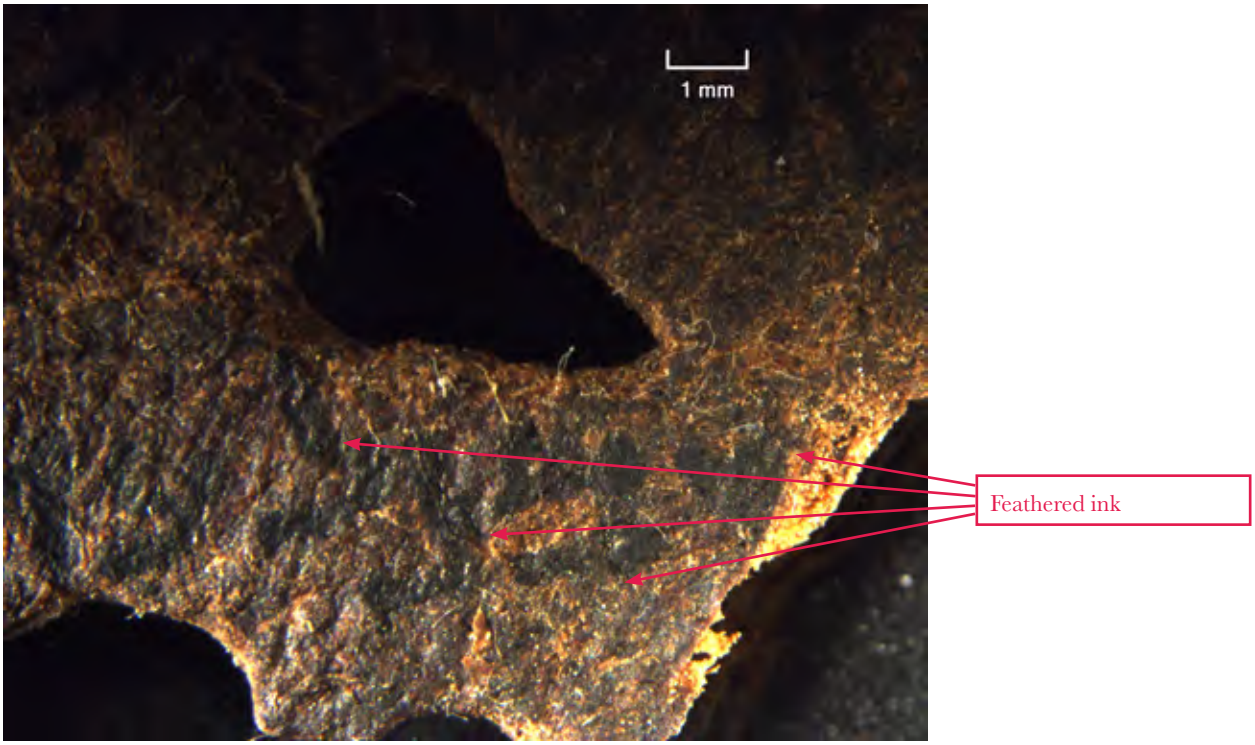

File Name:	MOTB.SCR.003171001.jpg (Hirox) 3
Description:	Detail of top edge, center, large crack with ink and dark amber glue pooling in crack. Follicle pattern more visible due to abrasion of oxidized grain layer.

File Name:	MOTB.SCR.003171/MOTB.SCR.003171002.jpg (Hirox) 3
Description:	Closer detail of top edge, center, large crack with ink and resinous material pooling in crack.

File Name:	MOTB.SCR.003171/MOTB.SCR.003171016.jpg (Hirox) 4
Description:	Bottom edge, far right corner, with ink falling over edge; thin white deposits lie on top of ink

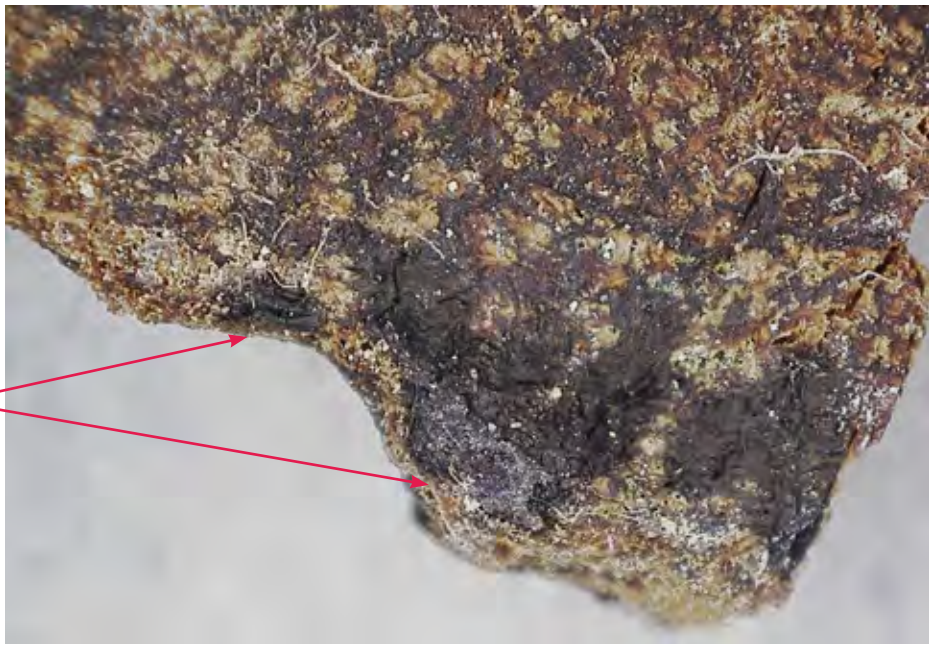

File Name:	MOTB.SCR.003171/MOTB.SCR.003171008.jpg (Hirox) 5
Description:	Third line of text above large hole showing missing grain and compressed fibers around perimeter of hole (white tissue is from hinge on the reverse).

File Name:	MOTB.SCR.003171/MOTB.SCR.003171014.jpg (stitched Hirox, horizontal) 6
Description:	Stitched image of incised ruling line that extends from left to right edge of fragment.

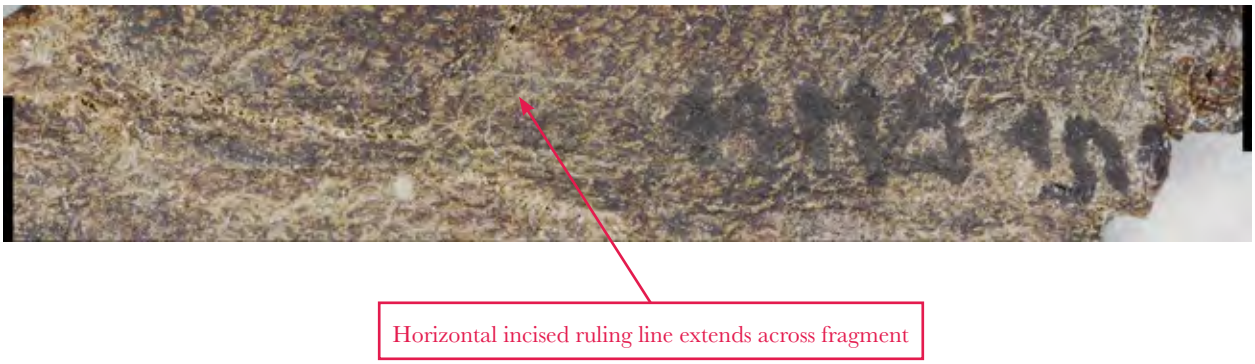

File Name:	MOTB.SCR.003171/MOTB.SCR.003171018.jpg (Hirox) 6
Description:	Stitched image of incised ruling line with green marking the outer edges of the line.

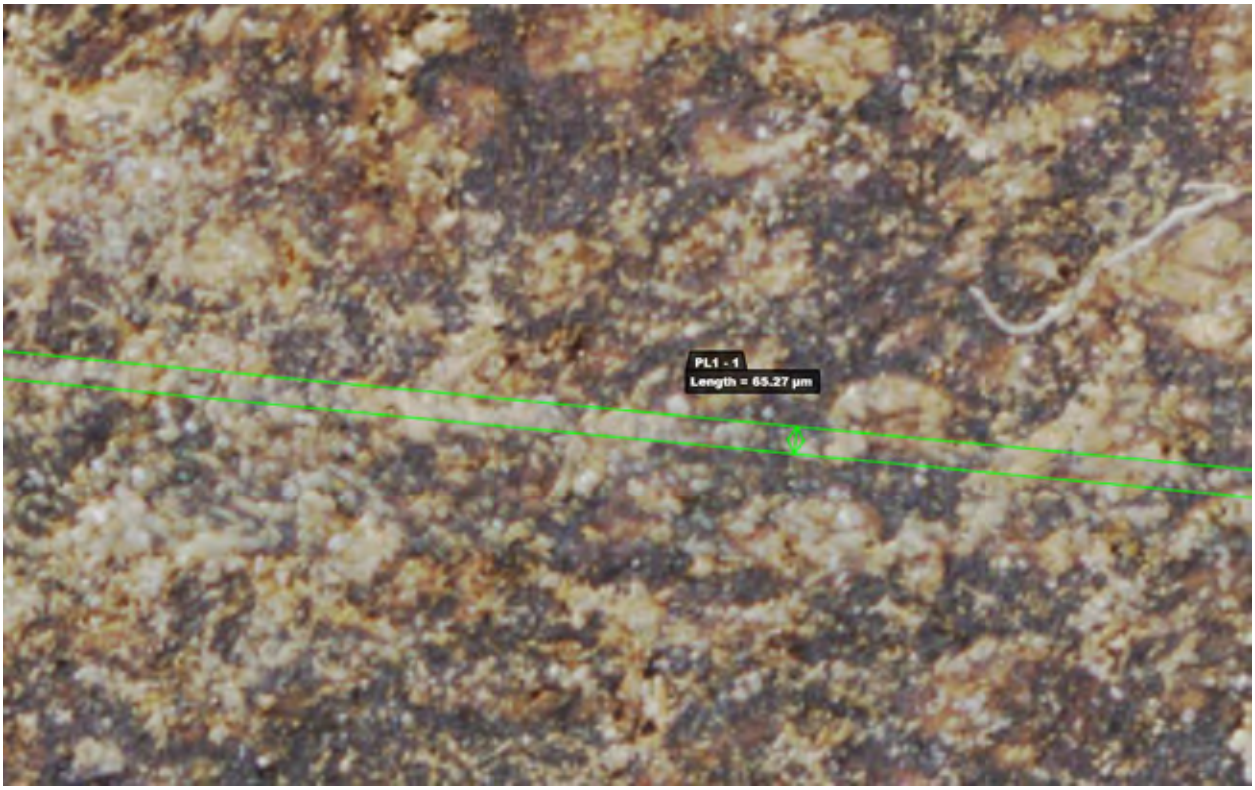

MOTB.SCR.003172 (Jeremiah)

Fragment No.	MOTB.SCR.003172
Text	Jeremiah
Inv Group	3
Notes	

File Name:	MOTB.SCR.003172_001_PM_NL.tif (Micrograph) 1
Description:	Detail of second line of text at top of fragment with particulate clusters.

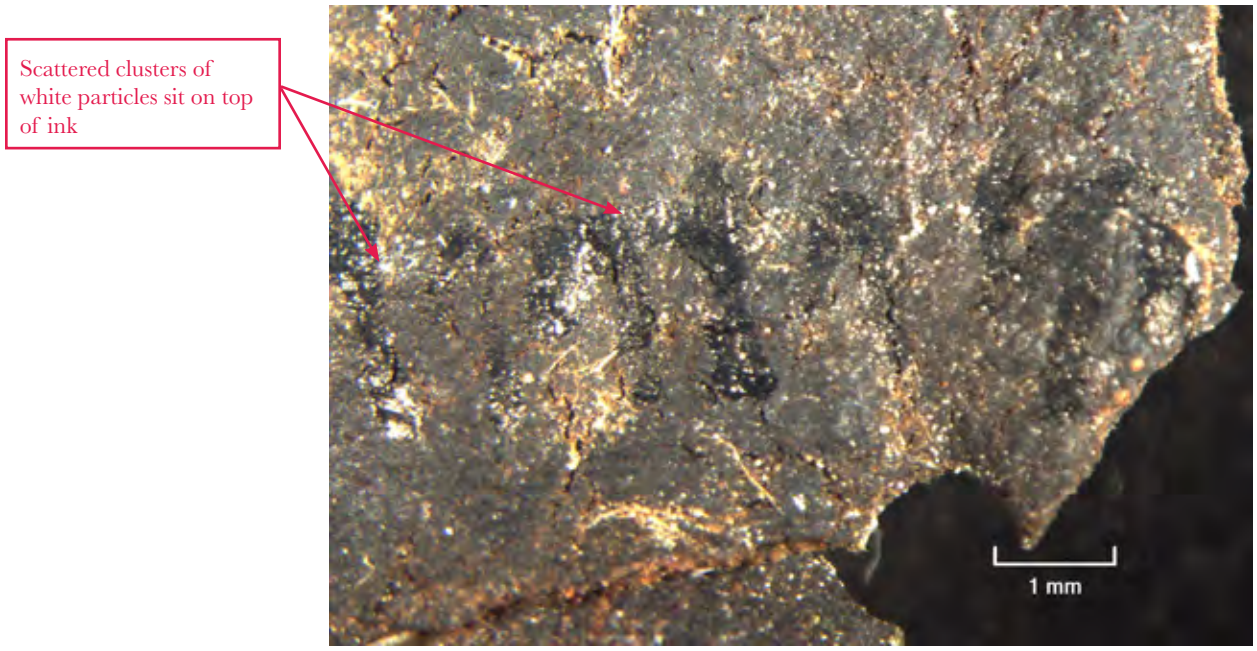

File Name:	MOTB.SCR.003172_003_PM_NL.tif (Micrograph) 2
Description:	Detail of right edge, above center, with area of lumpy surface texture created by an irregular area or defect in the leather substrate; follicle pattern very prominent in this area.

File Name:	MOTB.SCR.003172/MOTB.SCR.003172005.jpg (Hirox) 3
Description:	Sixth line of text to the right of center, with long semi-circular tear in support that widens towards the bottom edge of fragment; lighter brown areas are where the grain surface is abraded

File Name:	MOTB.SCR.003172/MOTB.SCR.003172006.jpg (Hirox) 3
Description:	Sixth line of text to the right of center, highlighting the very irregular surface topography that is a natural feature of the leather support in this area

File Name:	MOTB.SCR.003172/MOTB.SCR.003172001.jpg (Hirox) 3
Description:	Detail of sixth line of text to left of center, showing faint irregular line of white waxy material along the tops of the letters

File Name:	MOTB.SCR.003172/MOTB.SCR.003172003.jpg (stitched Hirox)
Description:	Stitched image that digitally marks traces of two faint artificial ruling lines, above and below sixth line of text, made with a white waxy material.

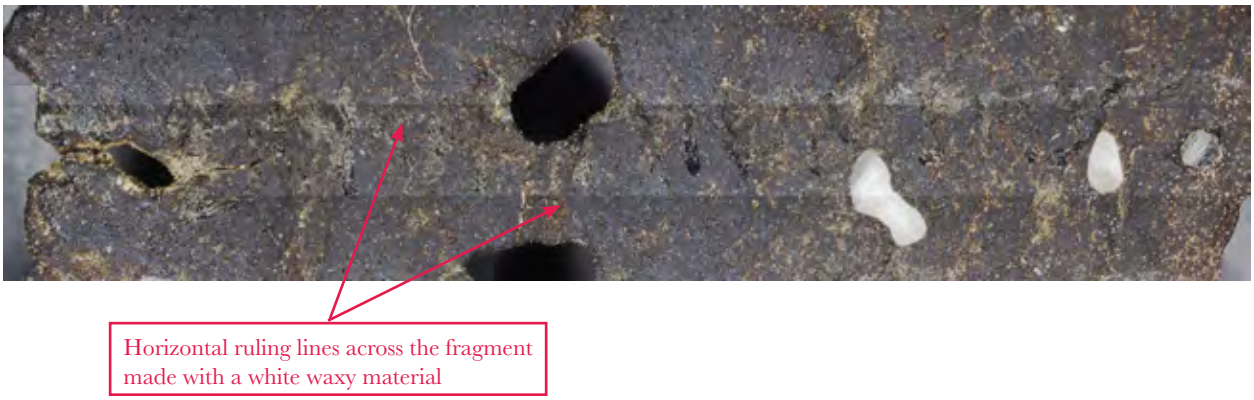

File Name:	MOTB.SCR.003172/MOTB.SCR.003172007.jpg (Hirox) 4
Description:	V-shaped crack at bottom left edge in sixth line of text, showing ink applied over an abraded area of the support that is coated with dark amber glue.

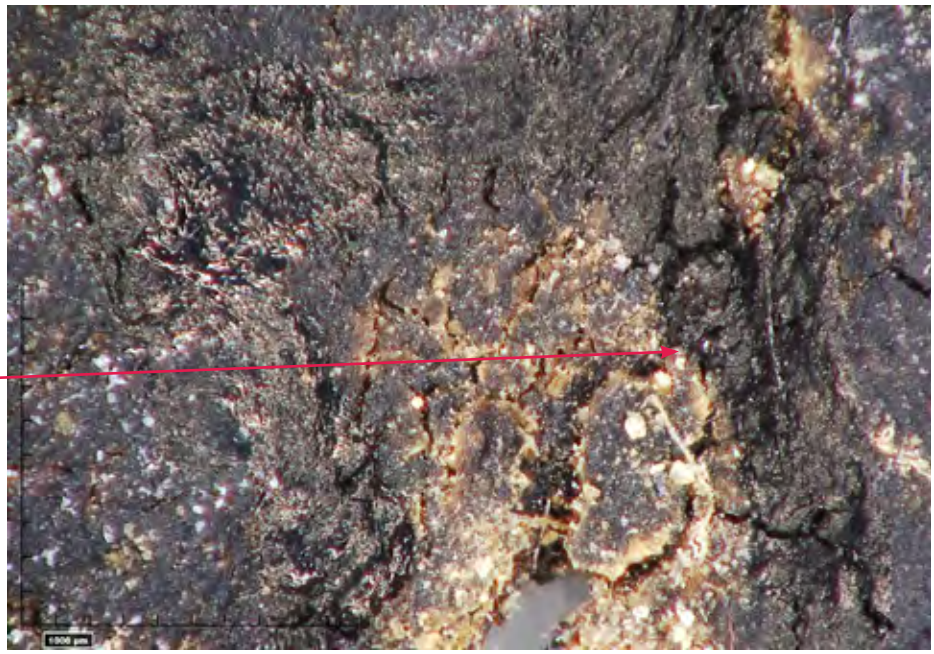

File Name:	MOTB.SCR.003172/MOTB.SCR.003172010.jpg (Hirox) 5
Description:	Shiny ink carries over onto bent left edge of fragment, in third line of text.

MOTB.SCR.003173 (Numbers)

Fragment No.	MOTB.SCR.003173
Text	Numbers
Inv Group	3
Notes	Included in BAM Report

File Name:	MOTB.SCR.003173_003_PM_NL_20190424.tif (Micrograph) 1
Description:	Far left edge of fragment with ink falling over worn edge; ink goes into surface crack parallel to edge.

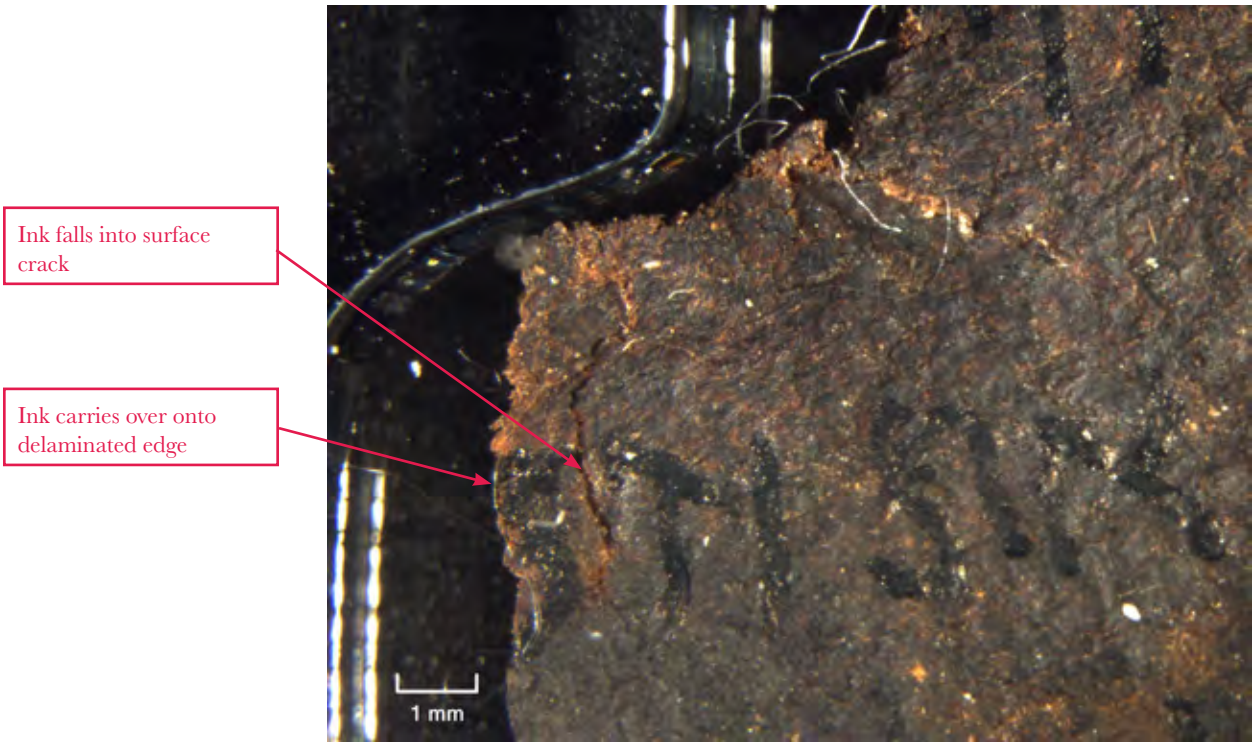

File Name:	MOTB.SCR.003173/MOTB.SCR.003172014.jpg (Hirox) 1
Description:	Closer detail, third line of text, left side, with ink continuing over on to damaged edge where fibers are frayed

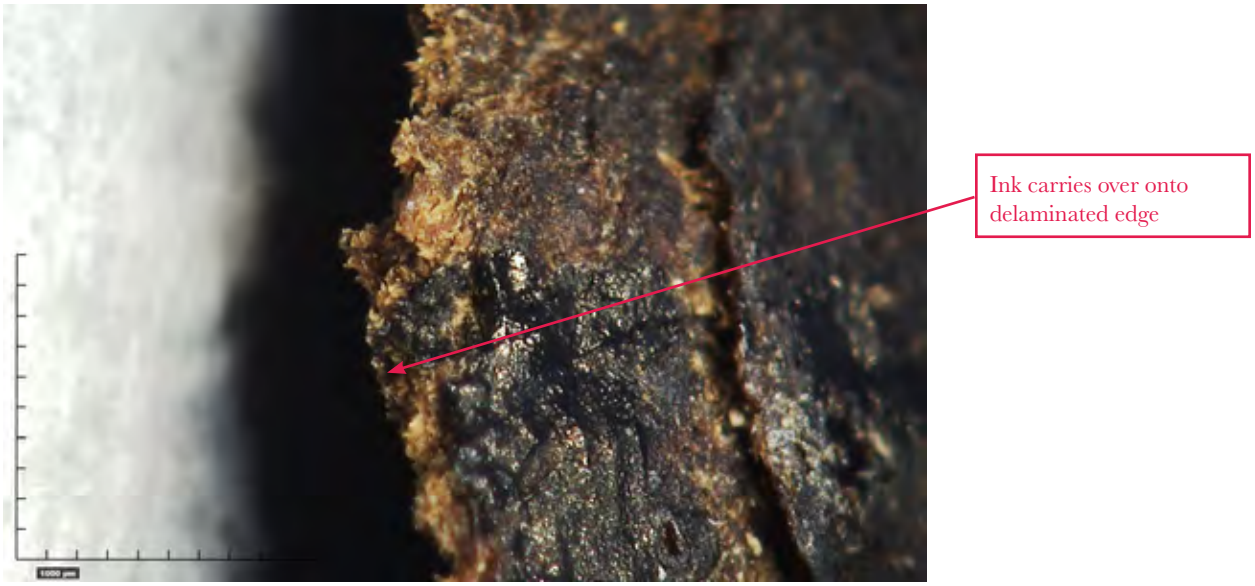

File Name:	MOTB.SCR.003173_002_PM_NL_20190424.tif (Micrograph) 2
Description:	Far left section of fragment with sharp bottom edge, possibly cut with a knife

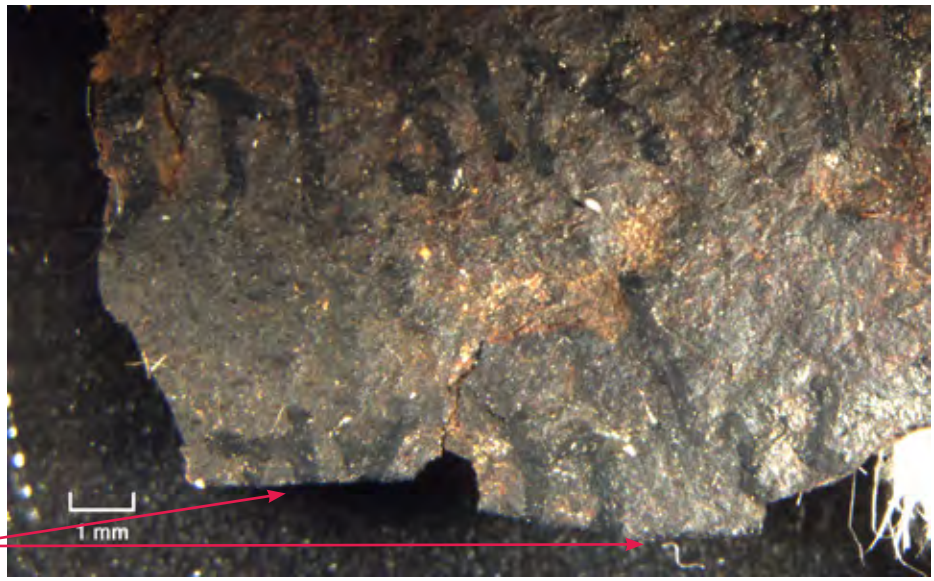

Apparent trimmed bottom edge of fragment

File Name:	MOTB.SCR.003173_004_PM_NL_20190424.tif (Micrograph) 3
Description:	Detail of top edge, where ink falls into a vertical crease and resinous amber material is present; the uneven, lumpy surface of the leather substrate is evident at far right

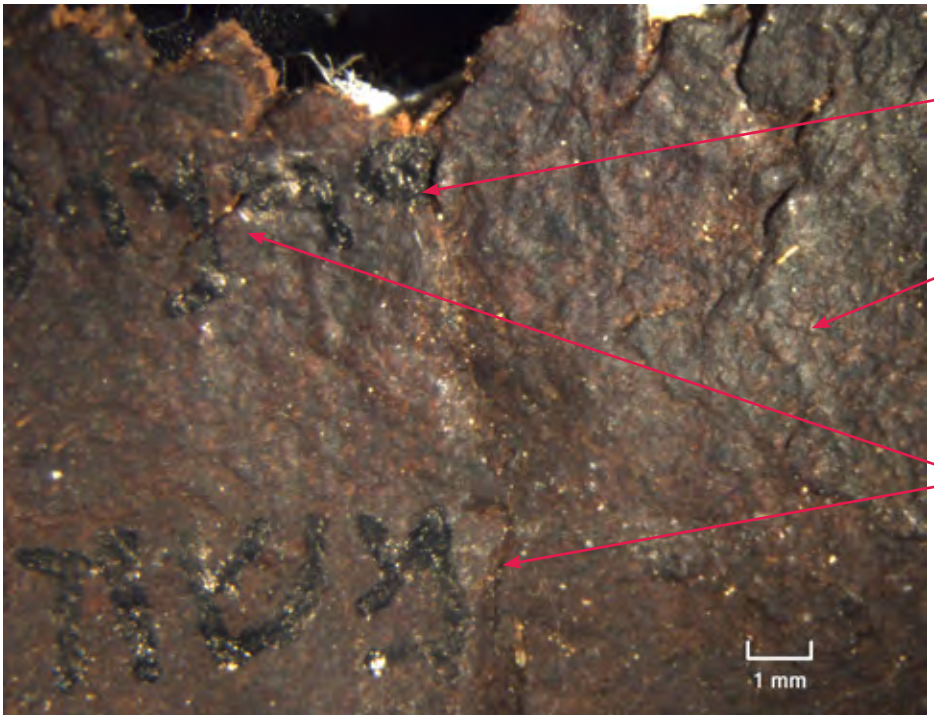

Ink falls into a vertical crease

Uneven, lumpy surface of leather substrate

Amber colored, resinous accretions

File Name:	MOTB.SCR.003173/MOTB.SCR.003173005.jpg (Hirox) 4
Description:	Top edge at center, with core of skin projecting beyond grain layer; both surfaces are blackened from oxidation

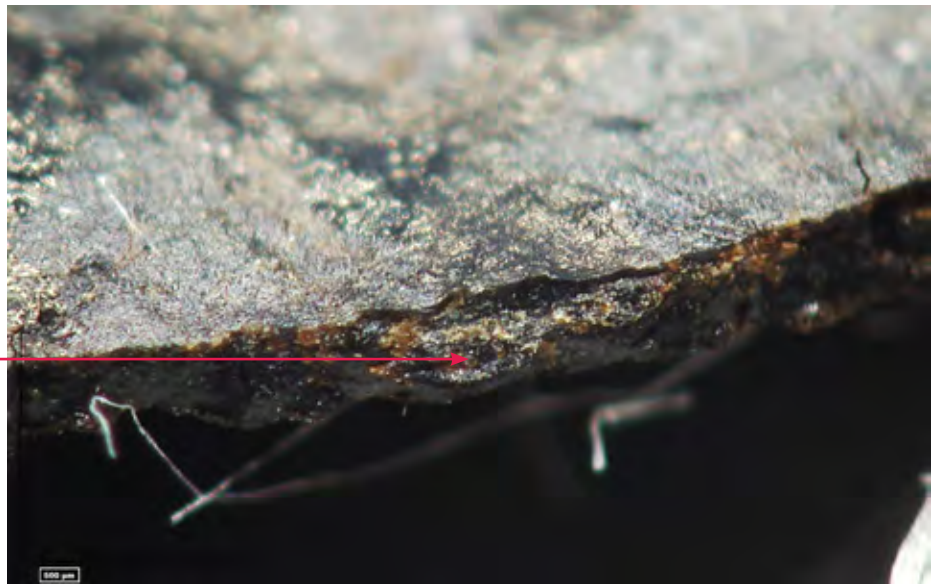

Fibers projecting beyond embrittled grain layer; both are blackened from oxidative damage

File Name:	MOTB.SCR.003173/MOTB.SCR.003173008.jpg (Hirox) 5
Description:	Fourth line of text to the left of center near a hole, with shiny, viscous ink puddling in diagonal crack

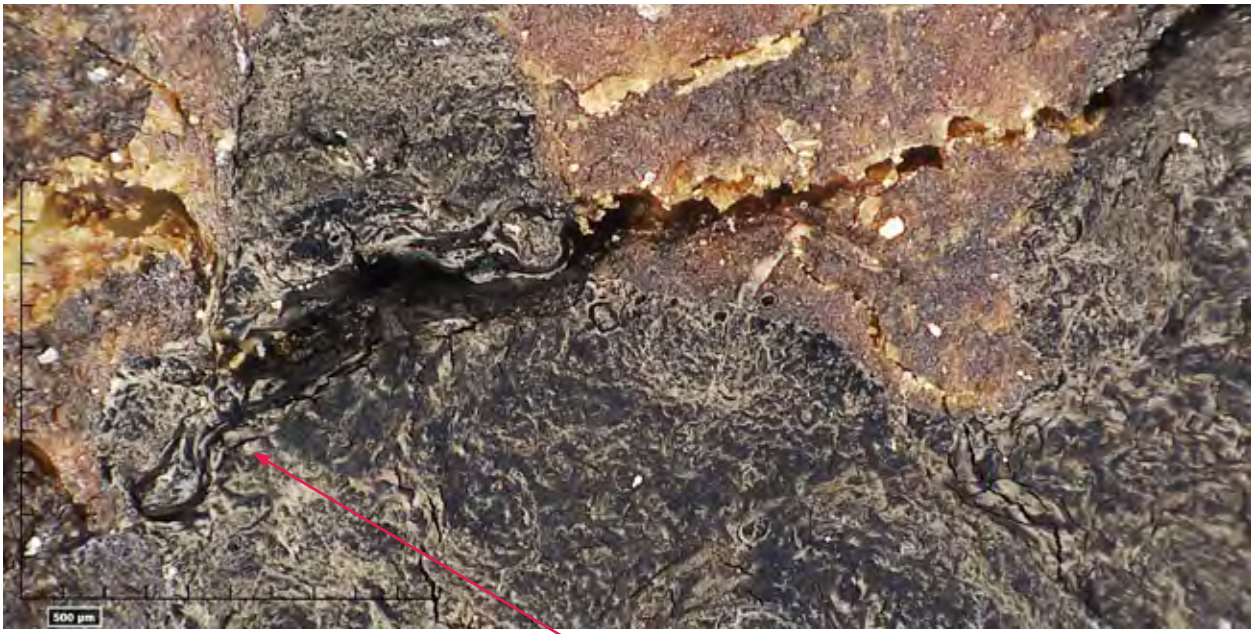

Shiny, viscous ink pooling within diagonal crack in the fragment

File Name:	MOTB.SCR.003173/3dimage_0022.jpg (3D Hirox) 5
Description:	3D image of ink in 4th line of text, left of center, waterfalling into a deep crack

File Name:	MOTB.SCR.003173/MOTB.SCR.003173010.jpg (Hirox) 6
Description:	Artificial horizontal and vertical ruling lines, made with a waxy white material; horizontal line traverses a large area of grain loss at center and goes across vertical cracks at left and right.

Artificial ruling lines made with a white, waxy material passing over an area of grain loss and vertical cracks

File Name:	MOTB.SCR.003173/MOTB.SCR.003173020.jpg (Hirox) 6
Description:	First line of text with artificial ruling line made with a white waxy material that extends over damaged edges at left and right.

File Name:	MOTB.SCR.003173/MOTB.SCR.003173019.jpg (Hirox) 6
Description:	Top edge at center, with ink falling into cracked, damaged area; artificial horizontal and vertical ruling lines intersect to right of letter (white deposits over ink have similar appearance to waxy material used for ruling)

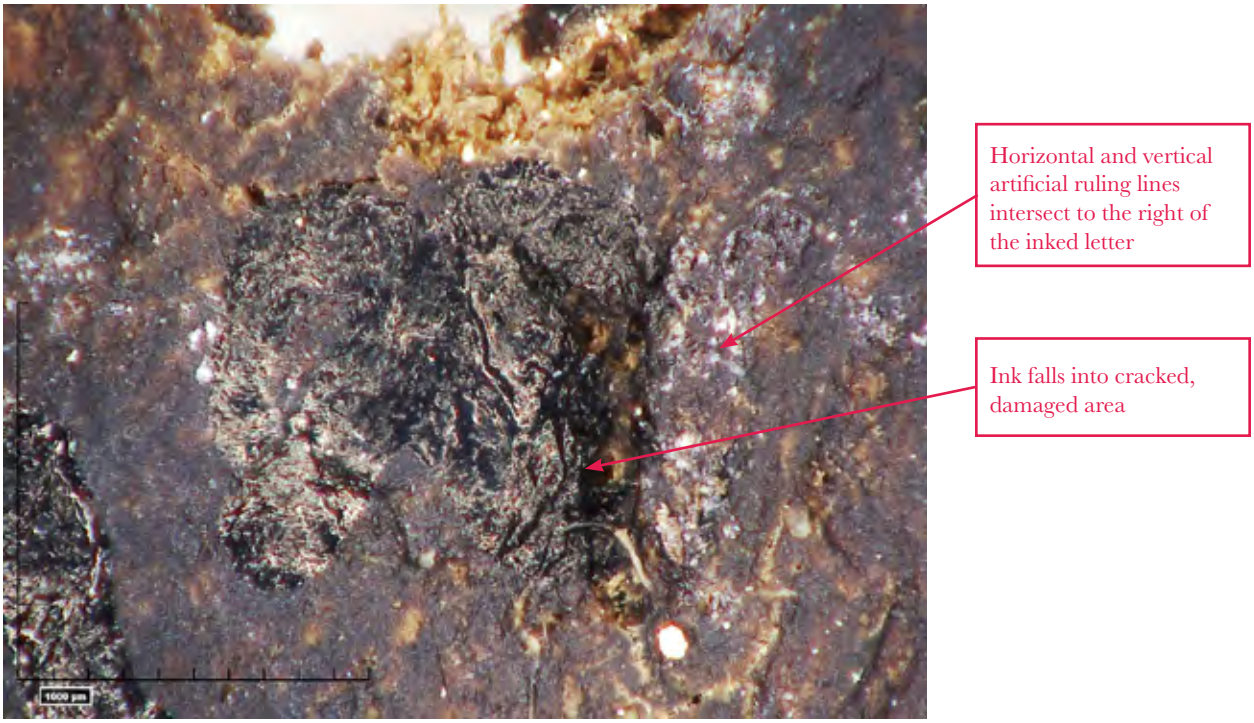

File Name:	MOTB.SCR.003173/MOTB.SCR.003173012.jpg (stitched Hirox, horizontal)
Description:	Stitched image of horizontal ruling line, made with white waxy material, that extends out to damaged right edge of fragment

Horizontal artificial ruling line extends over the damaged right edge of the fragment

File Name:	MOTB.SCR.003173/MOTB.SCR.003173014.jpg (stitched Hirox, vertical) 7
Description:	Stitched image of vertical ruling line, made with white waxy material, that intersects with similar horizontal ruling lines along full height of fragment. The vertical ruling line runs just left of an area of distortion in the support, passing within a recessed area of the cockling

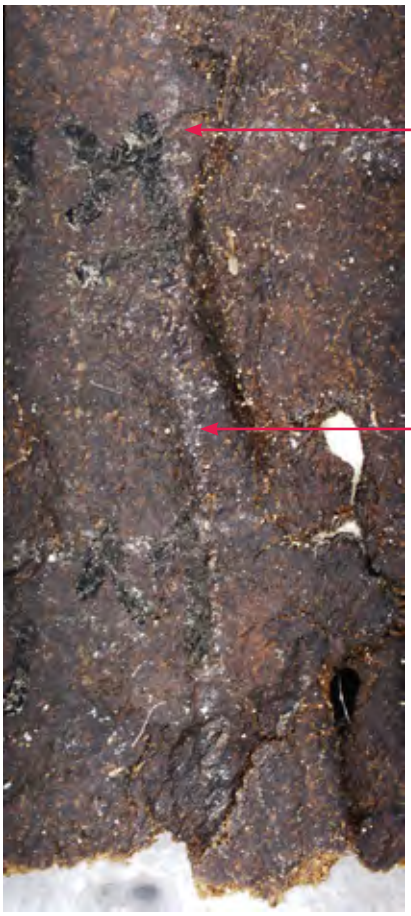

Horizontal ruling lines intersect a vertical ruling line across the height of the fragment

Vertical ruled line runs in a valley created by cockling (distortion) in the support

MOTB.SCR.003174 (Ezekiel)

Fragment No.	MOTB.SCR.003174
Text	Ezekiel
Inv Group	3
Notes	

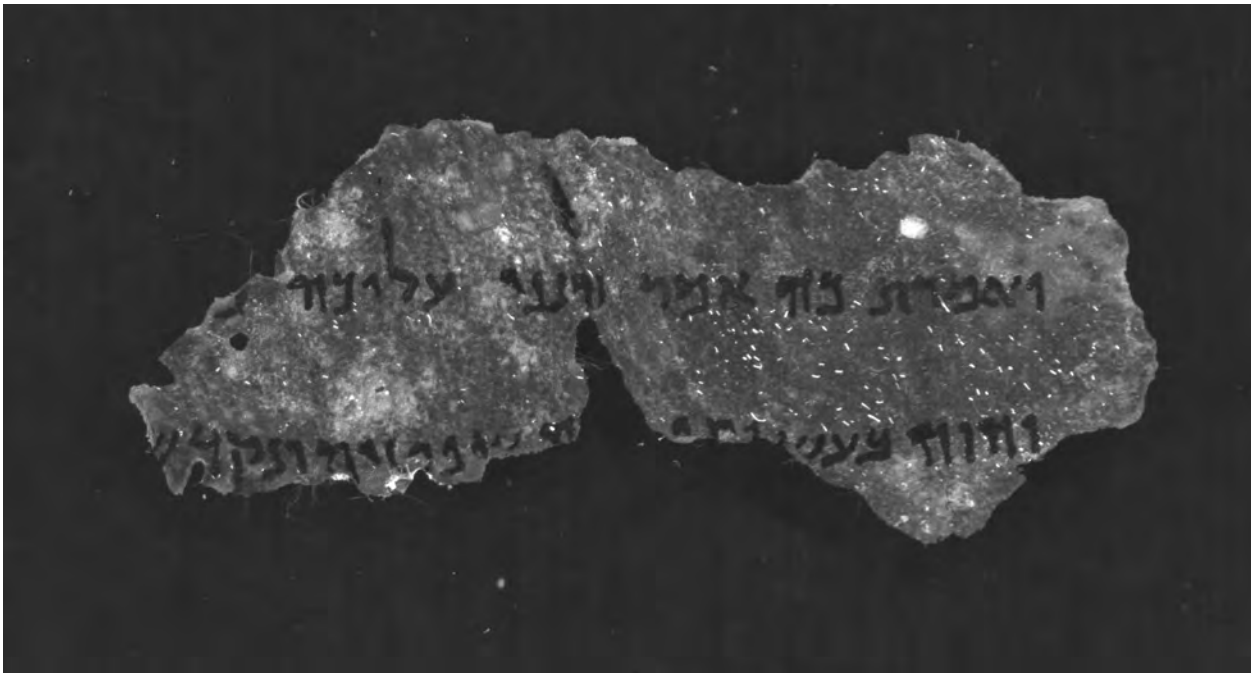

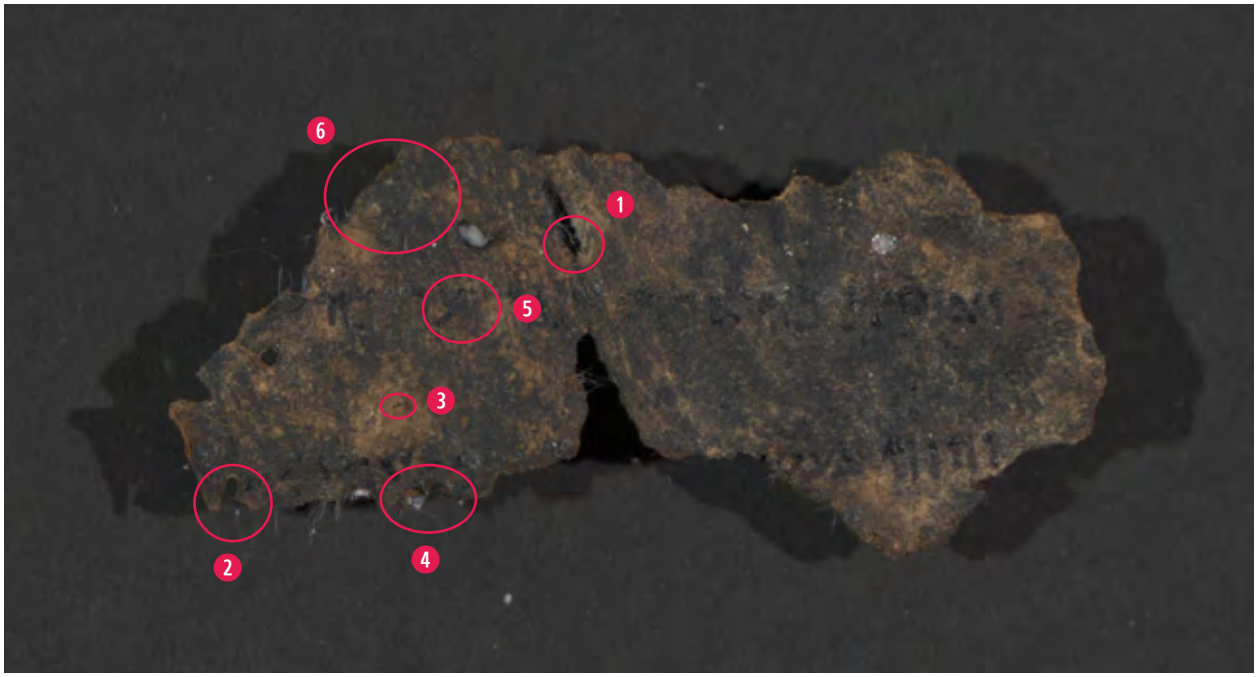

File Name:	MOTB.SCR.003174_001_PM_NL_20190424.tif (Micrograph) 1
Description:	Detail of resinous amber-colored material, likely animal skin glue, in and along mended crack and loss in top center of support

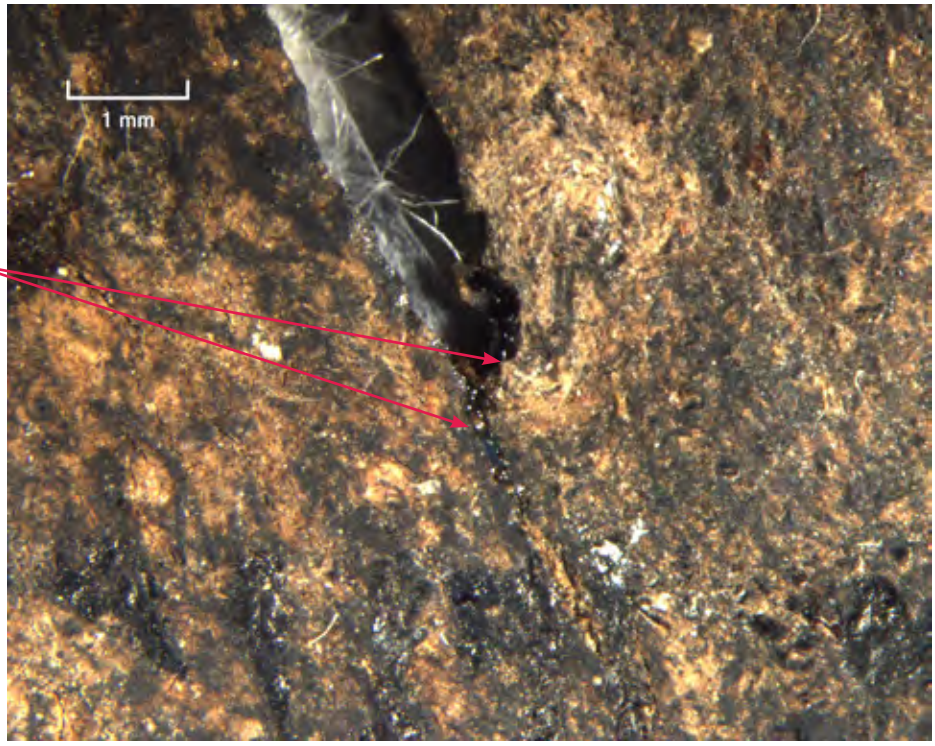

Resinous, amber-colored material (likely animal skin glue) in mended crack and loss area in the top center of the support

File Name:	MOTB.SCR.003174/MOTB.SCR.003174006.jpg (Hirox) 2
Description:	Bottom edge, right of center and large area of loss, where grain layer has broken off. Ink applied to this edge extends into vertical crack at right.

Ink extends into a vertical crack to the right of an area of grain loss

File Name:	MOTB.SCR.003174_003_PM_NL_20190424.tif (Micrograph) 3
Description:	Detail of stray ink located on top of sediment layer, left of center, above a line of text.

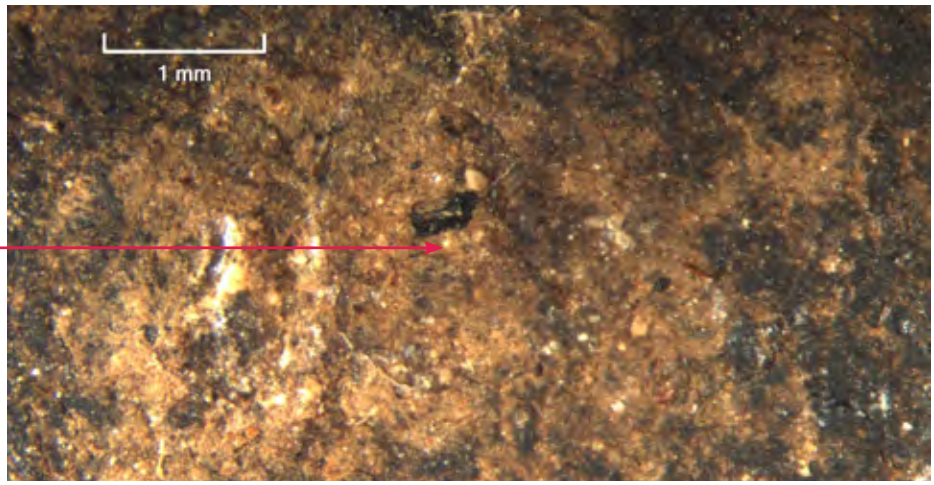

File Name:	MOTB.SCR.003174/MOTB.SCR.003174013.jpg (stitched Hirox, horizontal) 4
Description:	Stitched image of horizontal ruling line, made with a white waxy material, that extends from left to right edge of fragment.

File Name:	(MOTB.SCR.003174/MOTB.SCR.003174002.jpg (Hirox) 4
Description:	Bottom edge, left of center, where shiny ink extends onto a delaminated area of support; clear pressure-sensitive tape and fibrous white tissue extend out from the verso of fragment.

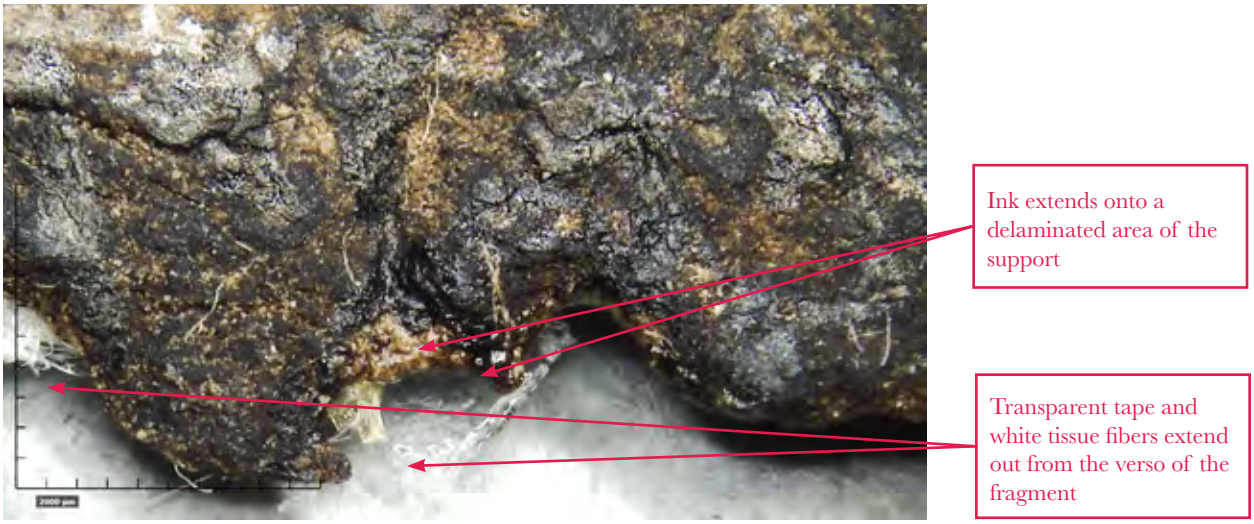

File Name:	MOTB.SCR.003174/MOTB.SCR.003174004.jpg (Hirox) 4
Description:	Detail of triangular tip of substrate along bottom edge, left of center, where ink appears to be covered with a shiny, transparent coating. Clear pressure-sensitive tape seen in background.

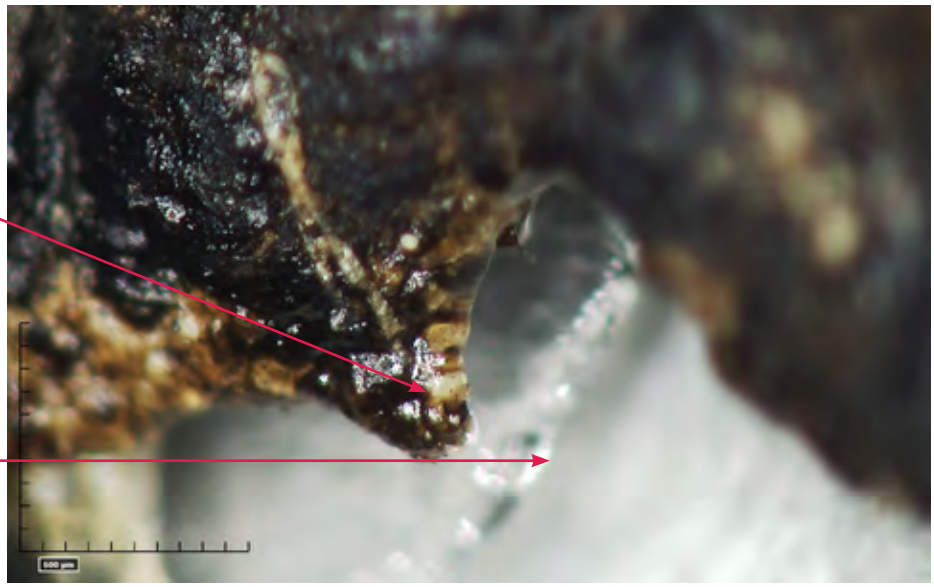

File Name:	MOTB.SCR.003174/MOTB.SCR.003174015.jpg (Hirox) 5
Description:	First line of text, to the left of two large losses, emphasizing three-dimensional nature of the ink.

File Name:	MOTB.SCR.003174/MOTB.SCR.003174016.jpg (Hirox) 5
Description:	Detail of the first line of text in higher magnification, showing the topography of the inked letters

The ink is thicker along the perimeter of the letters, where it has been pushed to the edges by the pressure of the writing tool

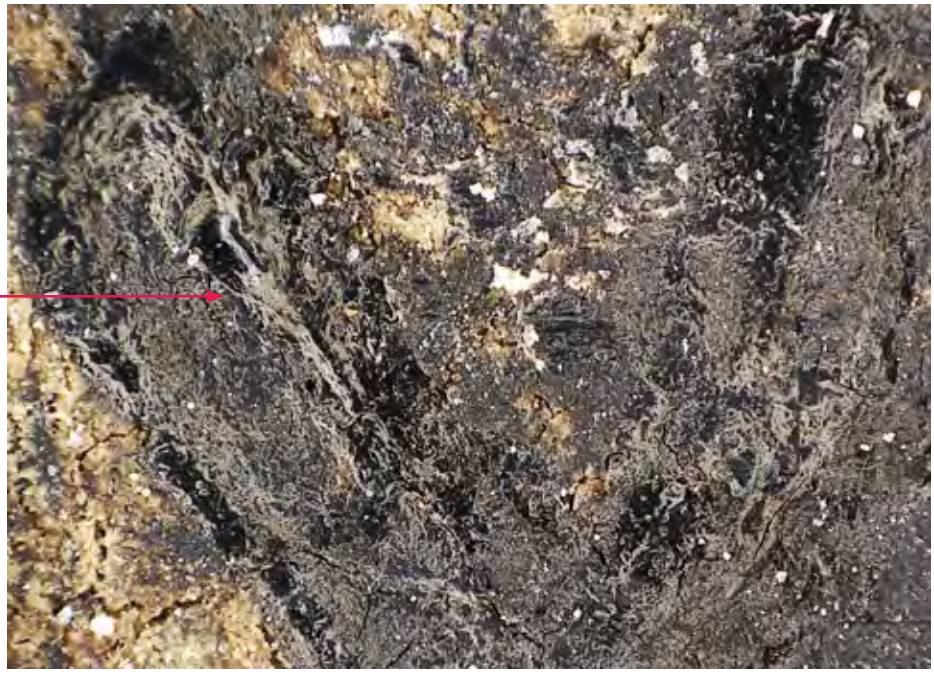

File Name:	MOTB.SCR.003174/MOTB.SCR.003174021.jpg (Hirox) 5
Description:	First line of text, left side, where faint vertical brush strokes run parallel to a stroke of thick, shiny ink

Striated lines, evidence of applied coating, are to the left of a letter in the first line of text

File Name:	MOTB.SCR.003174/MOTB.SCR.003174023.jpg (Hirox) 6
Description:	Vertical brush strokes indicating possible application of a transparent coating over cream and white surface deposits, visible in specular illumination This image suggests a clear coating over the blackened grain layer, with the lighting causing the brush marks to be very pronounced.

Brush strokes visible in specular light appear to indicate application of a transparent coating applied over granular surface deposits

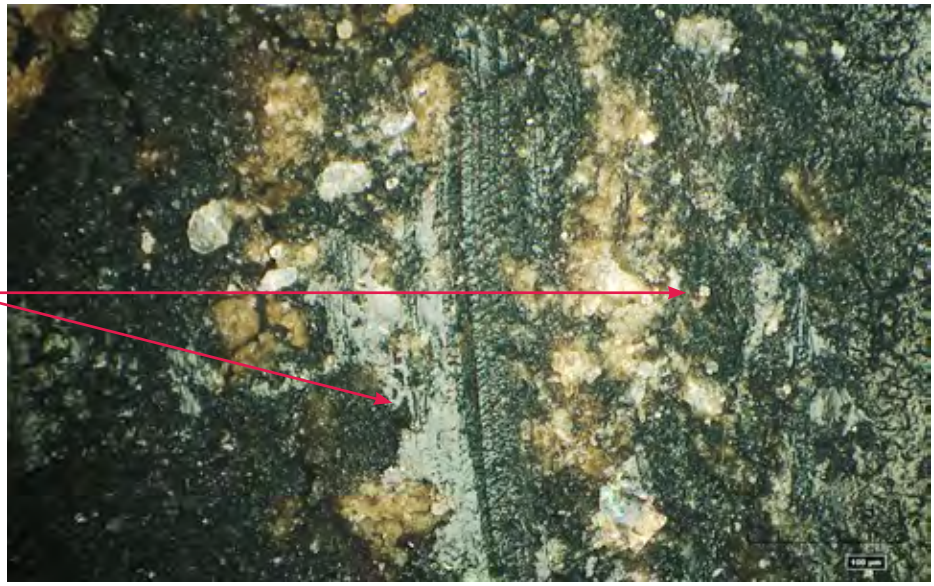

File Name:	MOTB.SCR.003174/3dimage_0034.jpg (3D Hirox) 6
Description:	Fine parallel brush strokes indicating possible application of a transparent coating over a blank area, above first line of text at left.

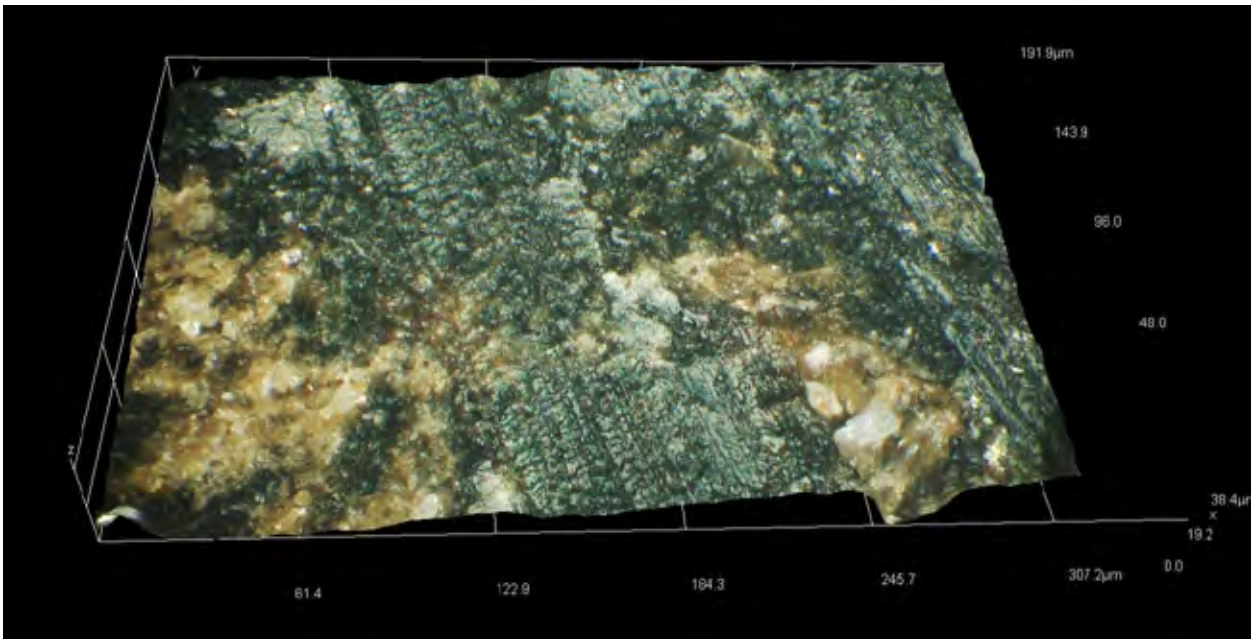

MOTB.SCR.003175 (Nehemiah)

Fragment No.	MOTB.SCR.003175
Text	Nehemiah
Inv Group	3
Notes	Included in BAM Report

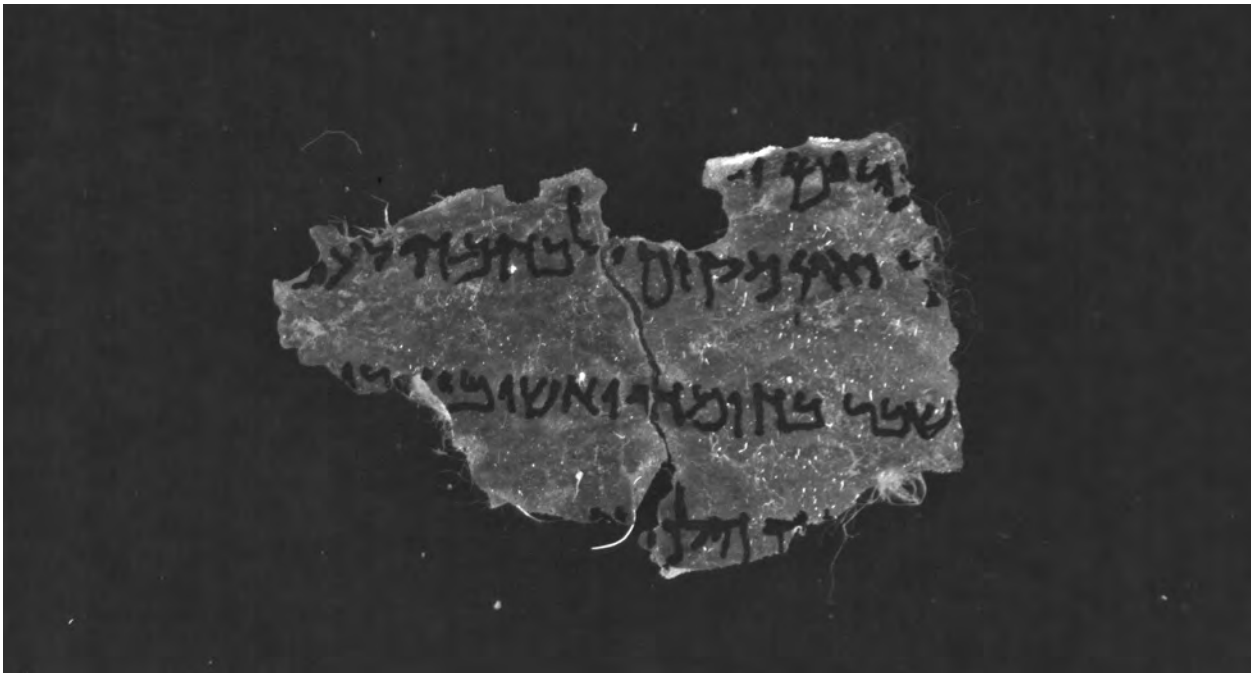

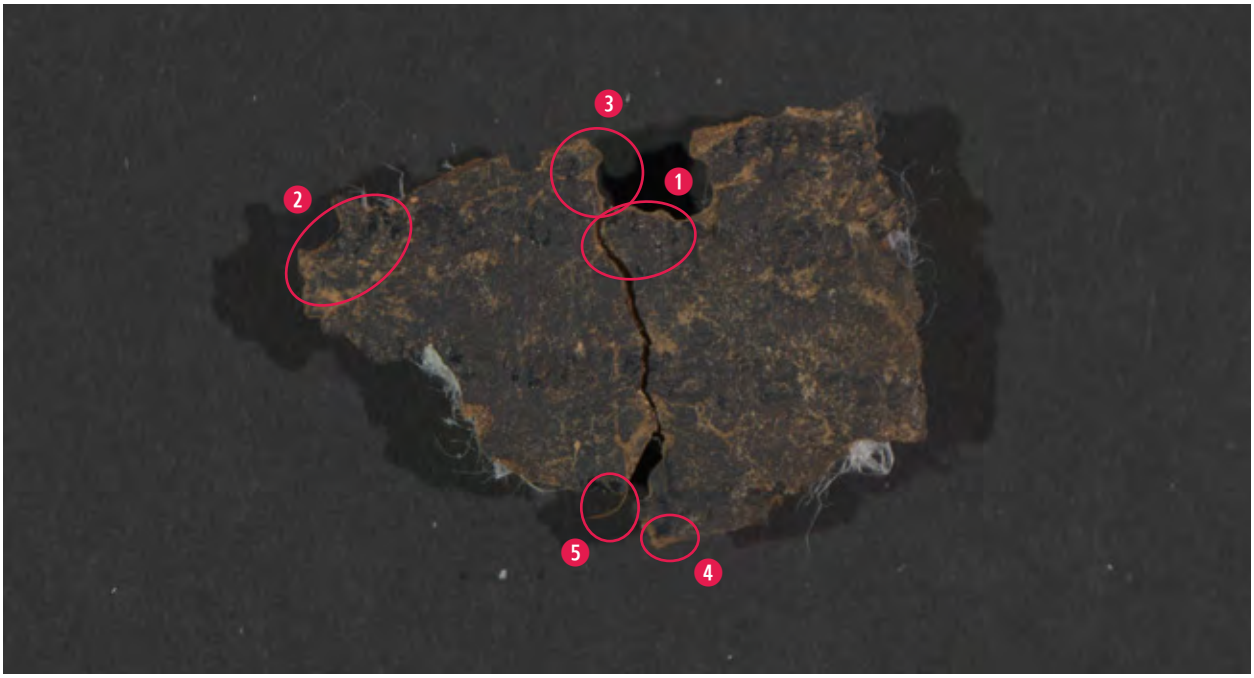

File Name:	MOTB.SCR.003175_001_PM_RL_20190424.tif (Micrograph) 1
Description:	Diagonal incised line, possibly from abrasion, located across the left section of the fragment above center, extending out to the damaged edge.

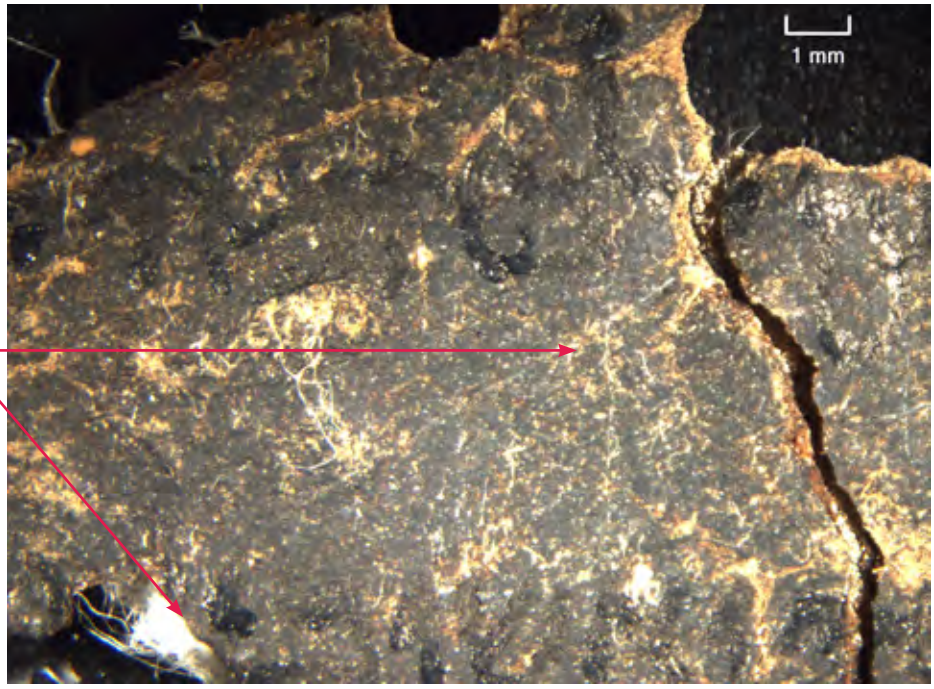

File Name:	MOTB.SCR.003175_004_PM_RL_20190424.tif (Micrograph) 2
Description:	Detail of diagonal incised line, possibly from abrasion, located across the left section of the fragment above center, passing through ink and over the worn left edge.

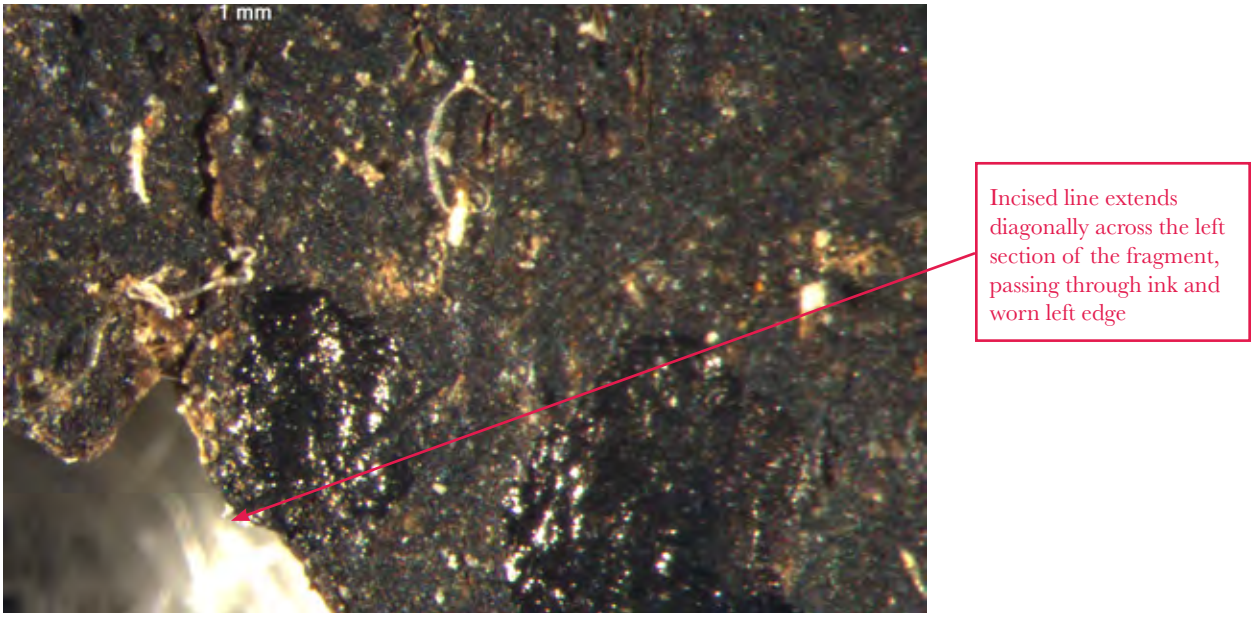

File Name:	MOTB.SCR.003175_002_PM_RL_20190424.tif (Micrograph) 3
Description:	Detail of ink (letter "lamed") passing over and sinking into cracks in support, top center.

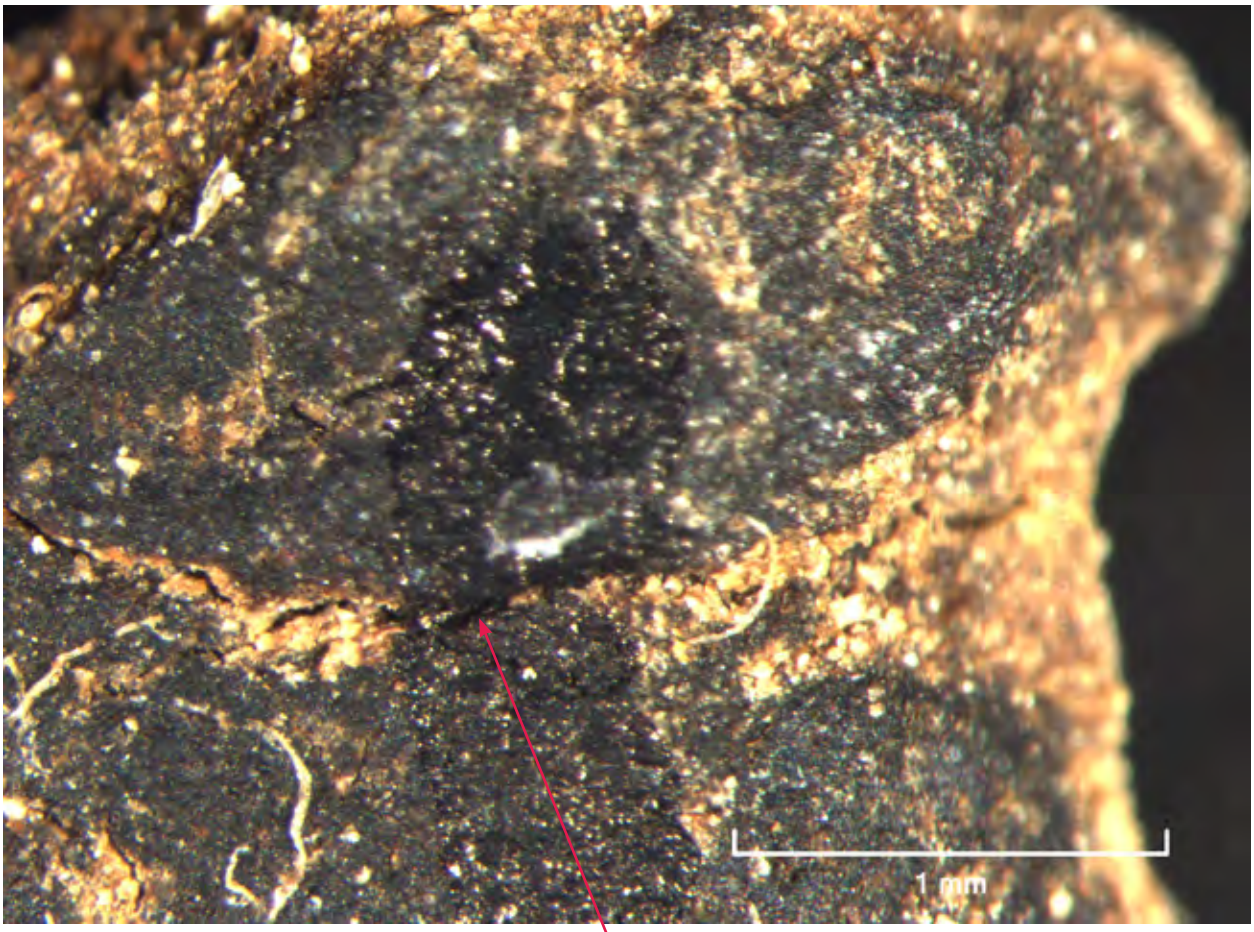

Ink sunk into cracks in the support

File Name:	MOTB.SCR.003175/MOTB.SCR.003175012.jpg (stitched Hirox, horizontal)
Description:	Stitched image of ruling line, made with white, waxy material, for third line of text.

Horizontal ruling line guiding third line of text, made of a white, waxy material

File Name:	MOTB.SCR.003175/MOTB.SCR.003175021.jpg (Hirox) 4
Description:	Detail of ink over delaminated area at bottom left edge

Ink passes over delaminated grain layer at bottom left edge

File Name:	MOTB.SCR.003175/MOTB.SCR.003175019.jpg (Hirox) 5
Description:	Detail of yellowish collagen fiber that projects out from damaged edge at bottom of left section

MOTB.SCR.003183 (Micah)

Fragment No.	MOTB.SCR.003183
Text	Micah
Inv Group	3
Notes	Sampled

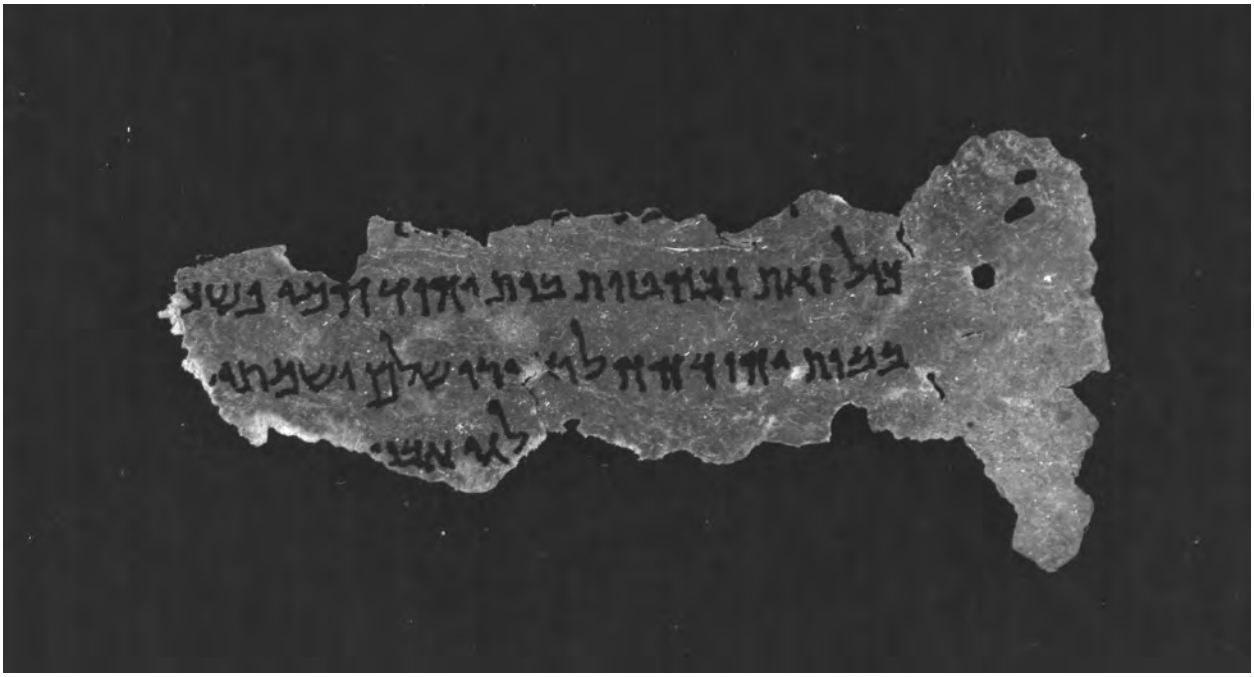

File Name:	MOTB.SCR.003183_002_PM_RL_20190424.tif (Micrograph) 1
Description:	Detail in raking light of third line of text and blank right margin, highlighting incised ruling lines; vertical line is doubled

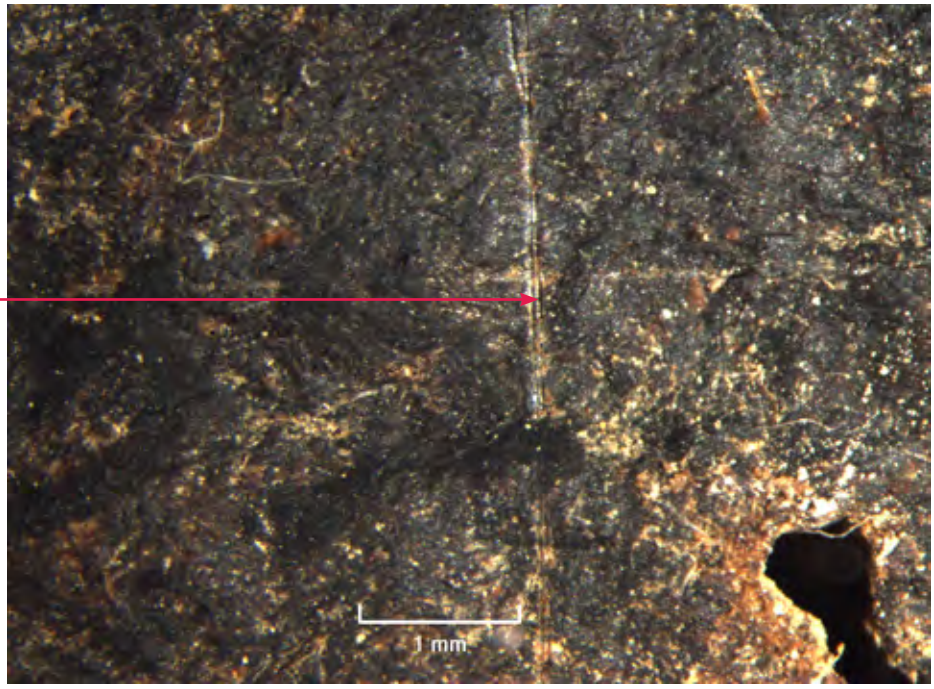

Intersecting single horizontal and double vertical ruling lines passing through third line of text

File Name:	MOTB.SCR.003183_003_PM_RL_20190424.tif (Micrograph) 1
Description:	Higher magnification detail of third line of text, with ink going over incised ruling line

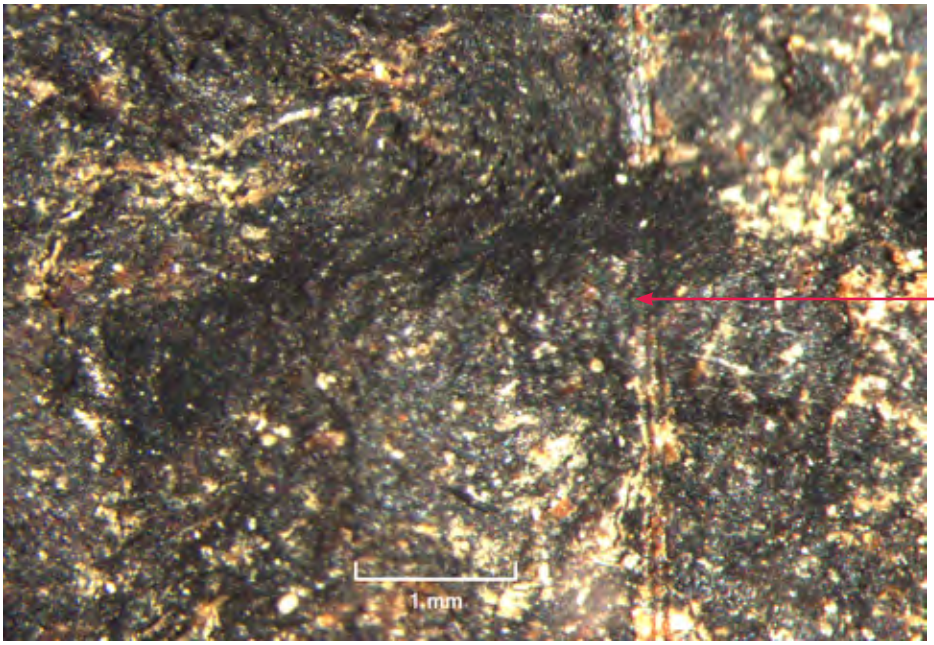

Detail of third line of text, where ink passes over vertical ruling lines

File Name:	MOTB.SCR.003183_002_PM_RL_20190424.tif (Micrograph) 1
Description:	Detail in raking light of third line of text and blank right margin, highlighting incised ruling lines; vertical line is doubled

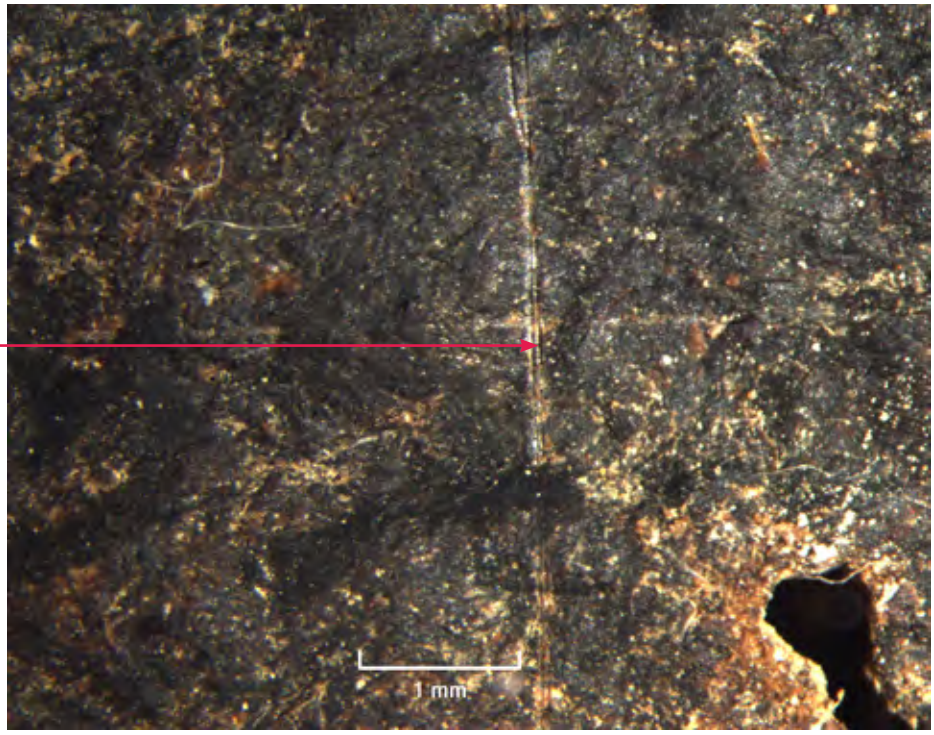

Intersecting single horizontal and double vertical ruling lines passing through third line of text

File Name:	MOTB.SCR.003183/MOTB.SCR.003183009.jpg (Hirox) 2
Description:	Vertical ruling line doubled above second line of text at right margin.

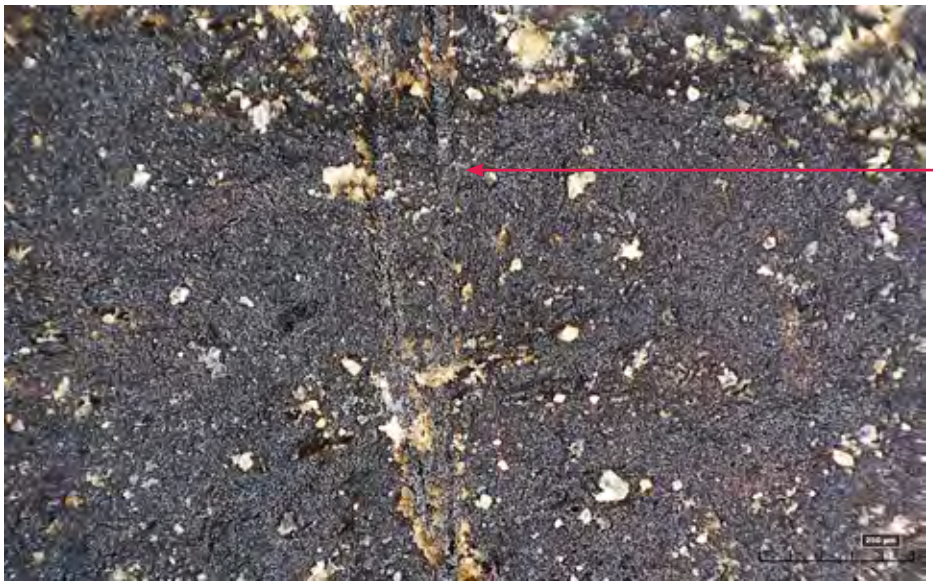

Parallel vertical ruling lines are slightly separated above the second line of text in the right margin

File Name:	MOTB.SCR.003183/3dimage_0036.jpg (3D Hirox) 2
Description:	3D detail of intersecting incised ruling lines along blank right margin

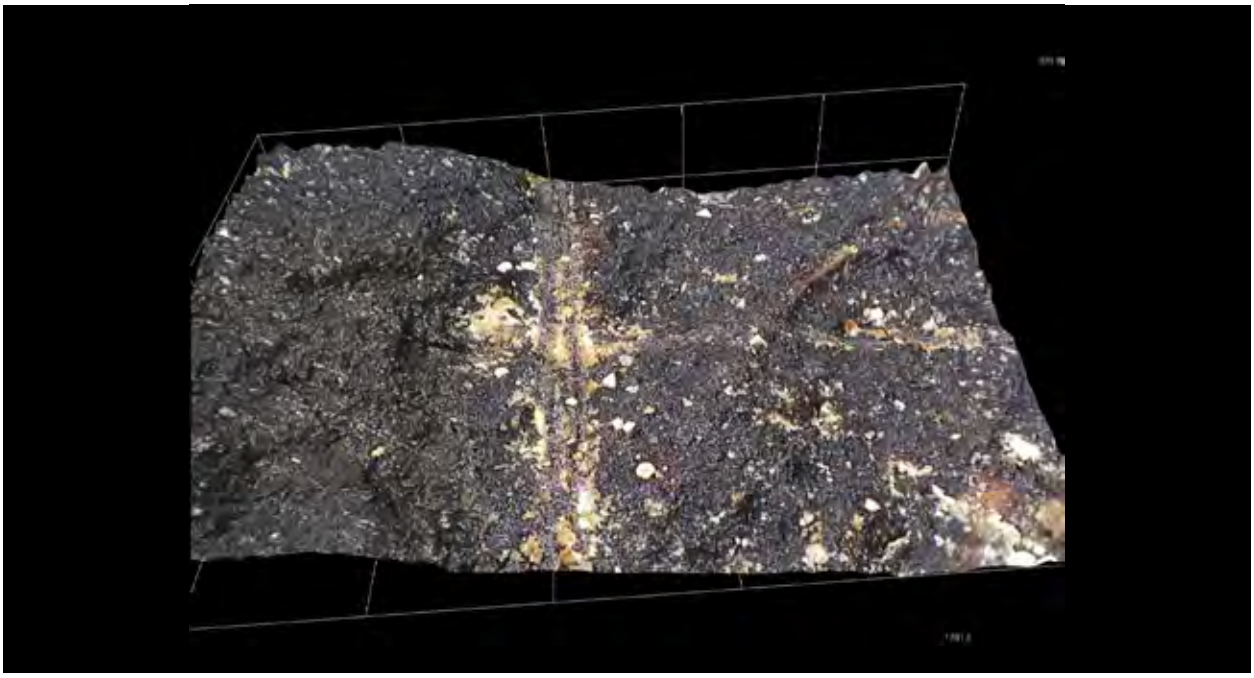

File Name:	MOTB.SCR.003183/3dimage_0037.jpg (3D Hirox) 2
Description:	Same as above

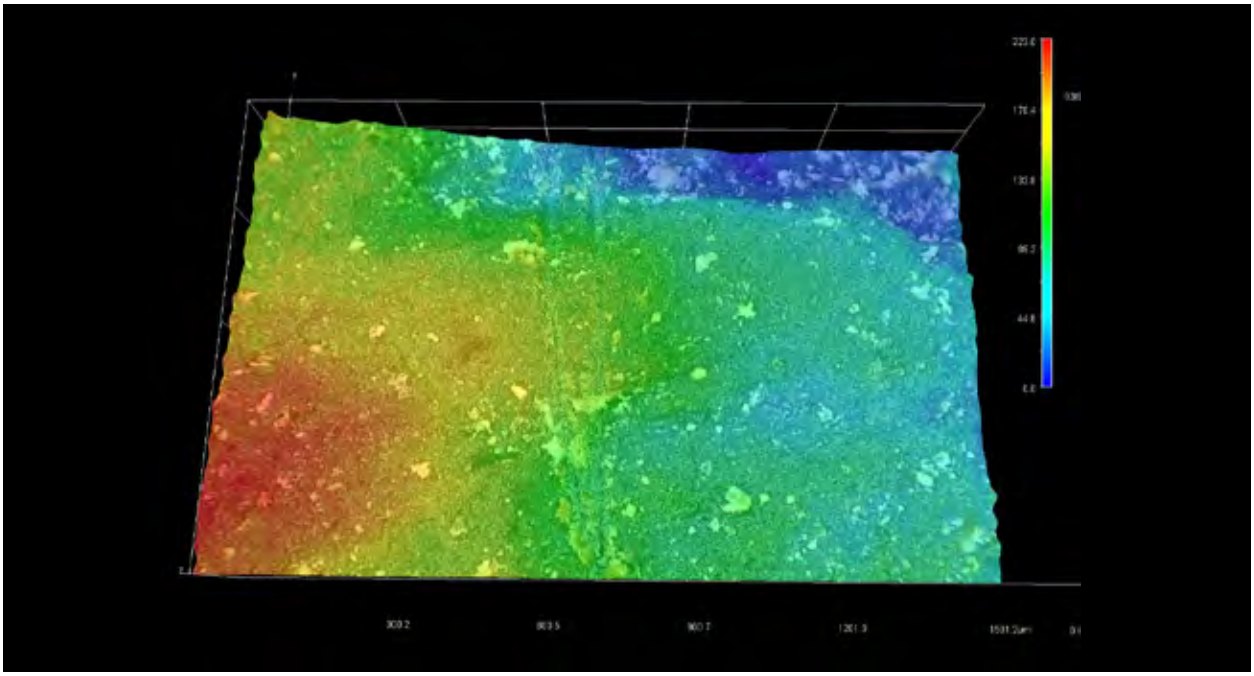

File Name:	MOTB.SCR.003183/MOTB.SCR.003183010.jpg (Hirox) 2
Description:	Detail in higher magnification of the striations in the parallel vertical ruling lines above the second line of text, in specular illumination.

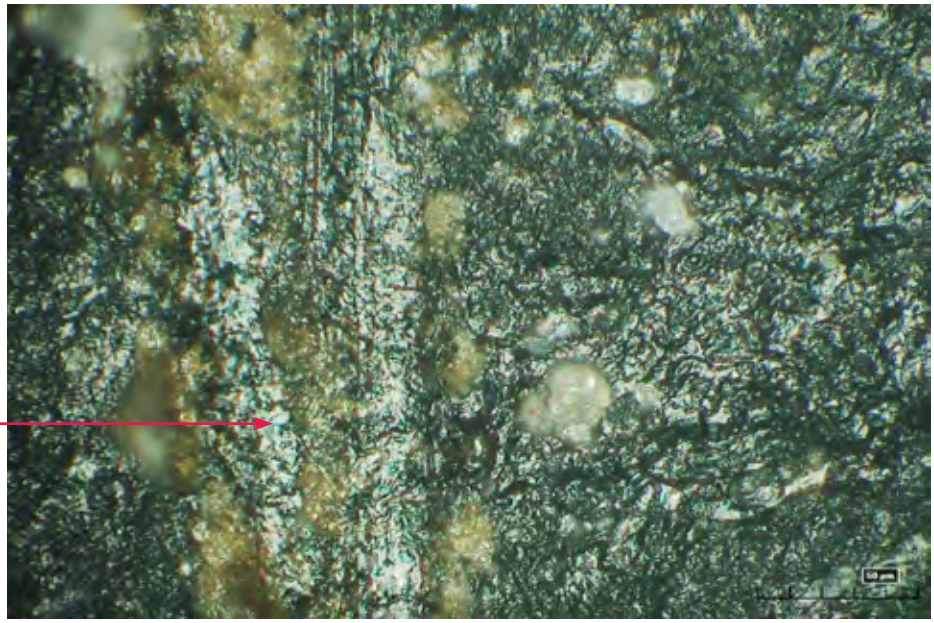

Striations in the vertical ruling lines above the second line of text, visible in specular illumination

File Name:	MOTB.SCR.003183/MOTB.SCR.003183026.jpg (Hirox) 3
Description:	Second line of text at center, with ink going over and into diagonal crack that radiates out from area of grain loss at left.

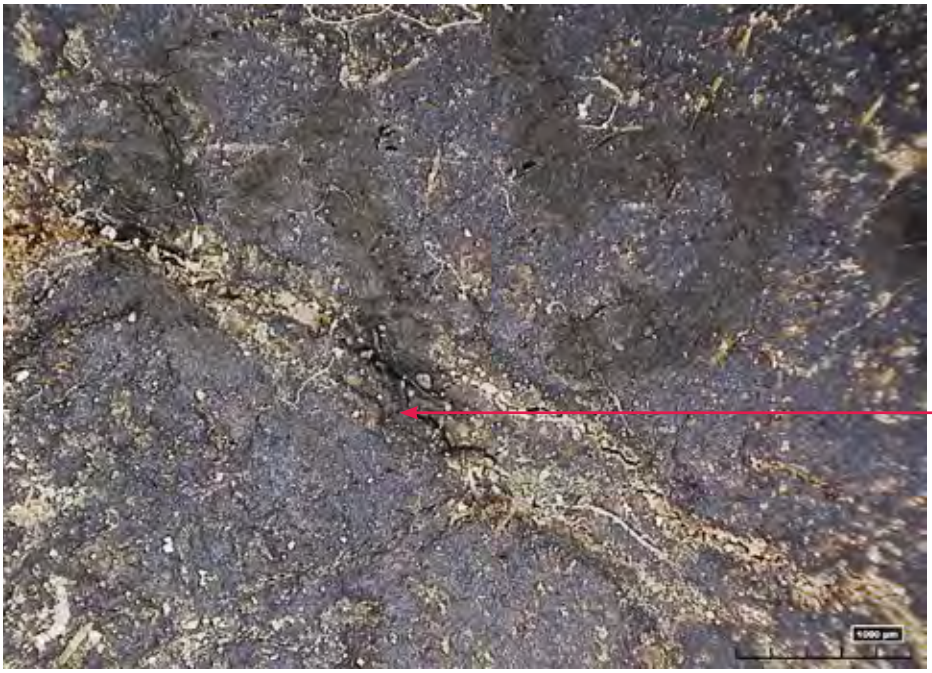

Ink passes over and falls into diagonal crack extending from an area of grain loss

File Name:	MOTB.SCR.003183/MOTB.SCR.003183021.jpg (Hirox) 4
Description:	Incised ruling line extends over left edge of fragment and across small defect at right

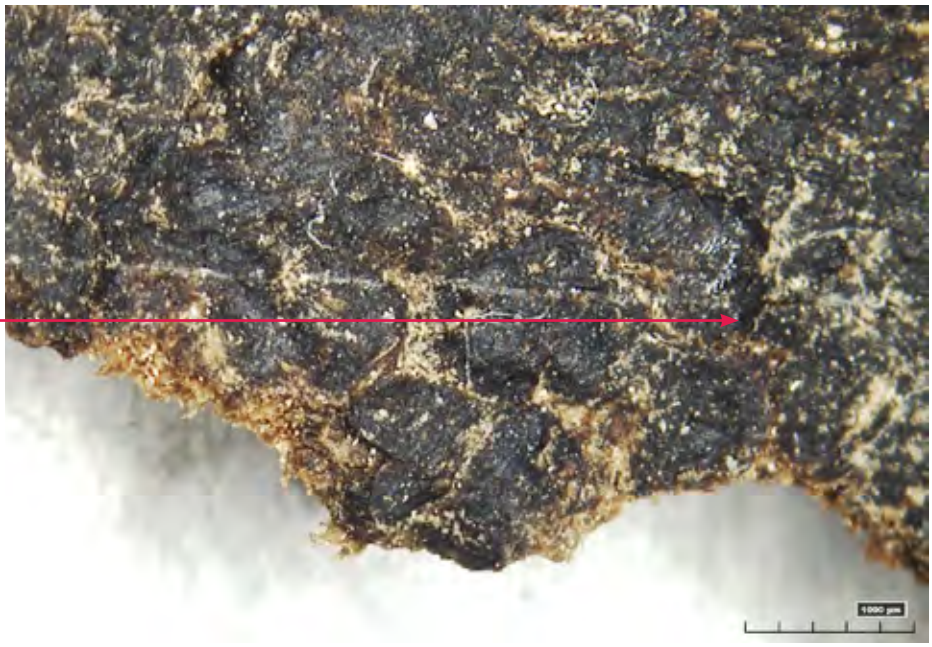

Ruling line extends across left edge, passing over small cracks in the support

File Name:	MOTB.SCR.003183/MOTB.SCR.003183028.jpg (Hirox) 5
Description:	Ruling line associated with first line of text is doubled on left side of hole

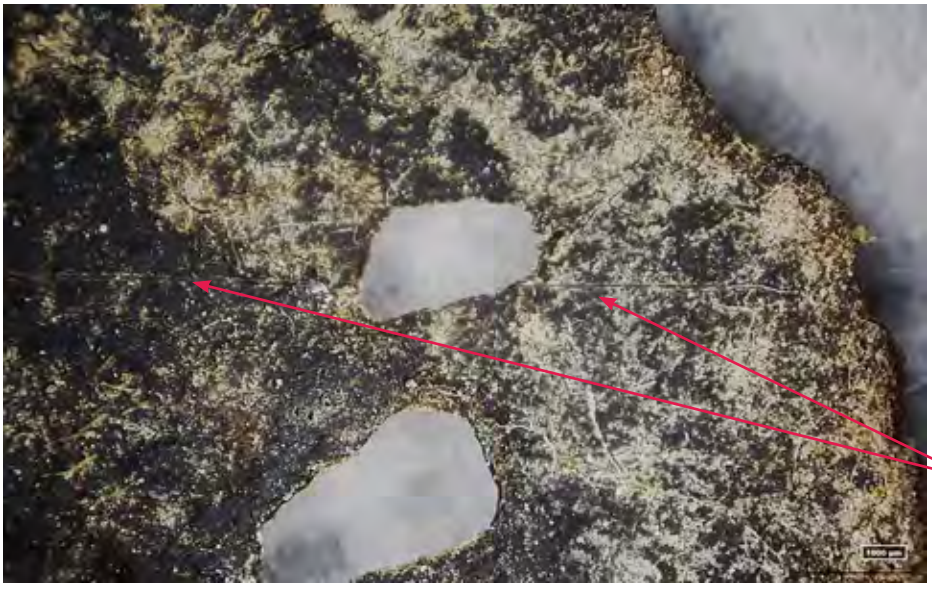

Ruling line guiding the first line of text is doubled on left side of loss area

File Name:	MOTB.SCR.003183/MOTB.SCR.003183012.jpg (Hirox) 6
Description:	Incised line is slightly doubled and lies underneath the second line of text near left edge

Horizontal ruling lines guiding the second line of text near the left edge of the fragment

File Name:	MOTB.SCR.003183/MOTB.SCR.003183017.jpg (stitched Hirox, horizontal)
Description:	Stitched image of incised ruling line for second line of text

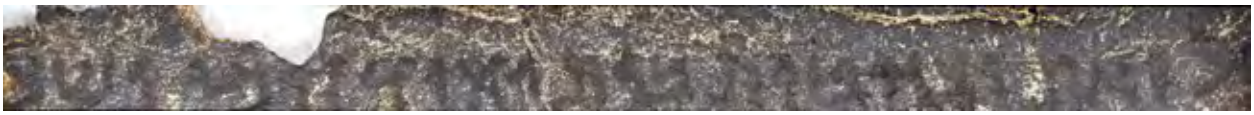

MOTB.SCR.0004742 (Leviticus)

Fragment No.	SIG.SCR.004742
Text	Leviticus
Inv Group	4
Notes	Included in BAM Report Sampled

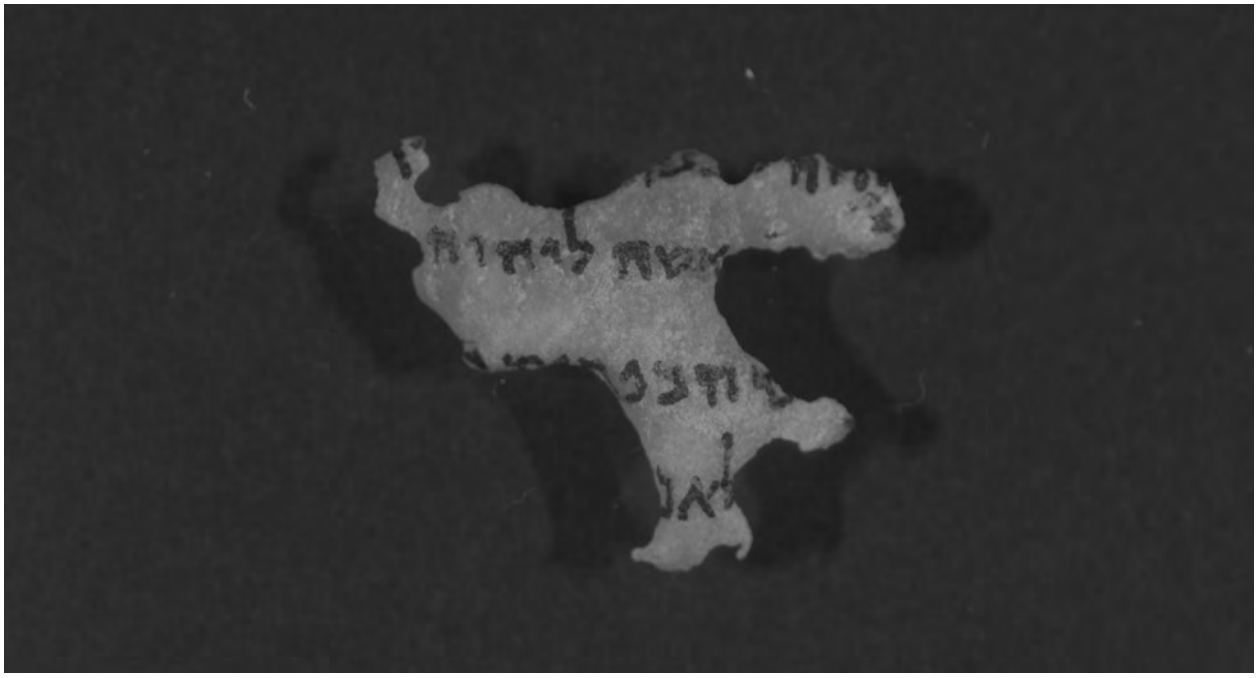

File Name:	MOTB.SIG.SCR.004742_001_PM_NL_20190424.tif (Micrograph) 1
Description:	Detail of bottom line of text; substrate is severely curled towards the verso (flesh side)

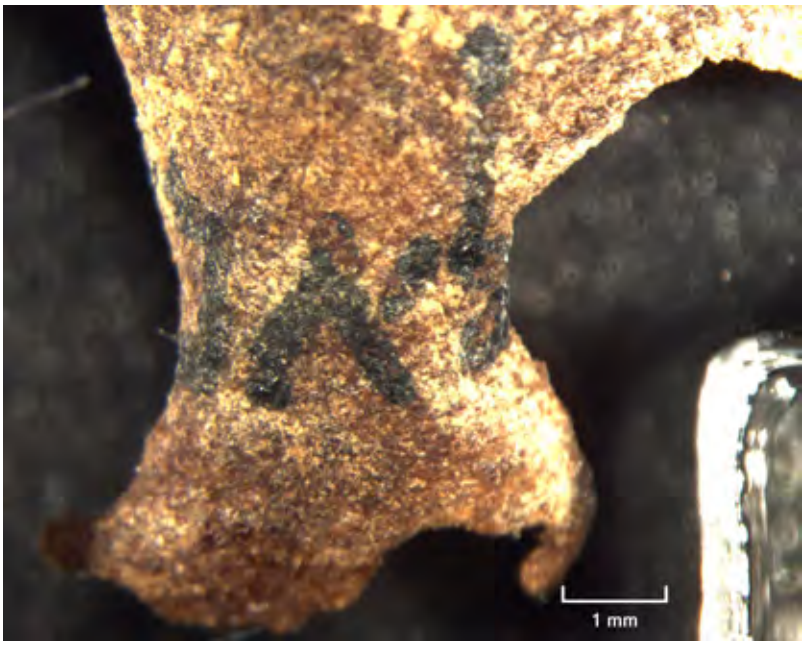

File Name:	MOTB.SIG.SCR.004742_007_PM_NL_TL_20190424.tif (Micrograph) 1
Description:	Detail of bottom line of text in transmitted and reflected illumination; translucency of substrate partially result of glue impregnation

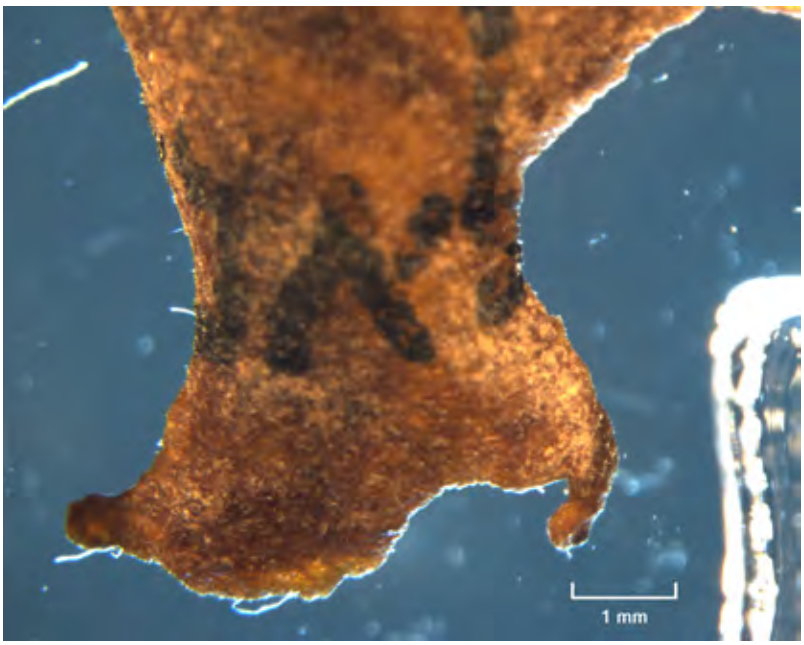

File Name:	MOTB.SIG.SCR.004742_002_PM_NL_20190424.tif (Micrograph) 2
Description:	Detail of incised line extending from left through the top of letter "hay" in third line of text

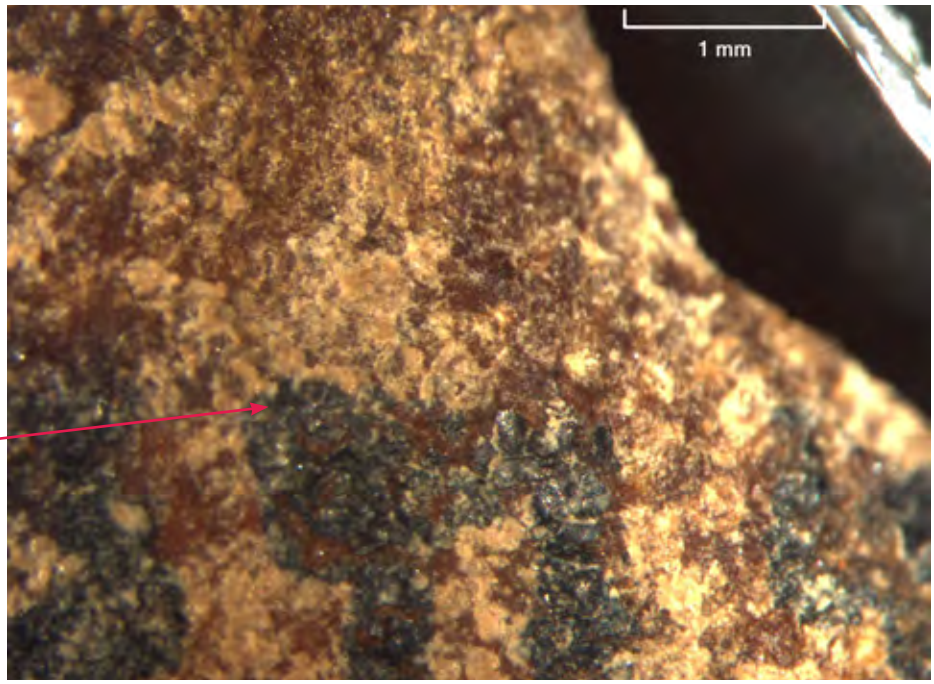

Faint incised line intersects with third line of text at center

File Name:	MOTB.SIG.SCR.004742_003_PM_NL_20190424.tif (Micrograph) 3
Description:	Detail of ink on top of deposits located below and right of center

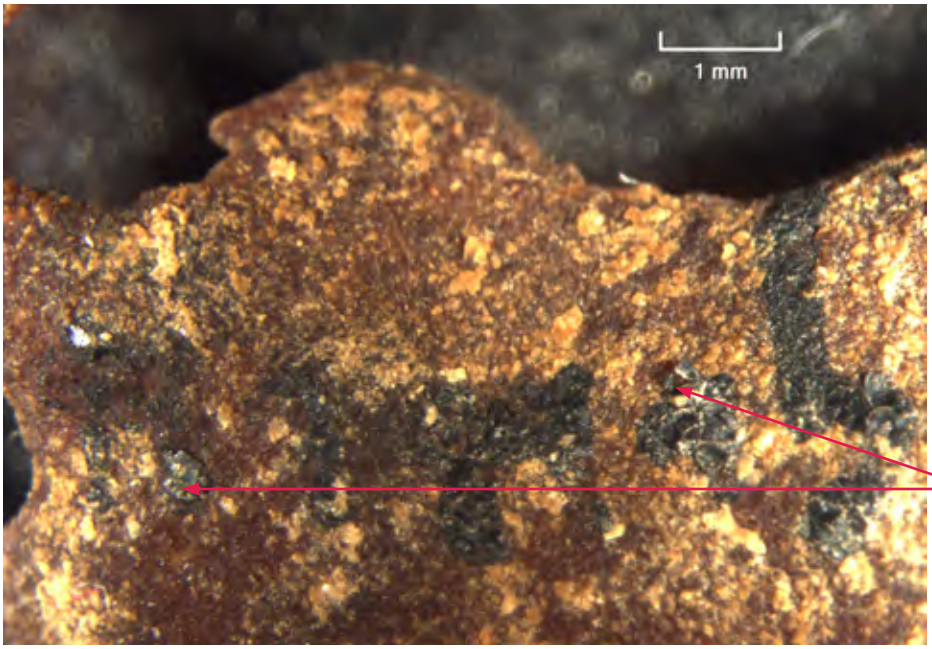

Ink applied on top of granular deposits on the fragment surface

File Name:	MOTB.SCR.004742/MOTB.SCR.004742002.jpg (Hirox)
Description:	Ink over surface deposits

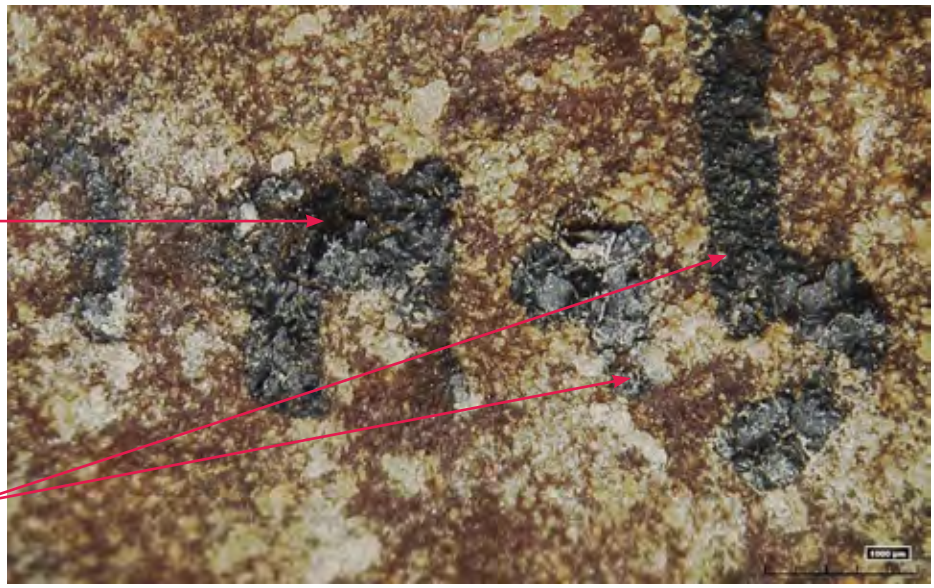

File Name:	MOTB.SCR.004742/MOTB.SCR.004742006.jpg (Hirox) 4
Description:	Ink flowing over edge

File Name:	MOTB.SCR.004742/MOTB.SCR.004742013.jpg (Hirox)
Description:	Detail of surface texture and amber color of substrate caused by glue impregnation

File Name:	MOTB.SCR.004742/MOTB.SCR.004742015.jpg (Hirox)
Description:	Detail in partial transmitted light to show uneven surface texture and translucency caused by glue impregnation

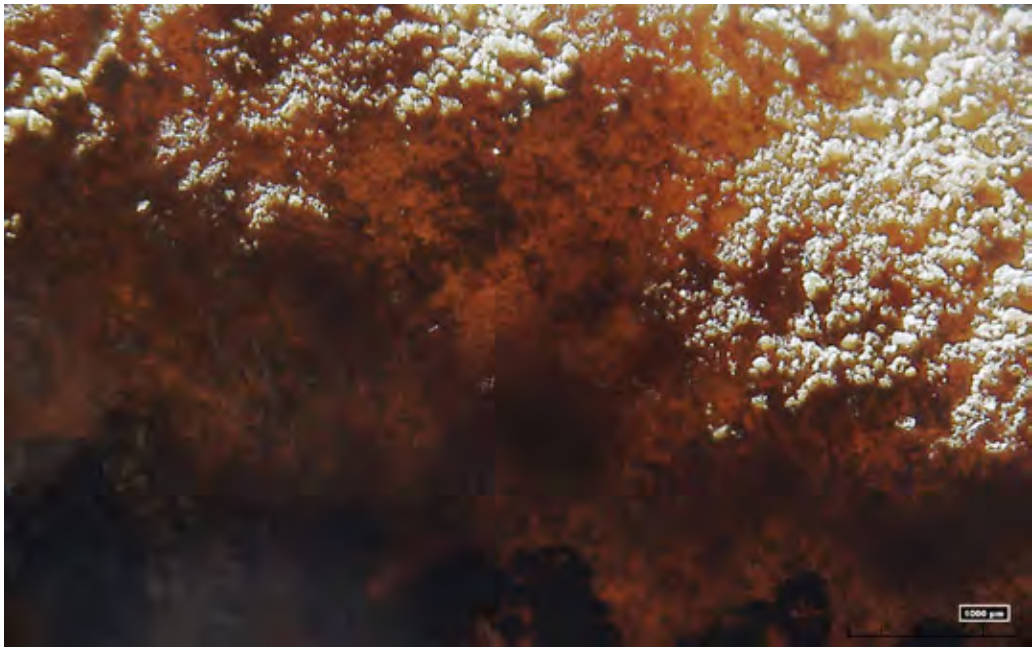

File Name:	MOTB.SIG.SCR.004742_005_PM_TL_20190424.tif (Micrograph)
Description:	Low magnification detail in transmitted light of top three lines of text highlighting texture of support and scattered dark stains most visible in transmitted light

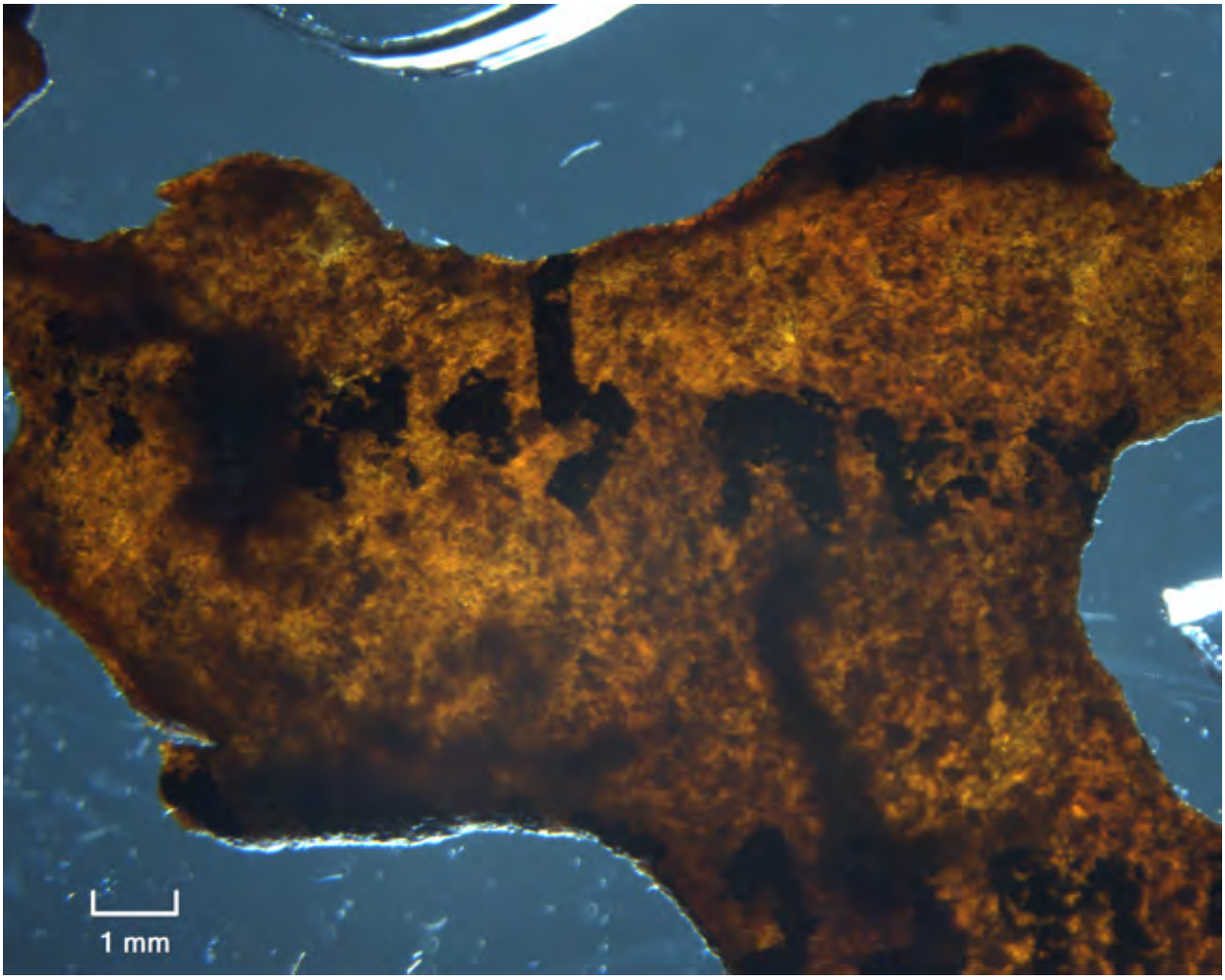

SCR.0004768 & SCR.004741

Fragment No.	SCR.004768 SCR.004741
Text	none
Inv Group	4
Notes	Previously connected Considered one material unit Not published Sampled

File Name:	MOTB.SCR.004768/MOTB.SCR.004768001.jpg (Hirox) 1
Description:	Bottom edge of fragment with the blackened grain layer curling up and the light brown core, which is saturated with dark amber glue, also delaminating.

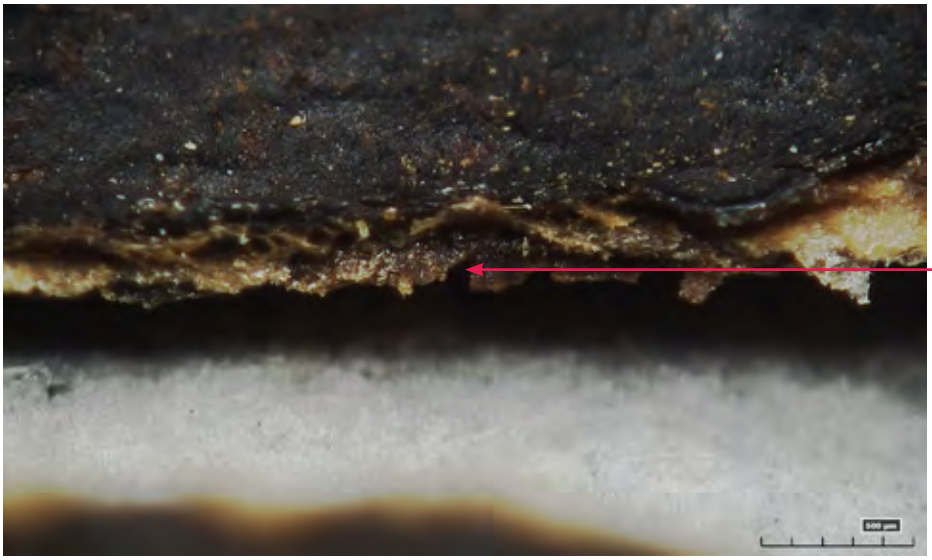

Delaminated, oxidized grain layer with lighter brown core of substrate saturated with amber glue

File Name:	MOTB.SCR.004768/MOTB.SCR.004768003.jpg (Hirox) 2
Description:	Lower left edge of fragment, with compressed fibers impregnated with amber glue; fine surface cracks radiate out from edge

Compressed, glue-impregnated fibers at edge where grain is missing; surface cracks radiate out from edge

File Name:	MOTB.SCR.004768/MOTB.SCR.004768004.jpg (Hirox) 2
Description:	Lower left edge of fragment with large white surface deposit and compressed fibers at edge; undulations grain layer are very pronounced

File Name:	MOTB.SCR.004741_001_PM_RL_20190424.tif (Micrograph) 3
Description:	Detail of top right edge of fragment, of what appears to be a horizontal incision line across edge. Multiple surface cracks radiate at a diagonal from top edge. Prominent rippling in grain layer at top left corner.

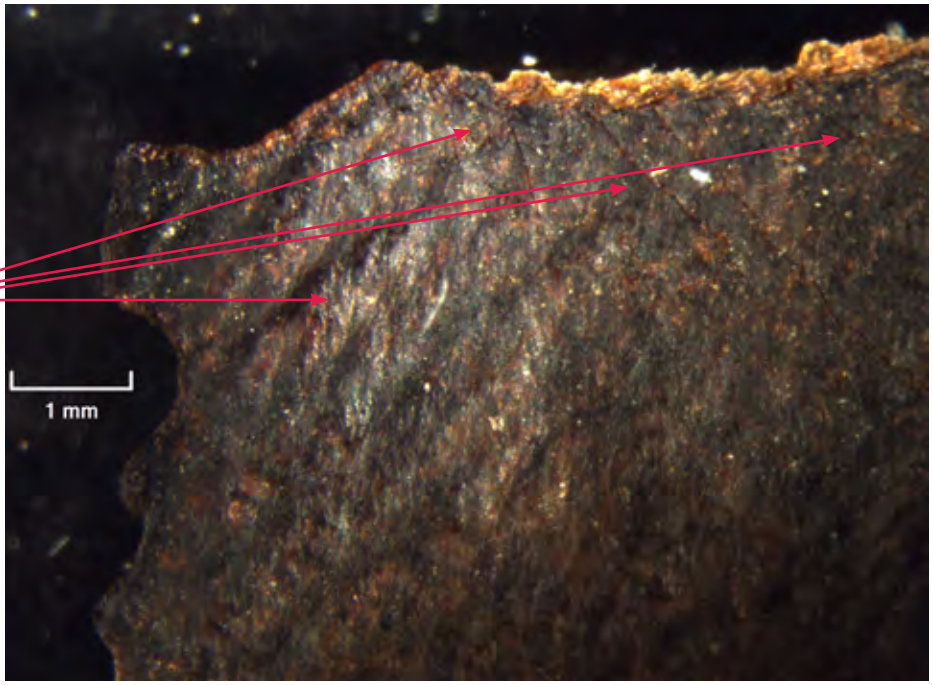

File Name:	MOTB.SCR.004741/MOTB.SCR.004741006.jpg (Hirox) 4
Description:	Bottom right tip of fragment that has delaminated, exposing light brown core and milky accretion that may be a modern acrylic adhesive

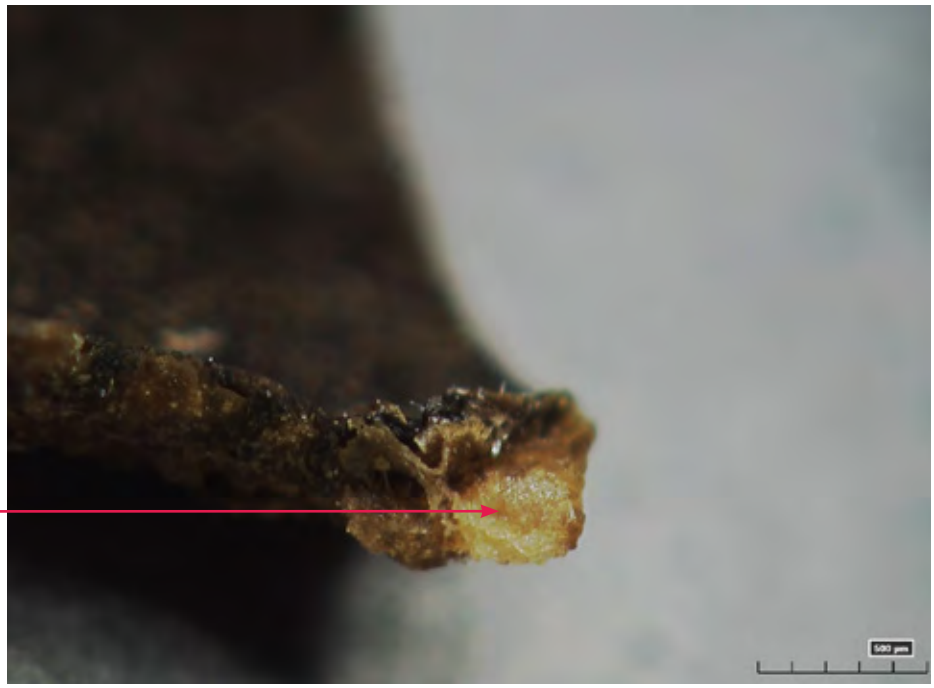

Milky white accretion (modern adhesive?) at tip of delaminated substrate

File Name:	MOTB.SCR.004741/MOTB.SCR.004741009.jpg(Hirox) 5
Description:	Right edge below center where oxidized grain layer is missing around perimeter of hole; intact grain beyond hole is delaminating

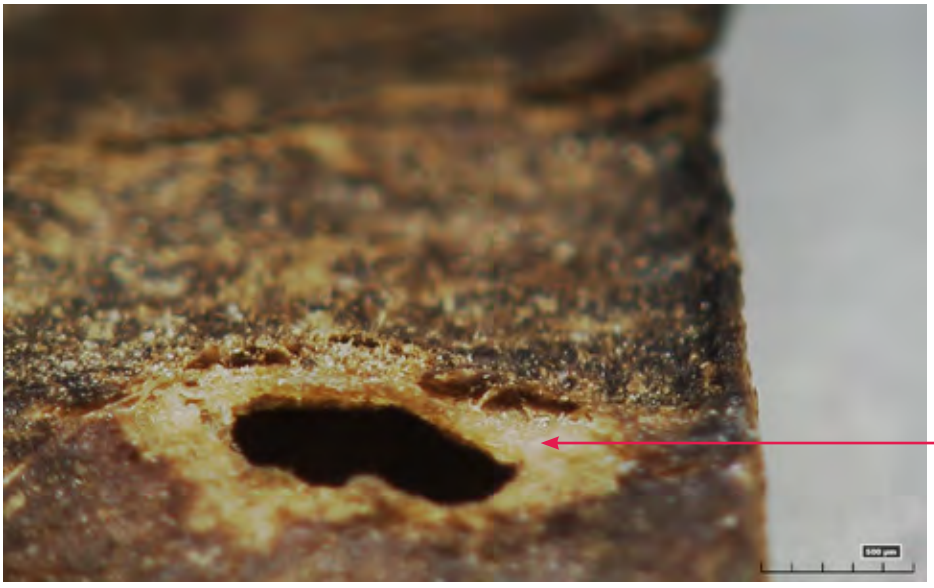

Oxidized grain layer appears to have been sliced off from around perimeter of hole

File Name:	MOTB.SCR.004741/MOTB.SCR.004741012.jpg (Hirox) 6
Description:	Left section of fragment, top edge with large loss. Substrate to left of loss is bent over, darkened grain layer continues to very edge. Rippling in grain layer is prominent.

Edges of substrate are bent over; oxidized grain layer extends to edge

SCR.004769

Fragment No.	SCR.004769
Text	Four visible letters
Inv Group	4
Notes	Not published

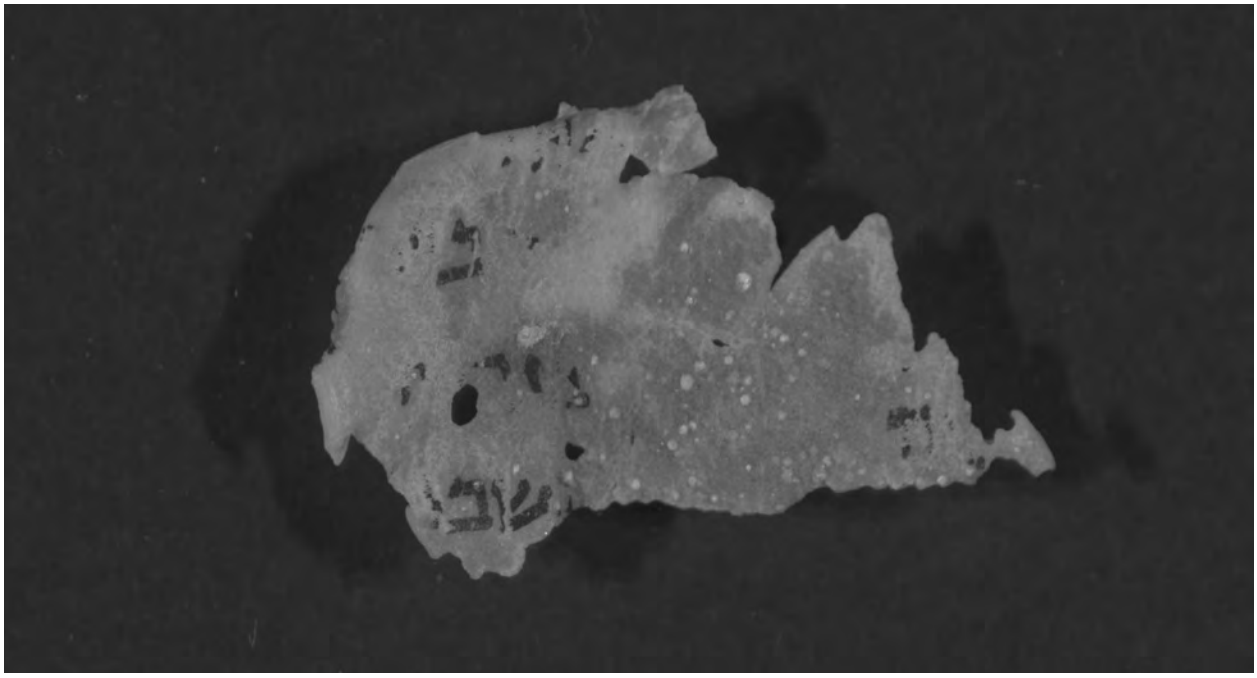

File Name:	MOTB.SCR.004769_002_PM_NL_20190424.tif (Micrograph)
Description:	Bottom edge, near left edge with ink fragments; thick, bulbous accretions and crusty surface deposits; substrate appears severely deteriorated with significant loss of grain layer and numerous cracks

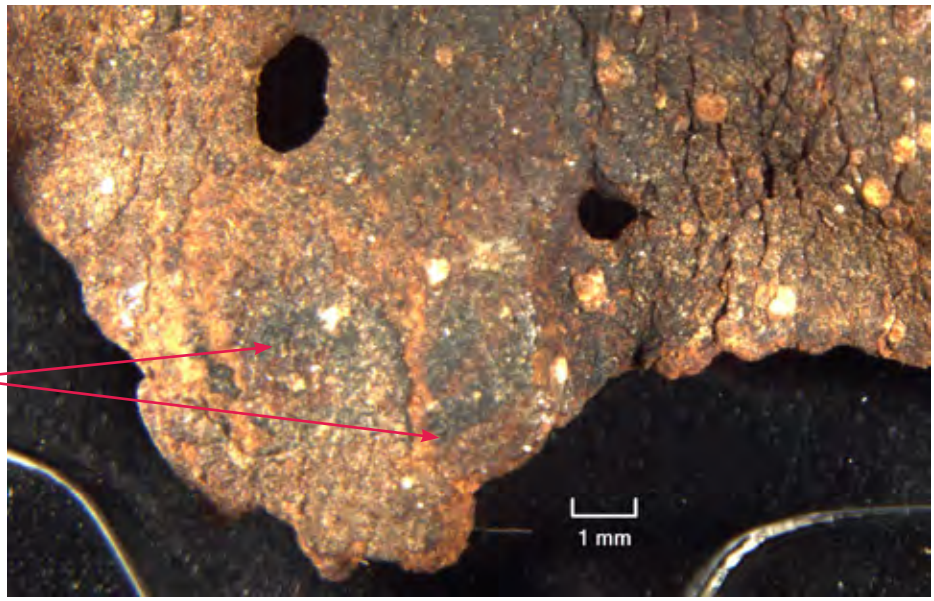

Fragments of inked letters on top of intact portions of grain layer

File Name:	MOTB.SCR.004769/MOTB.SCR.004769001.jpg (Hirox) 1
Description:	Crusted mineral deposits under fragments of inked letters

Mineral deposits under areas of inked letters; lighter brown areas are where grain layer is missing

File Name:	MOTB.SCR.004769/MOTB.SCR.004769002.jpg (Hirox) 1
Description:	Lower left quadrant, extensive loss of grain in center with surviving grain layer black from oxidation; surface covered with crusty deposits

Large area of grain loss bordered by intact grain that has blackened from oxidation; thick, crusty deposits over entire surface

File Name:	MOTB.SCR.004769_005_PM_NL_20190424.tif (Micrograph) 2
Description:	Bottom edge, left of center and to right of small hole. Detail of severe cracking and delamination in substrate with thick, crusty surface deposits

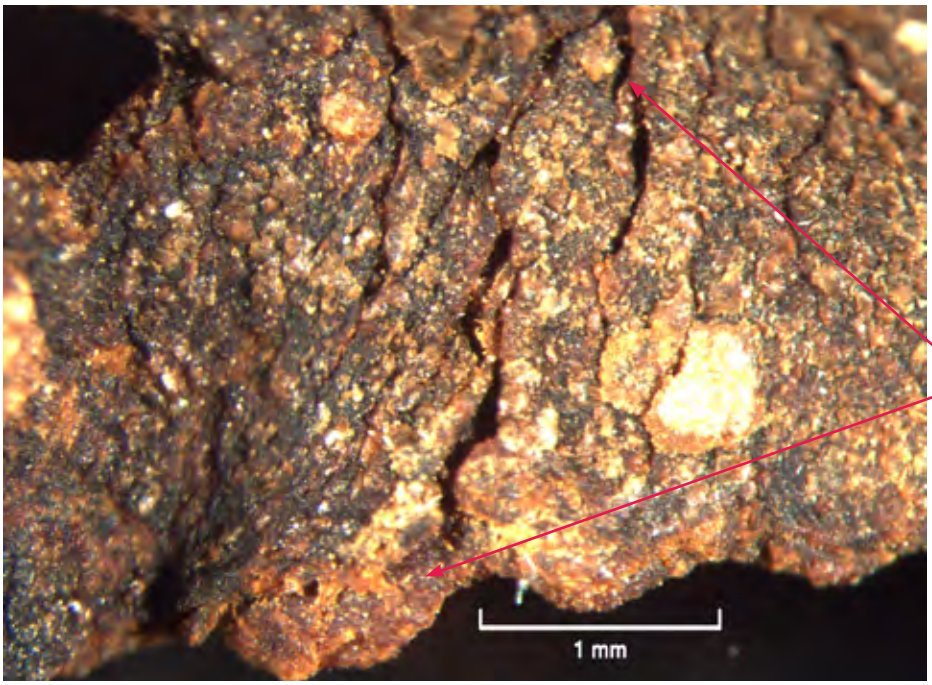

Extensive cracking and delamination of grain layer; crusty deposits

File Name:	MOTB.SCR.004769_004_PM_NL_20190424.tif (Micrograph) 3
Description:	Detail of large white deposits, right of center, that appear to be covered with finer deposits and a coating of amber glue

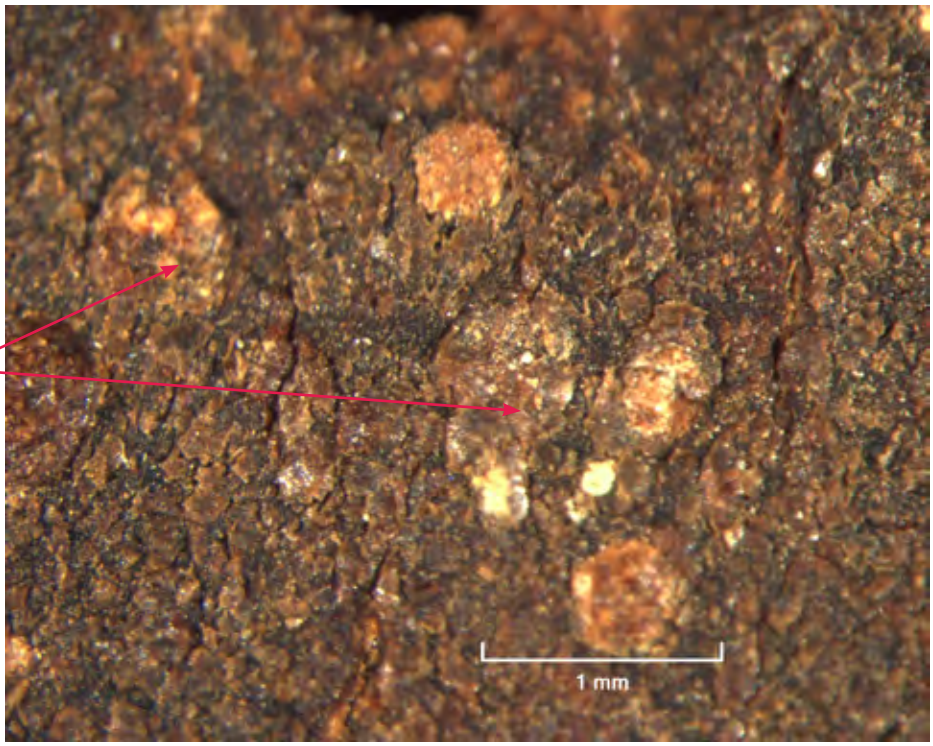

Large white deposits appear embedded in grain surface and covered with additional deposits and a layer of amber glue

File Name:	MOTB.SCR.004769/MOTB.SCR.004769010.jpg (Hirox) 4
Description:	Large crusty deposits on surface also coated with amber glue; grain layer exhibits losses and is very deteriorated

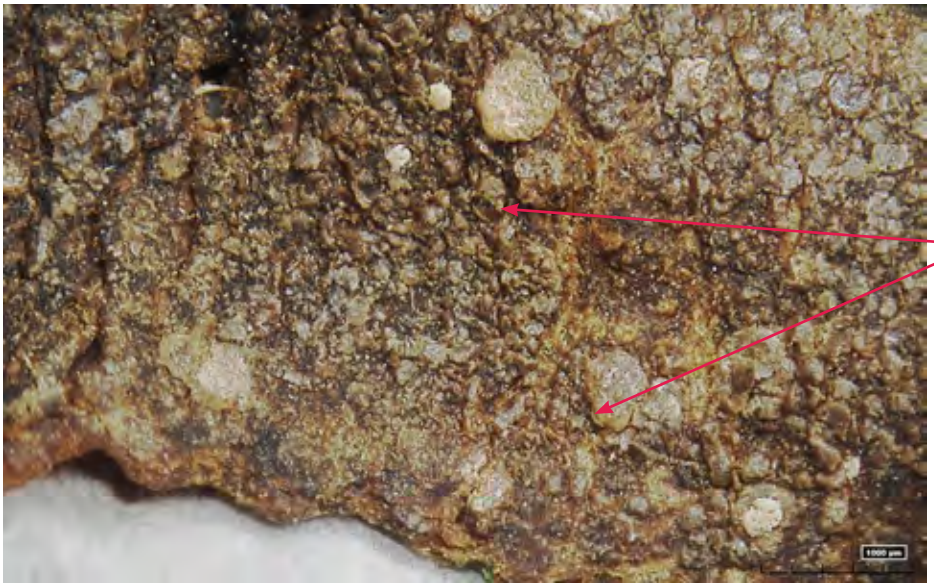

Thick, irregular mineral deposits on deteriorated fragment surface

File Name:	MOTB.SCR.004769_001_PM_NL_20190424.tif (Micrograph) 5
Description:	Bottom edge near right edge, broad view of deteriorated support surface with multiple cracks and large bulbous accretions; diagonal scratch or incision line originates at left

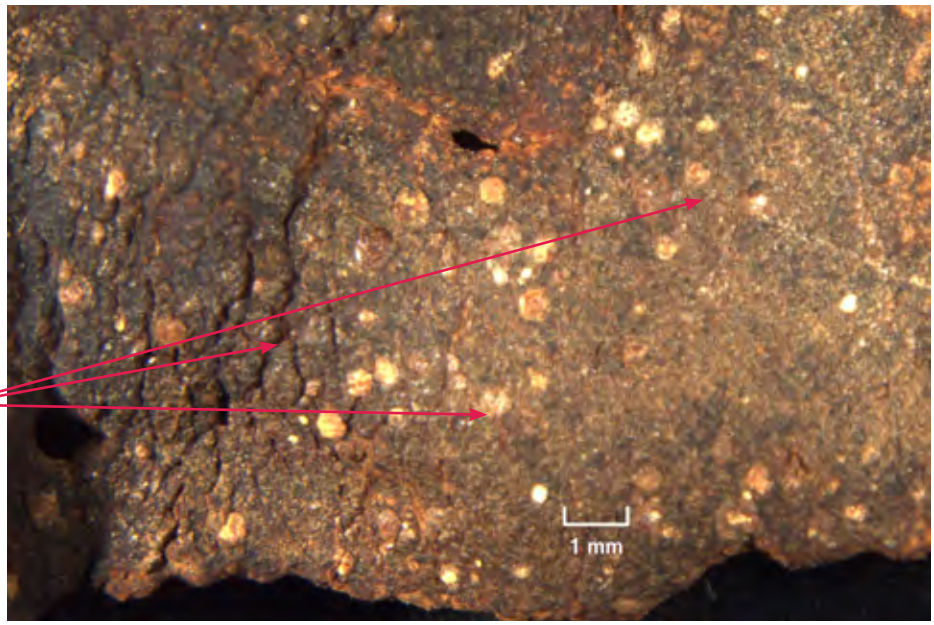

Large white accretions embedded in grain surface, multiple deep cracks; diagonal scratch or incision line at right

File Name:	MOTB.SCR.004769_003_PM_NL_20190424.tif (Micrograph) 6
Description:	Detail of top center, to the left of small loss with extant fragments of inked letters on deteriorated grain surface covered with crusty deposits

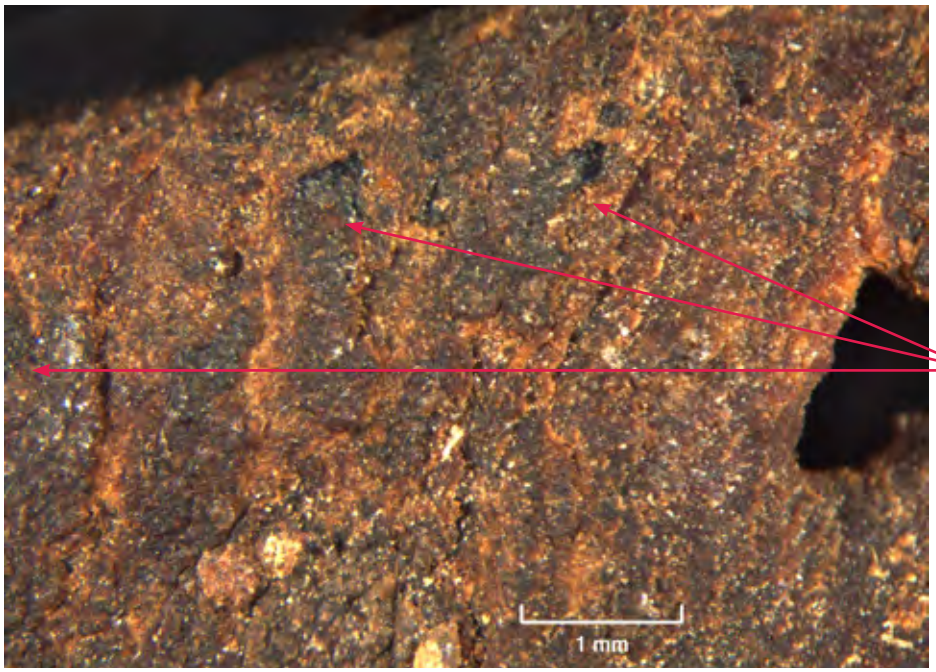

Fragments of inked letters over intact areas of the grain layer

File Name:	MOTB.SCR.004769/MOTB.SCR.004769003.jpg (Hirox) 7
Description:	Left edge where a large area of grain is missing; raised grain in right half of image is black from oxidatoin

Large area of grain missing on left; intact oxidized grain on right is very raised with a pronounced texture

File Name:	MOTB.SCR.004769/MOTB.SCR.004769017.jpg (Hirox) 8
Description:	Reverse of fragment with concave edges and partially detached portion at right impregnated with amber glue and slightly translucent

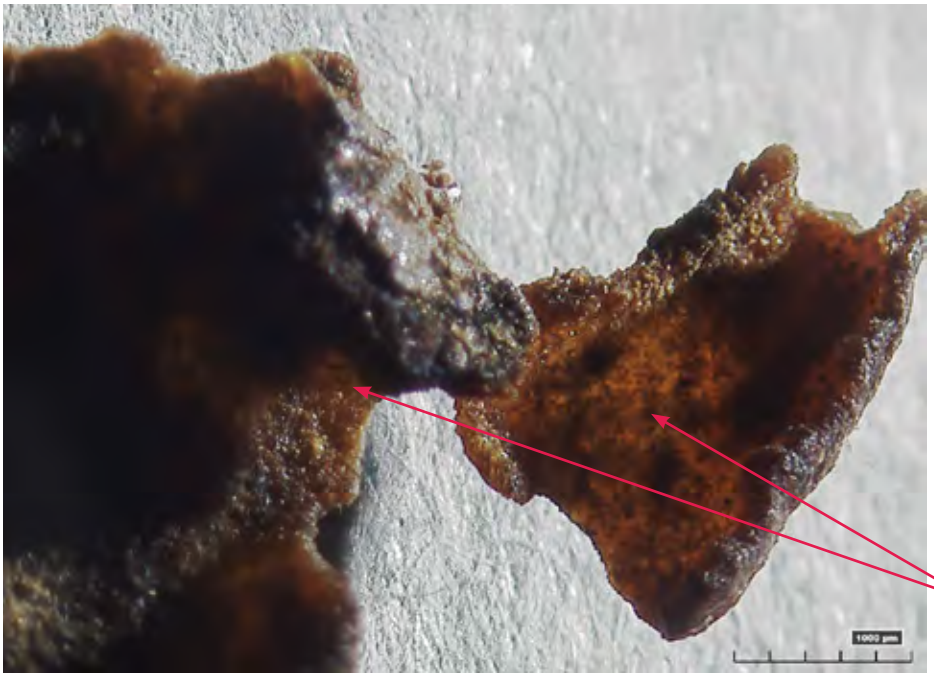

Edges of reverse of fragment are curled under; partially detached piece at right is translucent due to glue impregnation

Results of Molecular, Elemental and Chemical Analysis

FTIR Report (SAFA)..... 107
XRF Report (Aaron Shugar) 167
SEM Report (Aaron Shugar 187
Microchemical Test Summary (Rebecca Pollak)..... 206



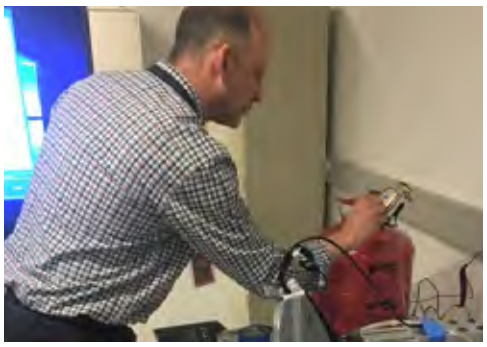





Scientific Analysis of Fine Art Report 1931

September 1, 2019

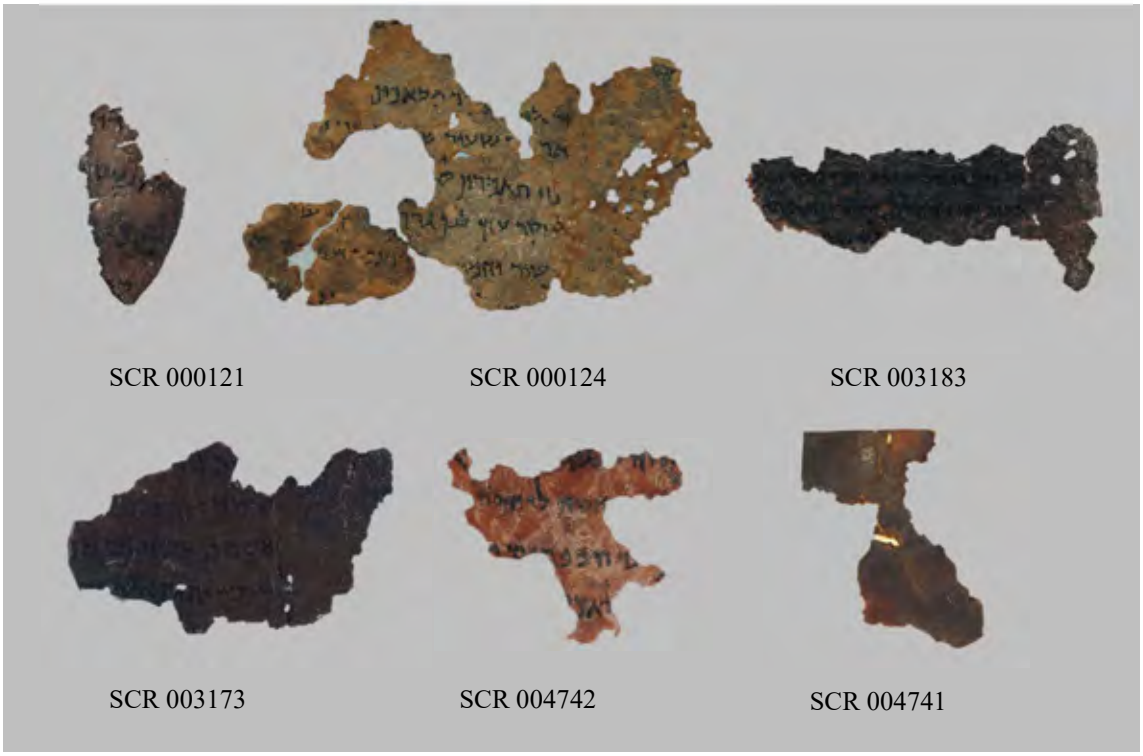

Accession number and description	Overall dimensions	
	horizontal (cm)	vertical (cm)
SCR 000121, text: Psalms, inventory group no. 1	2.0	2.5
SCR 000124, text: Genesis, inventory group no. 2	8.9	5.5
SCR 003173, text: Numbers, inventory group no. 3	4.4	2.5
SCR 003183, text: Micah, inventory group no. 3	6.1	2.9
SCR 004741, possible unidentified text, inventory group no. 5	ca. 1.9	ca. 1.2
SCR 004742, text: Leviticus, inventory group no. 4	2.1	2.5

Executive Summary

Molecular and mineralogical analysis of the Museum of the Bible Dead Sea Scroll surface sedimentary deposits, undocumented conservation treatments, other applied coatings (i.e., for artificial aging), and writing inks was carried out using Fourier transform infrared spectroscopy (FTIR). This technique is sensitive to inorganic materials such as the mineral deposits on the scroll fragments, and to organic materials such as ink binders and any transparent/translucent coatings applied to the parchment or leather substrates. In addition to materials that have been used to prepare the fragments, this technique can identify chemical changes that have occurred over time as the materials have interacted with each other and/or their environment (degradation/alteration products). Conservation and restoration treatments that have been applied to the fragments can also be identified.

All organic and inorganic phases identified in the inks, sediment deposits, and surface coatings of the six studied fragments are summarized in Table 1-3. Analytical results for each fragment are summarized in Table 4-9. Notable and/or representative samples are discussed in greater detail in the Context and Discussion sections below.

The fragment substrates are either parchment or leather, and the period technology anticipated for these substrates should be an enzymatic depilation rather than a lime process.[1] Alum treatment is suggested by a correlation of potassium, aluminum, and sulfur (see Aaron Shugar's MA-XRF report) [$KAl(SO_4)_2 \cdot 12H\ 2O$]. Evidence of alum has been observed previously by Rabin et al. for a Temple Scroll fragment.[2] No tannins were identified in any parchment or ink samples, suggesting it was not used in the preparation of the parchment for writing, nor is it a component of a natural gum or ink additive. The inks on all fragments are carbon based and are predominantly bound with tree gums such as gum Arabic. All findings of an animal skin glue are indicative of a protein coating on the fragments, either inherent in the preparation of the parchment or as a result of degradation of the collagen substrate. Infrared spectroscopy cannot identify which specific type of protein has been applied. For example, a mammalian hide glue protein will appear identical to a fish glue or a casein (milk protein) using this technique. A chromatography technique that identifies the amino acid distributions of the proteins, such as gas chromatography-mass

[1] Tigchelaar, E. "The Material Variance of the Dead Sea Scrolls: On Texts and Artefacts." *Hts Teologiese Studies/theological Studies* 72, no. 4 (2016): 6. 2016.; Poole, J. B, and R. Reed. "The Preparation of Leather and Parchment by the Dead Sea Scrolls Community." *Technology and Culture* 3, no. 1 (1962): 1-26.
[2] Rabin, I., and O. Hahn. "Characterization of the Dead Sea Scrolls by Advanced Analytical Techniques." *Analytical Methods* 5, no. 18 (2013): 4648-654.

spectrometry, would be required to distinguish among the different protein sources (however this technique requires a sample roughly ten times the size of an infrared spectroscopy sample).

The mineralogical findings from the FT-IR (and MA-XRF) data are consistent with the known compositions of mineral evaporites at the Dead Sea, the mineral deposits in the caves at Qumran, and the literature on the mineralogy of other studied DSS fragments.[3] The inorganic sediments identified on the fragments included calcite (chalk), clay minerals, quartz, gypsum, dolomite (a calcium and magnesium carbonate), ankerite (a mixed metal carbonate containing iron and manganese), and calcium silicates. The identification of calcium carbonate on each fragment, as well as changes in the amide I and II band positions observed in the FT-IR spectra of the studied parchment samples,[4] suggest a lime depilation process that would be anachronistic for the dates of the texts since lime depilation was not introduced until the fourth century CE.[5] However, deposition of carbonates from the surrounding burial environment is observed on artifacts from the Qumran caves.[6] Additionally, the changes in the amide I and II band positions and heights observed in the studied fragments may also be attributed to collagen denaturation and hydrolysis, which can also contribute to a similar phenomenon.[7]

Traces of cerussite impurity are also suggested in one fragment (a lead carbonate). The clay mineral spectra identified most closely correspond to kaolinite, illite, montmorillonite, and attapulgite clays. However, x-ray diffraction would be needed to go beyond classes of clays to specify all individual clay minerals. These minerals have highly substituted and variable formulations and frequently occur as complex mixtures. A more detailed discussion of the mineralogy of the deposits found on the fragments and how it relates to the MA-XRF findings is presented in the Discussion section of this report. Study of the chlorine to bromine ratios by SEM-EDS (scanning electron microscopy-energy dispersive x-ray spectrometry) for comparison to the ratios in the Rabin report is ongoing.

---

[3] Derrick, M. R. "Evaluation of the State of Degradation of Dead Sea Scroll Samples Using Ft-Ir-Spectroscopy." *Book and Paper Group Annual* 10 (1991): 49-65; Arieh Singer, Eliezer Ganor, Stefan Dultz, and Walter Fischer, "Dust Deposition over the Dead Sea", *Journal of Arid Environments* (2003), 53:41-59.

[4] Bicchieri, M., et al. "Non-Destructive Spectroscopic Characterization of Parchment Documents." *Vibrational Spectroscopy* 55, no. 2 (2011): 267-72.

[5] Poole, J. B, and R. Reed. "The Preparation of Leather and Parchment by the Dead Sea Scrolls Community." *Technology and Culture* 3, no. 1 (1962): 1-26.

[6] Rabin, I. "Archaeometry of the Dead Sea Scrolls." *Dead Sea Discoveries* 20, no. 1 (2013): 124-42.

[7] Derrick, M. R. "Evaluation of the State of Degradation of Dead Sea Scroll Samples Using Ft-Ir-Spectroscopy." *Book and Paper Group Annual* 10 (1991): 49-65; Vyskočilová, Gabriela, et al. "Model Study of the Leather Degradation by Oxidation and Hydrolysis." *Heritage Science* 7, no. 1 (2019): 1-13.

The degradation products identified on the fragments include calcium oxalate and calcium stearate. The calcium stearate is thought to be a reaction between the calcium-containing deposits on the parchment (likely chalk from a lime depilation) reacting with residual fats present in the animal hide substrate (stearic acid). Calcium oxalate is formed as a result of bacterial and fungal attack of chalk-containing parchment fragments. These processes are discussed more fully in the Context section below.

The conservation adhesives and consolidants identified on the fragments include an acrylic polymer, an alkyd resin (a type of synthetic drying oil), and, primarily, cellulosic materials such as cellulose gum(s) and wheatstarch. Repairs on the verso of the fragments indicate that they have undergone previous conservation treatments, but no conservation records are available. A biocidal material, isothiasolinone, was also suggested by the data.

Aside from unambiguous conservation materials, no anachronistic or anomalous materials were identified in the studied fragments. The state of degradation and minerology of the parchment samples suggests they may old or ancient, however, physical clues, such as the application of ink over delaminated support material and sediment, as well as cracks in several fragments, suggests that much or all of the ink may have been applied more recently. The mineral deposits and degradation products found are consistent with those identified on period archaeological parchment or leather. Without radiocarbon dating, however, an exact date cannot be assigned to the substrates. Radiocarbon dating of these pieces would be problematic, however, due to the carbon-containing conservation treatments the fragments have undergone. Similarly, if soot/carbon-black inks with no modern additions are used one cannot draw a conclusion about their age. The plant gum binder observed for the inks here has been used since antiquity.

Fourier Transform Infrared Spectroscopy (FT-IR) results of inks, sediment deposits, and coatings of studied fragments

Table 1. Inks - Summary of organic phases identified in the ink samples of the studied fragments.

Fragment	INK – organic phases identified	best match(es)
000121	animal skin glue cellulosic material	 hemicellulose
000124	animal skin glue tree gum cellulosic material	 gum Arabic cellulose
003173	animal skin glue tree gum	 gum Arabic

	calcium oxalate	
003183	NA	
004741	animal skin glue polysaccharide	sturgeon glue with honey
004742	animal skin glue	

Table 2. Sediments - Summary of inorganic phases identified in the sediment samples of the studied fragments.

Fragment	SEDIMENT – inorganic phases identified		best match(es)
000121	cream	calcium carbonate phyllosilicate clay quartz	illite
	tan	calcium carbonate phyllosilicate clay	kaolinite
	black	calcium carbonate phyllosilicate clay quartz	montmorillonite
000124	cream	calcium carbonate calcium oxalate calcium stearate gypsum phyllosilicate clay	attapulgite, montmorillonite
003173	cream	calcium carbonate gypsum phyllosilicate clay quartz	kaolinite, montmorillonite
003183	tan	calcium carbonate dolomite gypsum phyllosilicate clay quartz	kaolinite, montmorillonite
004741	cream	calcium carbonate cerussite	

		phyllosilicate clay quartz	illite
004742	cream	calcium carbonate phyllosilicate clay	kaolinite, montmorillonite
	tan	ankerite phyllosilicate clay calcium silicate	kaolinite, montmorillonite

Table 3. Coatings - Summary of organic phases identified in the coatings and other surface materials sampled from the studied fragments.

Fragment	COATING – organic phases identified		best match(es)
000121	saturated fibrils	animal skin glue cellulosic material bromine compound	 hemicellulose 2,5-dibromonitrobenzene
	pink accretion	alkyd polymer	Aralon 970
000124	fibrils	cellulosic material	cellulose
003173	fibrils	animal skin glue cellulosic material	 hemicellulose
	glossy material over ruled lines	acrylic copolymer	methyl methacrylate n-butyl acrylate
	mount adhesive	cellulosic material	wheat starch
003183	amber material	animal skin glue	
004741		cellulosic material calcium stearate	jute fiber, Kayocel 10-NC-50 [cellulose fiber with inorganic filler]
004742	orange resinous material	animal skin glue poss. biocide	 isothiasolinone

	parchment [diffuse reflectance]	cellulosic material	cellulose [microscope reflection], viscose rayon

Fourier Transform Infrared Spectroscopy (FT-IR) results of inks, sediment deposits, and coatings identified in each studied fragment

Figure 1. SCR 000121, text: Psalms, inventory group no. 1, figure of fragment recto (*left*) and verso (*right*) with sampling locations marked on it.

Table 4. SCR 000121 summary of Fourier Transform Infrared Spectroscopy (FT-IR) results

Sample	Material	Phases identified	
3	ink	animal skin glue, cellulosic material [best match hemicellulose]	
1	sediment	cream particle	calcium carbonate, phyllosilicate clay [best match illite], quartz
5		tan particle	calcium carbonate, phyllosilicate clay [best match kaolinite]

6		black particle	calcium carbonate, phyllosilicate clay [best match montmorillonite], quartz
5	coating	saturated fibrils	animal skin glue, cellulosic material [best match hemicellulose], poss. bromine compound [best match 2,5-dibromonitrobenzene]
4		pink accretion	alkyd polymer (a synthetic drying oil)

Figure 2. SCR 000124, text: Genesis, inventory group no. 2, figure of fragment with sampling locations marked on it.

Table 5. SCR 000124 summary of FT-IR results

Sample	Material	Phases identified	
2	ink	animal skin glue, tree gum, cellulosic material [best match cellulose]	
1	sediment	cream particle	calcium carbonate, calcium oxalate, calcium stearate, gypsum, phyllosilicate clay [attapulgite, montmorillonite]
2	coating	fibrils	cellulosic material [best match cellulose]

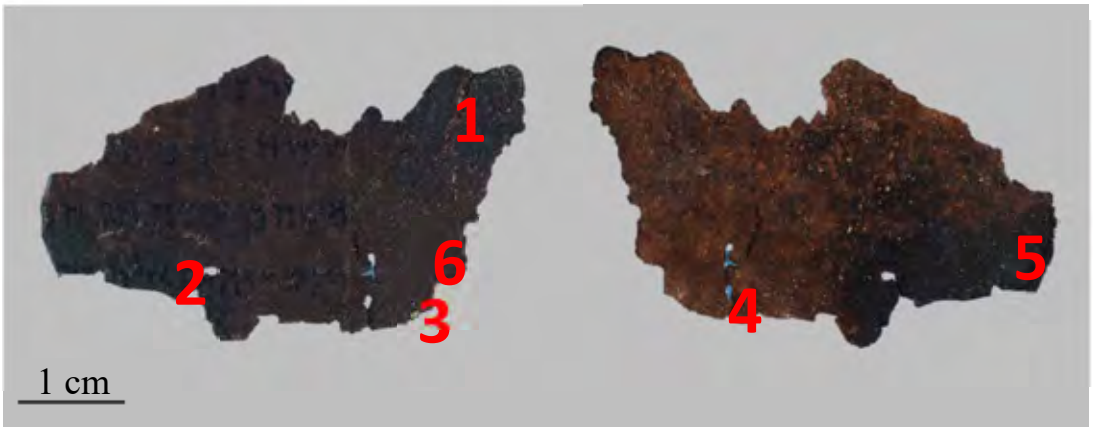

Figure 3. SCR 003173, text: Numbers, inventory group no. 3, figure of fragment recto (*left*) and verso (*right*) with sampling locations marked on it.

Table 6. SCR 003173 summary of FT-IR results

Sample	Material	Phases identified	
2	ink	animal skin glue, tree gum, calcium oxalate	
1, 3	sediment	cream particles	calcium carbonate, gypsum, phyllosilicate clay [best matches kaolinite, montmorillonite], quartz
4	coating	fibrils	animal skin glue, cellulosic material [best match hemicellulose]
6		glossy material over ruled lines	acrylic copolymer [best match methyl methacrylate n-butyl acrylate]
5		mount adhesive	cellulosic [best match wheat starch]

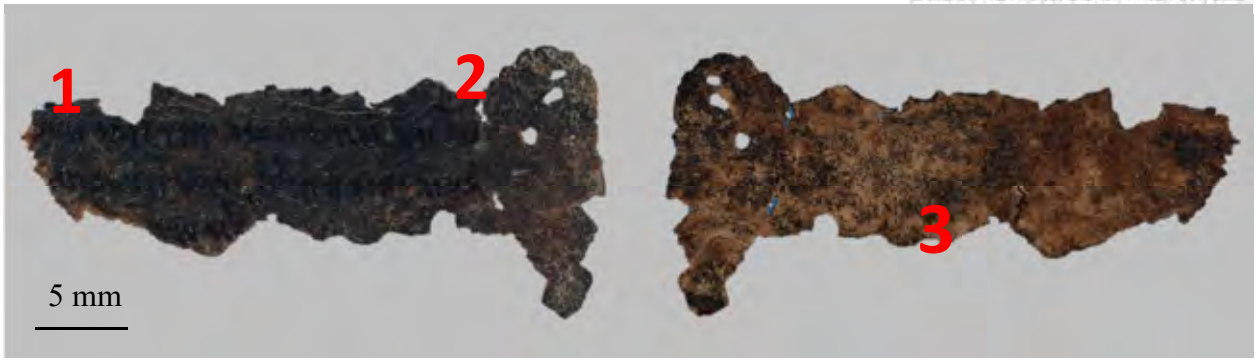

Figure 4. SCR 003183, text: Micah, inventory group no. 3, figure of fragment recto (*left*) and verso (*right*) with sampling locations marked on it.

Table 7. SCR 003183 summary of FT-IR results

Sample	Material	Phases identified	
	ink	NA	
3	sediment	tan particles	calcium carbonate, dolomite, gypsum, phyllosilicate clay [best matches kaolinite, montmorillonite], quartz
2	coating	amber material	animal skin glue

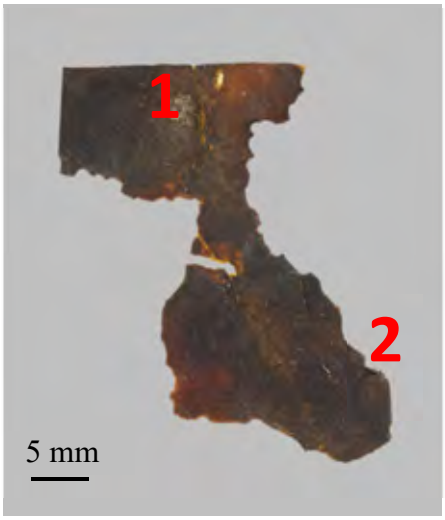

Figure 5. SCR 004741, possible fragments of unidentified text in two locations, inventory group no. 5, figure of fragment with sampling locations marked on it.

Table 8. SCR 004741 summary of FT-IR results

Sample	Material	Phases identified	
2	ink	animal skin glue, polysaccharide [best match sturgeon glue with honey]	
1	sediment	cream particle	calcium carbonate, cerussite, phyllosilicate clay [best match illite], quartz
1	coating	cellulosic material [best match cellulose], calcium stearate	

Figure 6. SCR 004742, text: Leviticus, inventory group no. 4, figure of fragment recto (*left*) and verso (*right*) with sampling locations marked on it.

Table 9. SCR 004742 summary of FT-IR results

Sample	Material	Phases identified	
2	ink	animal skin glue, calcium carbonate	
1	sediment	cream particle	calcium carbonate, phyllosilicate clay [kaolinite, montmorillonite]
3		tan and cream particles	ankerite, phyllosilicate clay [kaolinite, montmorillonite], calcium silicate
4	coating	orange resinous material	animal skin glue, poss. biocide [best match isothiasolinone]
NA		parchment [diffuse reflectance]	cellulosic material [best match cellulose]

Context

Summary of Parchment Production Technology in Antiquity

The main constituent of parchment is collagen, a structural organic polymeric protein composed of triple-helix units that arrange to form the fibrils that compose a collagen fiber. In contrast to leather, in parchment manufacture the animal skin undergoes a procedure to dehair the skin and dry it under tension to transform the three-dimensional fiber network to a flat, two-dimensional surface. Prior to the fourth century, the dehairing process was performed with enzymatic depilation.[8] After being flayed, the skin was soaked in water to prepare it for a prolonged bath of dung, flour, or fermented vegetable matter. Other materials described in the dehairing process include goat's milk, vegetable oils, and animal fat. Details regarding ancient methods and materials used to finish the skins are not well documented, but it is presumed that they are not dissimilar to methods recorded in the middle ages in which chalk and powdered pumice were applied to the flesh side to assist with degreasing and smoothing the surface. Vegetable tannins (plant polyphenols) were sometimes applied to the surface in the last stage after cleaning and drying, or were applied as a treatment before the writing surface would be inscribed with ink. Tannins bind to the collagen proteins in the outer layers of the skin, improving their resistance to water and bacterial degradation. Materials used for tanning included alum, wine, gallnuts and myrrh.[9] Ancient ritual procedures for parchment-like materials used for Jewish texts involved the application of small amounts of vegetable tannage or cedar oil on the writing support's surface, often together with alum and/or other salts.[10] However, tannins have not always been identified in period Jewish texts, nor were they identified in molecular analysis of the studied scroll fragments. It is possible that other organic tanning agents may be present in the studied fragments but in amounts too small to detect by infrared spectroscopy.[11]

---

[8] Poole, J. B, and R. Reed. "The Preparation of Leather and Parchment by the Dead Sea Scrolls Community." *Technology and Culture* 3, no. 1 (1962): 1-26.

[9] Bicchieri, M., et al. "Non-Destructive Spectroscopic Characterization of Parchment Documents." *Vibrational Spectroscopy* 55, no. 2 (2011): 267-72.

[10] Poole, J. B., and R. Reed. "The Preparation of Leather and Parchment by the Dead Sea Scrolls Community." *Technology and Culture* 3, no. 1 (1962): 1-26.

[11] Bicchieri, M., et al. "Non-Destructive Spectroscopic Characterization of Parchment Documents." *Vibrational Spectroscopy* 55, no. 2 (2011): 267-72.

The term "parchment" is formally used to describe a process established in the fourth century CE in which animal skins are depilated in a bath of calcium hydroxide (lime), dried under tension (typically on a wooden stretching frame), but are not tanned. The stretched skin would be scraped and polished to align the collagen fibers parallel to the surface. Some collagen breaks down to form a glue (gelatin) that hardens as the skin dries, helping to create a smooth, firm surface.

Differentiation of the two processes has been described based on microscopic examination and molecular analysis. Typically, limed parchment comprises a dense network of large, cylindrical, fibers that run parallel to the skin surface with gelatin localized on the surface.[12] In general, ancient preparations utilizing enzymatic depilation result in shorter fibers with a less ordered network, although many fibers do run parallel to the surface and can appear similar to modern parchment. Other morphological differences include more inclusions in the fiber structure as a result of organic materials applied in the enzymatic bath, and penetration of any applied tanning materials.[13] Lime processed parchment contains significant calcium embedded in the matrix, whereas calcium is not introduced in the primary processing of ancient skins and should not be expected to be the main inorganic impurity throughout the matrix. However, calcium is present in analyzed Dead Sea scroll fragments, both as an inorganic contaminant from the cave deposits and as a component of collagen, since it is naturally found in skin products.[14] One study differentiated enzymatic and lime processed parchment with infrared spectroscopy, identifying abatement of the amide I and II bands in enzymatic treatment.[15] This is observed in the studied fragments, however, changes in the amide I and II band positions and heights as a result of collagen denaturation and hydrolysis can also contribute to this phenomenon.[16]

Ink formulations used by ancient scribes

The ink formulations identified in Dead Sea scroll fragments are typically carbon inks, produced by mixing oily soot with tree resins and water. Light colored gums such as gum acacia (gum

---

[12] The presence of gelatin is due to both collagen denaturation caused by the highly alkali liming step (calcium hydroxide) during the manufacturing process and the exposure of the surface to other agents that cause denaturation-post production, such as ultraviolet radiation.
Gonzalez, L. G., and T. J. Wess. "The Effects of Hydration on the Collagen and Gelatine Phases Within Parchment Artefacts." *Heritage Science* 1, no. 1 (2013): 14.
[13] Poole, J. B., and R. Reed. "The Preparation of Leather and Parchment by the Dead Sea Scrolls Community." *Technology and Culture* 3, no. 1 (1962): 1-26.
[14] Rabin, I. "Archaeometry of the Dead Sea Scrolls." *Dead Sea Discoveries* 20, no. 1 (2013): 124-42.
[15] Bicchieri, M., et al. "Non-Destructive Spectroscopic Characterization of Parchment Documents." *Vibrational Spectroscopy* 55, no. 2 (2011): 267-72.
[16] Derrick, M. R. "Evaluation of the State of Degradation of Dead Sea Scroll Samples Using Ft-Ir-Spectroscopy." *Book and Paper Group Annual* 10 (1991): 49-65; Vyskočilová, Gabriela, et al. "Model Study of the Leather Degradation by Oxidation and Hydrolysis." *Heritage Science* 7, no. 1 (2019): 1-13.

Arabic) have been used in inks since antiquity due to their high water solubility. However, tannins, either from darker local gums or added vegetable matter, have been identified in a study of a Qumran scroll dating to ca. 1 century C.E.[17] If present, these tannins would chemically bind the ink to the parchment collagen, which would support the durability of the scroll inks when compared to typical carbon-based inks that are only adsorbed on a surface.[18] Other additives contained in ancient carbon based inks include animal glue, oil, or honey. These materials can affect the chemical and physical properties of parchment and cause its deterioration in the regions of ink application.[19]

The components of the ink are mixed into a paste and dried, then soaked and diluted with water before use. The ratio of chlorine and bromine ratios in inks, extant from evaporated water introduced during mixing, and dilution of the ink, has been used to geographically link scroll inks with manufacture or use in the Qumran region.[20]

The inks in the studied fragments appear to be carbon based likely with a tree gum binder. The presence of polysaccharide component was identified in one sample (SCR 00474). No tannins were identified in the inks. The presence of small quantities of gums and other components in the ink samples not identified with infrared spectroscopy may be detected with additional molecular analysis such as pyrolysis gas chromatography-mass spectrometry (py-GC-MS), although a larger sample is required for this technique.

Cellulosic material was identified in the inks located on two fragments (SCR 000121 and SCR 000124). As this material was identified as a coating in most of the studied fragments, its source here is likely from cellulosic adhesives frequently used as a consolidant in conservation treatment, such as methylcellulose, rather than as a component of the ink.

The ink microsamples were physically removed from the fragments with a size 11 steel scalpel blade. As a result, these microsamples were sometimes contaminated with adjacent materials such as degradation products, inorganic sediments, conservation treatments, and coating materials.

Evidence of degradation in parchment artifacts

Parchment preparation removes most of the fat, blood, and other components from the skin. Thus, parchment is primarily composed of aligned collagen fibrils, with interstitial

[17] Hahn, Oliver, et al. "On the Origin of the Ink of the Thanksgiving Scroll (1qhodayot[a])." *Dead Sea Discoveries* 16, no. 1 (2009): 97-106.
[18] Reed, R. *Ancient Skins, Parchments and Leathers*. Studies in Archaeological Science. London: Seminar Press, 1972
[19] Nir-El, Y. and M. Broshi. "The Black Ink of the Qumran Scrolls." *Dead Sea Discoveries* 3, no. 2 (1996): 157-67.
[20] Rabin, I. "Archaeometry of the Dead Sea Scrolls." *Dead Sea Discoveries* 20, no. 1 (2013): 124-42.

mucopolysaccharides, glycol proteins, and plasma proteins.[21] Both inherent and environmental factors – chemical, physical, and biological – contribute to collagen deterioration and cause parchment to become brittle, distorted, and darkened, or, alternatively, relaxed or gelatinized.

Collagen is vulnerable to irreversible degradation as a result of denaturation, hydrolysis, and oxidation. The denaturation process breaks down the collagen to form gelatin, a water soluble protein composed of polypeptide chains. This occurs when the basic structural units of collagen (tropocollagens), held in a triple helical structure via relatively weak hydrogen bonds, become disordered or "gelatinized" when exposed to elevated heat and/or moisture. Hydrolysis occurs when water ruptures the peptide linkages that form the amino acid end groups of proteins and is pH and humidity dependent. Oxidation of the peptide chain results in subsequent cross-linking and/or chain breakage depending on the position of the attack, and can cause embrittlement, cracking, and darkening.[22]

As a group, the studied scroll fragments all exhibit extensive aging and wear. This may be expected of prepared skin exposed to normal environmental changes, hydrolysis and other agents of deterioration over time, however, these processes can be accelerated by either intentional or unintentional exposure to extremes in heat, humidity, or bacterial attack. Parchment is not as prone to acid degradation as paper writing supports, due in part to alkaline agents such as lime and chalk that are used in the manufacturing process.

All studied fragments have darkened to varying degrees, with SCR 003173 being almost black-brown in color on the surface, seemingly similar to a black bituminous substance identified as a parchment decomposition product in an early description of a Dead Sea scroll fragment.[23] While the darkening visually appears to have been enhanced by a brush-applied coating, no specific pigment or other chromophore (colored molecular functional group) could be identified in the proteinaceous coating. Proteins do, however, inherently darken with age and so a naturally-formed chromophore cannot be excluded. The fragments are extremely brittle, with cracking, losses, abrasion, and delamination. Some of the delamination and surface losses on fragment SCR 000124 and SCR 003183 appear to result from insect grazing.

---

[21] The molecular structure is stabilized by a network of ionic interactions, hydrophobic regions and covalent intra and intermolecular crosslinkages to form an insoluble collagen fibril.
Bicchieri, M., et al. "Non-Destructive Spectroscopic Characterization of Parchment Documents." *Vibrational Spectroscopy* 55, no. 2 (2011): 267-72.

[22] Derrick, M. R. "Evaluation of the State of Degradation of Dead Sea Scroll Samples Using Ft-Ir-Spectroscopy." *Book and Paper Group Annual* 10 (1991): 49-65; Vyskočilová, G., et al. "Model Study of the Leather Degradation by Oxidation and Hydrolysis." *Heritage Science* 7, no. 1 (2019): 1-13.

[23] Caldararo, N. "Storage Conditions and Physical Treatments Relating to the Dating of the Dead Sea Scrolls." *Radiocarbon* 37, no. 1 (1995): 21, references Plenderleith, H. J. "Technical note on unwrapping of Dead Sea Scroll fragments." *In* Barthelemy, D. and J. T. Milik, *Discoveries in the Judaean Desert. Vol. 1. Qumran Cave 1*. Oxford, Clarendon Press: 39–40.

Calcium oxalate was identified in one ink sample (SCR 003173). Calcium oxalates [$CaC_2O_4.H_2O_x$], also identified by Rabin, are commonly occurring organic degradation products resulting from the formation of oxalic acid in reaction with calcium-rich minerals such as chalk or limestone. In parchment, oxalates can form as a result of biological deterioration, usually from fungal or bacterial attack, or could be due to the use of urine or plant extracts in the parchment manufacturing process, as well as degradation products observed in the breakdown of organic coatings such as oils.[24] Another metal carboxylate, calcium stearate, was identified in a sediment sample (SCR 000124) and coating (SCR 004741). This calcium soap formation would similarly form from reaction of the calcium in the carbonate deposits (and calcium sulfate present as gypsum, identified in SCR 000124, SCR 003173, and SCR 003183) with fatty acids of an oil introduced into the support through handling or treatment.[25] It could also form as a result of the reaction of the calcium salts with residual fats remaining in the parchment or leather.

None of the fragments exhibit visible evidence of mold damage or other biological attack. However, it is possible the conversion of calcium carbonate or sulfate in calcium oxalate could occur with fungi without significant effects on the collagen and fibers.[26]

SCR 004742 appears the most saturated of the fragments; its surface almost completely gelatinized. This can occur from exposure to elevated heat and moisture. Humidification with subsequent freezing, a treatment reportedly used to unroll and flatten the Dead Sea Scrolls, ultimately led to extensive gelatinization and re-crystallization of the salts used in the manufacturing process of the skin substrates.[27] This phenomenon can also be simulated by saturating the parchment with a dilute glue or other binder/coating.

---

[24] Bicchieri, M., et al. "Microscopic Observations of Paper and Parchment: The Archaeology of Small Objects." *Heritage Science* 7, no. 1 (2019): 1-12; Pinzari, F., G. Pinar and CialeiV. “A case study of ancient parchment biodeterioration using variable pressure and high vacuum scanning electron microscopy,” in Meeks, Nigel, and British Museum. *Conservation Research Section. Historical Technology, Materials and Conservation : Sem and Microanalysis*. London: Archetype Publications, in Association with the British Museum, 2012.

[25] Vichi, A., et al. "Study of the Degradation and Conservation of Historical Leather Book Covers with Macro Attenuated Total Reflection-Fourier Transform Infrared Spectroscopic Imaging." *Acs Omega* 3, no. 7 (2018): 7150-157. 2018; Y. Maor, et al., White halos surrounding the Dead Sea scrolls, Journal of Cultural Heritage (2017), http://dx.doi.org/10.1016/j.culher.2017.06.003 (accessed August 29, 2019).

[26] Piñar G, et al. "Unmasking the Measles-Like Parchment Discoloration: Molecular and Microanalytical Approach." *Environmental Microbiology* 17, no. 2 (2015): 427-43.

[27] A. Wallert, "Deliquescence and Recrystallization of Salts in the Dead Sea Scrolls," in Archaeological Conservation and its Consequences (ed. A. Roy and P. Smith; London: International Institute for Conservation, 1996), 198-201.

History and evidence of conservation treatments

Since their discovery, the Dead Sea Scrolls and associated fragments have been subject to multiple campaigns of treatment to flatten the parchment, clarify ink inscriptions, stabilize and preserve the fragments, and mount them for study and display. These treatments, along with decades of handling, have added nonoriginal material to the fragments that should be differentiated to better understand the history of each object.

Recorded interventions, which are likely not comprehensive, include the use of parchment size[28] sprayed or brushed on the surface as a consolidant (reported 1962), the application of pure castor oil or castor oil diluted with organic solvent to increase parchment flexibility (reported 1972), as well as treatment with moisture and oils to remove clay from fragment surfaces or to relax the collagen fibers. Other reported materials used for this purpose include spermaceti wax, neatsfoot oil, lanolin, milk, unbleached beeswax, Japan wax, nitrocellulose (in acetone), and glycerin. Alum was often applied by restorers to increase the adhesion of ink and to prevent mold.[29]

Adhesive tapes have been used to mend breaks and tears in the parchment, glass plates have been used to flatten parchment supports (as well as for storage and display).[30] Friable parchment, inks, and sediment have been consolidated in recent decades with acrylic and cellulosic consolidants, and fragments reinforced with Asian papers and starch pastes. Fuller's earth (a clay containing attapulgite and bentonite) has also been employed as a poultice material.[31]

---

[28] Parchment size is a dilute glue made from cooking parchment scraps in water, and is composed primarily of gelatin. Parchment size is more alkaline than gelatin due to the presence of residual calcium in the skin, and may also contain other residual compounds based on its method of manufacture.
Book and Paper Group, *Paper Conservation Catalog*, AIC, 1984, 1989. https://www.conservation-wiki.com/wiki/Parchment_(PCC)#Adhesives_and_Consolidants (accessed August 26, 2019).

[29] Caldararo, N. "Storage Conditions and Physical Treatments Relating to the Dating of the Dead Sea Scrolls." *Radiocarbon* 37, no. 1 (1995): 21.

[30] Y. Maor, et al., White halos surrounding the Dead Sea scrolls, Journal of Cultural Heritage (2017), http://dx.doi.org/10.1016/j.culher.2017.06.003 (accessed August 29, 2019).

[31] Rabin, I. "Archaeometry of the Dead Sea Scrolls." *Dead Sea Discoveries* 20, no. 1 (2013): 124-42.

Results and Discussion

The mineral phases identified among the fragments include calcite (chalk, $CaCO_3$ terrestrial phase), aragonite ($CaCO_3$ marine phase), gypsum (hydrated calcium sulfate, $CaSO_4.2H_2O$), quartz (SiO_2), kaolinite clay [$Al_2Si_2O_5(OH)_4$], a bentonite-group clay [bentonites are aluminosilicate clay minerals that can be sodium, potassium, or calcium rich], and talc [a magnesium silicate, $Mg_3Si_4O_{10}(OH)_2$]. Attapulgite [$(Mg,Al)_2Si_4O_{10}(OH)$] and montmorillonite clays are also suggested by the data. Montmorillonite has a complex chemistry; it is a hydrated sodium calcium aluminum magnesium silicate hydroxide $(Na,Ca)_{0.33}(Al,Mg)_2(Si_4O_{10})(OH)_2 \cdot nH_2O$. This type of chemical complexity for clay minerals is the result of these materials being comprised of aluminosilicate two-dimensional 'sheets' that are, like a phyllo dough pastry, stuffed with cations that often include sodium, potassium, magnesium, and calcium. Potassium, iron, and other cations are commonly observed substitutes in montmorillonite clays, and the exact ratio of any particular clay mineral varies with the geology of its source. As a result, correlations between many of the elements observed by x-ray fluorescence (XRF) can result because they occur together in clay minerals. Clay minerals associated with the Dead Sea region include smectite, kaolinite, illite, and small amounts of palygorskite.[32] Other silicate minerals that commonly occur on the earth's surface, such as feldspars, have a similar geochemistry and set of elemental correlations. Feldspars are a much less degraded/weathered form of rock than clays, and they have also been found to make up the geology of this region.[33] Different classifications of clay minerals are highly chemically and physically similar to one another, and as a result they can be broadly classified by FTIR. X-ray diffraction is the most definitive method for identifying clay minerals, and one MOTB scroll fragment deposit has been set aside for this experiment.

XRF results – relationship to FTIR results

The major elements identified by these experiments for the four fragments scanned (SCR000121, SCR000124, SCR003173, and SCR004742) included calcium, potassium, iron, chlorine, sulphur, silicon, and phosphorus. Other elements identified included sodium, manganese, aluminum, nickel, bromine, titanium, strontium, and magnesium. More unusual elements, suggestive of an external or man-made origin, included traces of selenium, zinc, and lead and more substantial amounts of copper. Positive correlations among the elements found on the fragments can be interpreted in terms of both the compounds identified by FTIR and the compounds that are not detectable by FTIR (because they do not absorb energy in the mid-infrared), such as most halides (chlorides and bromides) and all oxides and sulfides.

The correlations (covariance plots) generated by Prof. Aaron Shugar are consistent with the mineralogical findings from the FTIR data and the known compositions of mineral evaporites at

[32] A. Singer, et al. "Dust Deposition over the Dead Sea", *Journal of Arid Environments* (2003), 53:41-59.
[33] A. Singer, et al. "Dust Deposition over the Dead Sea", *Journal of Arid Environments* (2003), 53:41-59.

the Dead Sea, the mineral deposits in the caves at Qumran, and the literature on the mineralogy of other studied DSS fragments.[34] Study of the chlorine to bromine ratios by SEM-EDS (scanning electron microscopy) for comparison to the ratios in the Rabin report is ongoing.

Fragment SCR000121 shows the strongest positive correlations between:

- Aluminum and calcium, potassium, and silicon
- Calcium and chlorine, potassium
- Potassium and chlorine
- Iron and silicon, titanium
- Potassium and silicon
- Magnesium and aluminum, calcium, and silicon
- Phosphorus and calcium, potassium, and silicon
- Sulfur and calcium, potassium
- Silicon and calcium, potassium
- Bromine and potassium, chlorine

These correlations suggest the presence of aluminosilicate minerals including clay minerals (in which aluminum, silicon, calcium, magnesium, iron, potassium, and sodium will all have positive correlations). The presence of gypsum is suggested by the positive correlation between calcium and sulfur. The presence of potassium chloride, potassium bromide, and sodium chloride are suggested, although potassium chloride shows the stronger correlation. The correlation of and magnesium is characteristic of their geochemical relationship, and also suggestive of dolomite/dolomitic limestone. The presence of ilmenite ($FeTiO_3$) or another iron and titanium-containing clay accessory mineral is suggested by the correlation between iron, titanium, and silicon (this is an accessory mineral found in many clays). The presence of talc is suggested by a correlation between magnesium and silicon. These correlations in the case of aluminosilicate minerals cannot conclusively prove the presence of a specific molecule (for example there are many types of magnesium silicates besides talc), but in the context of the extant FTIR data the correlations can be better understood and interpreted. Magnesium and silicon correlations are also suggestive of palygorskite/attapulgite clays [$(Mg,Al)_2Si_4O_{10}(OH)\cdot 4(H_2O)$]. X-ray diffraction is required to definitively identify the bromides and chlorides since they are not active in the mid-infrared.

Fragment SCR000124 shows the strongest positive correlations between:

- Calcium and sulfur, aluminum, magnesium, phosphorus, and silicon
- Aluminum and silicon, sulfur

[34] Derrick, M. R. "Evaluation of the State of Degradation of Dead Sea Scroll Samples Using Ft-Ir-Spectroscopy." *Book and Paper Group Annual* 10 (1991): 49-65

- Bromine and potassium, calcium
- Chloride and calcium
- Iron and titanium (lesser correlation with aluminum and silicon)
- Potassium and aluminum, silicon, and sulfur
- Magnesium and aluminum, calcium, silicon, and sulfur
- Sulfur and silicon

These data are strongly suggestive of gypsum, aluminosilicate clay minerals, potassium bromide, calcium bromide, calcium chloride, talc, ilmenite ($FeTiO_3$, one of many iron and titanium-containing accessory minerals in clays and sands). The correlation between sulfur and silicon as well as sulfur and magnesium is not understood at this time – they may be due to sulfate mineral evaporites (although these were not detected by FTIR). The correlations of aluminum, potassium, and sulfur are suggestive of the presence of alum. The correlation of calcium and phosphorus observed here is suggestive of a calcium phosphate mineral evaporite such as apatite. Phosphates are known geochemically in the Dead Sea region (phosphate mining occurs within 50 miles of the coast), and apatite [$Ca_5(PO_4)_3(OH,F,Cl)$] makes up 1-5% of environmental dust deposition over the Dead Sea.[35] The correlation of magnesium and calcium is suggestive of dolomite/dolomitic limestone.

Fragment SCR 003173 shows the strongest positive correlations between:

- Aluminum and silicon
- Calcium and manganese, phosphorus, and sulfur
- Iron and silicon
- Potassium and aluminum, chlorine, and silicon
- Manganese and sulfur
- Silicon and aluminum, iron, potassium
- Titanium and iron, silicon

These data are suggestive of aluminosilicate clay minerals, gypsum, ilmenite ($FeTiO_3$) or other iron and titanium containing clay accessory mineral, and potassium chloride. The manganese and sulfur correlation is unexpected, as black manganese deposits along the Dead Sea coastline have been found to be predominately manganese oxides. However, these manganese deposits are incompletely characterized at this time. The calcium and manganese deposits are consistent with aragonite and poorly crystalline manganese oxide/hydroxide crusts that have been observed on the shores of the Dead Sea.[36]

Fragment SCR 004742 shows the strongest possible correlations between:

---

[35] A. Singer, et al. "Dust Deposition over the Dead Sea", *Journal of Arid Environments* (2003), 53:41-59.
[36] Garber, R. A., et al. "Modern deposition of manganese along the Dead Sea shore", *Sedimentary Geology*, 30(4), December 1981, 267 – 274.

- Aluminum and silicon
- Silicon and iron
- Potassium and chlorine

These data are suggestive of aluminosilicate clay minerals and feldspars and potassium chloride.

Data

Fourier Transform Infrared Spectroscopy

This technique identifies the molecular components of the samples. Sample locations are shown in Figures 1 – 6.

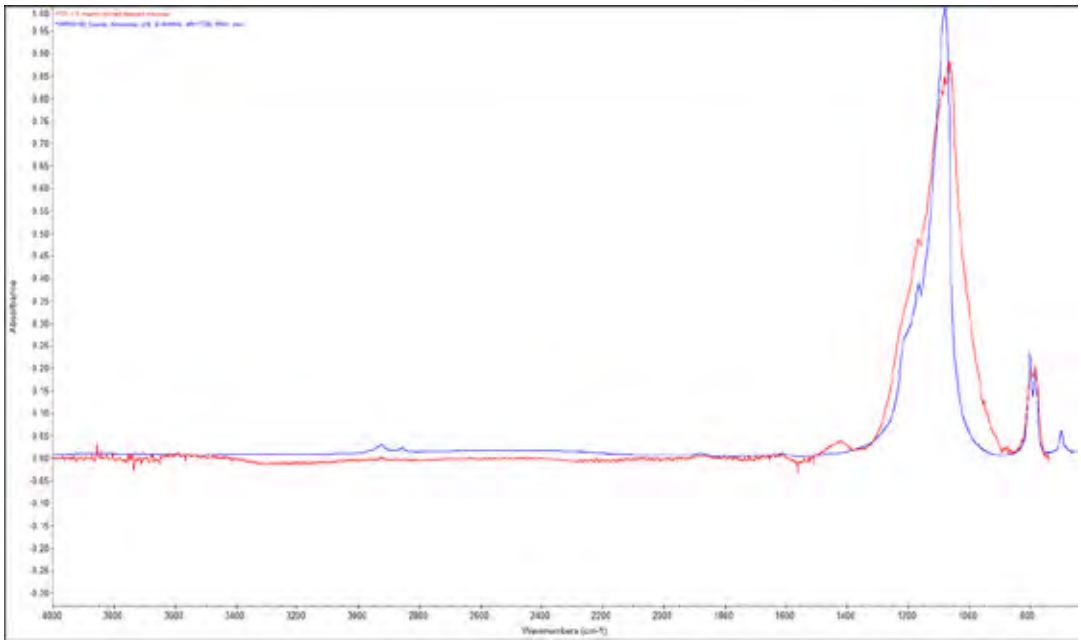

Figure 7. Fragment sample 121, region 1, spectrum 1. Cream colored deposit, overlaid.

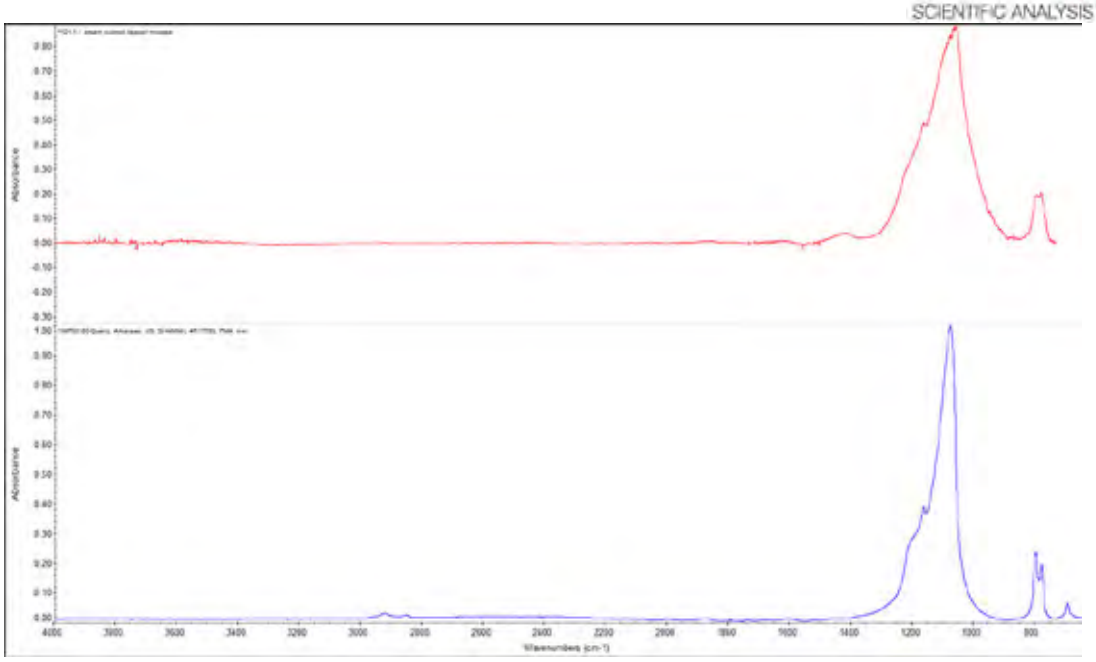

Figure 8. Sample 121, region 1, spectrum 1. Cream colored deposit, stacked.

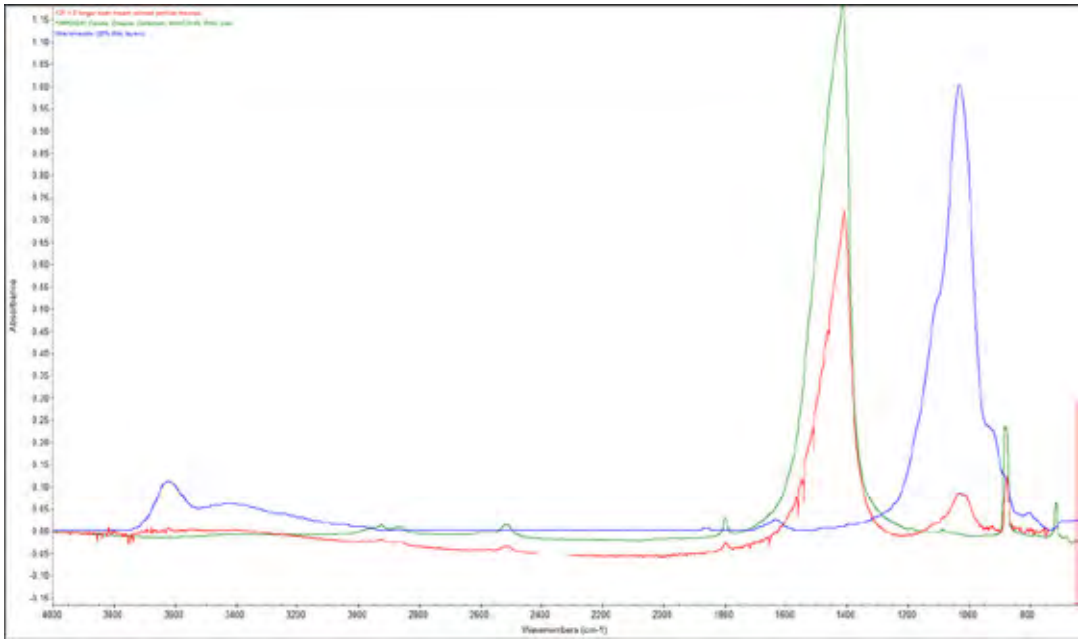

Figure 9. Sample 121, region 1, spectrum 3. Longer scan on cream colored particle, overlaid.

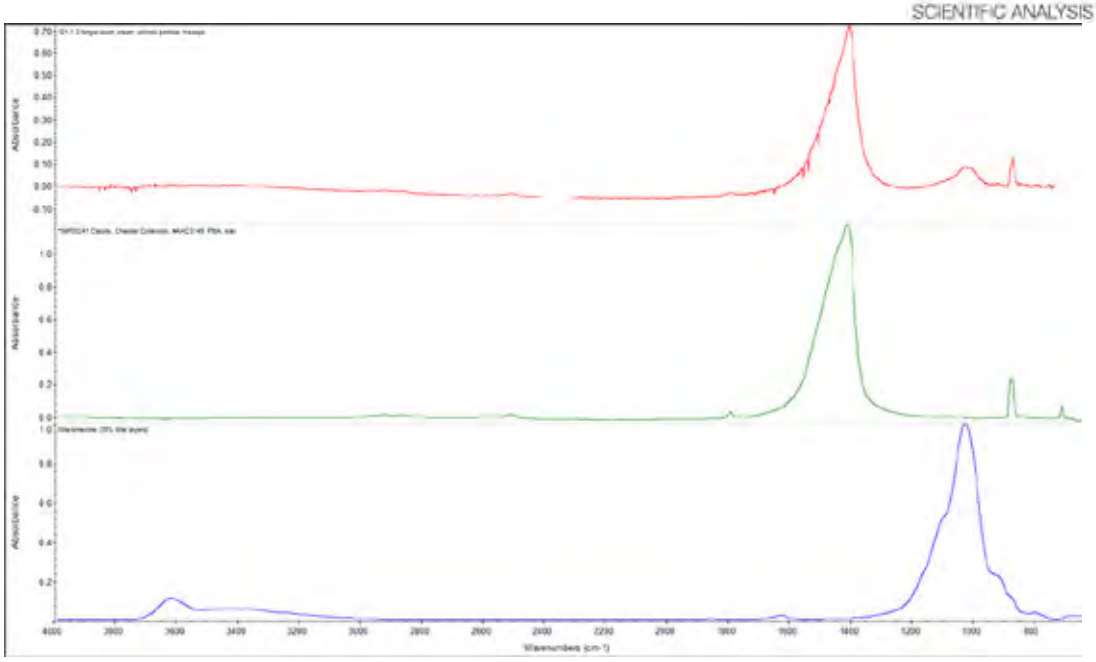

Figure 10. Sample 121, region 1, spectrum 3. Longer scan cream colored particle, stacked.

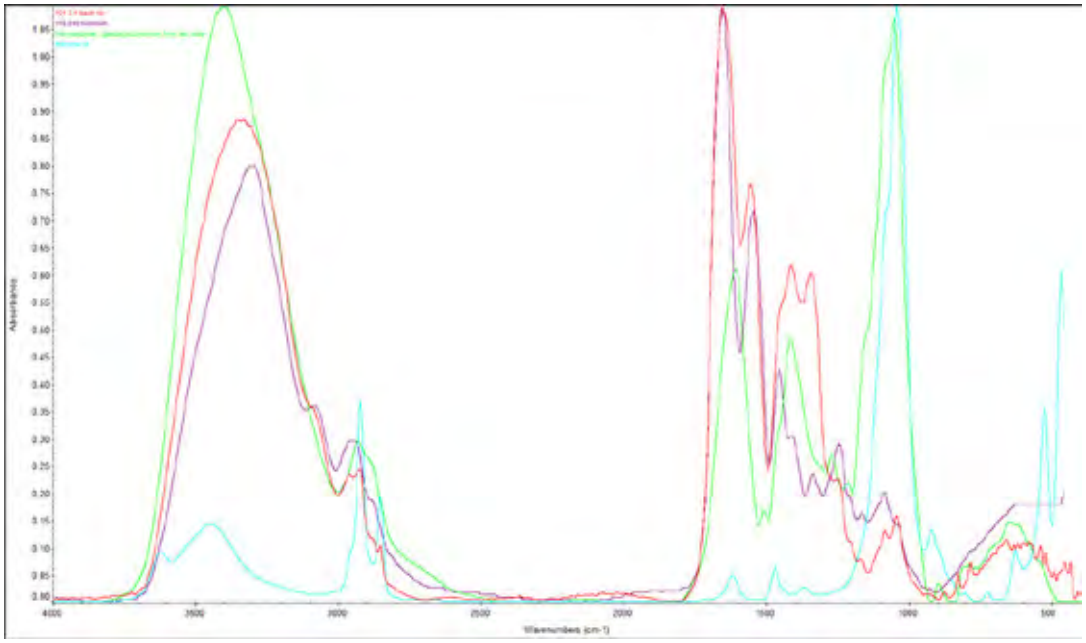

Figure 11. Sample 121, region 3, spectrum 1. Black ink, overlaid.

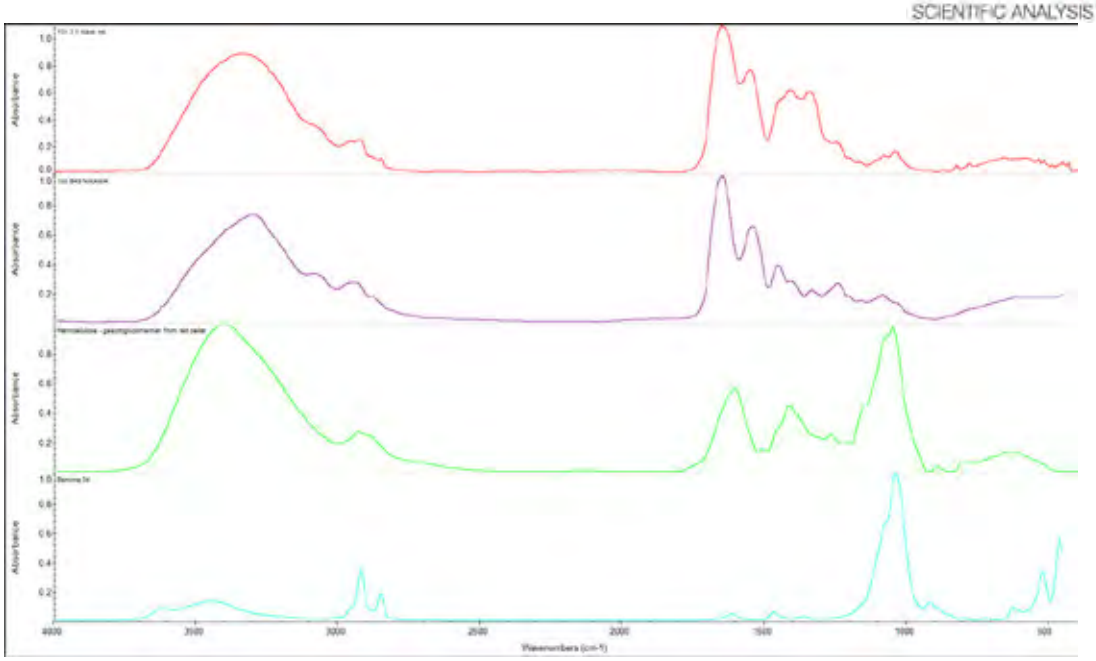

Figure 12. Sample 121, region 3, spectrum 1. Black ink, stacked.

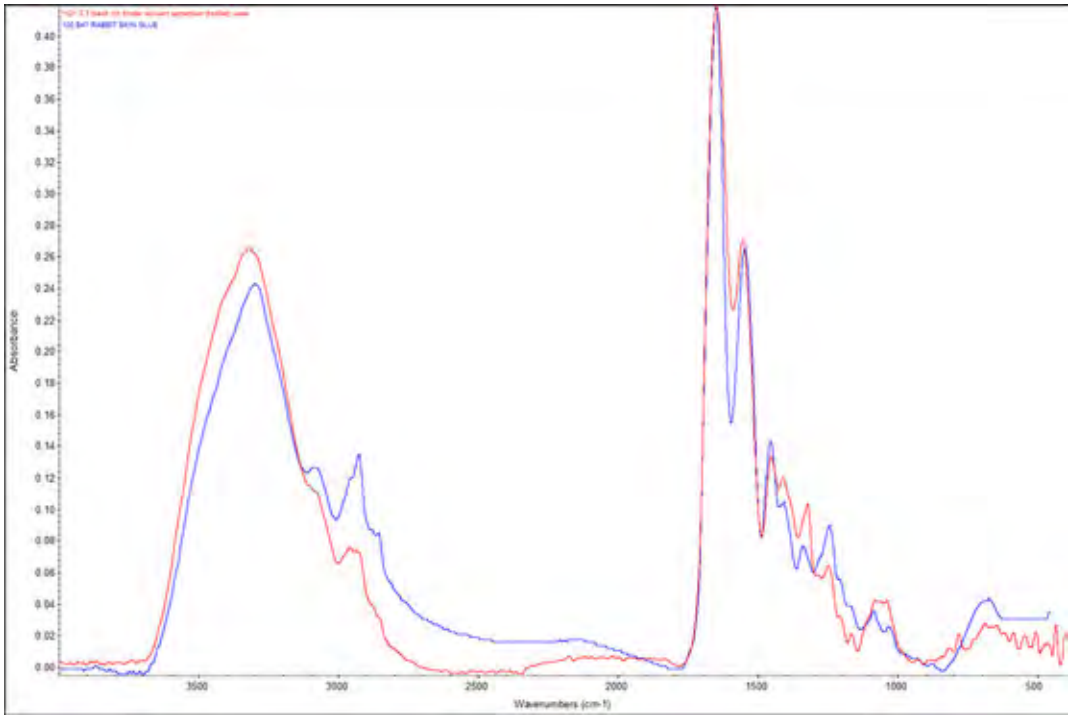

Figure 13. Sample 121, region 3, spectrum 3. Black ink binder distilled water extraction, overlaid.

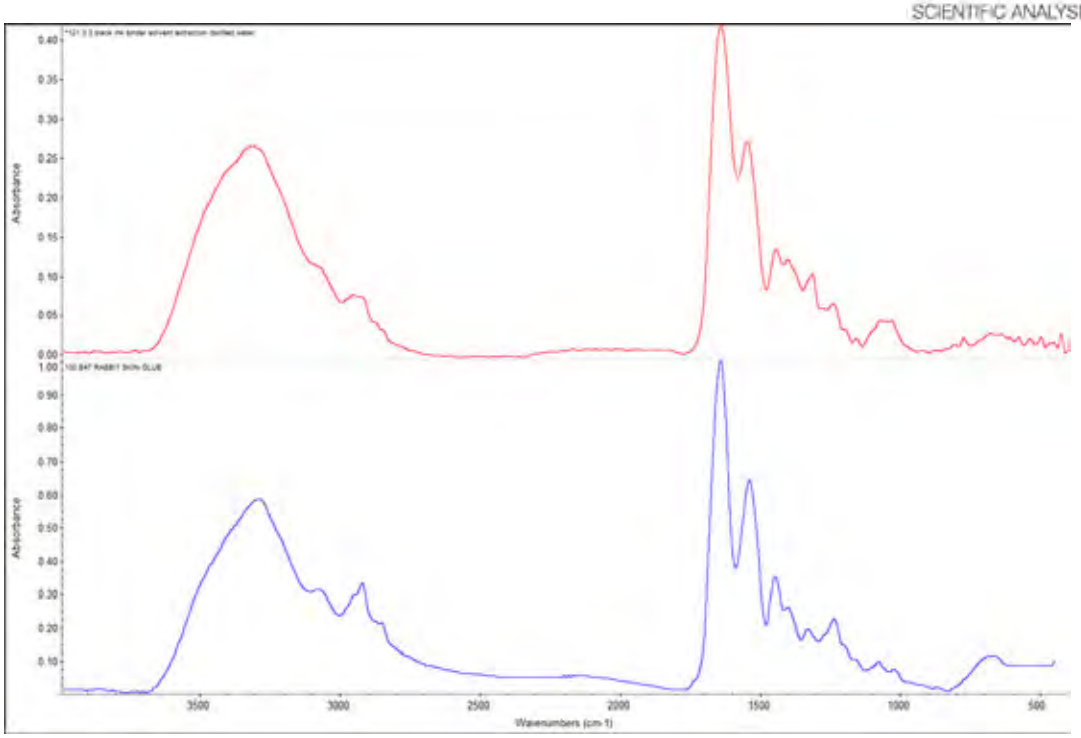

Figure 14. Sample 121, region 3, spectrum 3. Black ink binder, distilled water extraction, stacked.

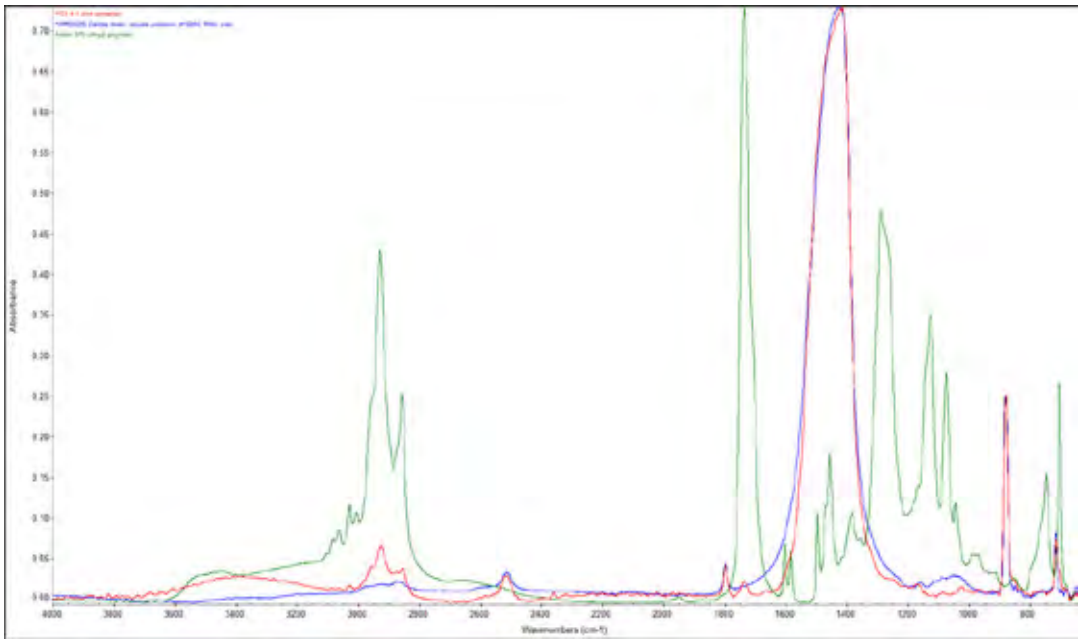

Figure 15. Sample 121, region 4, spectrum 1. Pink accretion, overlaid.

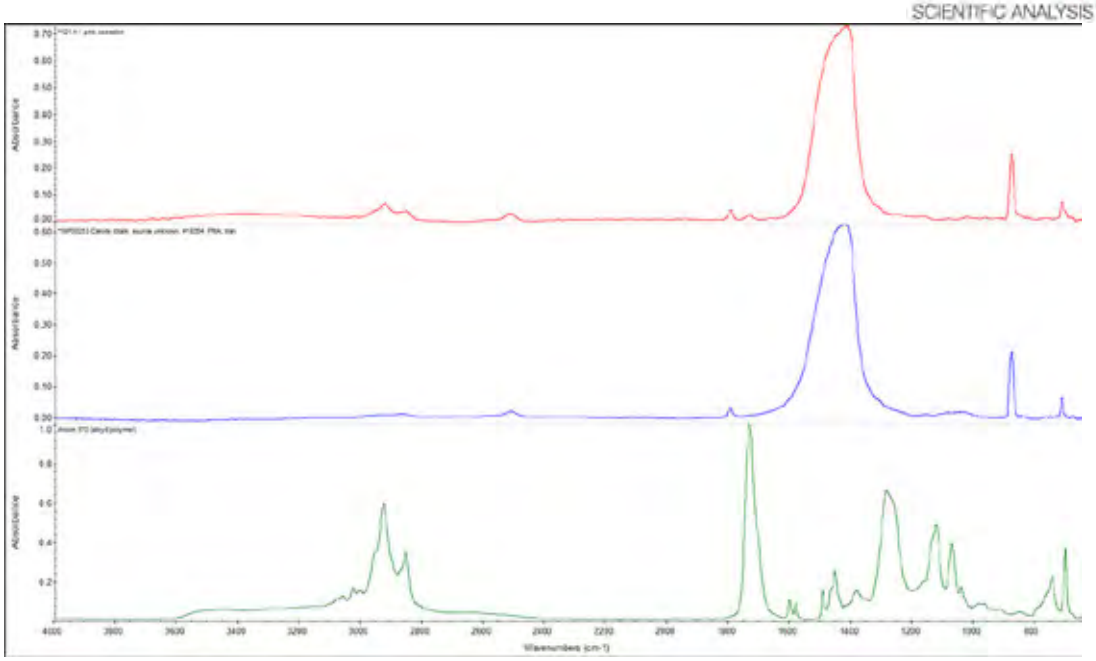

Figure 16. Sample 121, region 4, spectrum 1. Pink accretion, stacked.

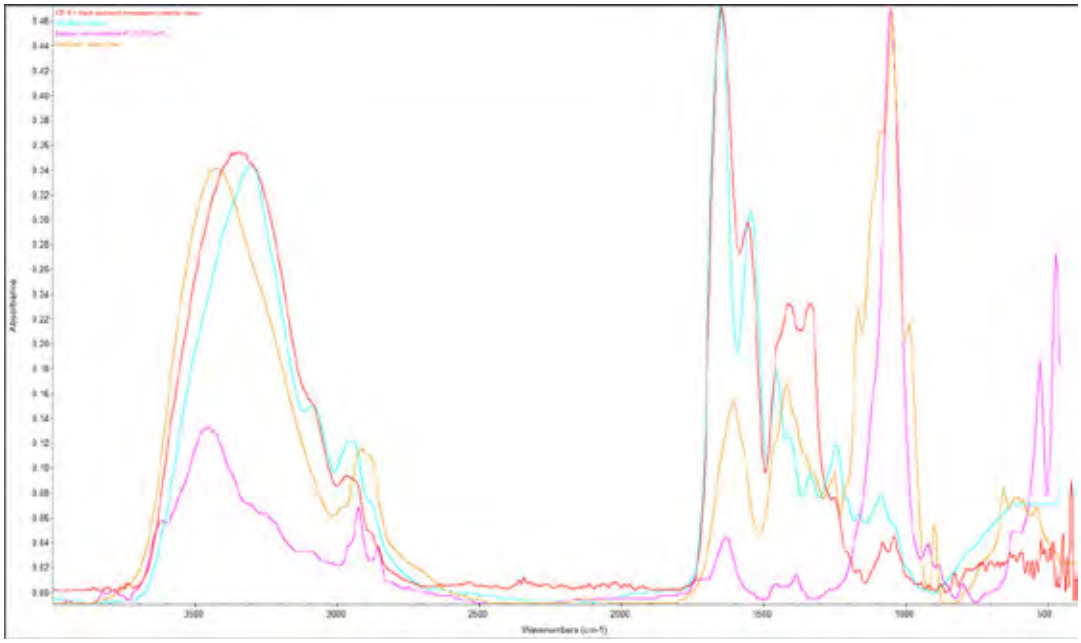

Figure 17. Sample 121, region 5, spectrum 1. Black sediment, transparent material verso, overlaid.

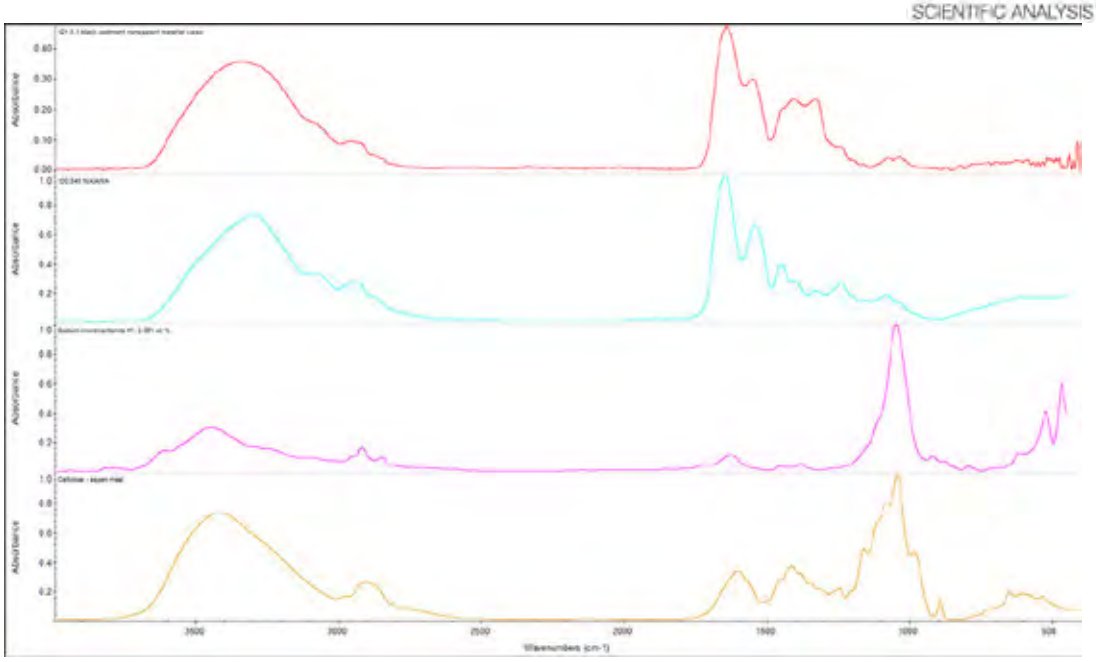

Figure 18. Sample 121, region 5, spectrum 1. Black sediment, transparent material verso, stacked.

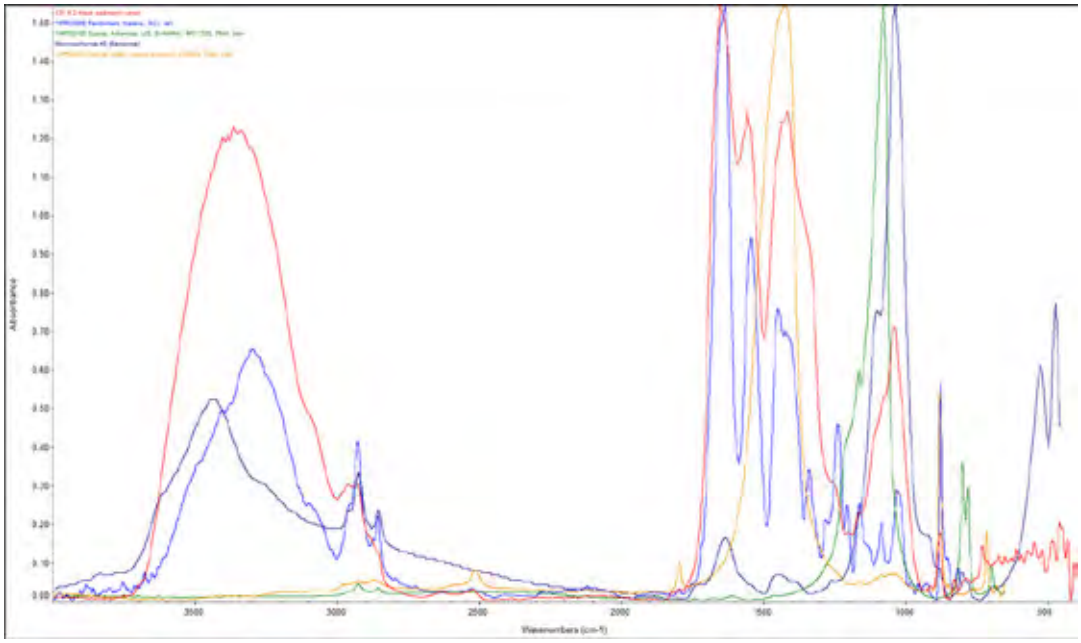

Figure 19. Sample 121, region 5, spectrum 2. Black sediment verso, overlaid.

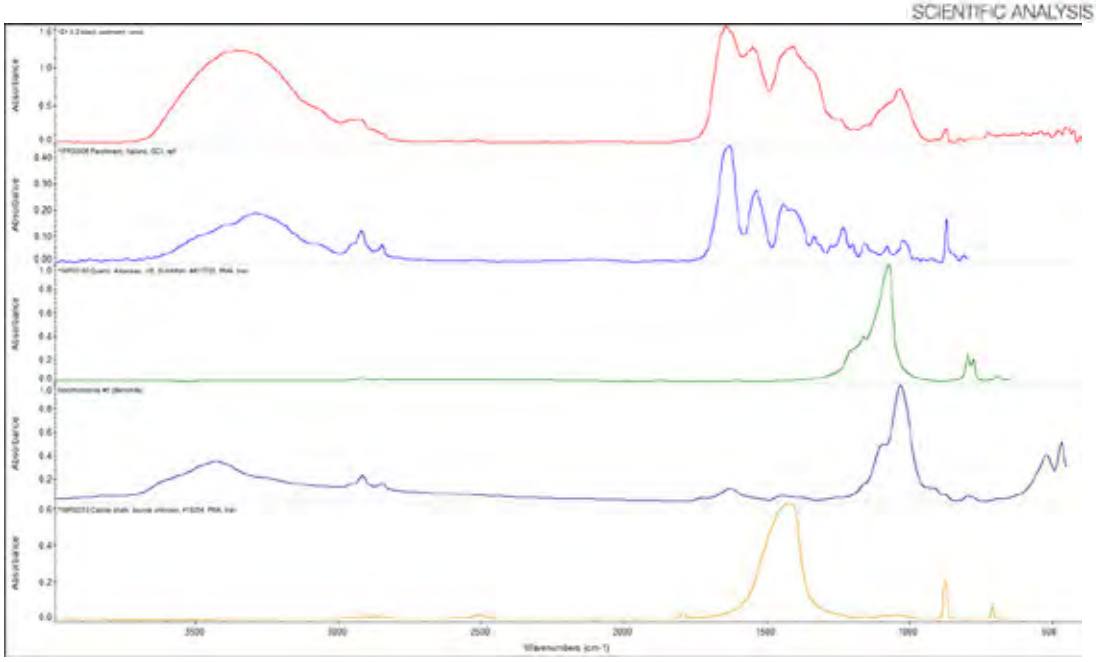

Figure 20. Sample 121, region 5, spectrum 2. Black sediment verso, stacked.

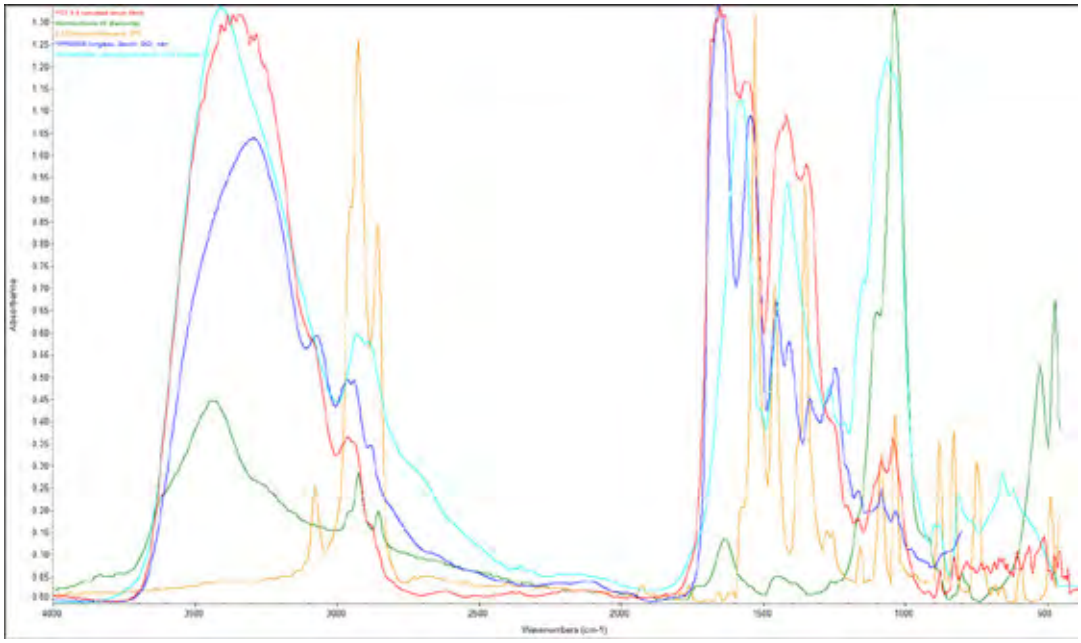

Figure 21. Sample 121, region 5, spectrum 3. Saturated brown fibrils (with bromine pesticide compound), overlaid.

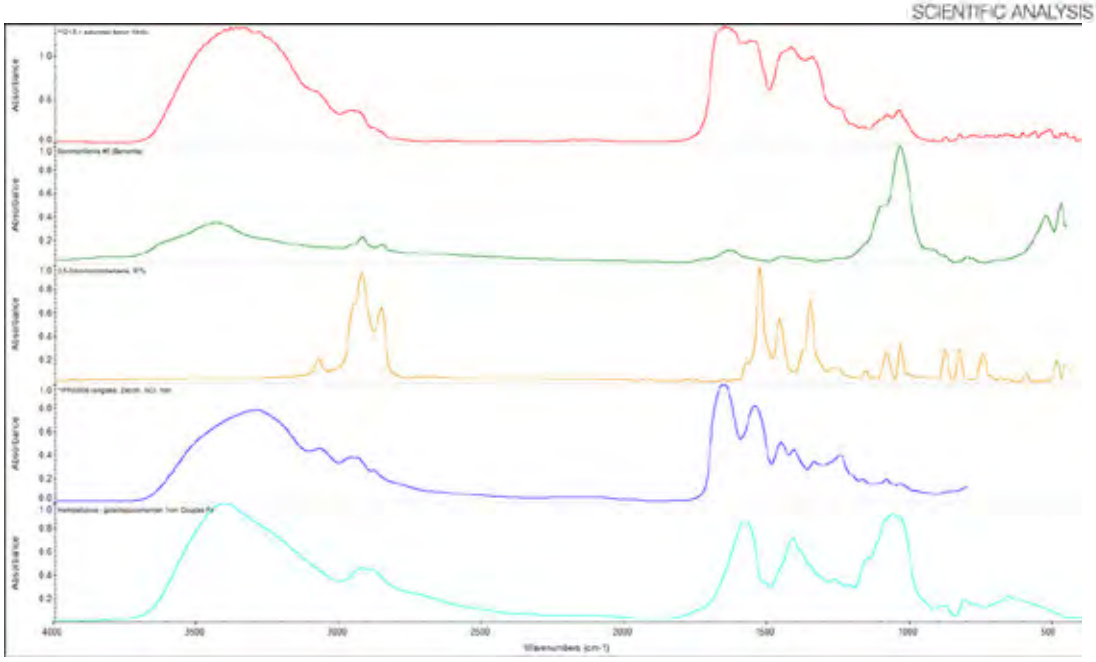

Figure 22. Sample 121, region 5, spectrum 3. Saturated brown fibrils (with bromine pesticide compound), stacked.

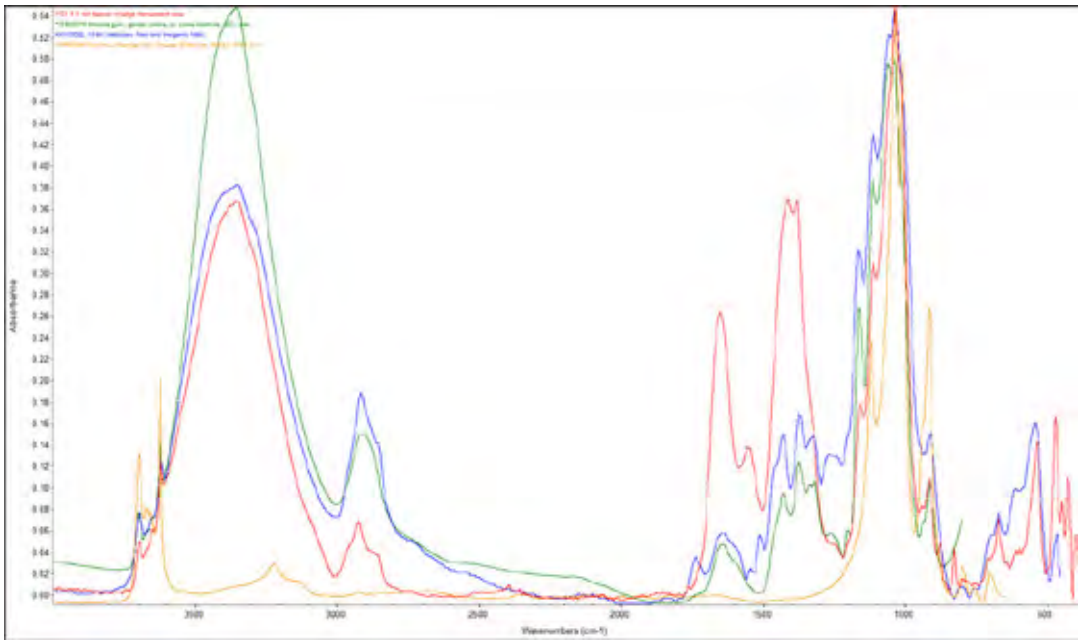

Figure 23. Sample 121, region 6, spectrum 1. Tan deposit, center-left edge, transparent area, overlaid.

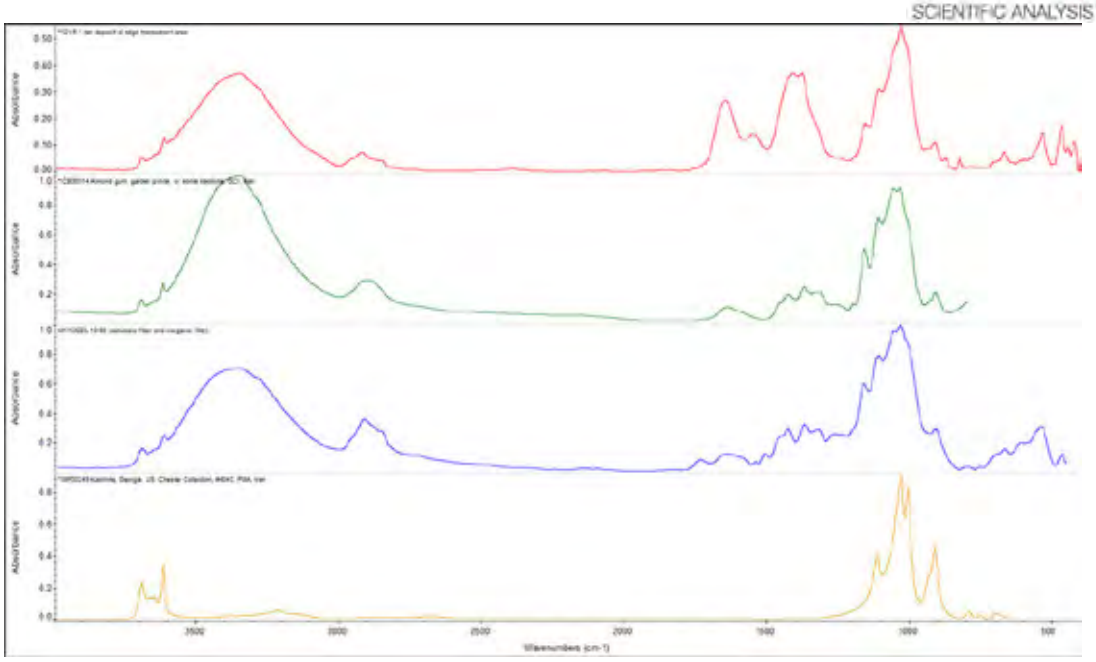

Figure 24. Sample 121, region 6, spectrum 1. Tan deposit, center-left edge, transparent area, stacked.

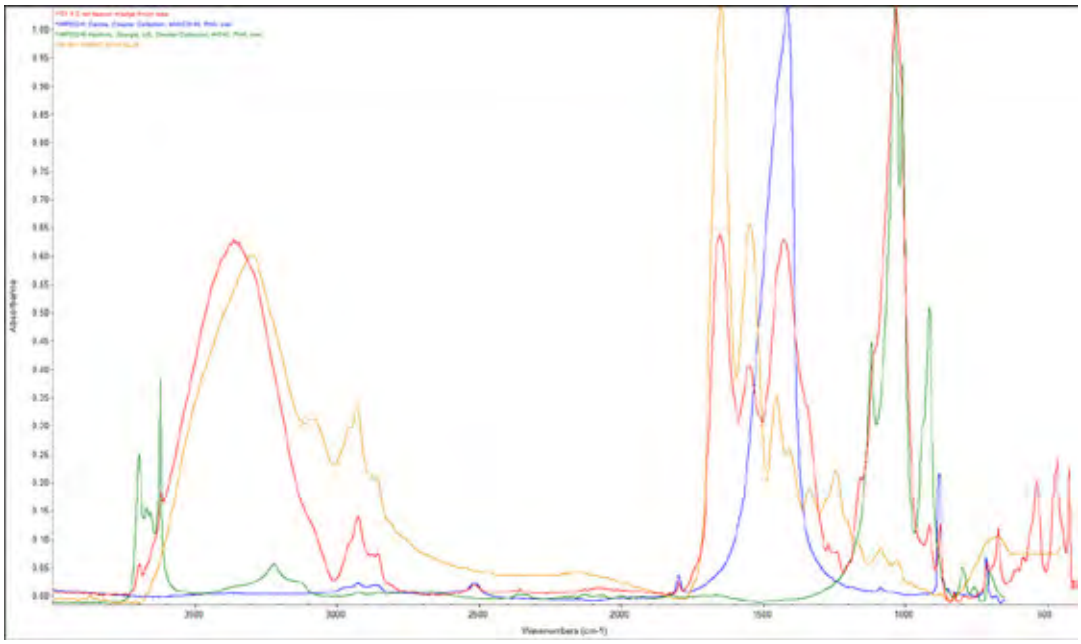

Figure 25. Sample 121, region 6, spectrum 2. Tan deposit, center-left edge, brown area, overlaid.

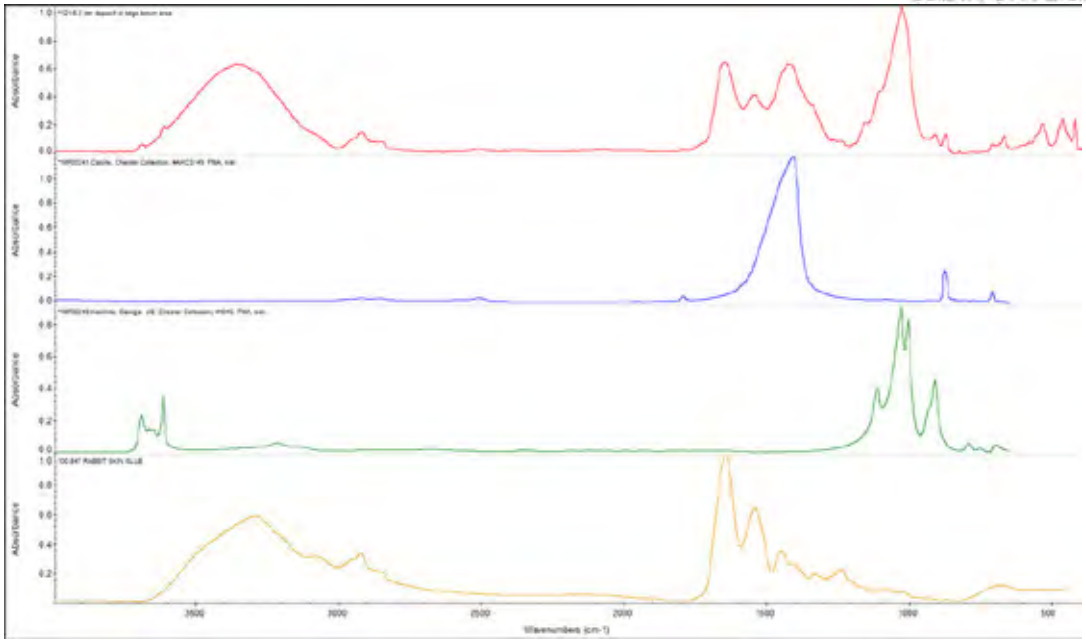

Figure 26. Sample 121, region 6, spectrum 2. Tan deposit, center-left edge, brown area, stacked.

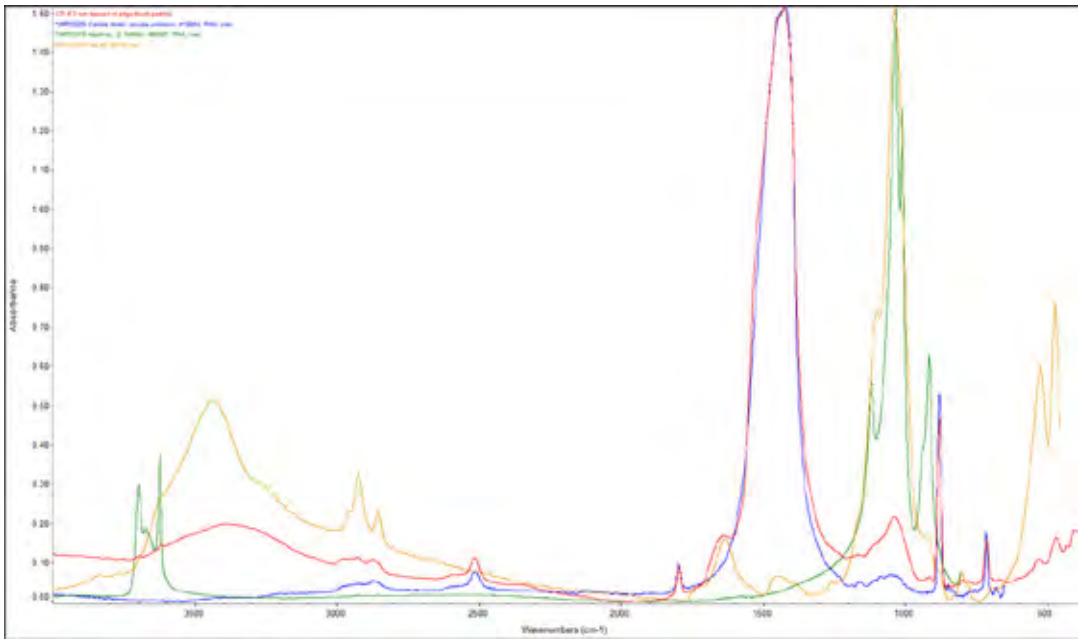

Figure 27. Sample 121, region 6, spectrum 3. Tan deposit, center-left edge, black particle, overlaid.

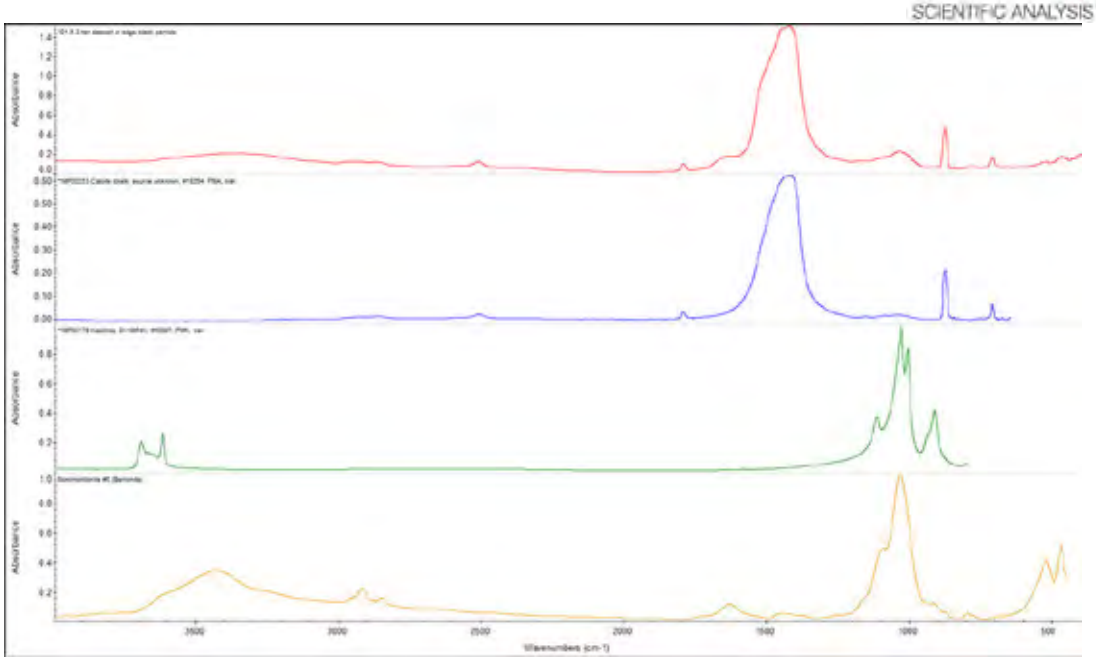

Figure 28. Sample 121, region 6, spectrum 3. Tan deposit, center-left edge, black particle, stacked.

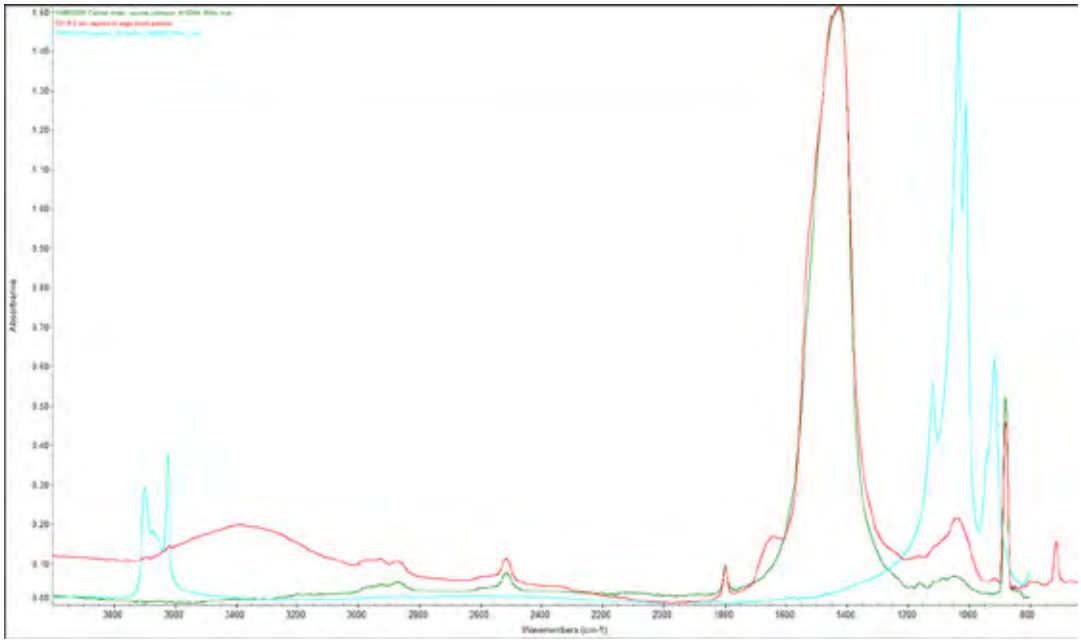

Figure 29. Sample 121, region 6, spectrum 4. Tan deposit, center-left edge, black particle, overlaid.

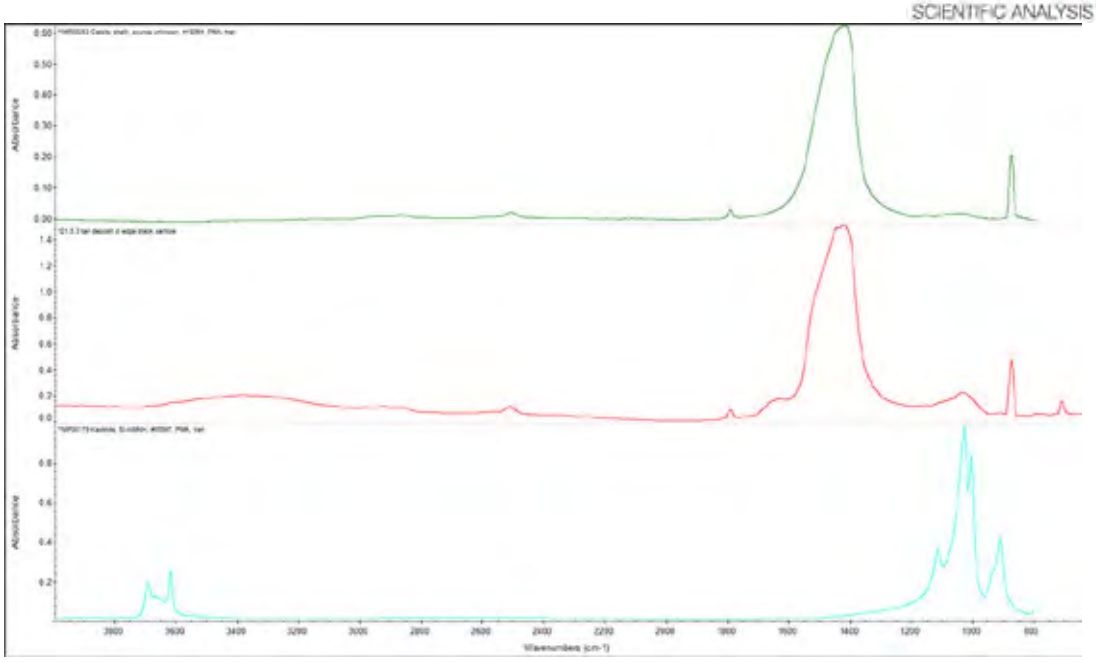

Figure 30. Sample 121, region 6, spectrum 4. Tan deposit, center-left edge, black particle, stacked.

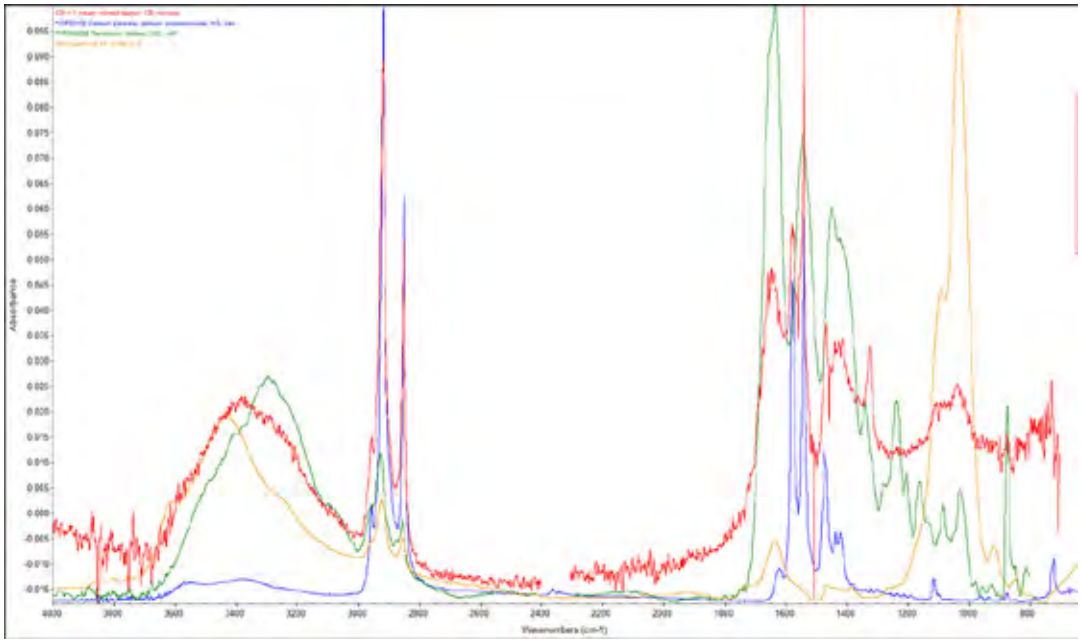

Figure 31. Sample 124, region 1, spectrum 1. Cream colored deposit, overlaid (spectral noise due to using Continuum microscope without a nitrogen flush).

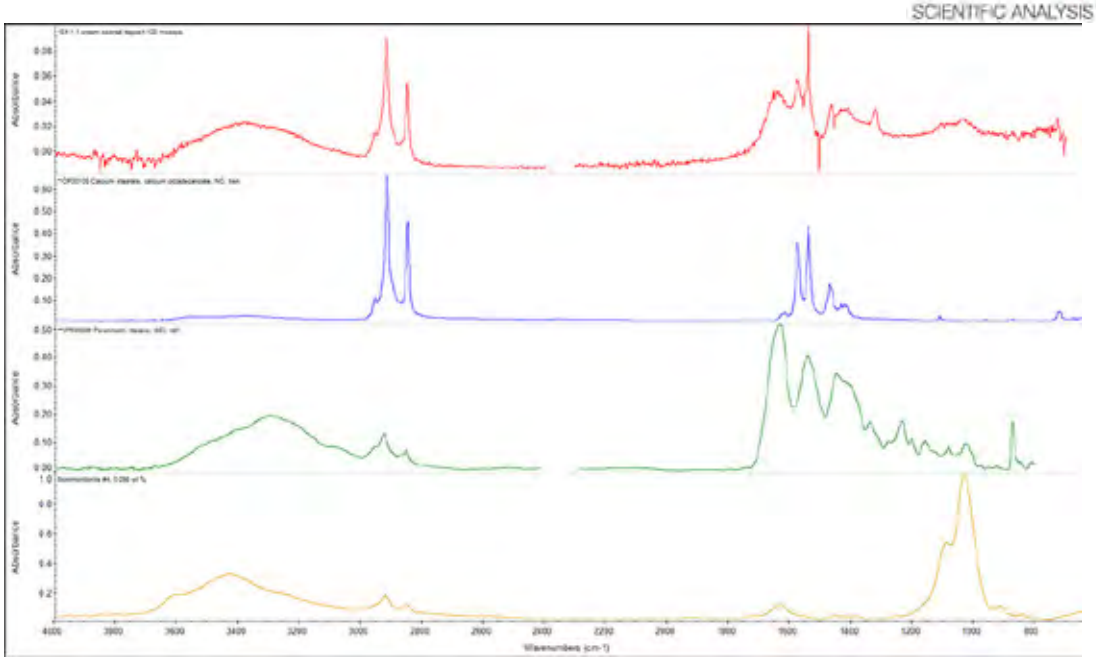

Figure 32. Sample 124, region 1, spectrum 1. Cream colored deposit, stacked overlaid (spectral noise due to using Continuum microscope without a nitrogen flush).

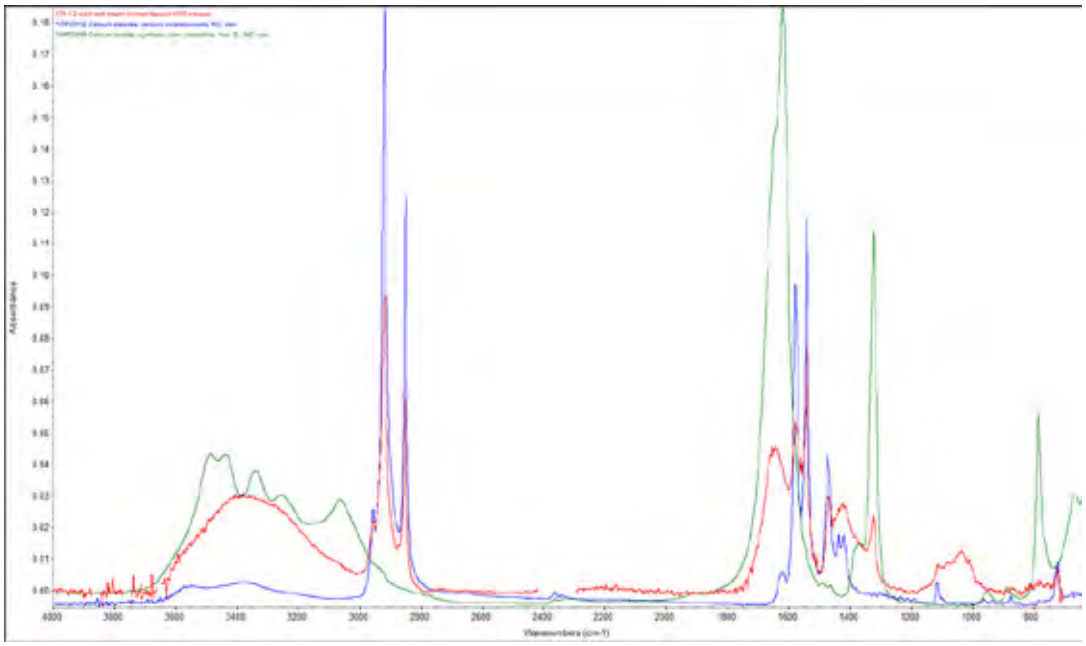

Figure 33. Sample 124, region 1, spectrum 2. Resin and cream-colored deposit overlaid overlaid (spectral noise due to using Continuum microscope without a nitrogen flush).

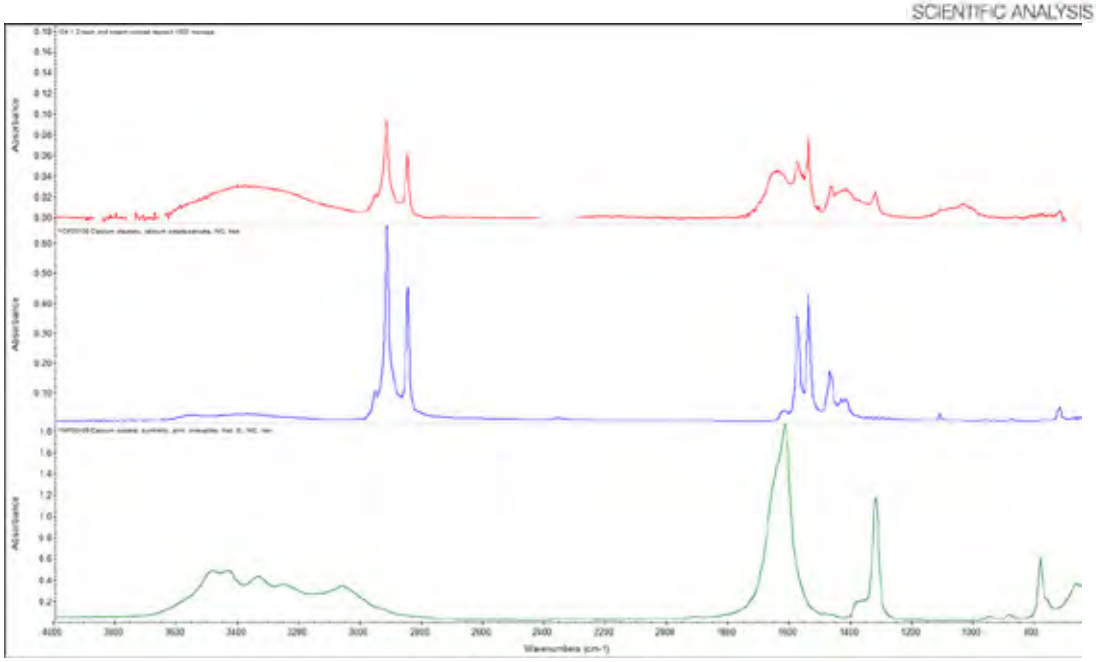

Figure 34. Sample 124, region 1, spectrum 2. Resin and cream-colored deposit stacked (spectral noise due to using Continuum microscope without a nitrogen flush).

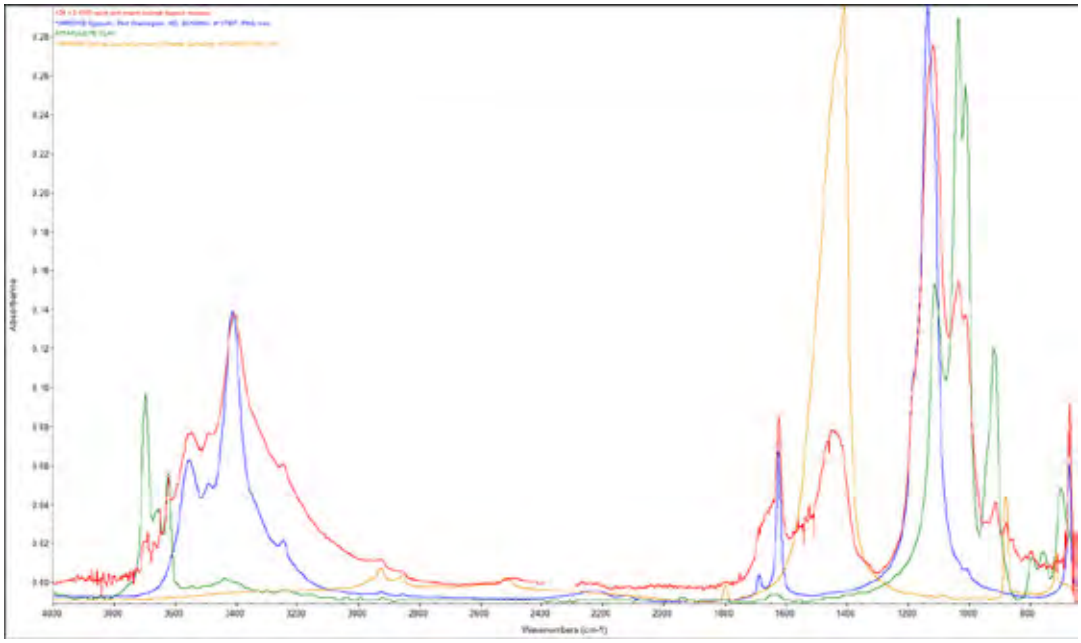

Figure 35. Sample 124, region 1, spectrum 3. Resin and cream-colored deposit overlaid (spectral noise due to using Continuum microscope without a nitrogen flush).

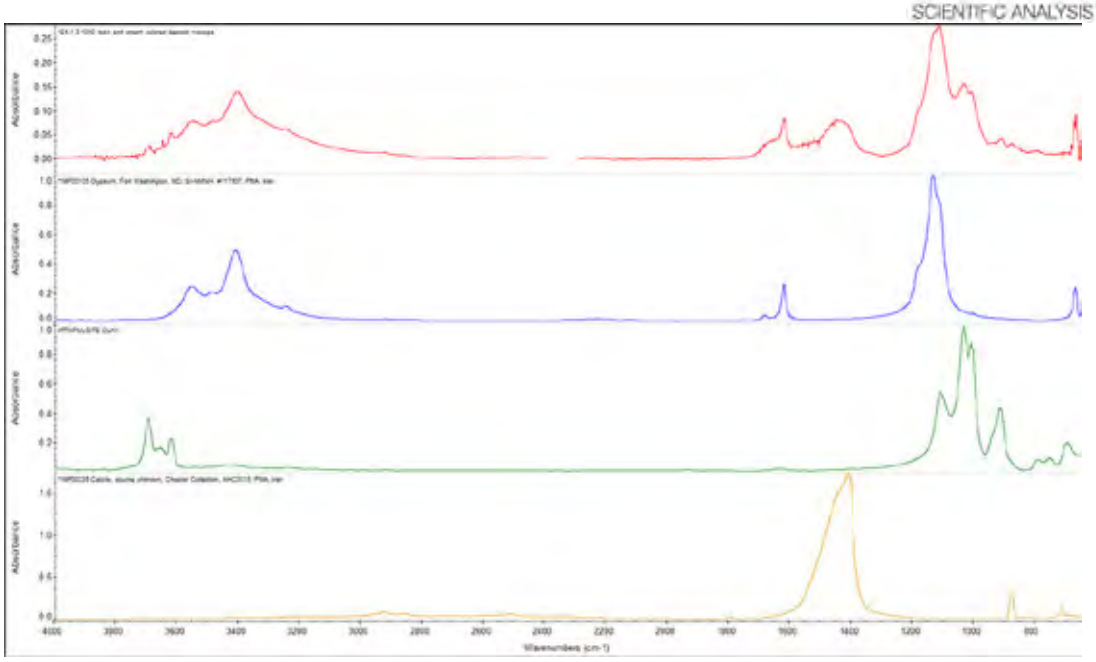

Figure 36. Sample 124, region 1, spectrum 3. Resin and cream-colored deposit, stacked (spectral noise due to using Continuum microscope without a nitrogen flush).

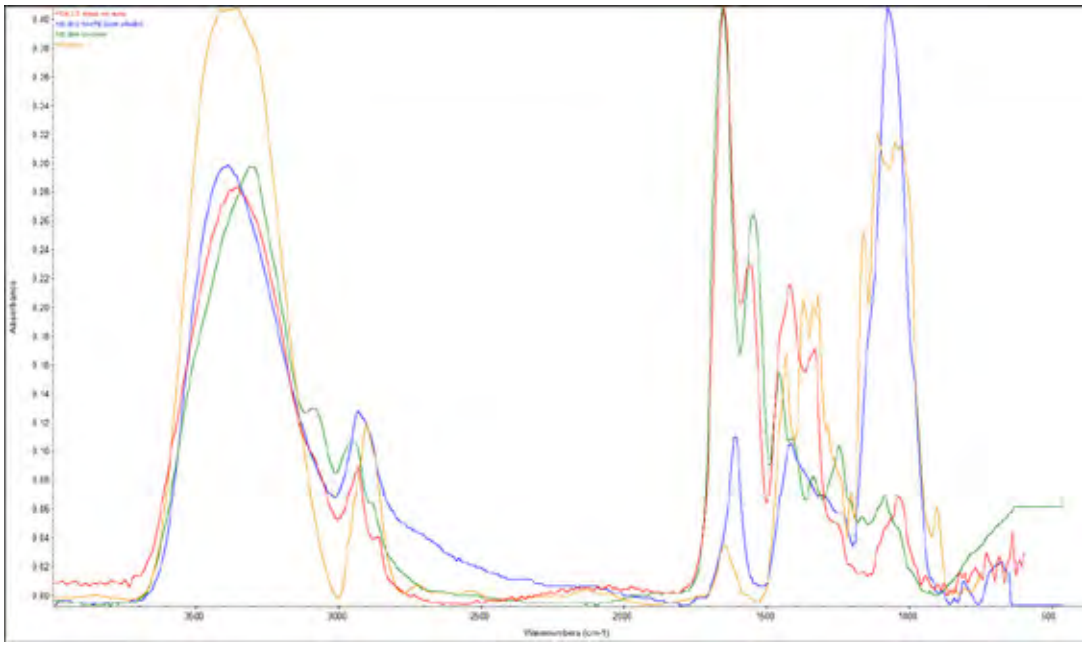

Figure 37. Sample 124, region 2, spectrum 2. Black ink recto, overlaid.

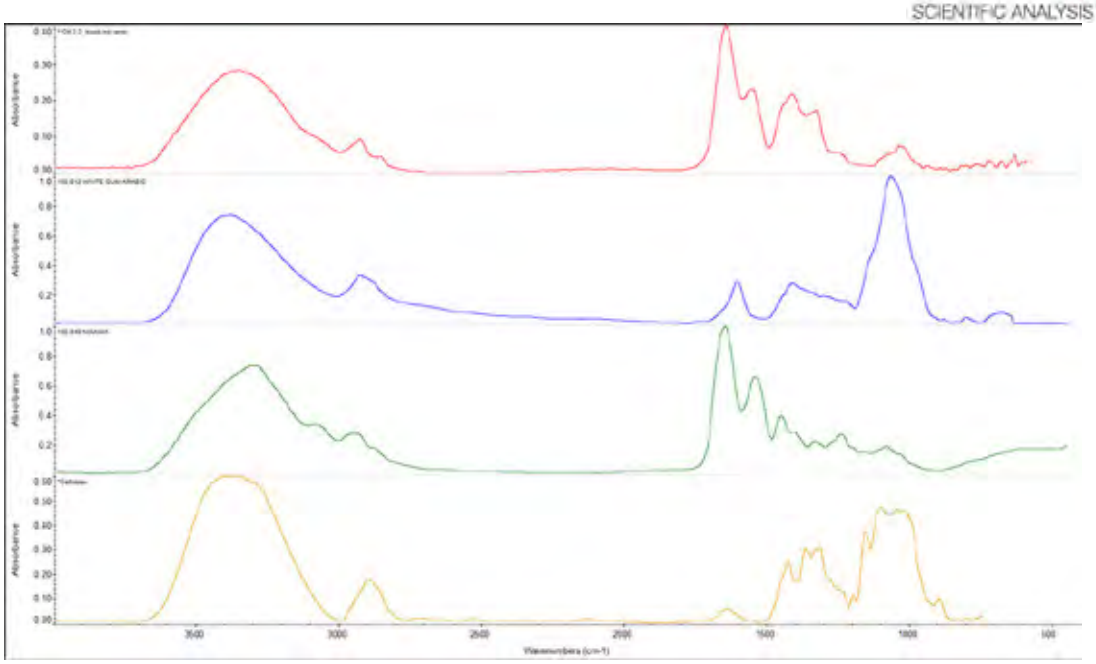

Figure 38. Sample 124, region 2, spectrum 2. Black ink recto, stacked.

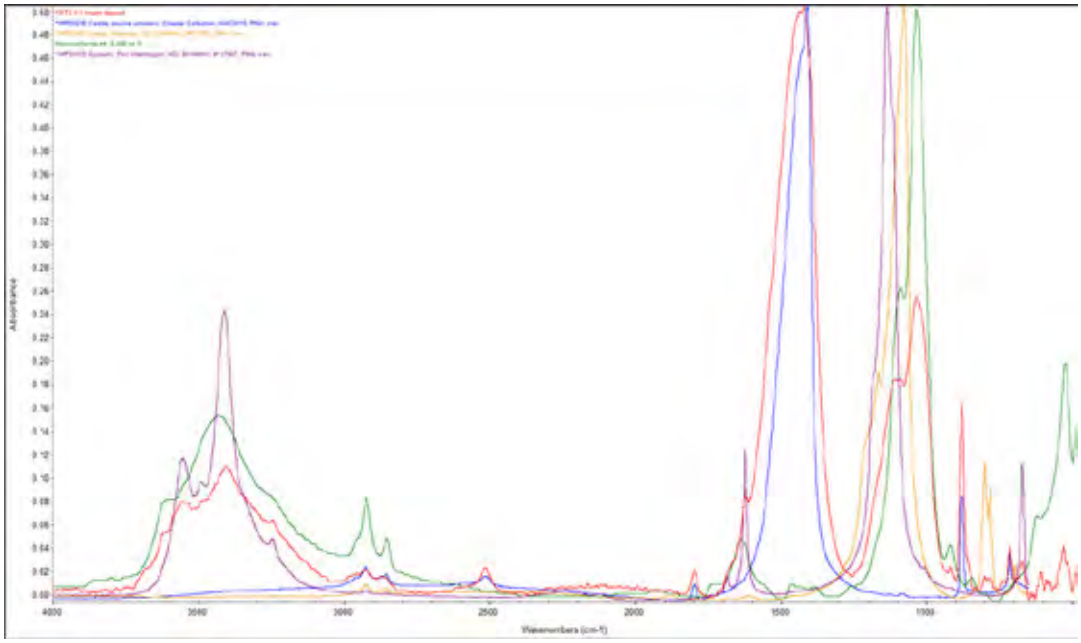

Figure 39. Sample 3173, region 1, spectrum 1. Cream-colored deposit, overlaid.

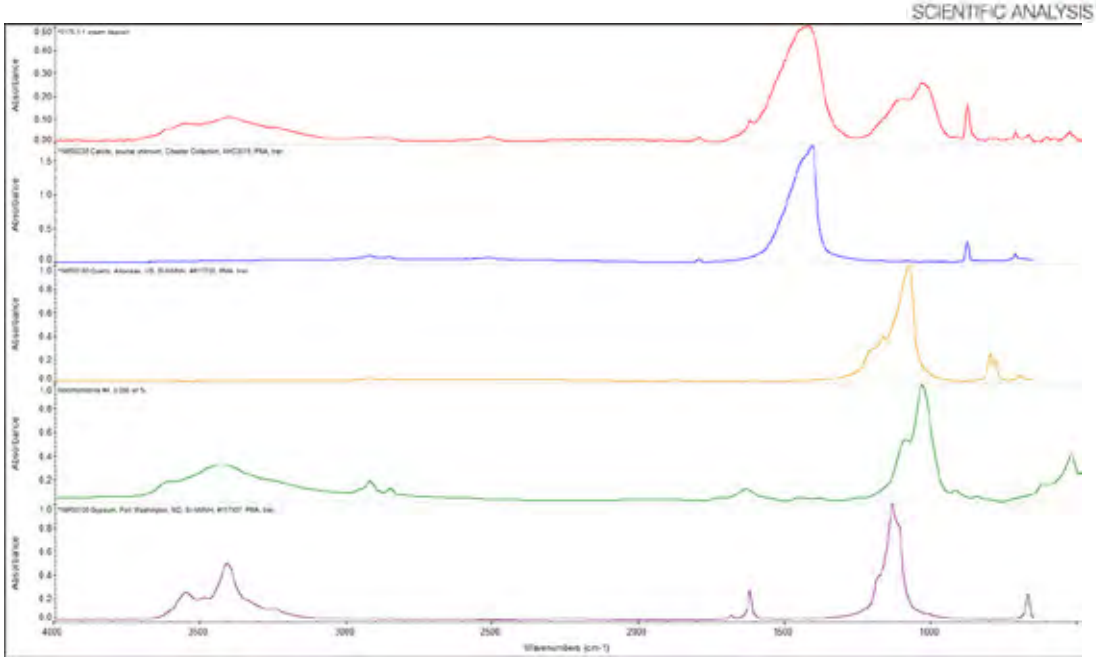

Figure 40. Sample 3173, region 1, spectrum 1. Cream-colored deposit, stacked.

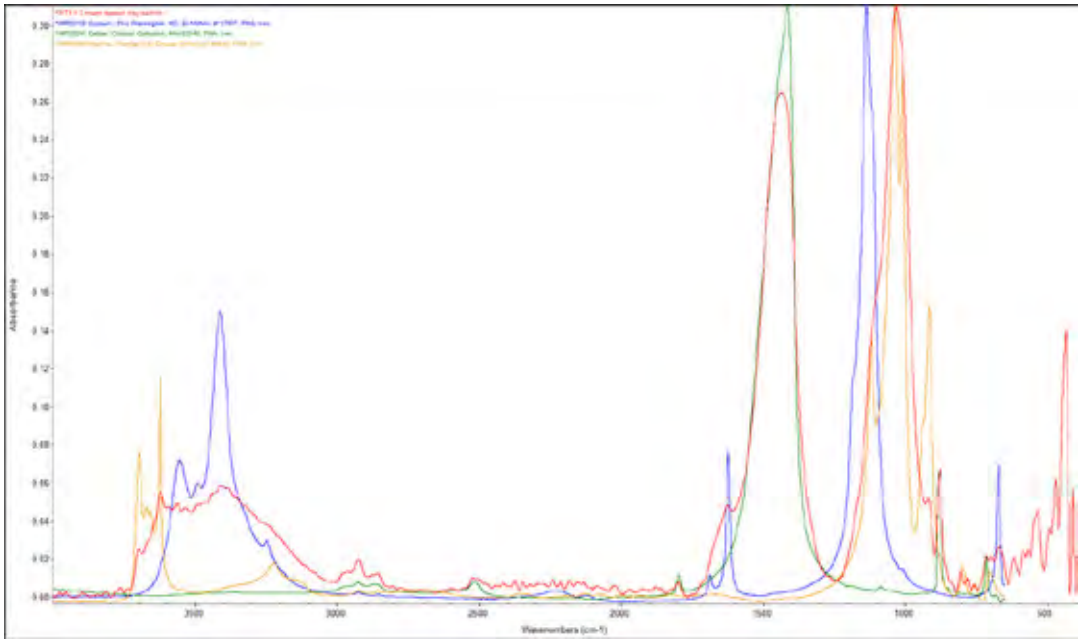

Figure 41. Sample 3173, region 1, spectrum 2. Cream-colored deposit clay particle, overlaid.

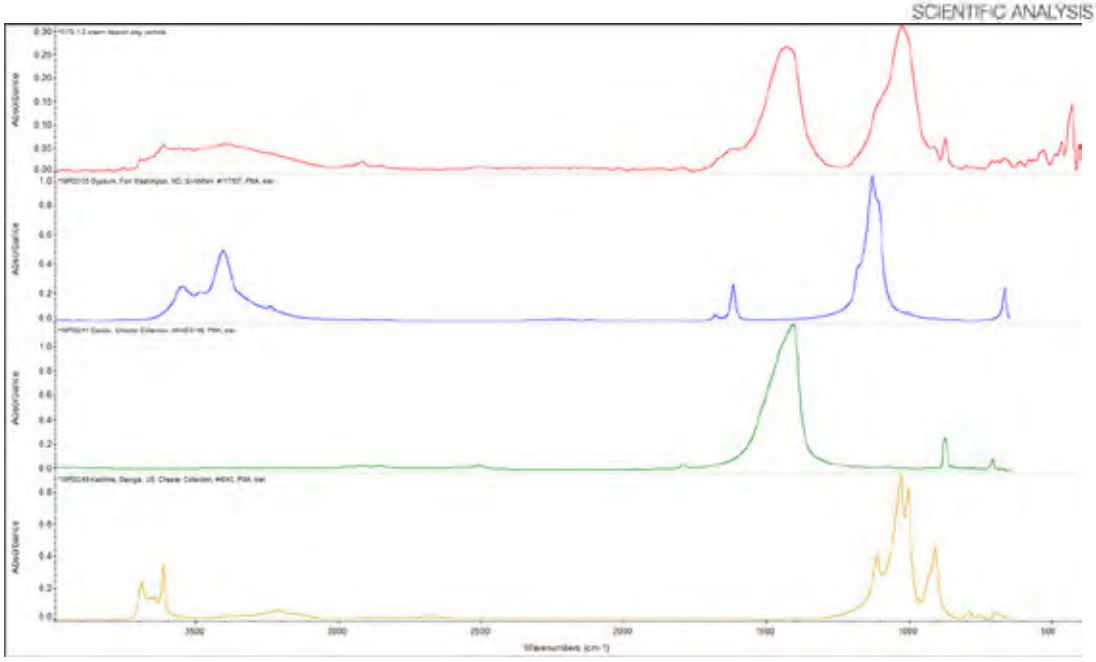

Figure 42. Sample 3173, region 1, spectrum 2. Cream-colored deposit clay particle, stacked.

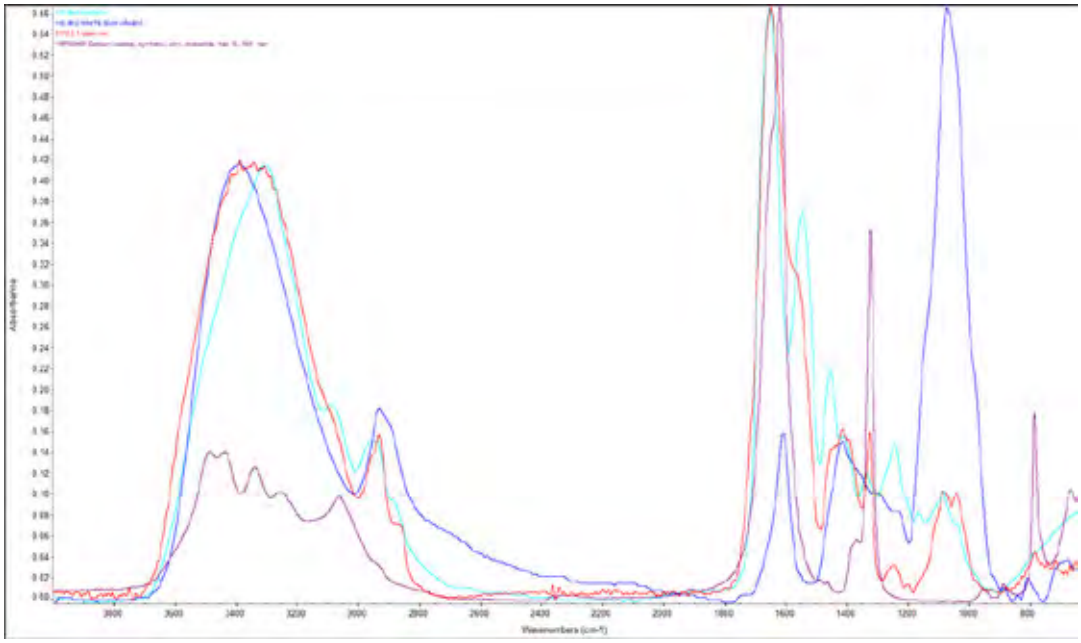

Figure 43. Sample 3173, region 2, spectrum 1. Black ink, overlaid.

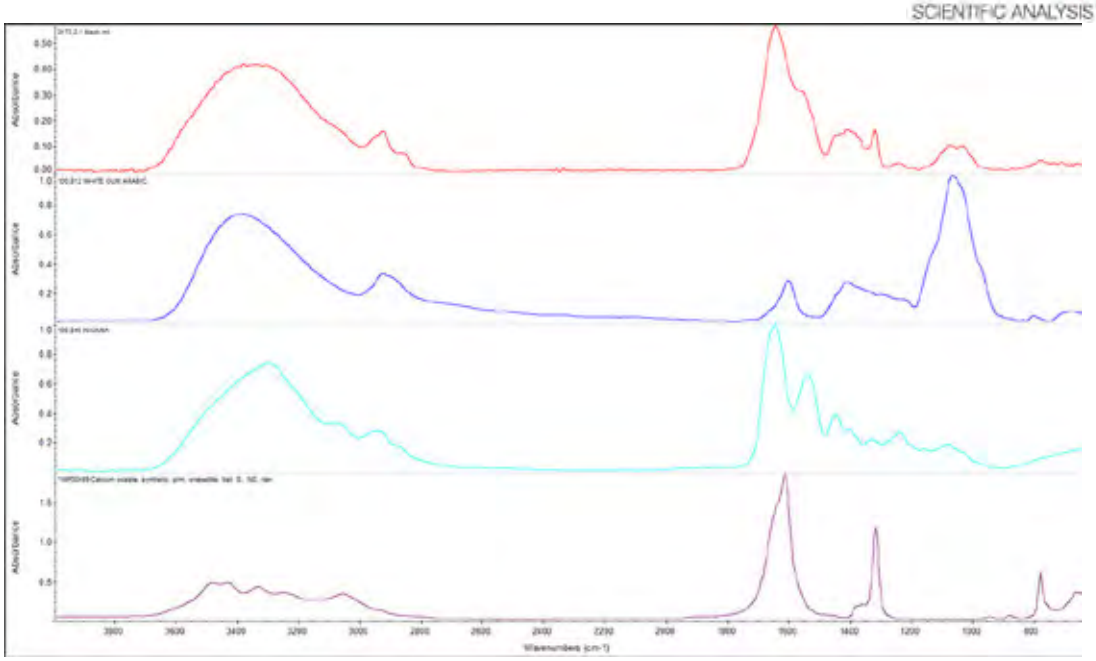

Figure 44. Sample 3173, region 2, spectrum 1. Black ink, stacked.

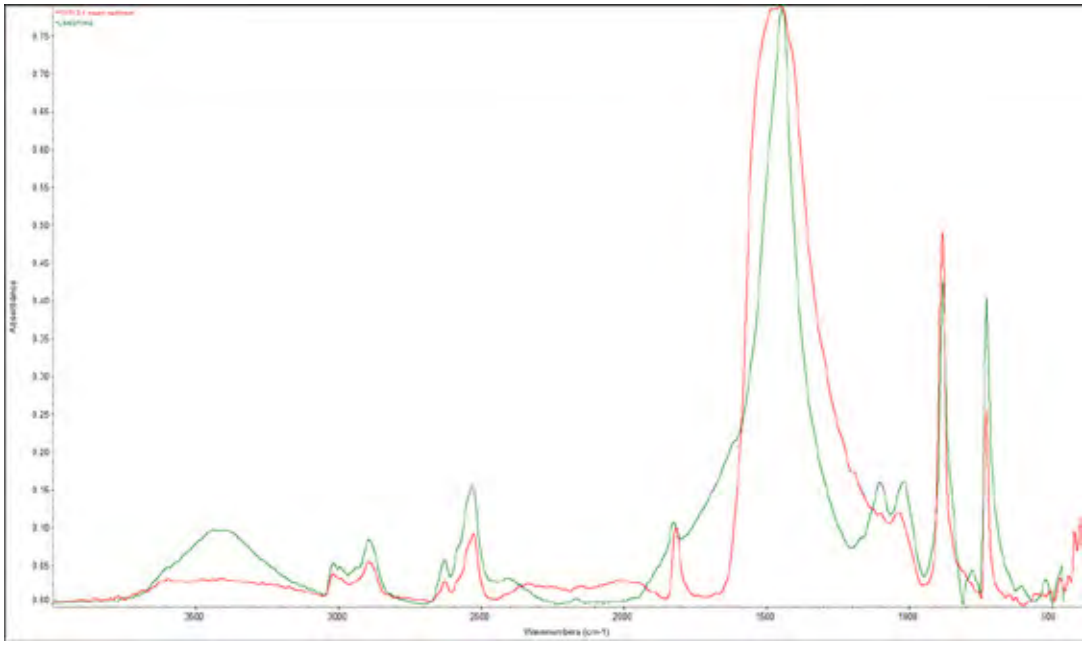

Figure 45. Sample 3173, region 3, spectrum 1. Cream-colored sediment, overlaid.

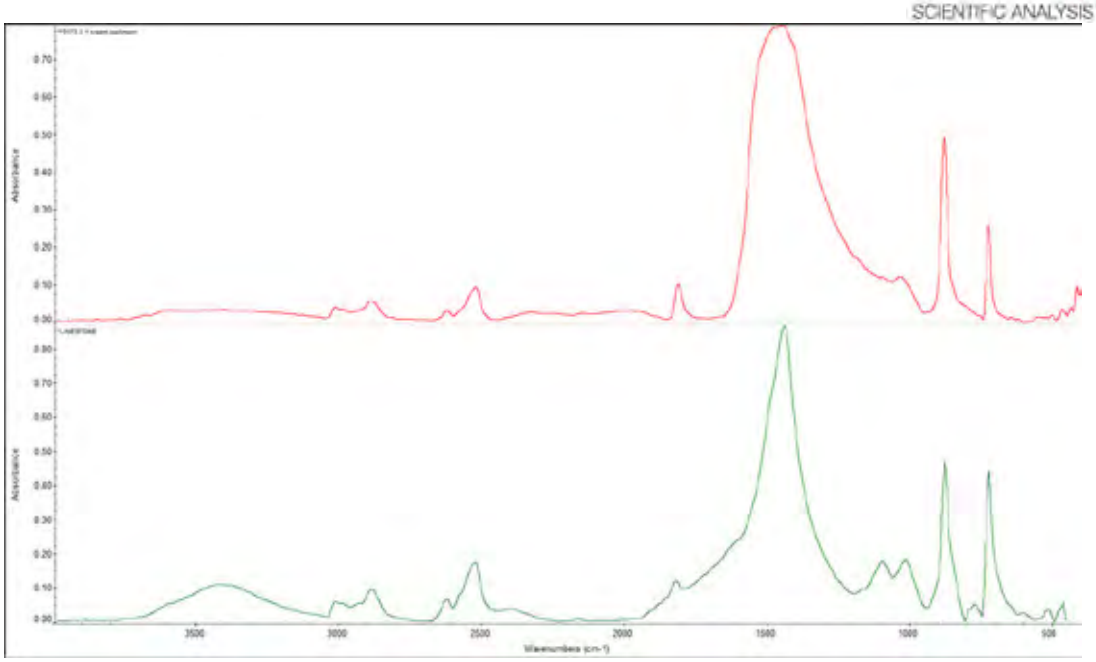

Figure 46. Sample 3173, region 3, spectrum 1. Cream-colored sediment, stacked.

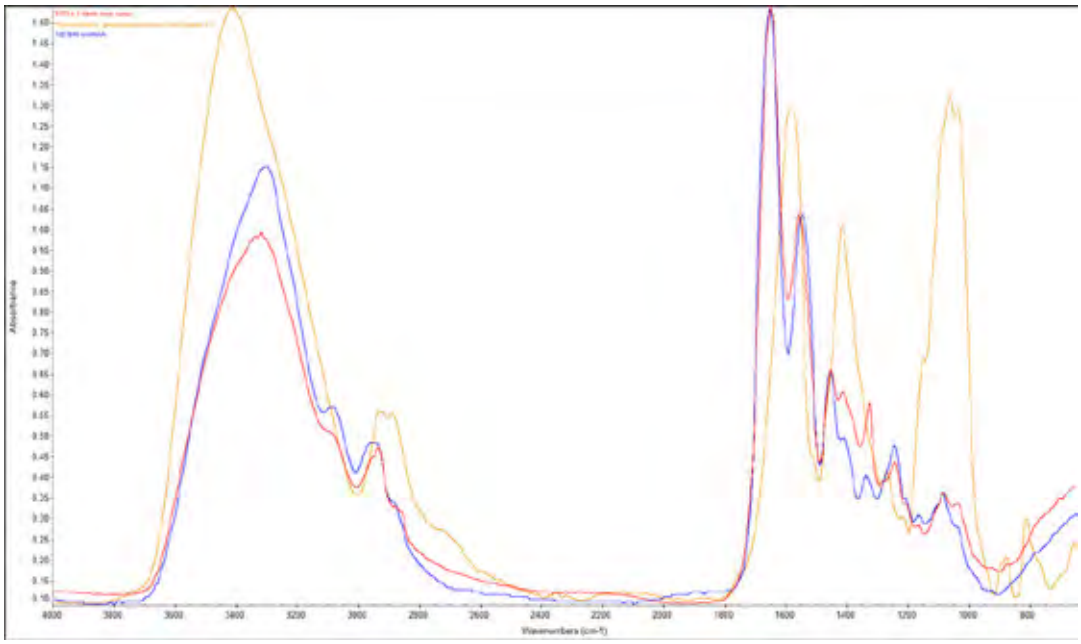

Figure 47. Sample 3173, region 4, spectrum 1. Fibrils from verso, overlaid.

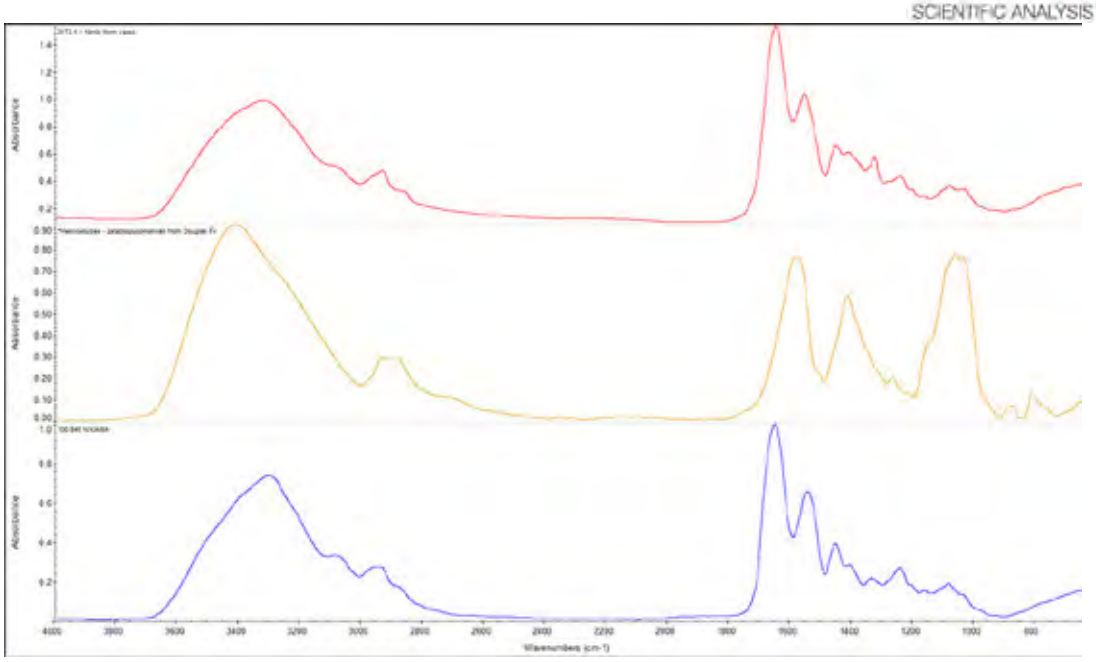

Figure 48. Sample 3173, region 4, spectrum 1. Fibrils from verso, stacked.

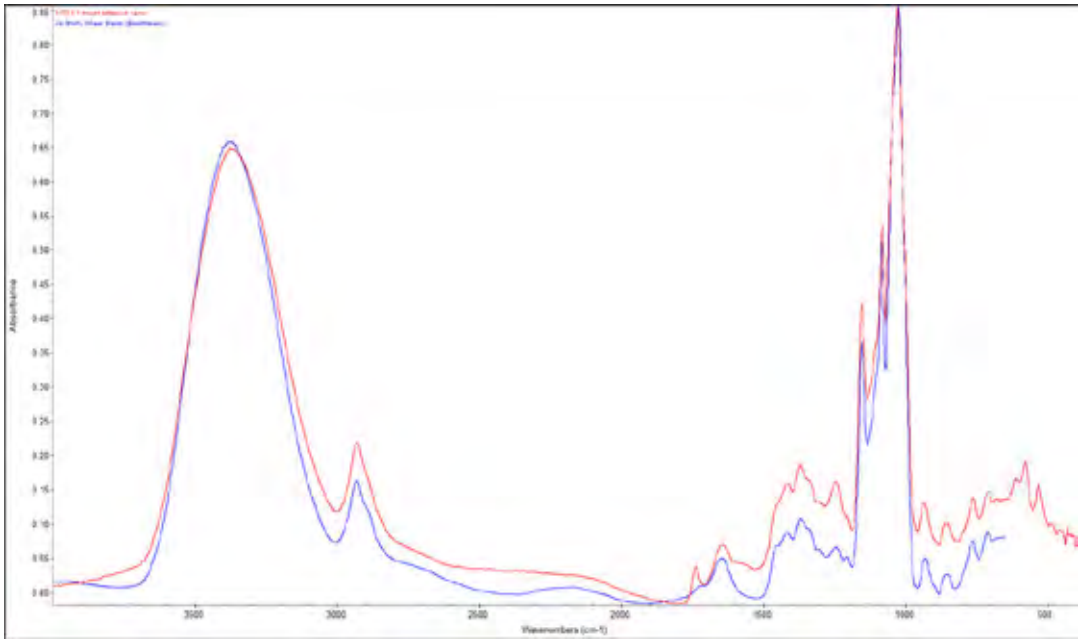

Figure 49. Sample 3173, region 5, spectrum 1. Mount adhesive verso, overlaid.

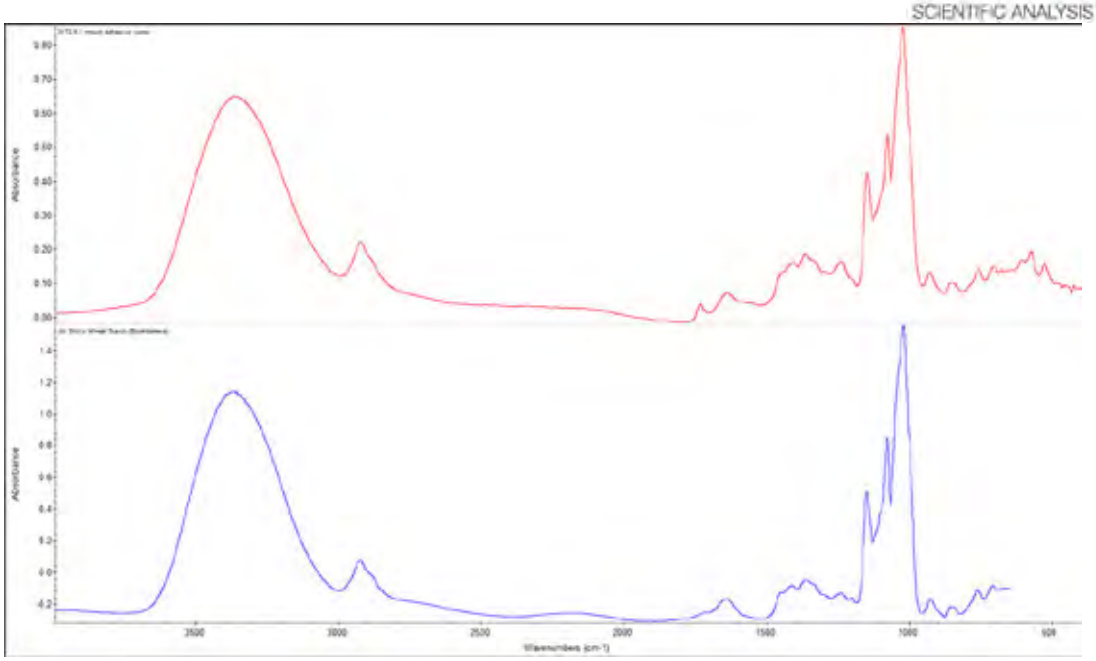

Figure 50. Sample 3173, region 5, spectrum 1. Mount adhesive verso, stacked.

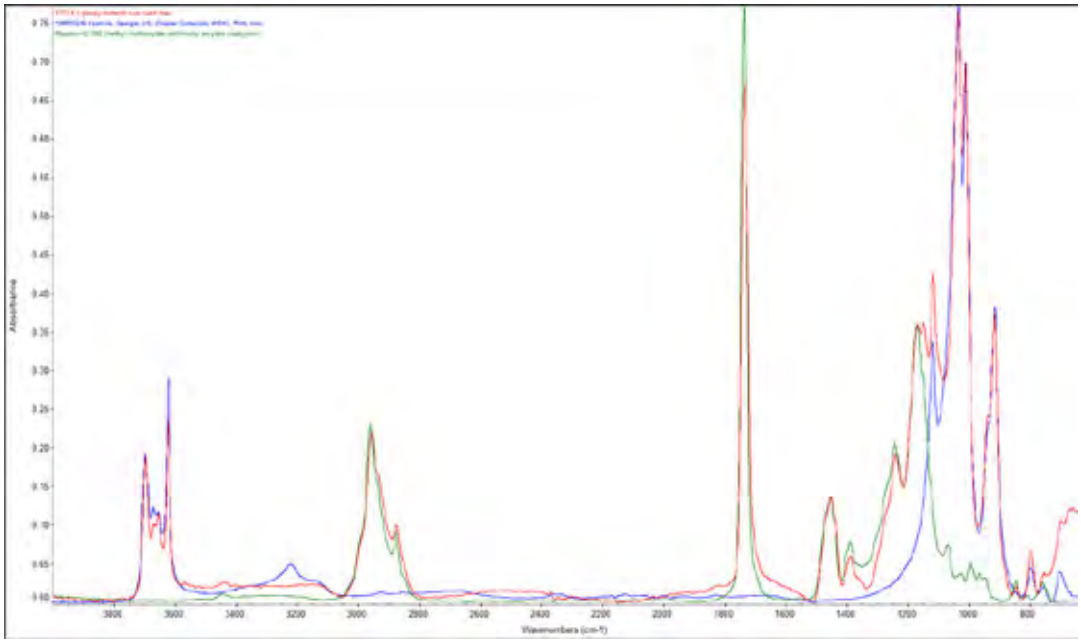

Figure 51. Sample 3173, region 6, spectrum 1. Glossy material ruled lines, overlaid.

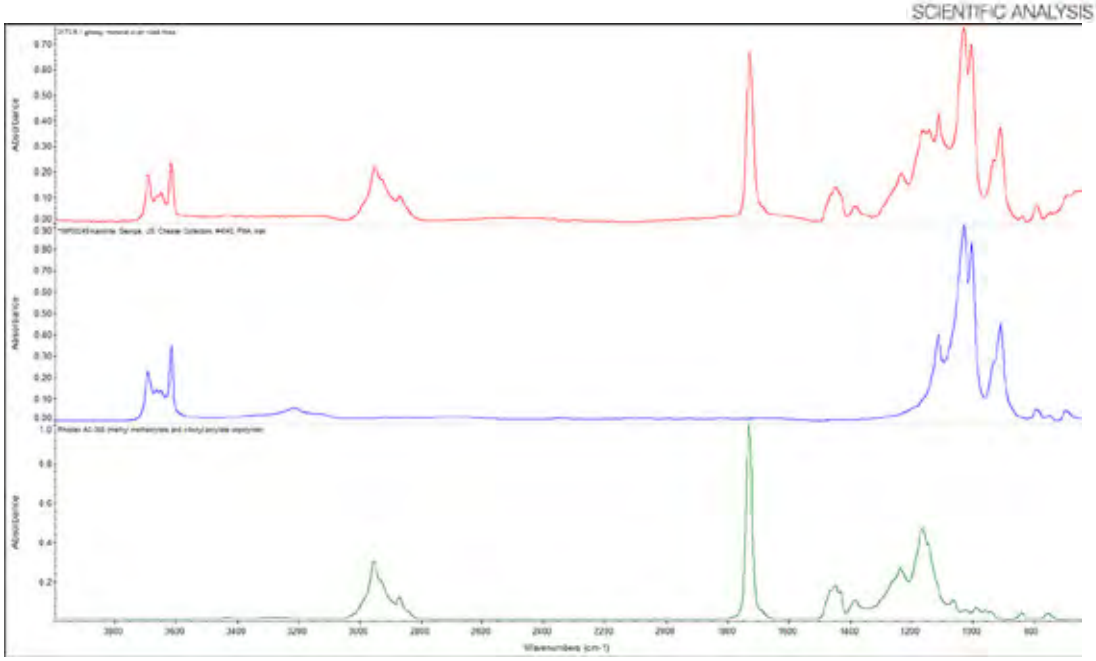

Figure 52. Sample 3173, region 6, spectrum 1. Glossy material ruled lines, stacked.

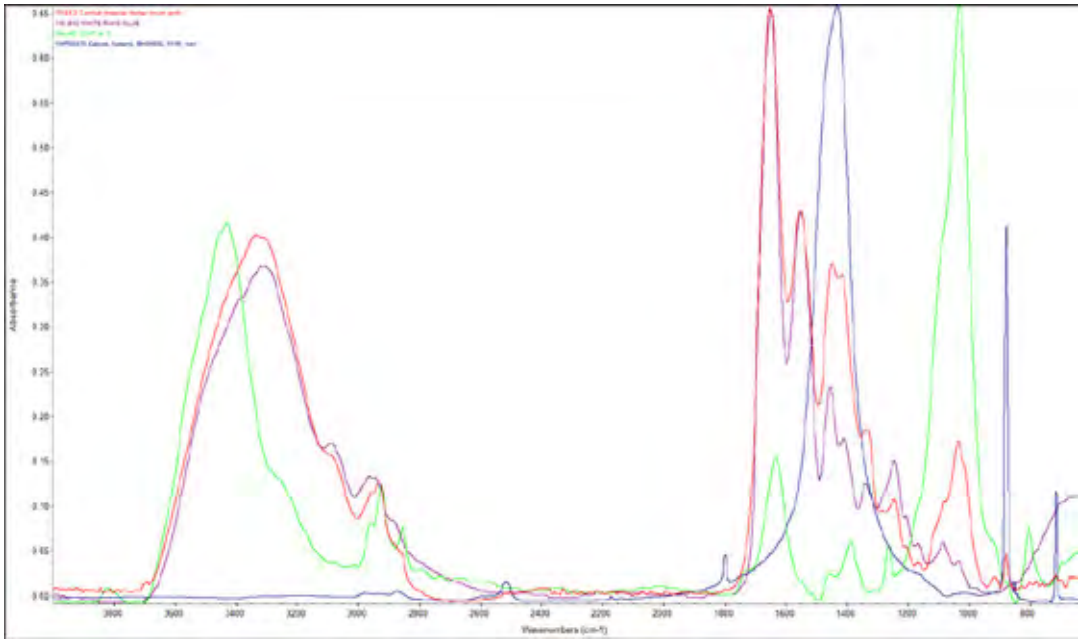

Figure 53. Sample 3183, region 2, spectrum 2. Amber material, darker brown recto, overlaid.

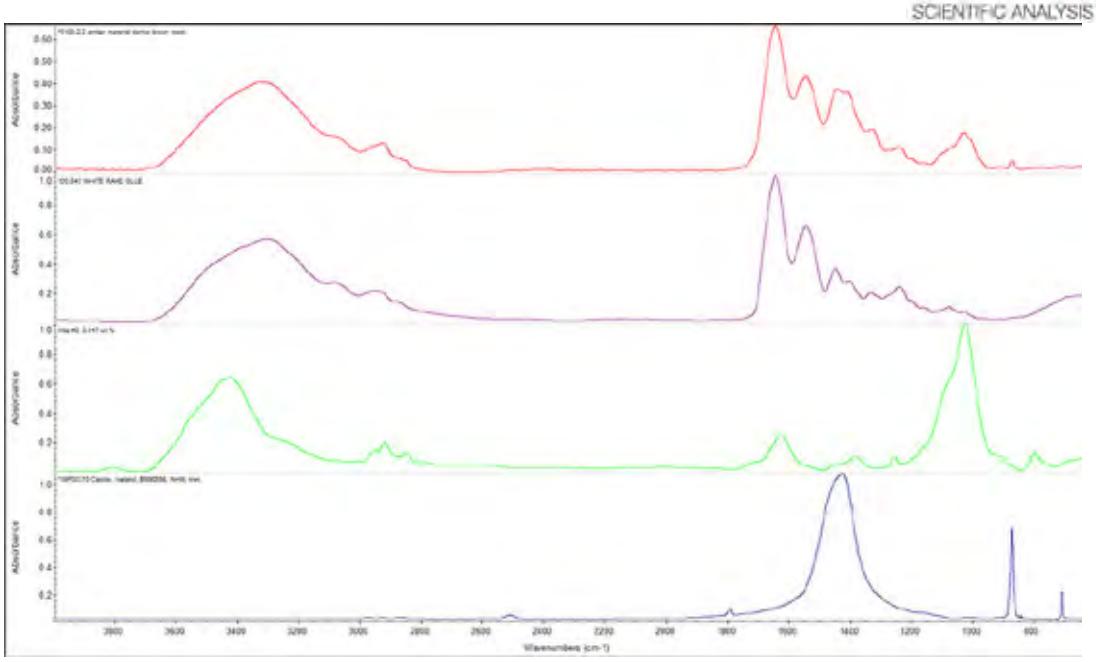

Figure 54. Sample 3183, region 2, spectrum 2. Amber material, darker brown recto, stacked.

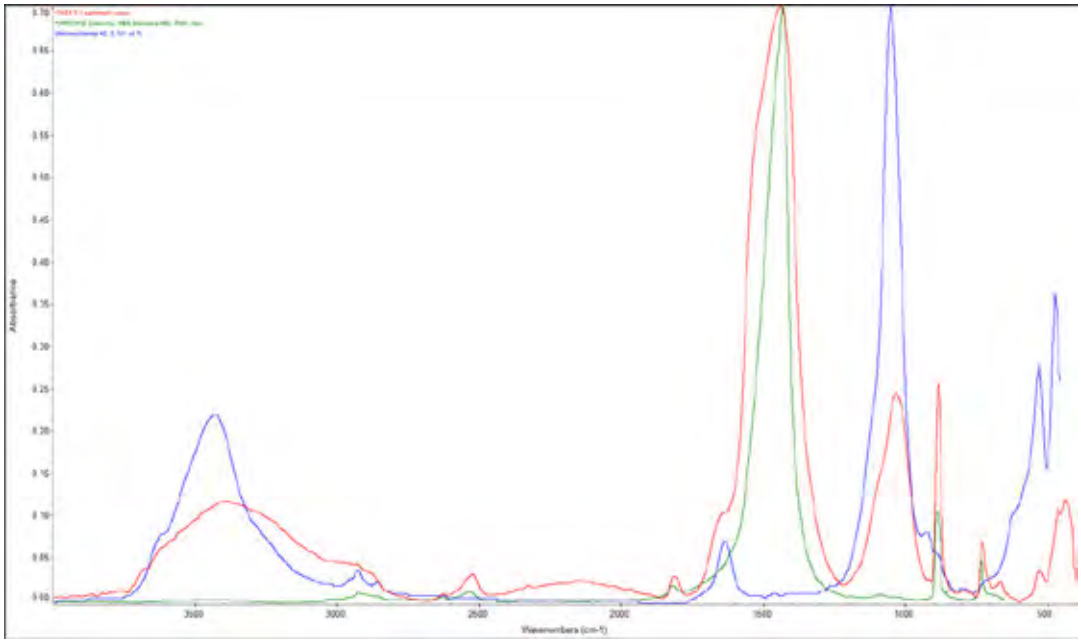

Figure 55. Sample 3183, region 3, spectrum 1. Sediment verso, overlaid.

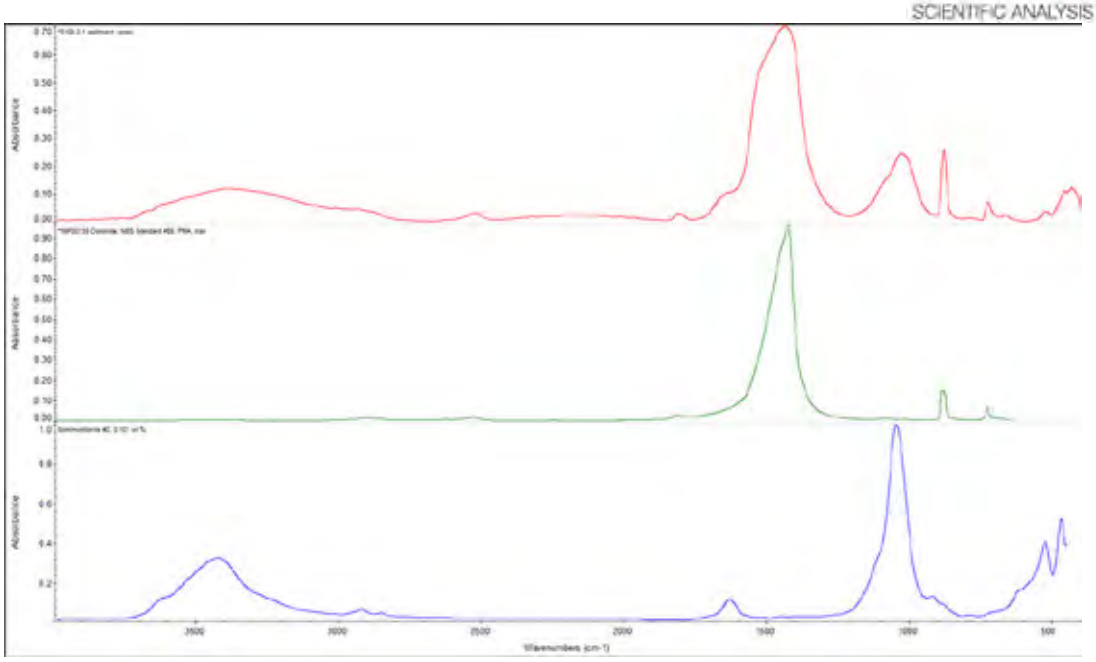

Figure 56. Sample 3183, region 3, spectrum 1. Sediment verso, stacked.

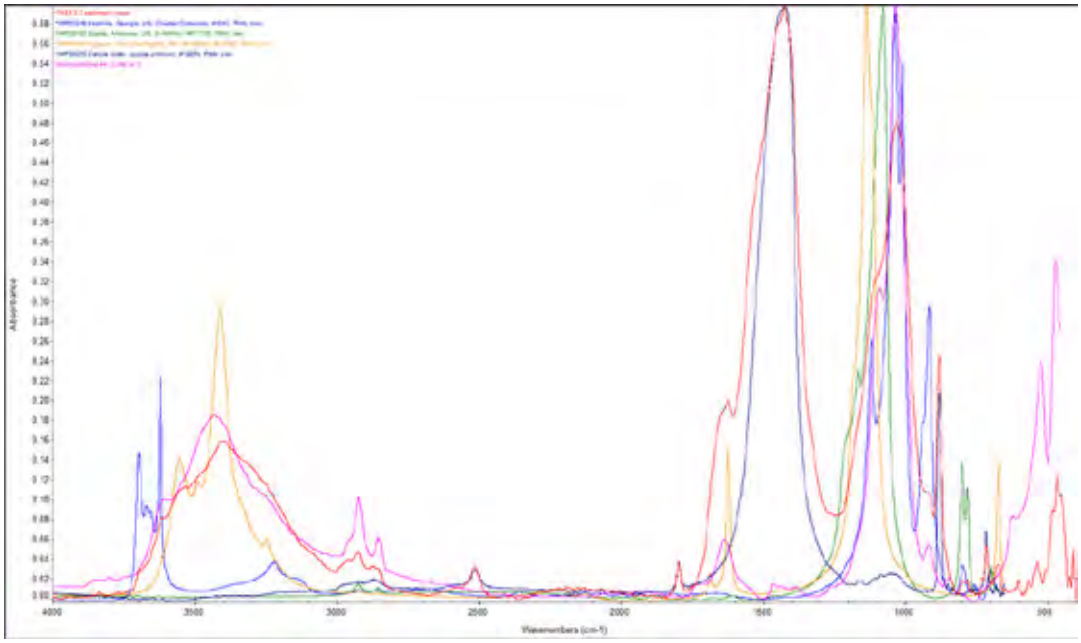

Figure 57. Sample 3183, region 3, spectrum 2. Sediment verso, overlaid.

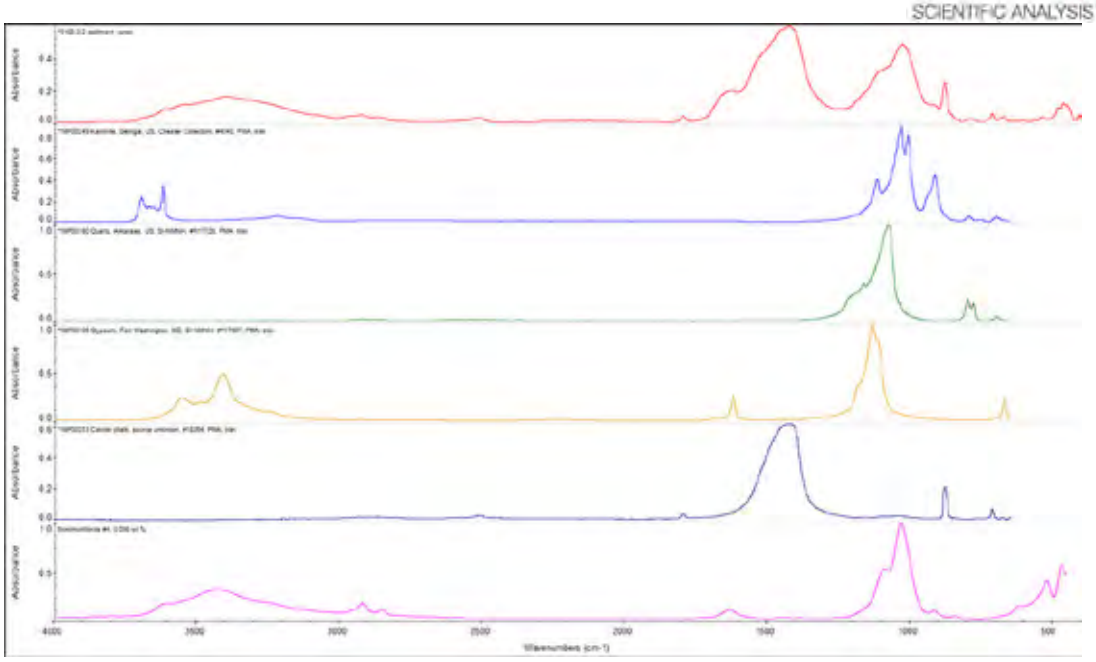

Figure 58. Sample 3183, region 3, spectrum 2. Sediment verso, stacked.

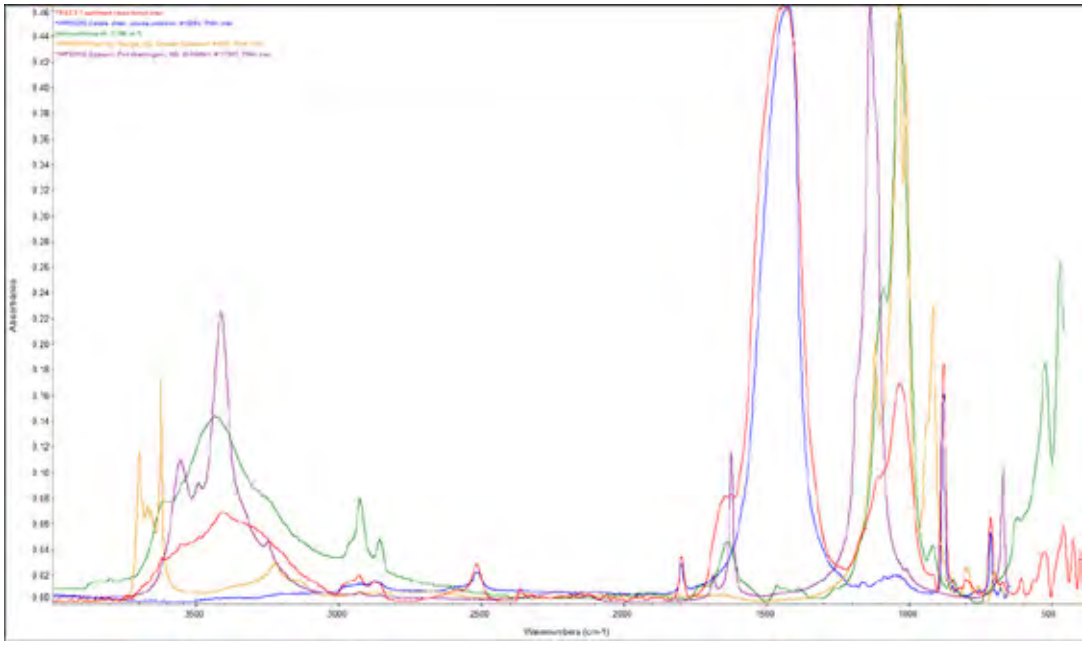

Figure 59. Sample 3183, region 3, spectrum 3. Sediment verso, brown area, overlaid.

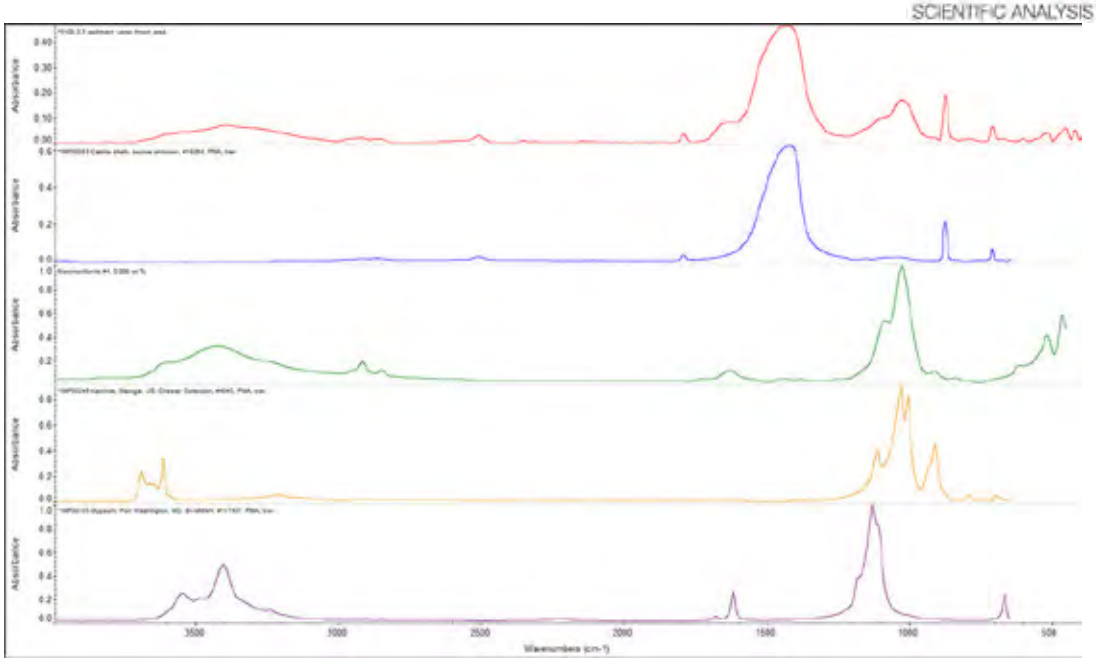

Figure 60. Sample 3183, region 3, spectrum 3. Sediment verso, brown area, stacked.

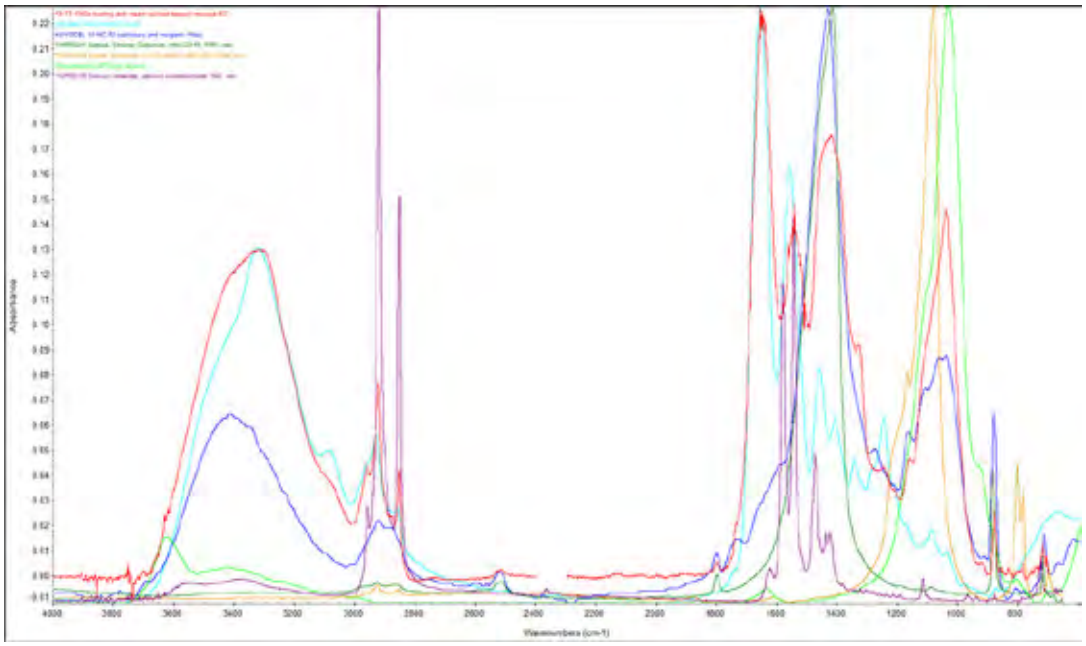

Figure 61. Sample 4741, region 1, spectrum 1. Coating and cream-colored deposit, overlaid (spectral noise due to using Continuum microscope without a nitrogen flush).

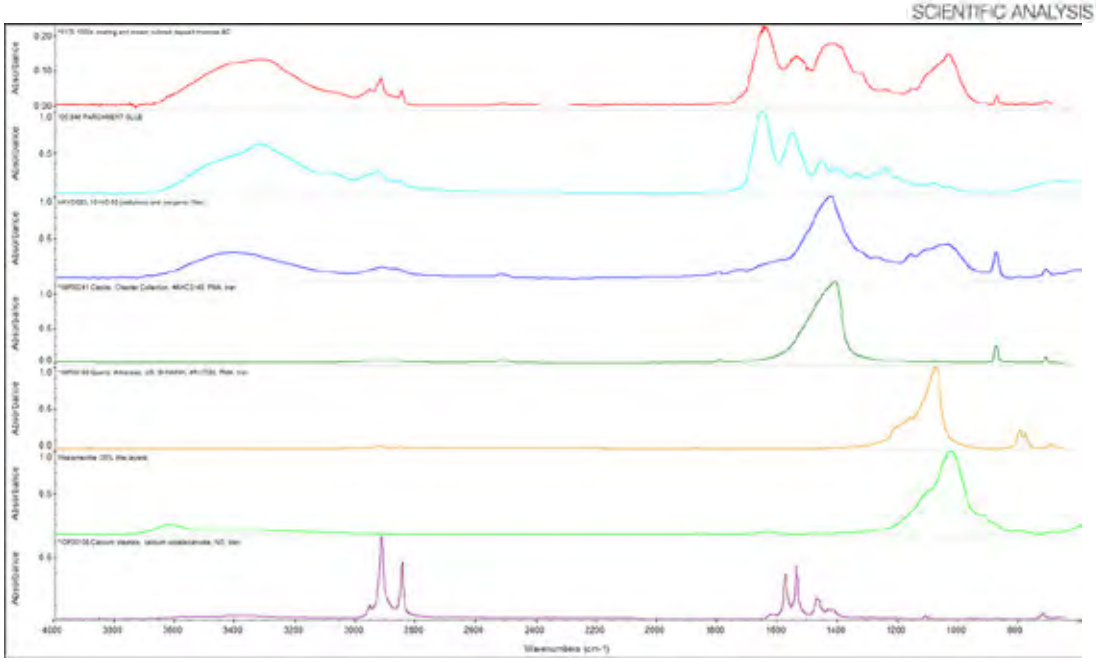

Figure 62. Sample 4741, region 1, spectrum 1. Coating and cream colored deposit, stacked (spectral noise due to using Continuum microscope without a nitrogen flush).

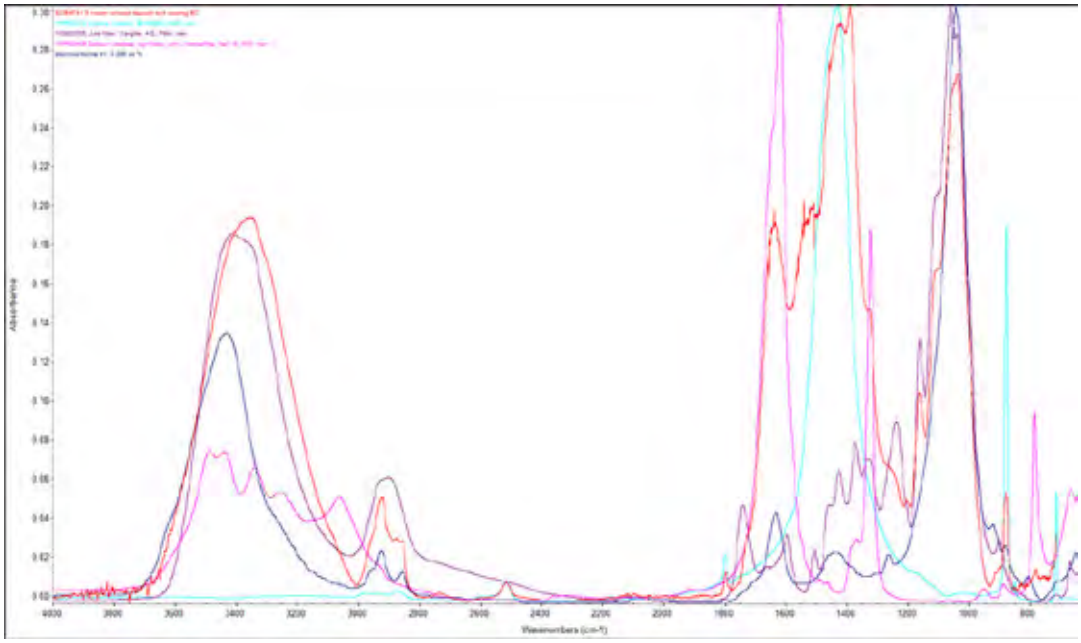

Figure 63. Sample 4741, region 1, spectrum 3. Cream colored deposit and coating, overlaid.

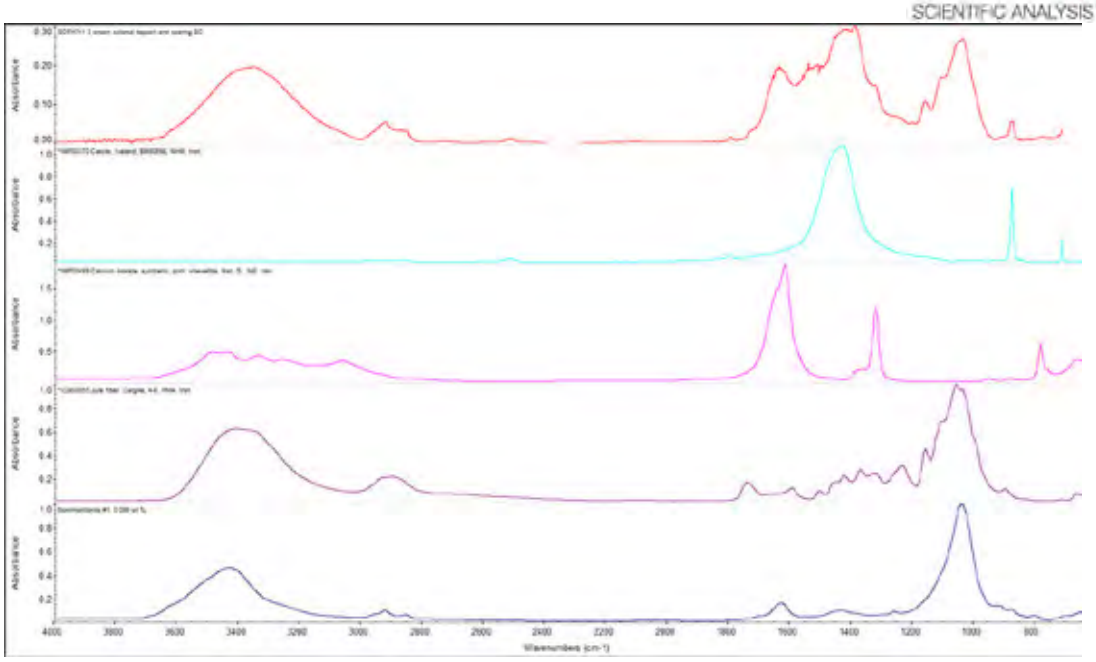

Figure 64. Sample 4741, region 1, spectrum 3. Cream colored deposit and coating, stacked.

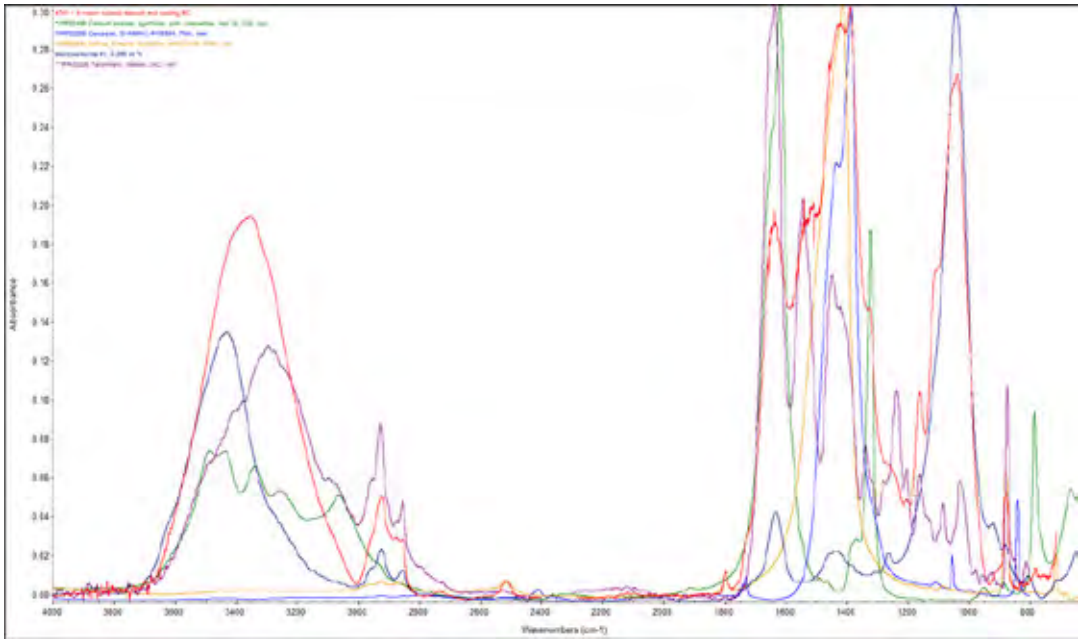

Figure 65. Sample 4741, region 1, spectrum 4. Cream colored deposit and coating, overlaid (spectral noise due to using Continuum microscope without a nitrogen flush).

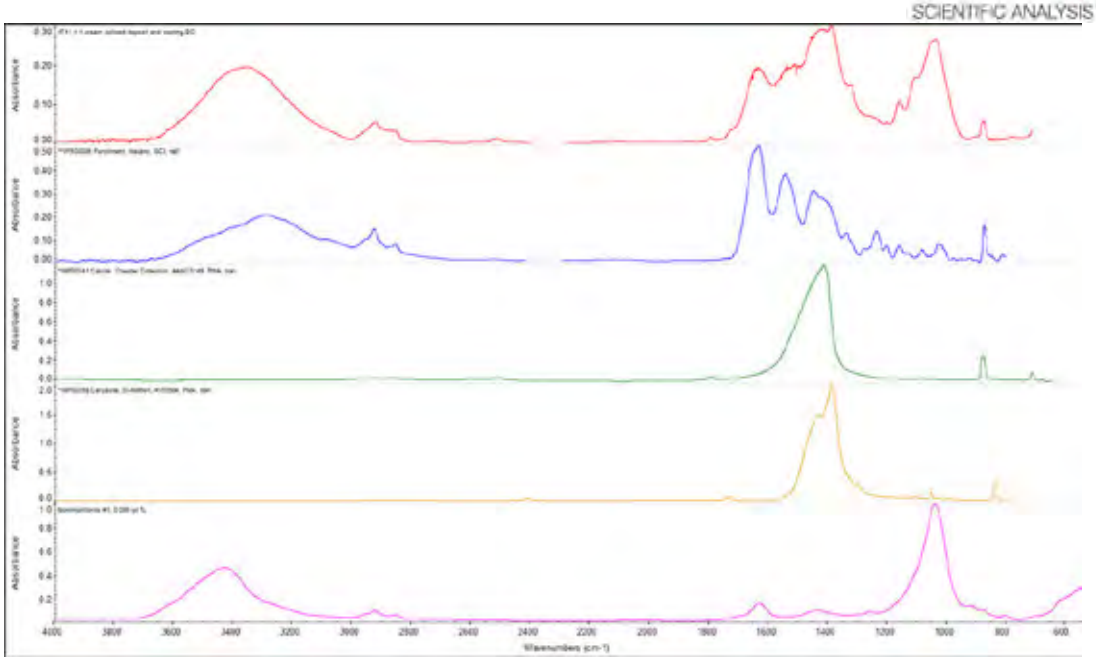

Figure 66. Sample 4741, region 1, spectrum 4. Cream colored deposit and coating, stacked (spectral noise due to using Continuum microscope without a nitrogen flush).

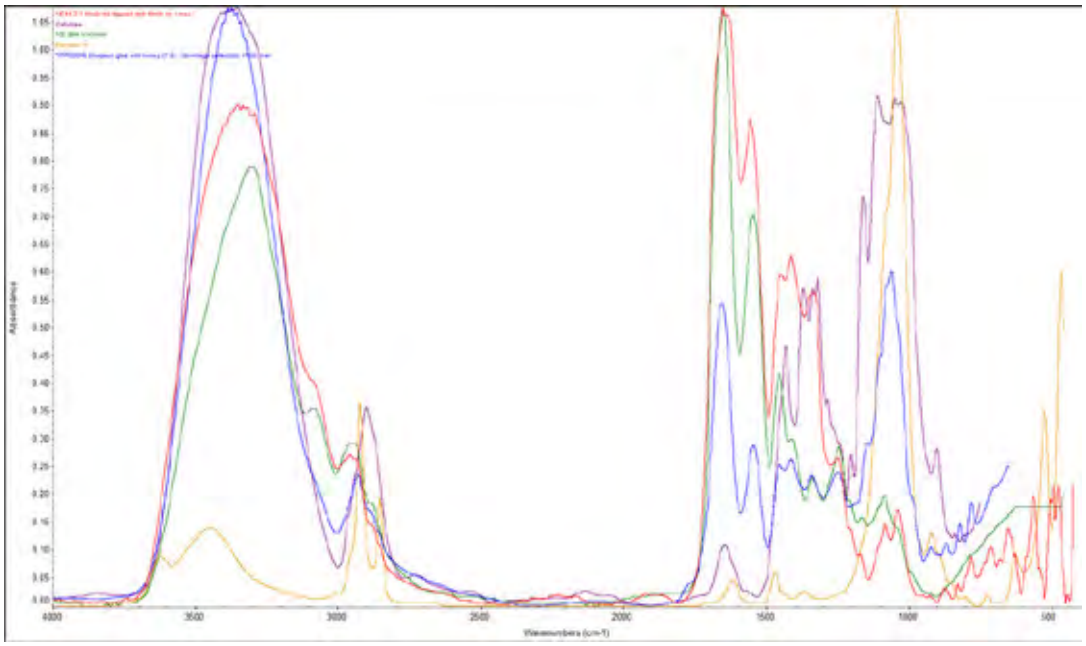

Figure 67. Sample 4741, region 2, spectrum 1. Black ink deposit and fibrils on verso, overlaid.

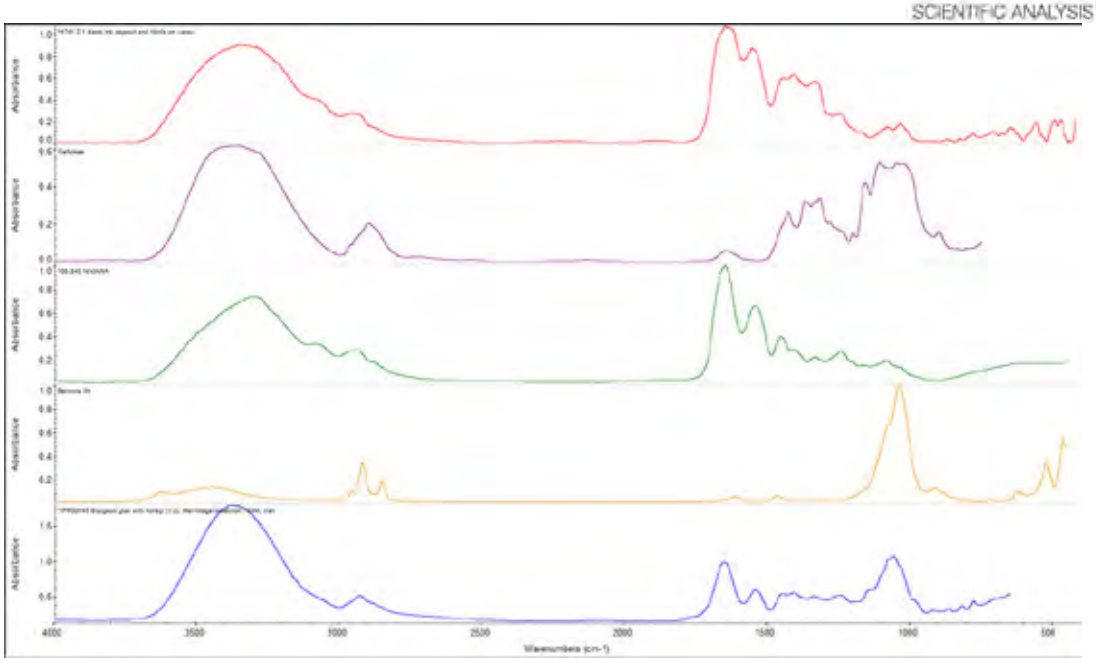

Figure 68. Sample 4741, region 2, spectrum 1. Black ink deposit and fibrils on verso, stacked.

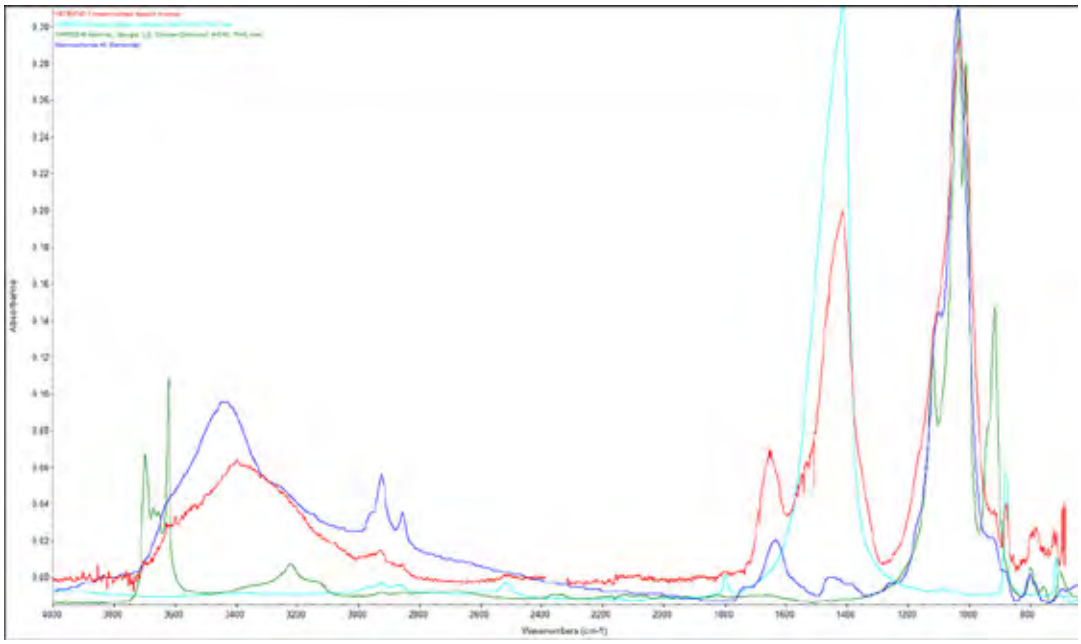

Figure 69. Sample 4742, region 1, spectrum 1. Cream colored deposit, overlaid (spectral noise due to using Continuum microscope without a nitrogen flush).

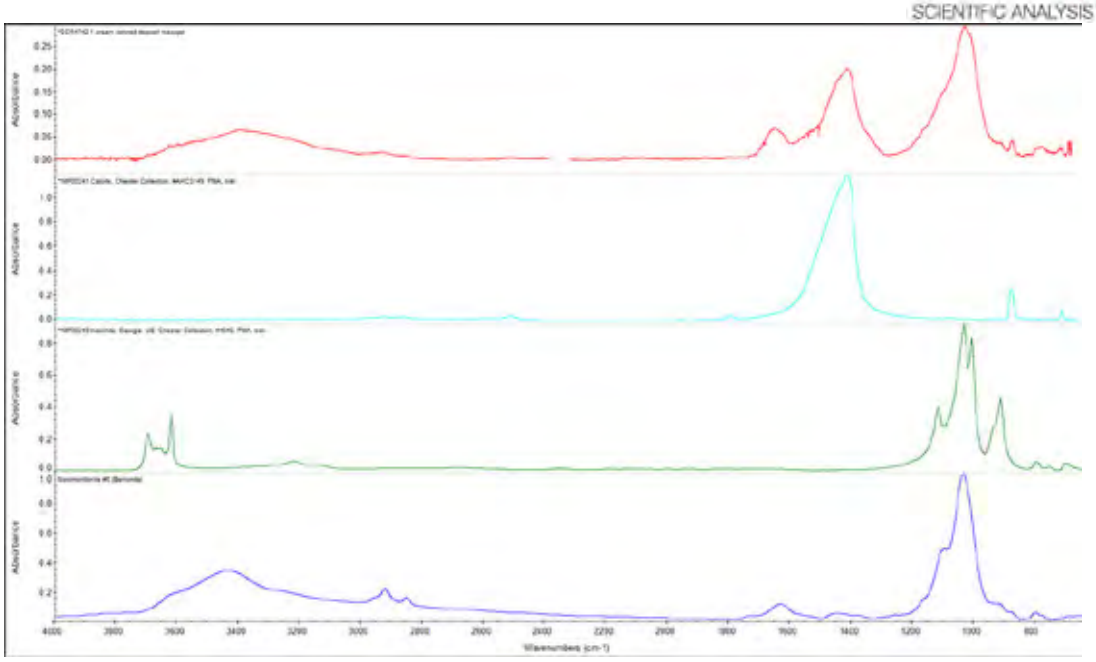

Figure 70. Sample 4742, region 1, spectrum 1. Cream colored deposit, stacked (spectral noise due to using Continuum microscope without a nitrogen flush).

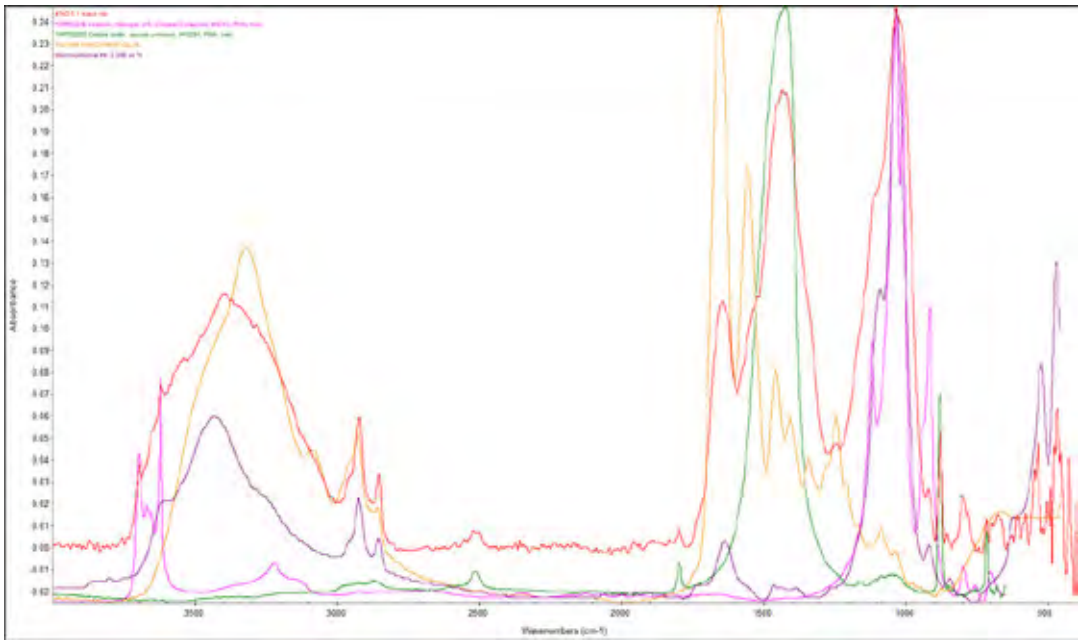

Figure 71. Sample 4742, region 2, spectrum 1. Black ink verso, overlaid (spectral noise due to using Continuum microscope without a nitrogen flush).

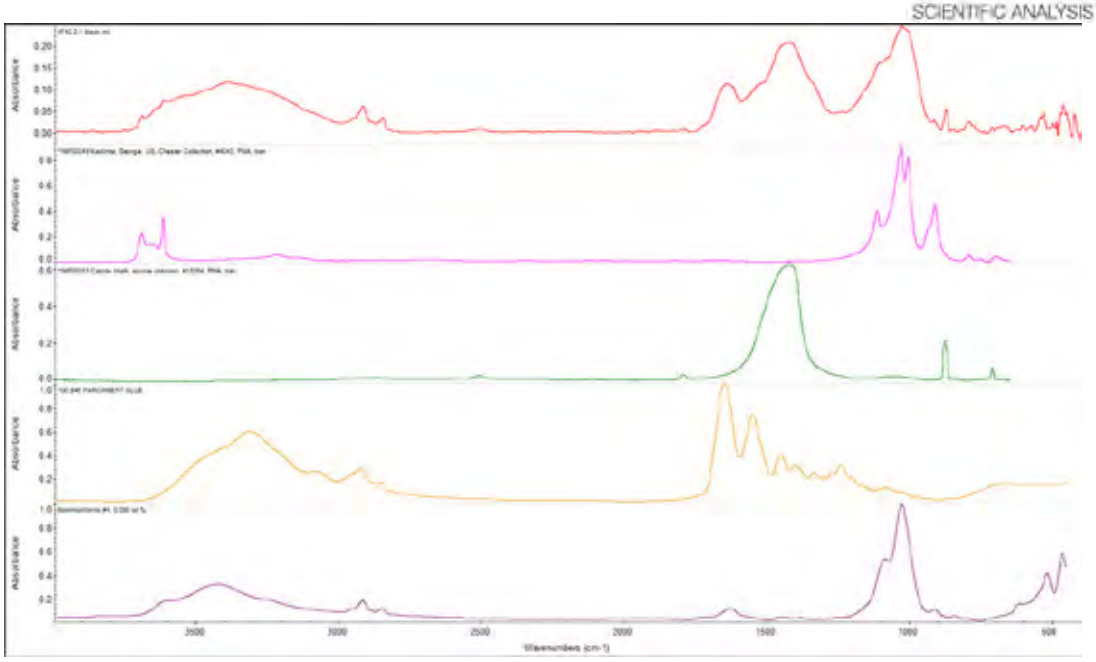

Figure 72. Sample 4742, region 2, spectrum 1. Black ink verso, stacked (spectral noise due to using Continuum microscope without a nitrogen flush).

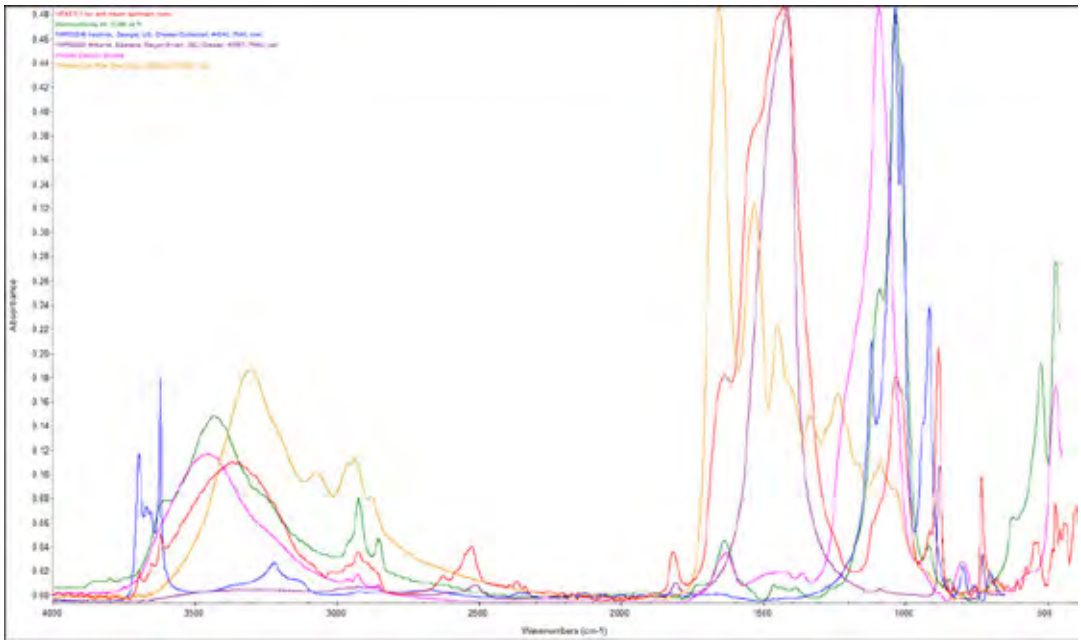

Figure 73. Sample 4742, region 3, spectrum 1. Tan and cream sediment, verso, overlaid.

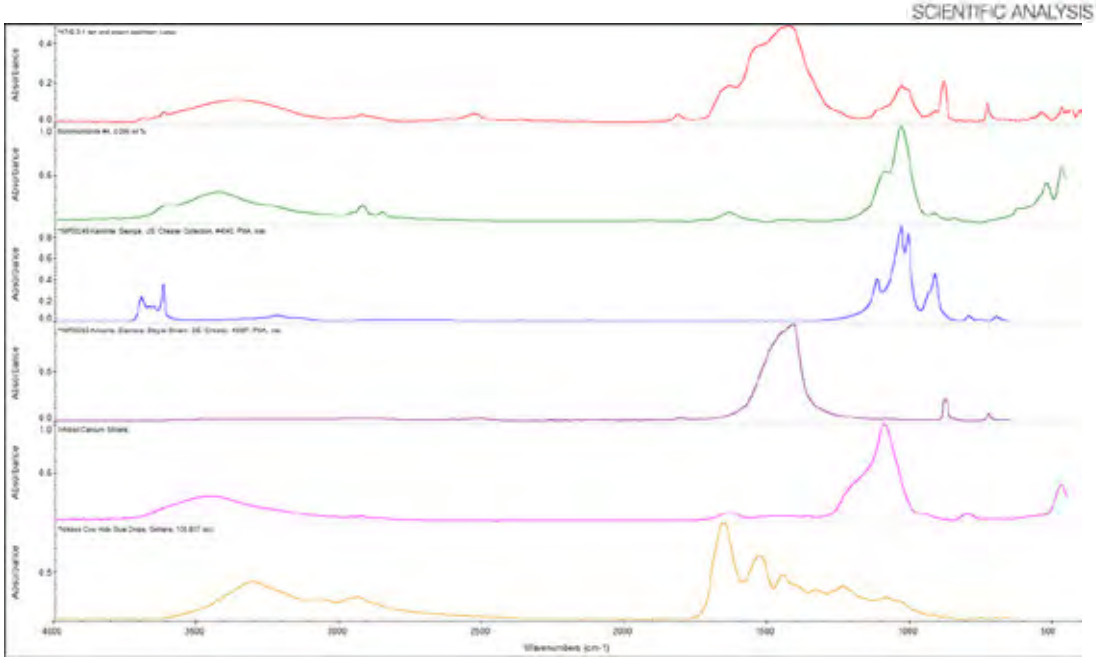

Figure 74. Sample 4742, region 3, spectrum 1. Tan and cream sediment, verso, stacked.

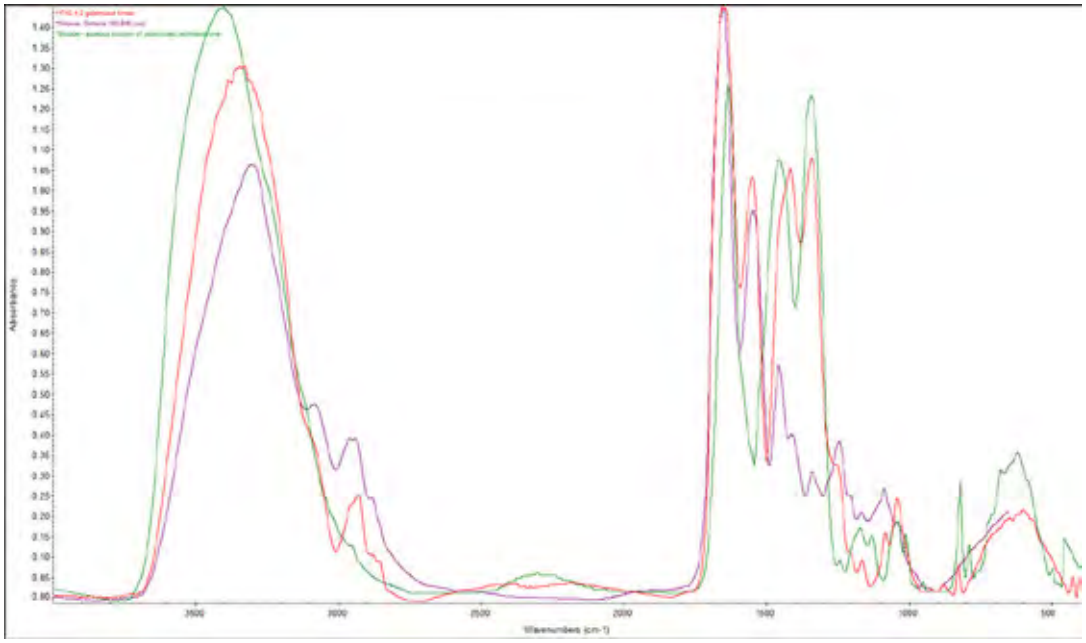

Figure 75. Sample 4742, region 4, spectrum 2. Gelatinized fibrils or coating, overlaid.

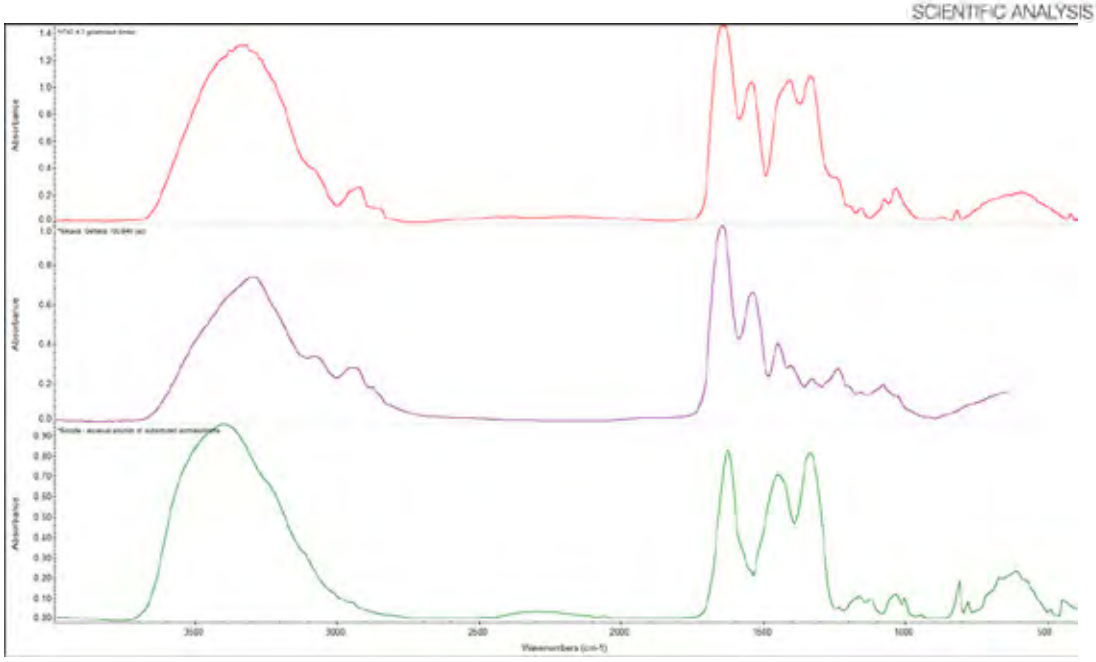

Figure 76. Sample 4742, region 4, spectrum 2. Gelatinized fibrils or coating, stacked.

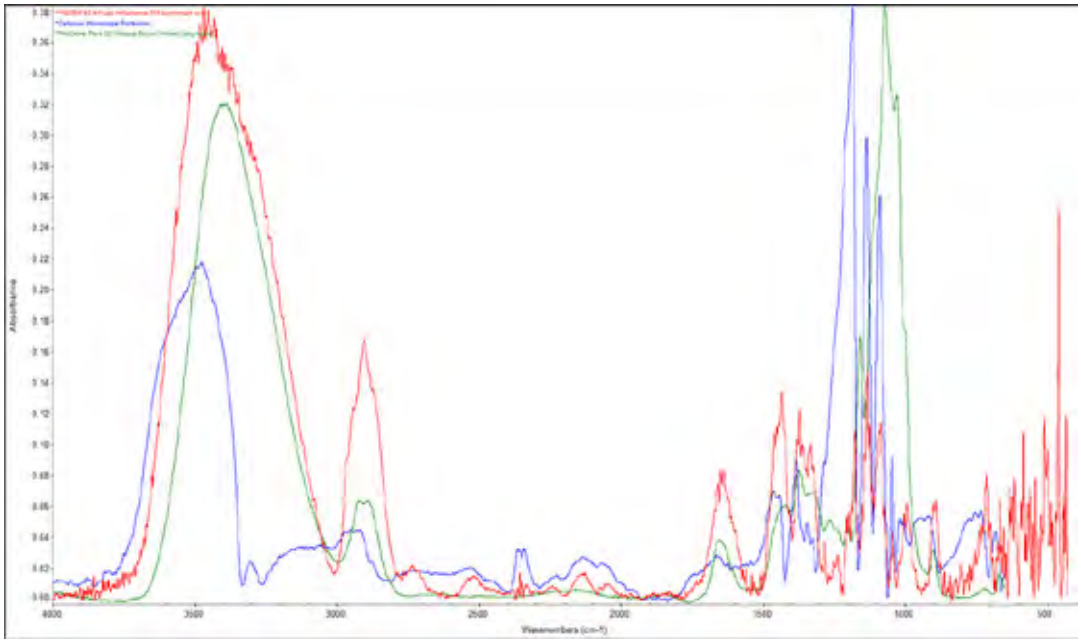

Figure 77. Sample 4742. Diffuse reflectance parchment only, overlaid.

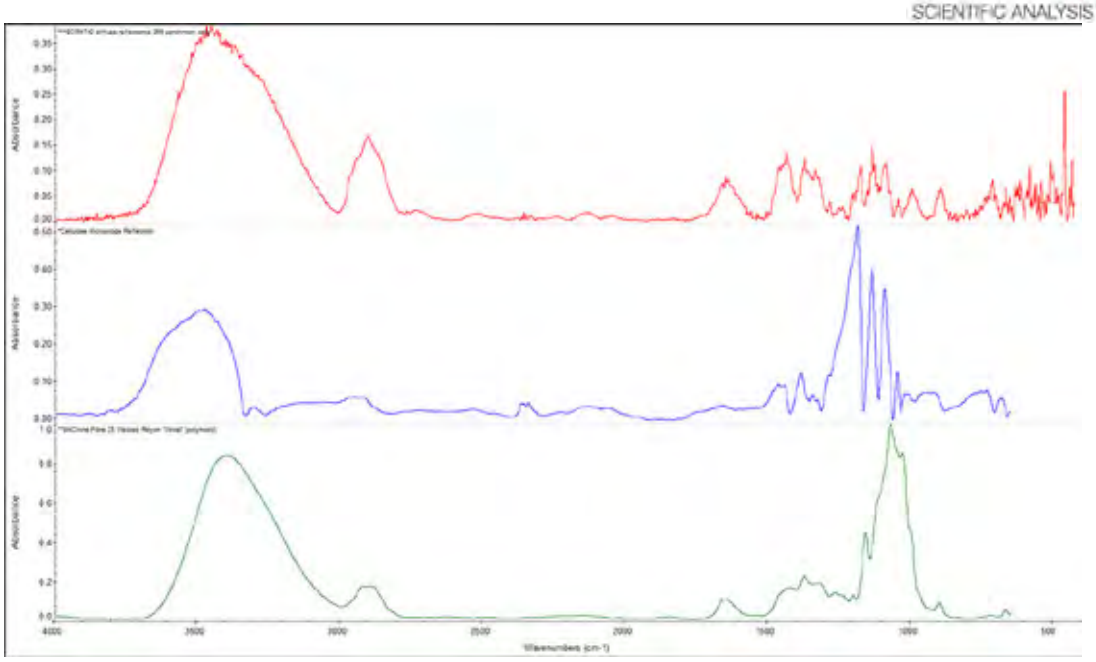

Figure 78. Sample 4742. Diffuse reflectance parchment only, stacked.

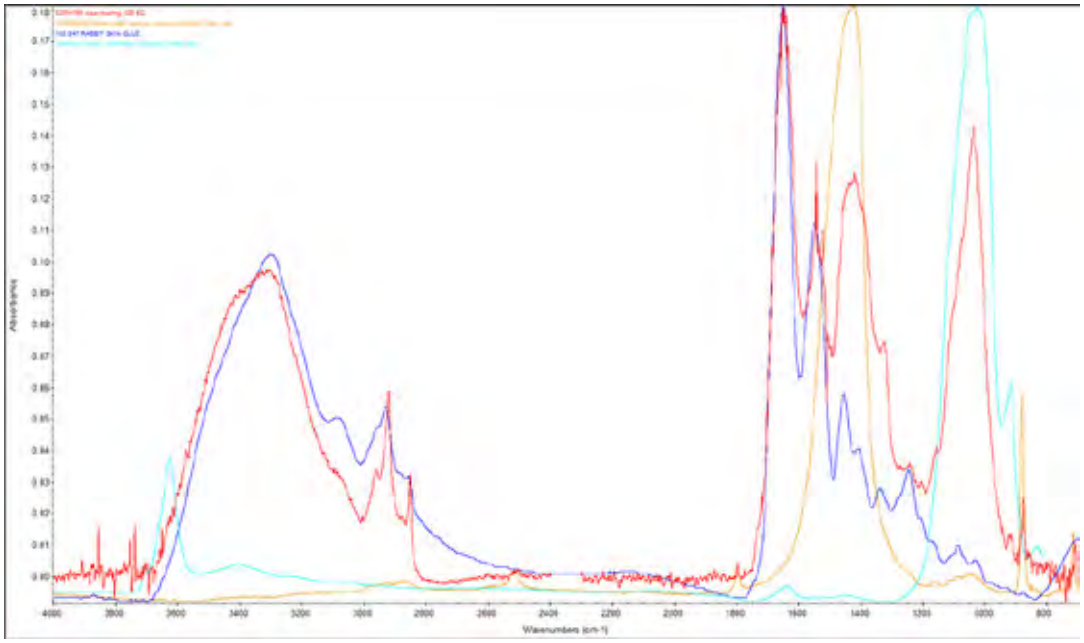

Figure 79. Sample 4760. Clear coating, overlaid (spectral noise due to using Continuum microscope without a nitrogen flush).

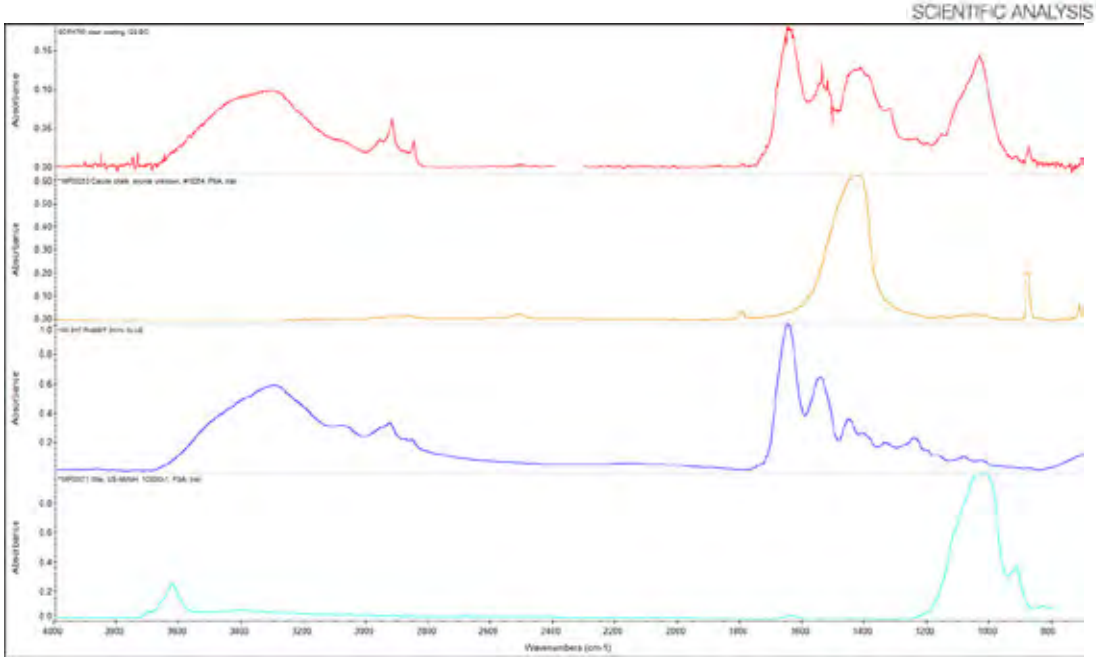

Figure 80. Sample 4760. Clear coating, stacked (spectral noise due to using Continuum microscope without a nitrogen flush).

Analytical Methodology

FTIR

Molecular analysis of the Museum of the Bible Dead Sea Scrolls fragments was carried out by Fourier transform infrared spectroscopy onsite using a Thermo-Fisher bench with a Continuum microscope and a nitrogen-cooled MCT detector. Microgram-sized samples were removed from the scroll fragments using a size 11 steel scalpel blade and transferred under a microscope to a diamond half-cell support. A total of 128 scans in transmission mode were collected over a spectral range of 4000 – 650 cm-1 with a spectral resolution of 4 cm-1. Each sample was then rolled flat to increase its transparency in the infrared using a steel roller tool. Follow-up analysis was conducted using a Thermo NicoletiN-10 spectrometer. Samples transported to New York for analysis were transported and housed in glass well slides.

Data at SAFA were acquired and analyzed with a Thermo Scientific Nicolet iN-10 FTIR microscope controlled by OMNIC Picta software. A total of 128 scans were collected over a spectral range of 4000 – 650 cm-1 with a spectral resolution of 4 cm-1. A number of publicly available cultural heritage and commercial spectral databases were used for identification. Multicomponent spectral deconvolutions and sample identifications were performed with OMNIC Specta software.

Report

MA-X-Ray Fluorescence Scanning of Four Dead Sea Scroll Fragments

Fragments SCR 000121

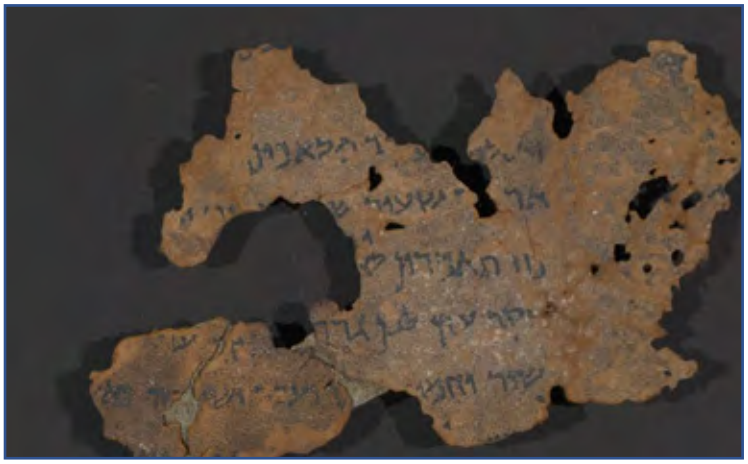

Fragment SCR 000124

Fragment SCR 003173

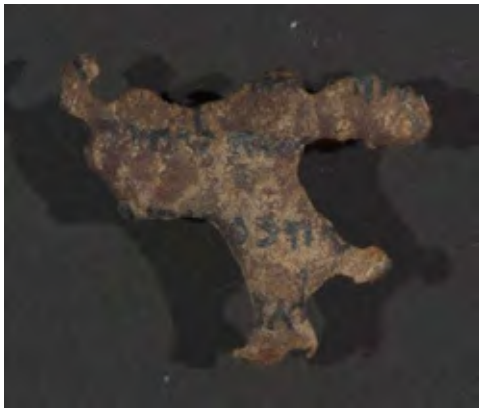

Fragment SCR 004742

Report by Aaron N.Shugar

Analysis performed on June 7th and 8th 2019
For: Museum of the Bible

July 26, 2019

Executive Summary

MA-XRF scanning was performed on four Dead Sea scrolls housed at the Museum of the Bible. The scanning produces elemental maps that relate to elemental distribution across the surface of the samples. The elemental maps of the four Dead Sea Scroll fragments show clear similarities. Major elements found include Ca, K, Fe, Cl, S, Si, and P. Minor elements identified include Mn, Al, Ni, Br, Ti, and Mg. Cu was occasionally found, mainly in isolated regions. Traces of Se, Sr, Zn, and Pb were also found evenly distributed on the fragments. Sodium was also identified but the low Z element has very low energy and is easily attenuated by material on the surface as well as the environment between the sample and the detector.

No identifiable elements were associated with the inks used. Many of the elements with strong correlation are likely related to accretions on the surface of the fragments. In many cases, these are best seen under UV irradiation at 365nm. A better understanding of the relationship of the elements to the particulate surface will be made by comparing XRF results with FTIR.

Introduction

X-ray fluorescence is a non-destructive, non-invasive analytical technique used extensively for the identification of elements present in samples across a wide range of disciplines (Adriaens 2005, Janssens et al. 2000, Shugar 2013, Shugar and Mass 2012). Within the world of Art Conservation, XRF has successfully been used to investigate paintings, paper artifacts, photographs, pigment identification, alloy characterization, and many other areas of study. The application of this technique was traditionally spot analysis, providing information on individual regions. The technology as developed and XRF is now being used to perform large area data cube analysis of artifacts.

MA-XRF scanning has become a staple for the technical study of works of art. Initially undertaken using high flux synchrotron sources (Alfeld et al. 2013, Dik et al. 2008, Ravaud et al. 2016), this technology has advanced allowing for lab-based systems to be developed. MA-XRF scanning systems have been developed in house (i.e. The National Gallery of Art, USA) and commercially (Bruker M6 Jetstream). The use of handheld XRF instruments to perform macro scanning has typically been limited by the relatively large beam spot size and the speed of collection. Early attempts were successful at scanning on a relatively small scale (~ 10x10cm). Newer advancements have created larger armatures to mount instruments resulting in larger scan areas. Artifacts with larger areas can be stitched together to reveal the relationship of various elements to one another and establish an artist's palette or the elemental distribution on an artifact. Small beam collimators have now been developed and can provide resolution as low as 0.25 mm (Shugar 2019).

Sample Condition and Preparation for Analysis

All four fragments were delicate and appear to have undergone some minor dimensional changes since they were last photographed. This is likely due to changes in temperature and humidity. The fragments were placed on a suspended inert paper support for analysis. This was designed to protect the sample during scanning and provide an air layer barrier behind the fragment and the scanner base. The fragments were only handled by conservators. Once placed on the scanner, scanning time ranged from approximately 1 hour to 15 hours depending on the size of the fragment.

Results

For all four fragments, the ink used for the text (best visualized at 940nm) was not identified. This suggested that it is a carbon-based ink which cannot be measured by the XRF. The elemental maps of the four fragments show some clear similarities. Major elements found include Ca, K, Fe, Cl, S, Si, and P. Minor elements identified include Mn, Al, Ni, Br, Ti, and Mg. Cu was occasionally found, mainly in isolated regions, Traces of Se, Sr, Zn, and Pb were also found evenly distributed on the fragments. Sodium was also identified but this element has very low energy and is easily attenuated by material on the surface of the fragments as well as the environment between the sample and the detector. Even so, Na was detected in various intensities on the samples.

The specifics for each sample will be presented below.

Fragment SCR 000121

Scanning details: 24mm in the X and 12.5mm in the Y. Total time: 55 minutes.

See attached PowerPoint file to see all the elemental maps and overlay images onto specific maps.

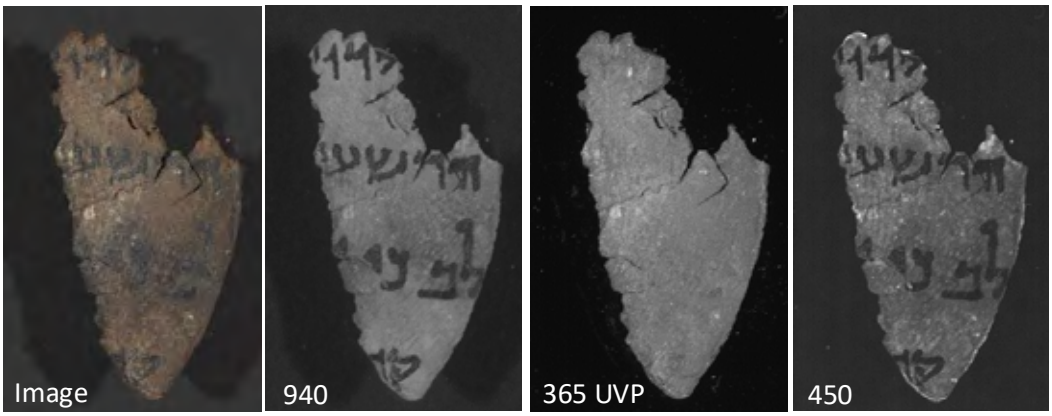

Figure 1: Multi-modality imaging of fragment SCR 000121 at 365nm, 450nm and 940nm. These wavelengths best show the variation in surface particulate and text.

Fragment SCR 000121 has clear fracturing in several locations with one main fracture across the center running left to right. The text is most clearly seen at 940nm while the light accretions seen in the raw image are visible in the 365 nm UVP image. Under 450nm additional enhancements can be seen as bright spots. The fracture is closely associated with higher concentrations of Si, Al, Ti and Fe, likely due to the increased surface area exposed to the XRF beam (see Fig. 2).

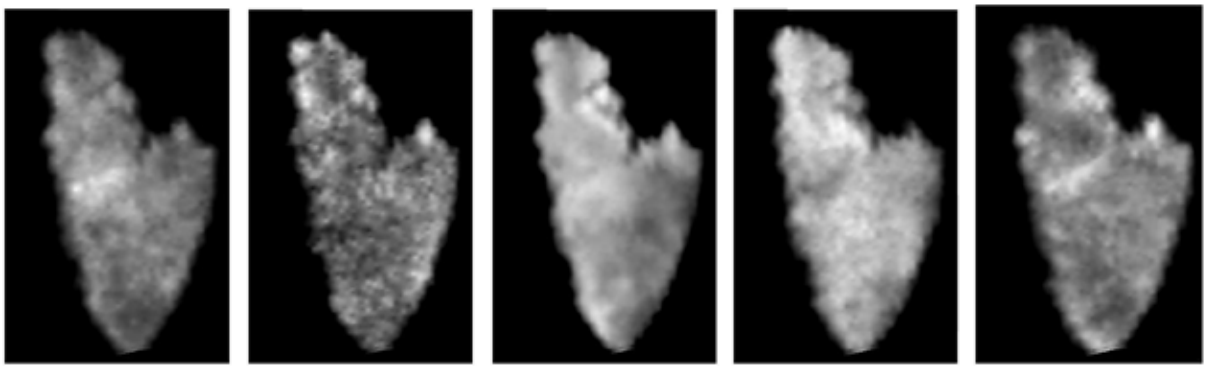

Figure 2; Selected elemental maps from SCR 000121. Data shows correlation between crack in fragment and Si and Fe, a general distribution of Ca, a slight increase in Cl at the smaller fragment in the upper middle right and a correlation between Fe and P.

There is a general Ca concentration across the sample. Concentration of Si and Al are closely associated with the accretions seen in the full spectrum image. In addition, there are higher concentrations of Fe, Si and Ti at the break crossing the fragment. Isolated concentrations of P are mostly associated with the upper part of the sample at the edges. The elemental correlation can be seen in the covariance plot (Fig. 3). Many elements positively correlate, but some of the strongest correlations are between Si and Al, Ca, K, S and Si (Figs. 4 and 5).

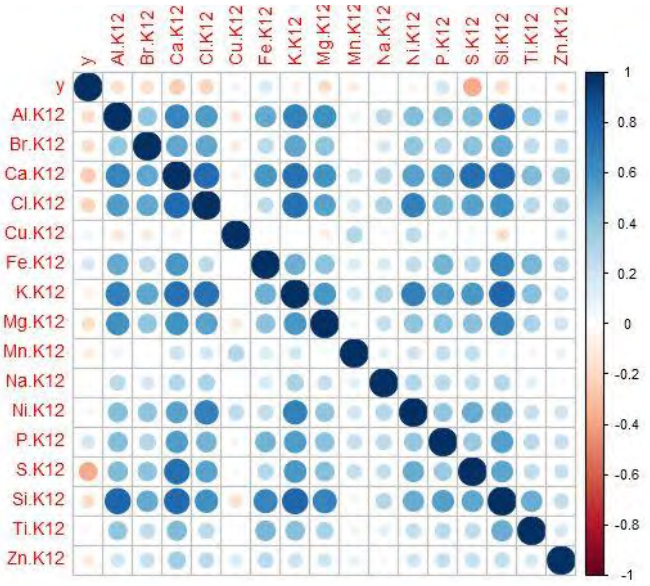

Figure 3: Covariance plot showing the relationship of elements to one another.

With the generally uniform coverage of the elements on the fragment, there are limited separation of the elements. By comparing the scatter plots of Cl and K and Cl and Na, the data suggests a stronger correlation for a potassium salt (Fig. 4). This should be considered under caution as the signal for sodium is greatly attenuated as compared to that of Cl and K.

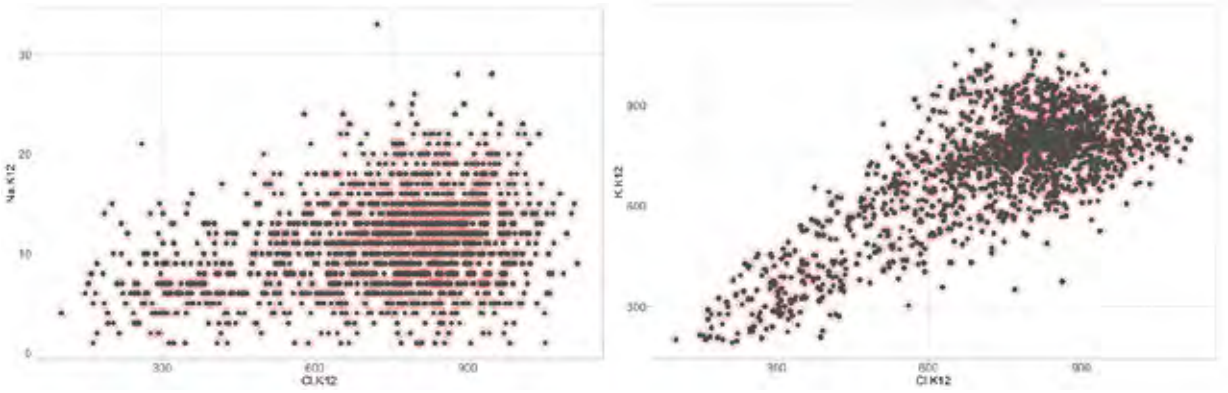

Figure 4: Scatter plots for Na vs Cl and K vs Cl. The data shows a stronger positive correlation for K and Cl than Na and Cl.

The strongest correlation is between Si and Al suggesting an alumino-silicate based material (Fig. 5).

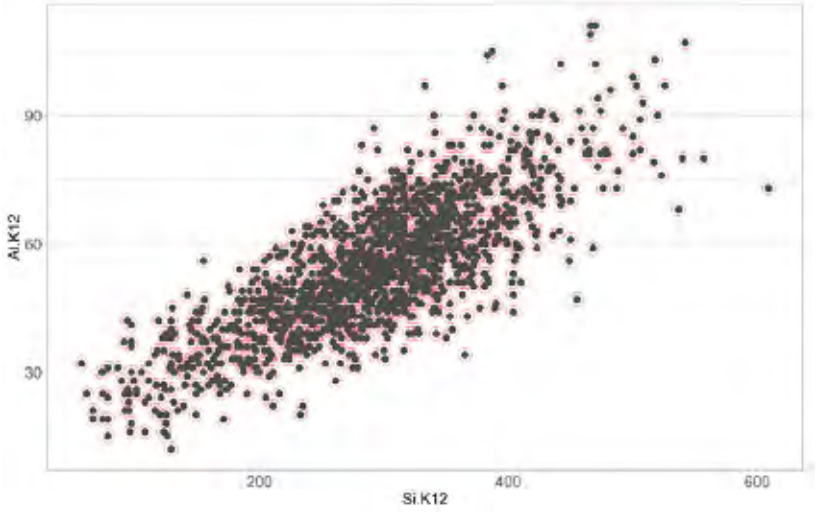

Figure 5: Scatterplot of Al vs Si showing a high positive correlation between the two elements.

Fragment SCR 00124

Scanning details: 90mm in the X and 56mm in the Y. Total time: 14.6 hours.

See attached PowerPoint file to see all the elemental maps and overlay images onto specific maps.

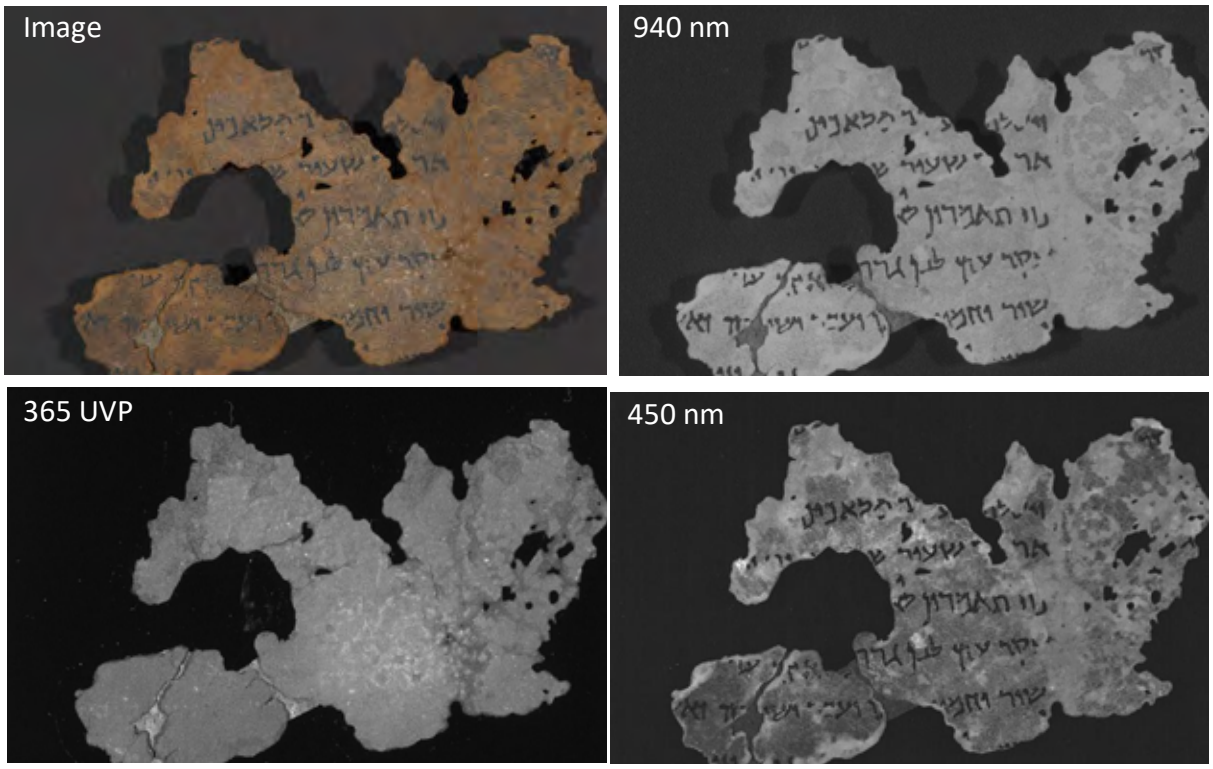

Figure 6: Multi-modality imaging of fragment SCR 000124 at 365nm, 450nm and 940nm. These wavelengths best show the variation in surface particulate. Note the inverse relationship in intensity between 365nm and 450nm.

Fragment SCR 000124 is the largest of the samples scanned. Through multi-modality imaging you can see clearly regions of response to different surface features/materials. The highlighted regions seen in the 365 nm UVP image closely relate to a surface feature visible in the raw image, possibly remnant sediment or delamination of the substrate (Fig. 6). These have direct elemental relationship with Br, Cl and Ca in particular. Bromine and Ca are positively correlated with the higher intensity regions in the 365 UVP image while Cl is more positively correlated with the higher intensities of the 450 nm scan (Fig 7).

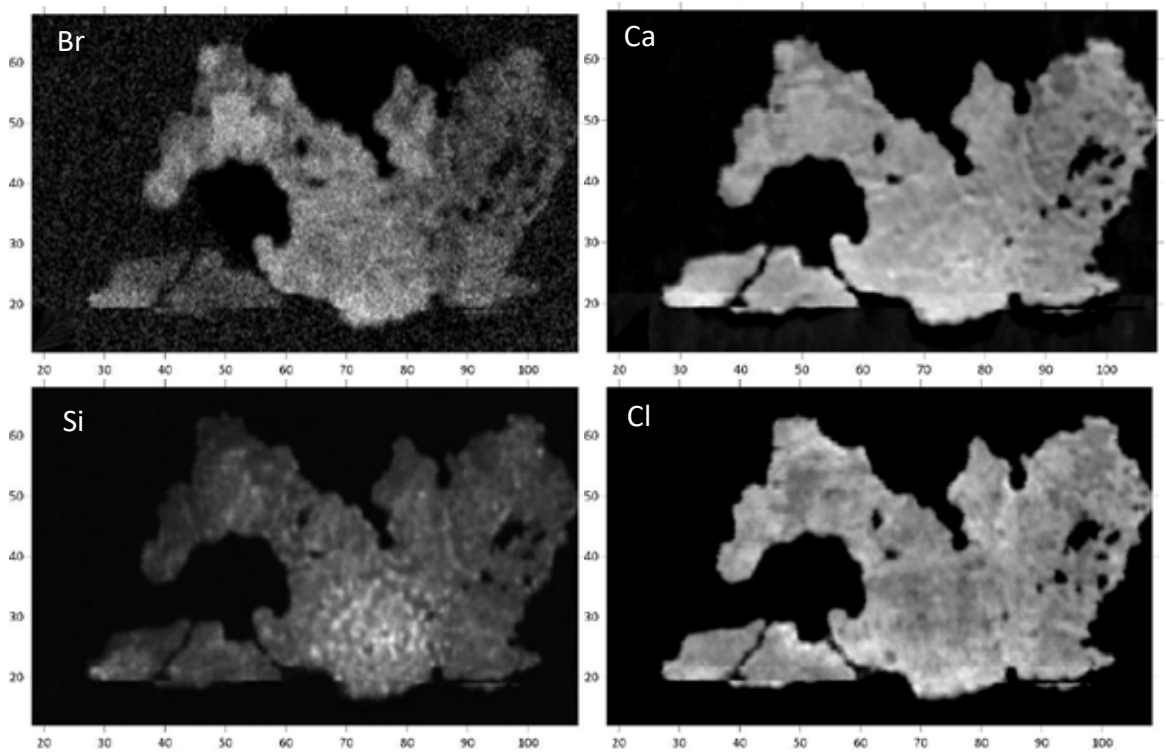

Figure 7: Elemental maps of Br, Ca, Si, and Cl. Note the inverse relationship between Br and Cl.

The elemental maps for Si, S, Mg, and Al all correspond strongly with the upper layer of the fragment and, in particular, the lighter areas seen in the raw image and the highest intensity responses in the 365nm UVP image (Figure 7). Previous studies (Hahn and Rabin 2018) did not note a correlation between Ca and the brighter locations seen in the 365nm UVP image but the elemental map clearly shows some increase in Ca concentration at these same locations. Iron also has a smaller intensity in the same areas and is likely due to some type of sediment on the surface. The assessment for water-based treatment of the fragment being the cause for Pb concentrations (Hahn and Rabin 2018) cannot be confirmed in these scans. The signal is very weak and although there are some minor regions of increased Pb concentrations they should be considered insignificant (see Fig. 8). Extracting a spectrum from one of the enriched Pb regions shows the limit of peak formation. Although there is Pb found across the fragment, without knowing the specifics of the regional soil, it would be hard to assign a particular source for it.

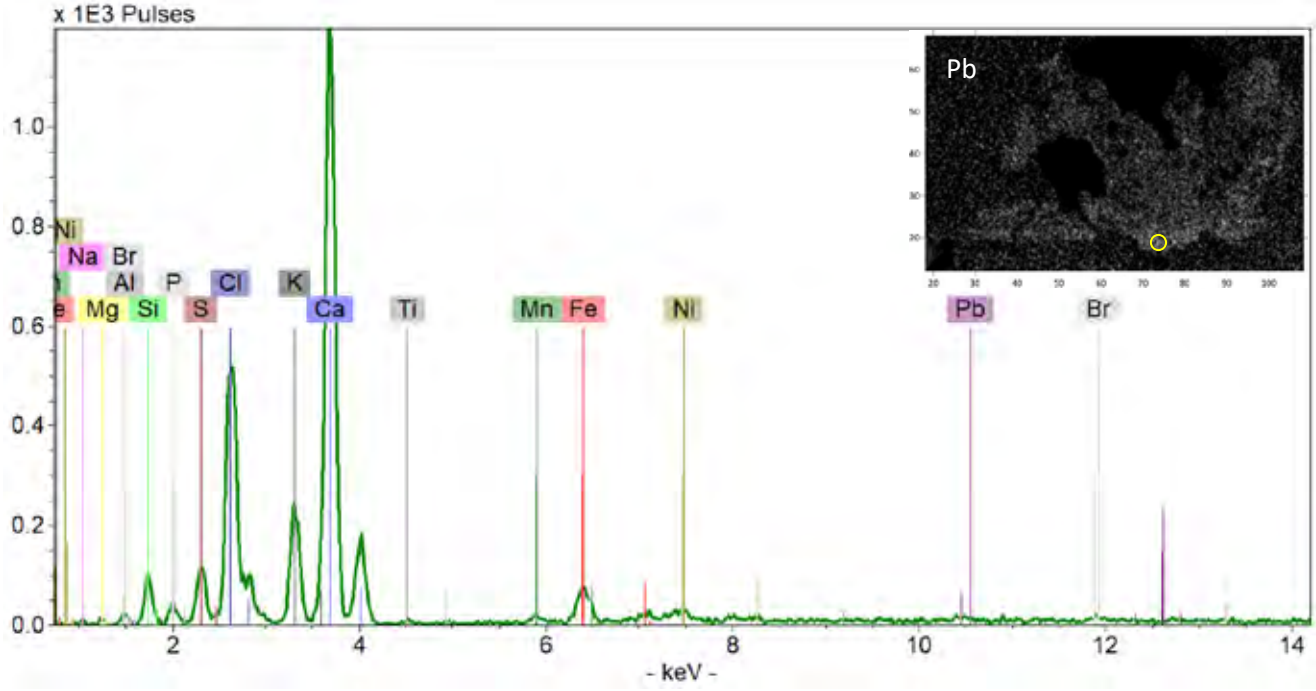

Figure 8: Spectrum from location 73.48x and 18.80y showing the elements associated with this pixel. Note the trace level of Pb in the region even though the map shows a slightly higher concentration at this point.

There is also a noticeable correlation between Ca and S, suggestive of potential gypsum being present (see Fig. 9).

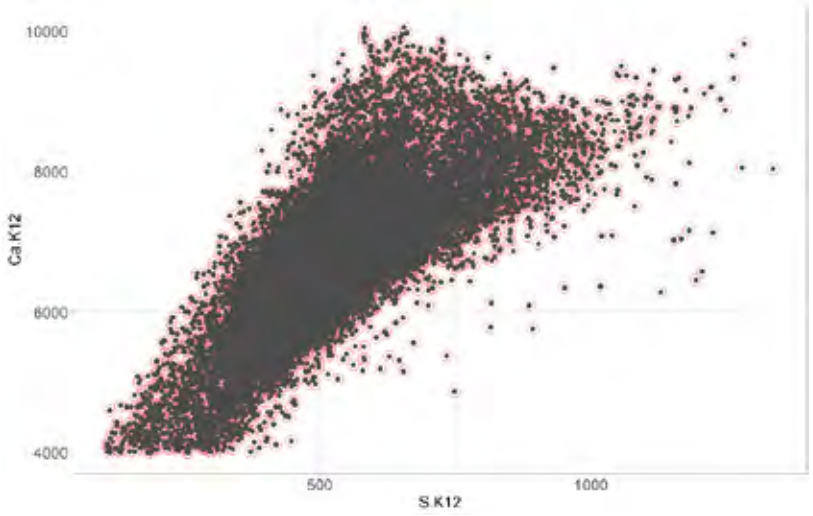

Figure 9: Scatterplot of Ca vs S showing a positive correlation between the two elements. This suggests the possibility of a calcium sulphate (gypsum) component.

The covariance plot shows some clear trends in positive correlation between elements. In particular, the strongest of these correlations are Al and Si, S and Si and Ca and S.

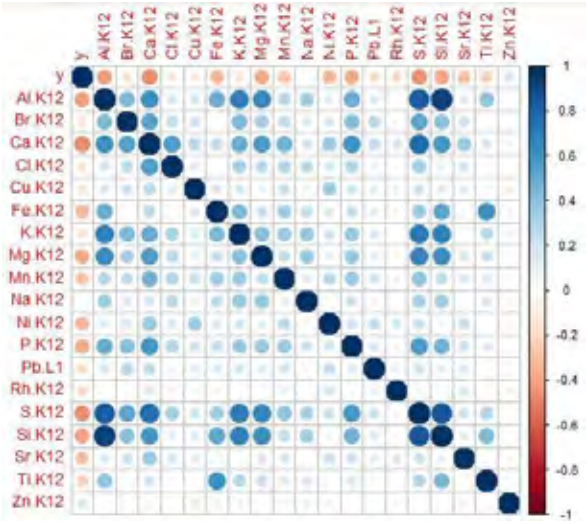

Figure 10 Covariance plot showing elemental relationships with one another.

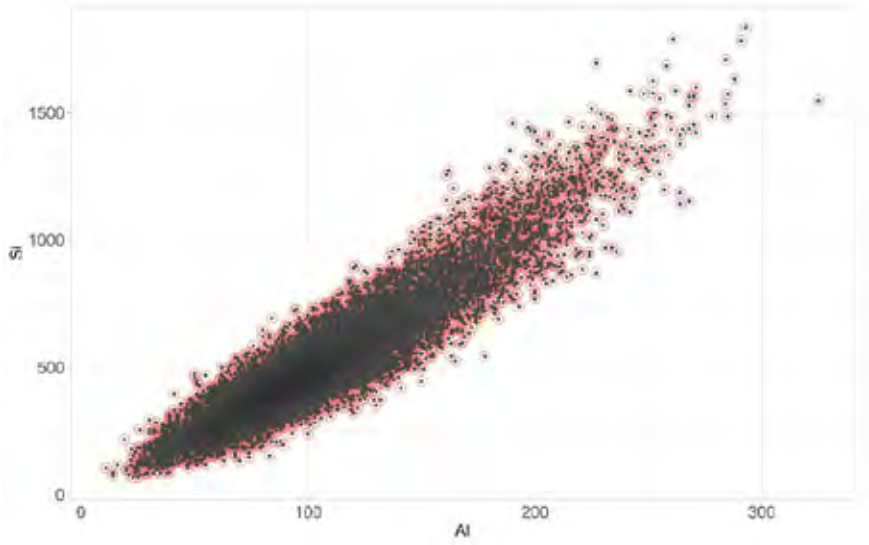

Figure 11: Clear positive correlation between Si and Al. Magnesium has a similar positive relationship as well

Comparisons of the XRF mapping done on the M6 and the Tracer show that the two techniques revealed similar results. The resolution is slightly higher on the M6 but the areas of increased elemental concentrations are clearly seen in both scans.

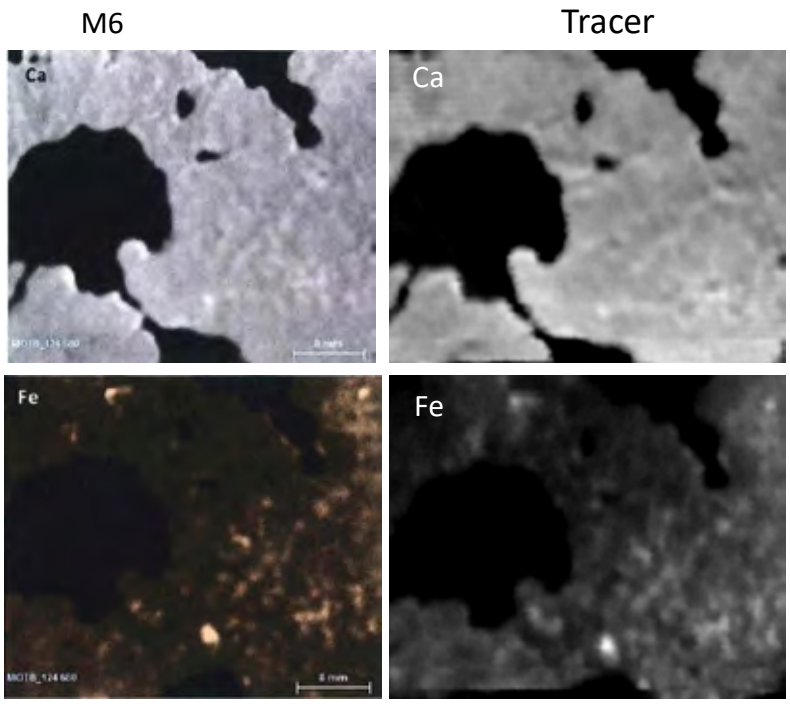

Figure 12: Comparison of the Bruker M6 XRF scan to the Tracer 5g scan showing the same region and similar results for elemental concentrations.

Fragment SCR 003173

Scanning details: 45mm in the X and 30.2mm in the Y. Total time: 215 minutes.

See attached PowerPoint file to see all the elemental maps and overlay images onto specific maps.

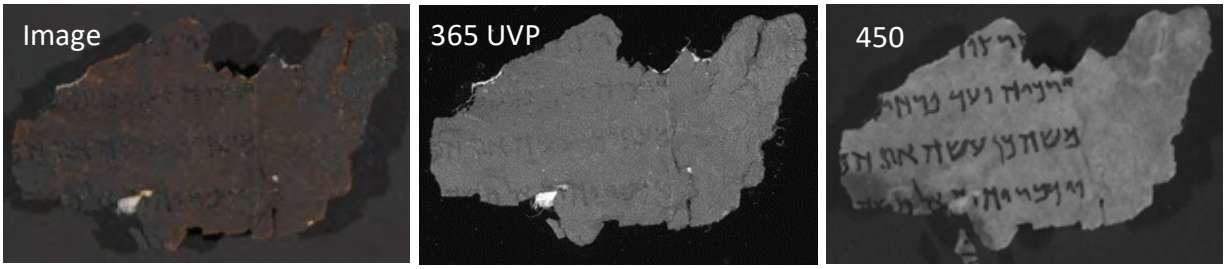

Figure 13: Multi-modality imaging of fragment SCR 003173 at 365nm and 450nm. These wavelengths best show the variation in surface particulate.

Fragment SRC 003173 is a fairly thick sample with clear breaks best seen in the 365 UVP image. It has a fairly uniform elemental composition. Around the fracture lines there is a clear increase in Cl, K, Fe, and Si (Fig. 14). This may be due to the cross section increasing surface area allowing for a higher signal from the XRF. Correlations between the darker surface accretions seen in the raw image at the upper right and mid lower left and Fe are clear, but the mid lower left region has a high concentration of P. This increased P must be near the surface as it is a light element that can only escape from approximately 5um from the surface itself.

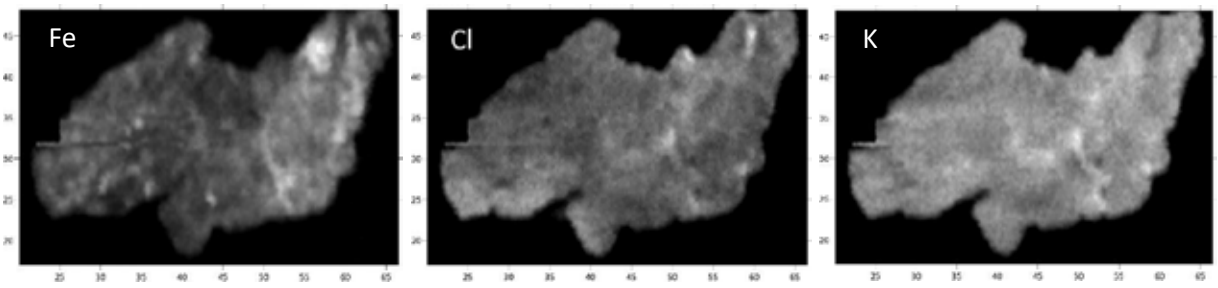

Figure 14: Elemental maps of Fe, Cl, and K. All three maps show increased concentrations around the lower right fracture in the fragment. The higher concentrations of Fe are associated with the darker surface of the fragment at the upper right.

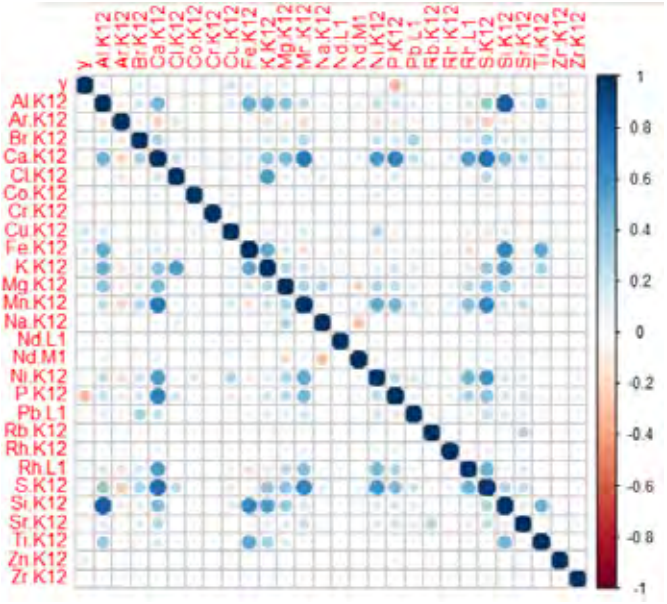

Figure 15: The covariance plot showing elemental correlation.

The covariance chart shows a strong correlation between Al and Si which can clearly be seen in the scatter plot of the two elements (Fig. 16). There is also a good corelation between Ca and S suggesting the presence of gypsum (Fig. 17). Interestingly, the relationship between Fe and Si indicates that there are two separate forms of Fe/Si present on the sample as indicated by the two clear groupings of data (Fig. 16). This may be due to two different forms of iron deposition, one associated with the darker areas on the fragment, and the other with general accretions. Chlorine is most strongly associated with K in this sample. (Fig. 17).

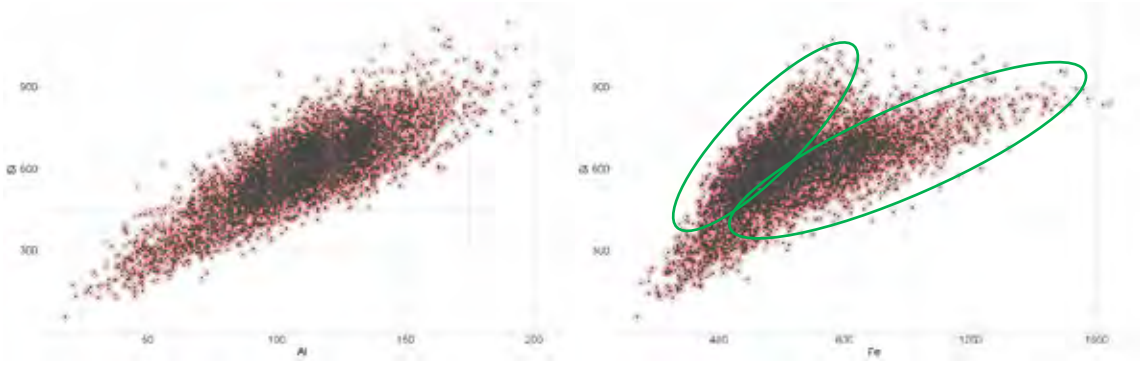

Figure 16: Scatterplots Si vs Al showing a strong positive correlation and Fe vs Si showing two different data set groupings.

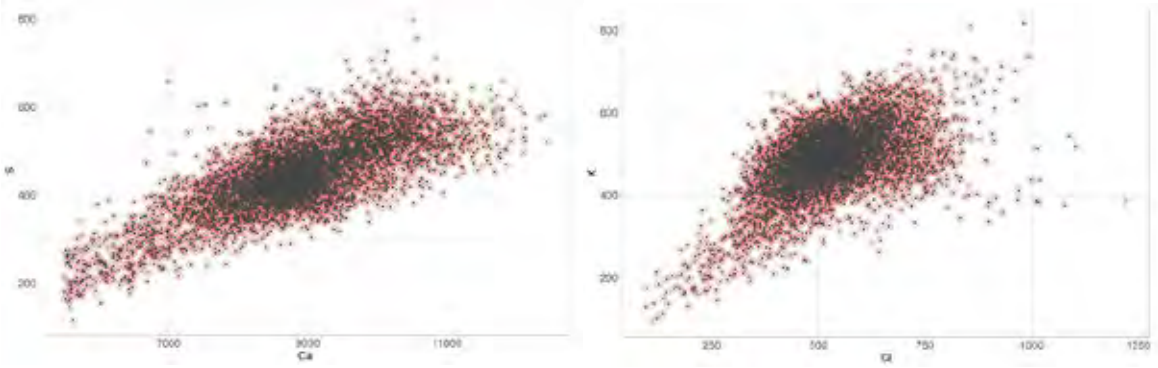

Figure 17: Scatterplots of Ca vs S showing a positive correlation and Cl vs K showing a mildly strong positive correlation.

As was found in previous studies (Hahn and Rabin 2018), there is a strong contribution from copper in this sample with no direct explanation.

Scanning details: 25.5mm in the X and 25mm in the Y. Total time: 100 minutes.

See attached PowerPoint file to see all the elemental maps and overlay images onto specific maps.

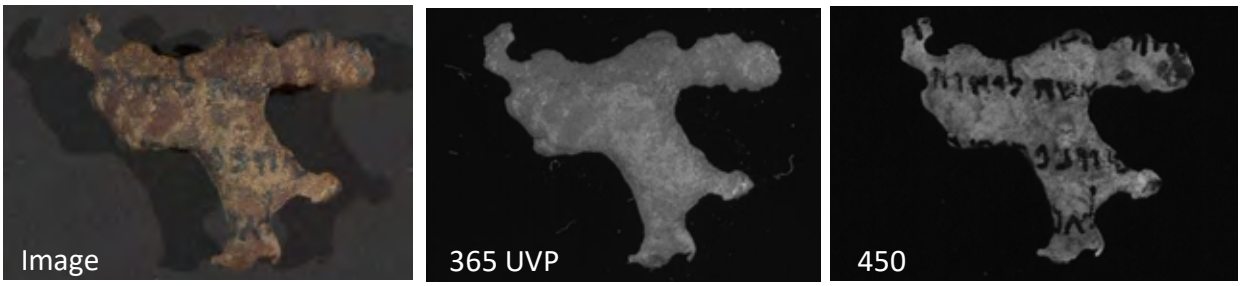

Figure 18: Multi-modality imaging of fragment SCR 004742 at 365nm and 450nm. These wavelengths best show the variation in surface particulate.

Fragment SCR 004742 has a natural curvature to the surface which creates a slight preferential spectral response to the right hand side. Each scan will have a slightly higher intensity along that side and does not represent even values across the surface. In addition, the sample has reduced in size from when it initially was photographed, likely from changes in humidity and temperature. From the multi-modality images, one can see the lighter accretions clearly in the raw image and the 365 nm UVP image while the 450nm image clearly shows the text and increased intensity negatively correlated with the other two images.

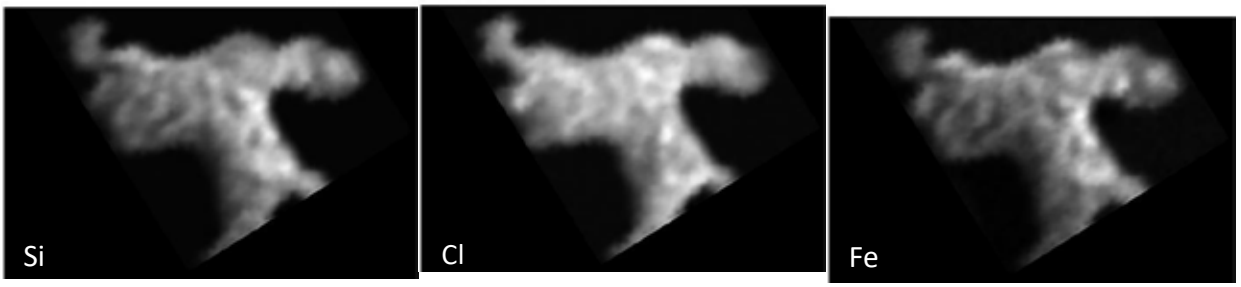

Figure 19: Elemental maps of Si, Cl, and Fe showing the positive correlation of Si and Fe with the lighter accretions seen in the 450nm image and the inverse relationship of Cl to the other two elements.

Elemental maps show clear correlation between Si, Al, and Fe (Fig 20) likely indicative of a soil accretion mainly associated with the lighter colors seen in the raw image of the fragment. The

relatively inverse relationship of Cl to Fe can be seen in Figure 21 along with a mildly positive correlation between Cl and K.

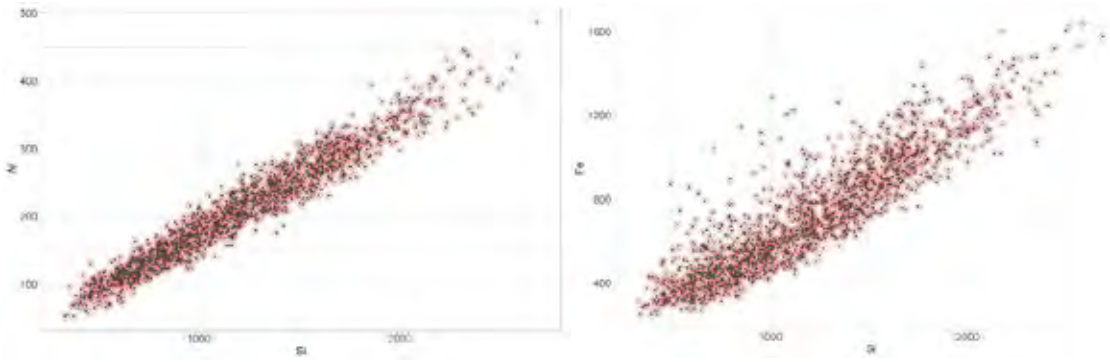

Figure 20: Scatter plots of Si vs Al and Si vs Fe both showing strong positive correlations.

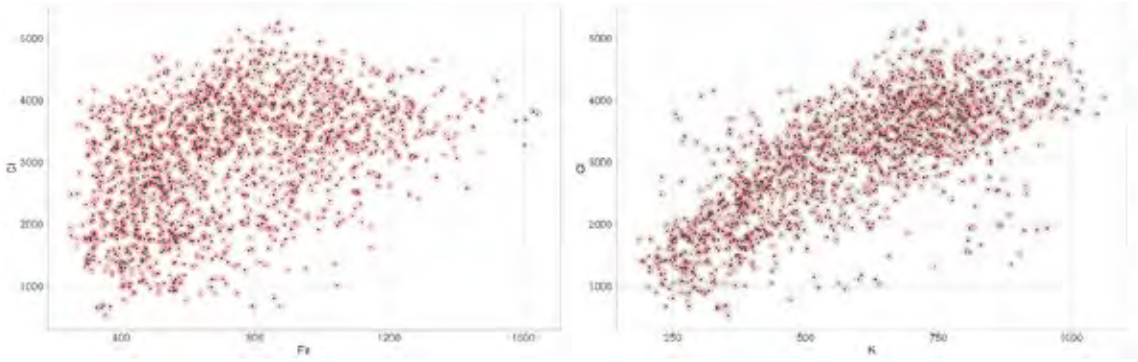

Figure 21: Scatter plots of Fe vs Cl showing no clear association between the two elements and K vs Cl showing a slight positive correlation.

Previous studies (Hahn and Rabin 2018) showing a negative correlation between Fe and Ca were not confirmed here. It is possible that the higher resolution of the Bruker M6 allowed for a difference to be seen, but this was not clear in the scan undertaken using the Tracer 5g.

Analytical Methodology

MA-XRF maps were collected using a Bruker Tracer 5g handheld XRF mounted to a DeWitt MSS-150E mobile scanner. This scanner allows for step sizes down to 0.1mm in both the X and Y axis. Data was compiled in DeWitt proprietary software, exported to Bruker Artax software for deconvolution processing, and individual elemental maps were built in Golden Software's Surfer software. The Tracer 5g is an energy-dispersive X-ray fluorescence spectroscopy (XRF) with a rhodium X-ray tube, a silicon drift detector, and a graphene window on the detector

allowing for light element identification. The analytical conditions were set at a tube voltage of 30 kV at 125 µA, with no filter and a Helium flush. A 0.5mm collimator was used to reduce the spot size. Scans were run at a rate of 0.3mm in the X direction and 0.4mm in the Y direction at 0.3mm/sec.

Summary

All four fragments show similar elemental compositions although their distributions are varied. In most cases there are clear differences seen between surface deposition/accretion and elemental composition. Attributing specific mineralization with these accretions is difficult through XRF alone. A more complete study would strengthen an accurate interpretation. This would involve multiple analytical techniques such as was done by Davis et al (2017). The elemental correlations found through XRF scanning will provide valuable information for more accurate FTIR and Raman interpretation.

One aspect of previous studies (Rabin 2013) suggests that the ratio of Cl/Br may be indicative of degradation state, or potential to atmospheric exposure. These two elements can easily be measured by XRF although the attenuation of Cl is fairly strong limiting its contribution in the spectrum to the upper layers of the fragment, while the Br signal can come throughout almost the entire thickness of the fragment. Nevertheless, the Cl/Br ratio can be calculated for the four fragments.

Looking at the logarithmic boxplot of Cl/Br shows potential relationships between fragments SCR000124 and SCR004742 and between fragments SCR000121 and SCR003173. This may suggest a similar source for the two related fragments or similar treatment/degradation. Further study would be required to fully comprehend this phenomenon.

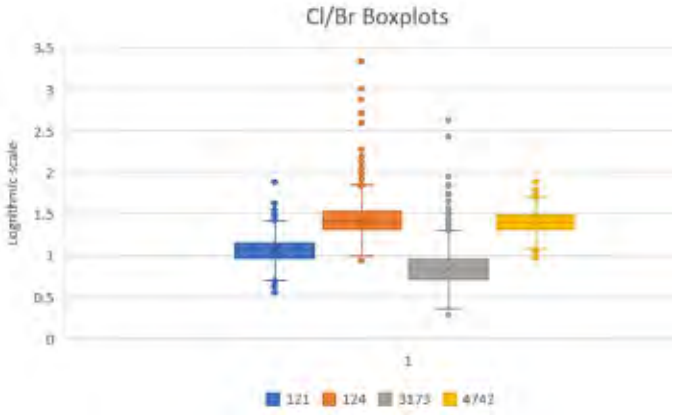

Figure 22: Boxplots showing the Cl/Br ratios for all four fragments in a log(10) scale.

Bibliography

Adriaens, Annemie. 2005. "Non-destructive analysis and testing of museum objects: An overview of 5 years of research." *Spectrochimica Acta Part B: Atomic Spectroscopy* 60 (12):1503-1516.

Alfeld, Matthias, Geert Van der Snickt, Frederik Vanmeert, Koen Janssens, Joris Dik, Karen Appel, Luuk van der Loeff, Meta Chavannes, Teio Meedendorp, and Ella Hendriks. 2013. "Scanning XRF investigation of a Flower Still Life and its underlying composition from the collection of the Kröller–Müller Museum." *Applied Physics A* 111 (1):165-175.

Bicchieri, Marina, Armida Sodo, Ira Rabin, Anka Kohl, and Giovanna Piantanida. 2018. "New results in Dead Sea Scrolls non-destructive characterisation. Evidence of different parchment manufacture in the fragments from Reed collection." *Journal of Cultural Heritage* 32:22-29. doi: https://doi.org/10.1016/j.culher.2018.01.014.

Broshi, Magen. 2004. "The Dead Sea Scrolls, the sciences and new technologies." *Dead Sea Discoveries* 11 (2):133-42.

Davis, Kipp, Ira Rabin, Ines Feldman, Myriam Krutzsch, Hasia Rimon, Årstein Justnes, Torleif Elgvin, and Michael Langlois. 2017. "Nine dubious "Dead Sea Scrolls" fragments from the twenty-first century." *Dead Sea Discoveries* 24 (2):189-228.

Dik, Joris, Koen Janssens, Geert Van Der Snickt, Luuk Van Der Loeff, Karen Rickers, and Marine Cotte. 2008. "Visualization of a lost painting by Vincent van Gogh using synchrotron radiation based X-ray fluorescence elemental mapping." *Analytical chemistry* 80 (16):6436-6442.

Frydman, Sam, Josef Charrach, and Ian Goretsky. 2008. "Geotechnical properties of evaporite soils of the Dead Sea area." *Engineering Geology* 101 (3):236-244. doi: https://doi.org/10.1016/j.enggeo.2008.06.003.

Galor, Katharina, Jean-Baptiste Humbert, and Jürgen Zangenberg. 2006. "Qumran: the Site of the Dead Sea Scrolls Archaeological Interpretations and Debates." In *Qumran: The Site of the Dead Sea Scrolls: Archaeological Interpretations and Debates*, 279-284. Brill.

Hahn, Oliver, and Ira Rabin. 2018. Material Analysis if Five DSS Fragments. BAM.

Janssens, Koen, G Vittiglio, I Deraedt, A Aerts, Bart Vekemans, Laszlo Vincze, F Wei, I De Ryck, O Schalm, and F Adams. 2000. "Use of microscopic XRF for non-destructive analysis in art and archaeometry." *X-Ray Spectrometry: An International Journal* 29 (1):73-91.

Lisker, Sorin, Roi Porat, Uri Davidovich, Hanan Eshel, Stein-Erik Lauritzen, and Amos Frumkin. 2007. "Late Quaternary environmental and human events at En Gedi, reflected by the geology and archaeology of the Moringa Cave (Dead Sea area, Israel)." *Quaternary Research* 68 (2):203-212. doi: https://doi.org/10.1016/j.yqres.2007.03.010.

Mantouvalou, Ioanna, Timo Wolff, Oliver Hahn, Ira Rabin, Lars Lühl, Marcel Pagels, Wolfgang Malzer, and Birgit Kanngiesser. 2011. "3D micro-XRF for cultural heritage objects: new analysis strategies for the investigation of the Dead Sea Scrolls." *Analytical chemistry* 83 (16):6308-6315.

Maor, Yonah, Pnina Shor, and Zeev Aizenshtat. 2017. "White halos surrounding the Dead Sea scrolls." *Journal of Cultural Heritage* 28:90-98. doi: https://doi.org/10.1016/j.culher.2017.06.003.

Marengo, Emilio, Marcello Manfredi, Orfeo Zerbinati, Elisa Robotti, Eleonora Mazzucco, Fabio Gosetti, Greg Bearman, Fenella France, and Pnina Shor. 2011. "Development of a

technique based on multi-spectral imaging for monitoring the conservation of cultural heritage objects." *Analytica Chimica Acta* 706 (2):229-237. doi: https://doi.org/10.1016/j.aca.2011.08.045.
Müller, M, B Murphy, M Burghammer, C Riekel, E Pantos, and J Gunneweg. 2007. "Ageing of native cellulose fibres under archaeological conditions: textiles from the Dead Sea region studied using synchrotron X-ray microdiffraction." *Applied Physics A* 89 (4):877-881.
Nir-El, Yoram, and Magen Broshi. 1996. "The black ink of the Qumran Scrolls." *Dead Sea Discoveries*:157-167.
NIR-EL, Yoram, and Magen Broshi. 1996. "The red ink of the Dead Sea Scrolls." *Archaeometry* 38 (1):97-102.
Palchan, Daniel, Yigal Erel, and Mordechai Stein. 2018. "Geochemical characterization of contemporary fine detritus in the Dead Sea watershed." *Chemical Geology* 494:30-42. doi: https://doi.org/10.1016/j.chemgeo.2018.07.013.
Palchan, Daniel, Yigal Erel, and Mordechai Stein. 2019. "Mobilization of fine detritus to the Dead Sea Basin during the late glacial and early Holocene." *Quaternary Science Reviews* 218:395-405. doi: https://doi.org/10.1016/j.quascirev.2019.05.028.
Rabin, Ira. 2013. "Archaeometry of the Dead Sea scrolls." *Dead Sea Discoveries* 20 (1):124-142.
Rabin, Ira. 2016. "Material analysis of the fragments."
Rabin, Ira, and Oliver Hahn. 2013. "Characterization of the Dead Sea Scrolls by advanced analytical techniques." *Analytical Methods* 5 (18):4648-4654.
Rabin, Ira, Oliver Hahn, Timo Wolff, Emanuel Kindzorra, Admir Masic, Ulrich Schade, and Gisela Weinberg. 2010. "9. Characterization Of The Writing Media Of The Dead Sea Scrolls." In *Holistic Qumran*, 123-134. Brill.
Rasmussen, Kaare Lund, Anna Lluveras Tenorio, Ilaria Bonaduce, Maria Perla Colombini, Leila Birolo, Eugenio Galano, Angela Amoresano, Greg Doudna, Andrew D. Bond, Vincenzo Palleschi, Giulia Lorenzetti, Stefano Legnaioli, Johannes van der Plicht, and Jan Gunneweg. 2012. "The constituents of the ink from a Qumran inkwell: new prospects for provenancing the ink on the Dead Sea Scrolls." *Journal of Archaeological Science* 39 (9):2956-2968. doi: https://doi.org/10.1016/j.jas.2012.04.041.
Ravaud, E, L Pichon, E Laval, V Gonzalez, M Eveno, and T Calligaro. 2016. "Development of a versatile XRF scanner for the elemental imaging of paintworks." *Applied Physics A* 122 (1):17.
Roberts, David G. 2000. "The Dead Sea: The Lake and its Setting: Tina M. Niemi, Zvi Ben-Avraham, Joel R. Gat, Oxford Monographs on Geology and Geophysics, No. 36, 1998, 286 pp., ISBN 0-19-508703-8, £57.50." *Marine and Petroleum Geology* 17 (4):557-558. doi: https://doi.org/10.1016/S0264-8172(99)00053-7.
Shugar, A. 2019. "Advancing handheld macro-XRF scanning: Development of collimators for sub-mm resolution." Technart Bruges, Belgium, 7-10 May.
Shugar, Aaron N. 2013. "Portable X-ray fluorescence and archaeology: limitations of the instrument and suggested methods to achieve desired results." In *Archaeological chemistry VIII*, 173-193. ACS Publications.
Shugar, Aaron N, and Jennifer L Mass. 2012. *Handheld XRF for art and archaeology*. Vol. 3: Leuven University Press.

Sobel, Harry, and Henry Ajie. 1992. "Modification in amino acids of dead sea scroll parchments." *Free Radical Biology and Medicine* 13 (6):701-702. doi: https://doi.org/10.1016/0891-5849(92)90044-H.

Wolff, Timo, Ira Rabin, Ioanna Mantouvalou, Birgit Kanngießer, Wolfgang Malzer, Emanuel Kindzorra, and Oliver Hahn. 2012. "Provenance studies on Dead Sea scrolls parchment by means of quantitative micro-XRF." *Analytical and bioanalytical chemistry* 402 (4):1493-1503.

Report created by:

Aaron N. Shugar, Ph.D.

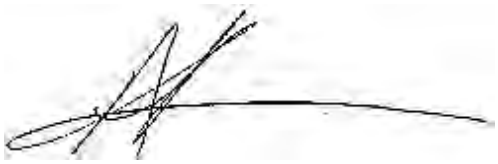

Ph: 716.512.0783
E-mail: aaron.shugar@gmail.com

For: MOTB

7/26/2019

REPORT

Optical Microscopy, SEM, and Reflectance FTIR analysis of two DSS Fragments of Sample SCR000121

Report by Aaron N.Shugar
Analysis performed on September 11, 12, 13, 2019
For: Museum of the Bible
September 25, 2019

Introduction

Two small fragments from SCR000121 were mounted in epoxy resin and polished to reveal the samples in section. The samples were polished and finished with 2um paper. The samples were investigated by optical microscopy and scanning electron microscopy (SEM) to investigate the range and types of surface accretions as well as help clarify the manufacturing process of the fragments (if it can elucidate whether it is leather or parchment). Images were taken under dark field reflected light and two forms of UV irradiation. SEM imaging was coupled with EDS analysis to provide chemical compositional analysis of particles. Reflectance FTIR was also performed to further the analysis of the sections.

Executive Summary

The two samples show some similarity and differences in their sections. Sample **a** shows a higher concentration of oils on the bottom half. Sample **b** shows some evidence of oil as well, but not as extensive. This might be what has attributed to the darkening of the fragment as a whole. The fiber structures of the samples are similar as well. They are highly compressed at the base and show some more flowing fibers at the top. Determining directionality is difficult, most likely due to the degradation of the parchment and gelatinization that has occurred over time. Images taken under UV irradiation display this feature best. SEM analysis shows high calcium concentrations in the main parchment surrounding fibers. These may be associated with oxalate or stearate formations but could be further characterized by FTIR. SEM mapping shows the clear distribution of elements throughout the structures and shows the higher atomic number elements associated with the accretions on the surface of the fragments. Estimated mineralization includes calcium oxides (i.e. calcite $CaCO_3$), gypsum ($CaSO_4 \cdot 2H_2O$), calcium phosphates (apatite ($Ca_{10}(PO_4)_6(OH)_2$) and derivatives thereof), clay bodies, iron calcium alumino silicates (i.e. omphacite (Ca, Na)(Mg, Fe^{2+}, Al)Si_2O_6), quartz and possibly rutiled quartz, calcium silicates (Ca_2SiO_4), and variable salts (Na, Mg, and K based). FTIR analysis confirms these findings and shows the presence of calcium oxalate as well.

Analysis performed to determine potential bromine concentration was hampered as the Br L lines overlap Al K lines. The higher energy Br K lines were not excited as this would have required running the SEM at higher voltage that might have resulted in damage to the section. This analysis can be revisited if deemed needed now that the remainder of analysis has been performed.

Analytical Methodology

Zeiss Optical Microscope

A Zeiss Axio Imager A1m equipped with illuminators for reflected light and fluorescent microscopy was used. Samples were viewed under brightfield and darkfield illumination. Objective magnifications range between 50x and 1000x for reflected light microscopy. Fluorescent microscopy images were obtained using a mercury lamp. Spectral regions of excitation and emission were controlled using DAPI and FITC filter cubes. Images were taken using ZEN 2 software.

SEM-EDS

Secondary electron and backscatter electron images were obtained using a Tescan Vega3 XMU tungsten variable pressure scanning electron microscope. Samples were analyzed under high vacuum (or low vacuum). The accelerating voltage used was 15 kV. X-ray spectra were collected using an accelerating voltage of 15 kV. The data was processed with an Oxford Instrument 50 mm2 X-Maxn Silicon Drift Detector (SDD) and AZtecEnergy analysis software. Samples were carbon coated to reduce surface charging.

Reflection FTIR

Reflected Infrared spectra were collected using a Continuum microscope coupled to a Nicolet 6700 FTIR spectrometer (Thermo Scientific). Samples were analyzed after being polished in cross section. An approximately 50 um x 100 um rectangle microscope aperture was used to isolate the sample area for analysis. The spectra are the average of 64 scans at 4 cm-1 spectral resolution. Correction routines were applied as needed to eliminate interference fringes and sloping baselines. Sample identification was aided by searching a spectral library of common conservationandartists'materials(Infrared and Raman Users Group, http://www.irug.org) using Omnic software (Thermo Scientific).

Results of Analysis

Two samples were taken from SCR000121 (121a and 121b). They have slightly different features but are mostly similar with regard to the mineralization and accretions. The two samples will be discussed separately.

Sample 121a

Optical Microscopy

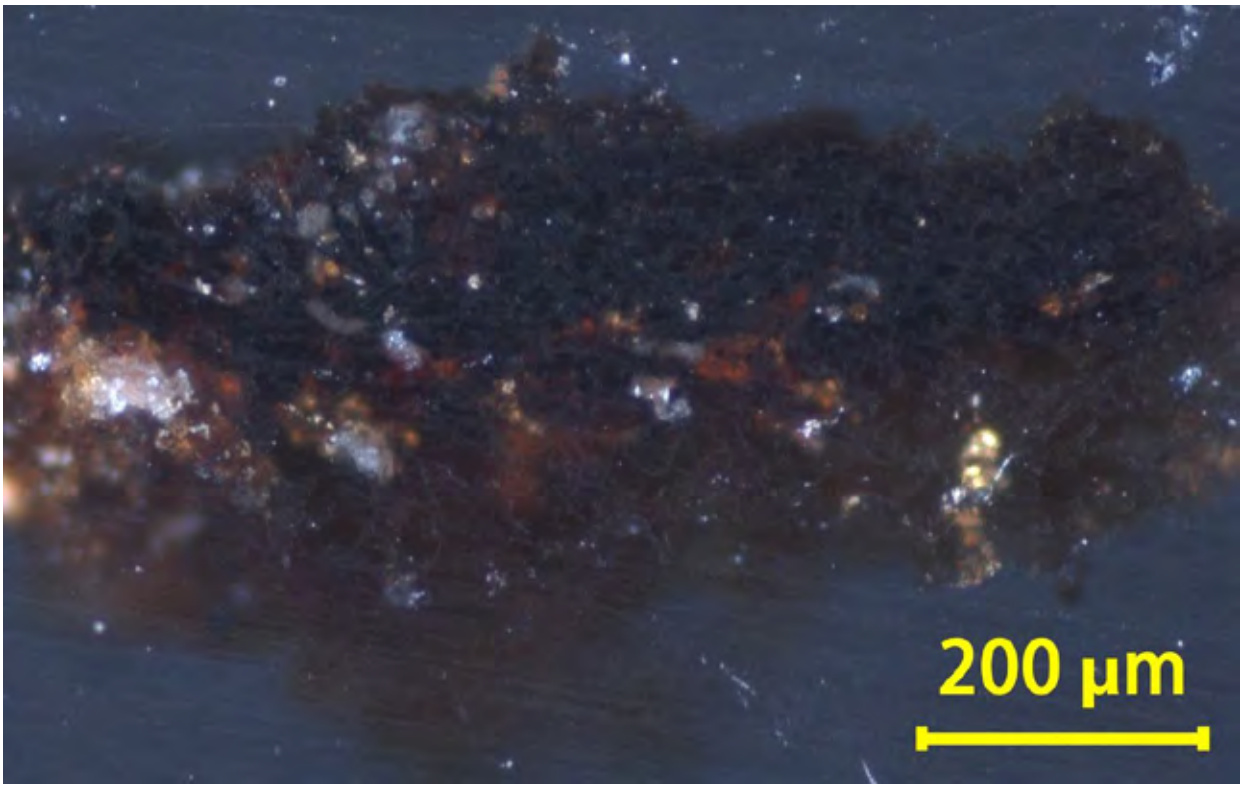

Figure 1: Darkfield image of samples 121a showing some mineralization (white features to the left) and some darkening discoloration of the sample as a whole. (The sample is hard to characterize using brightfield or darkfield illumination.)

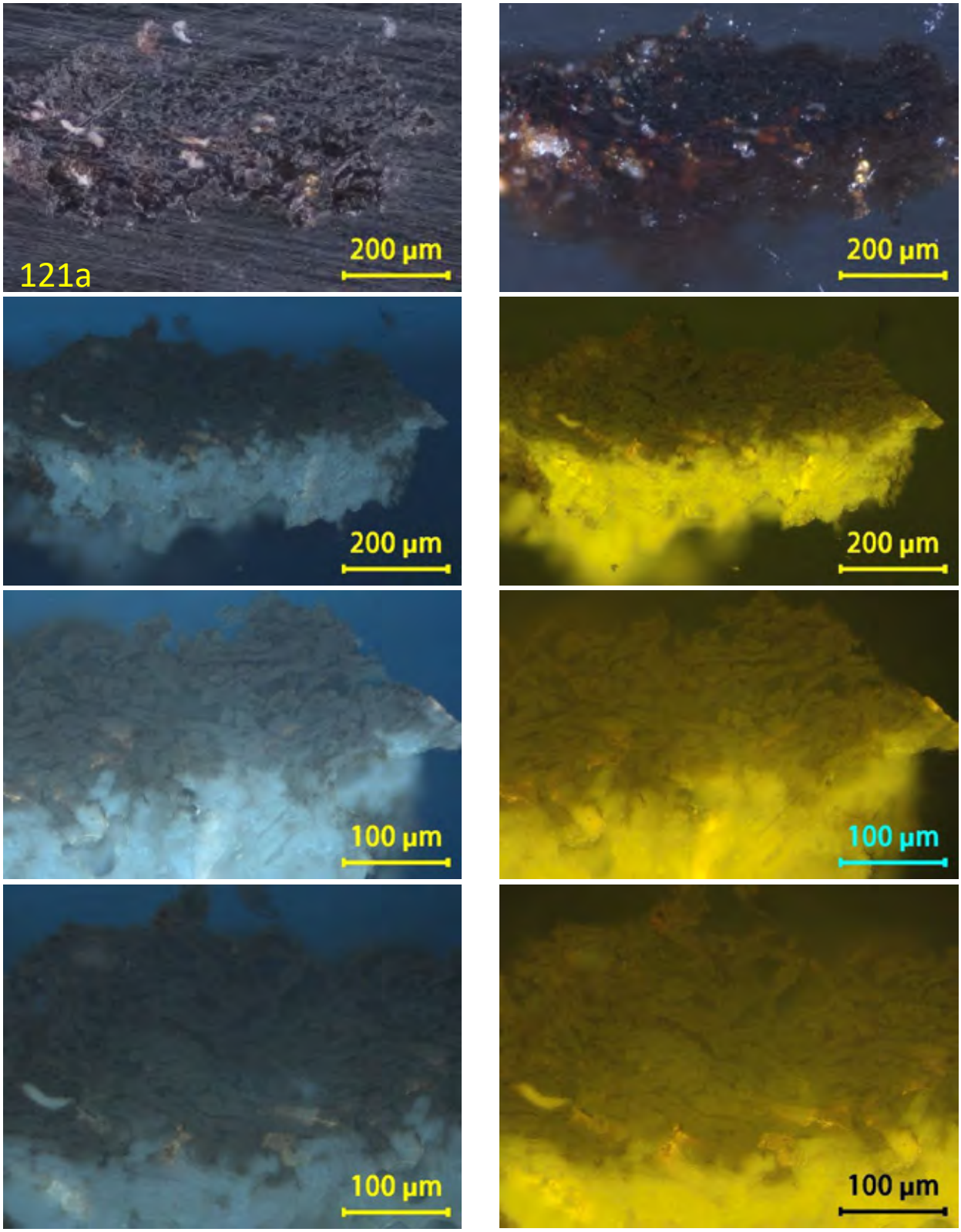

Figure 2: Images of sample 121a showing brightfield and darkfield images at the top (L and R respectively). The images below are taken under UV irradiation using DAPI illumination on the left and FITC illumination on the right. The images show the fibrous structure of the leather towards the top of the images. There does not appear to be significant elongation of the fibers. The lower region fluorescence is indicative of an oil impregnation.

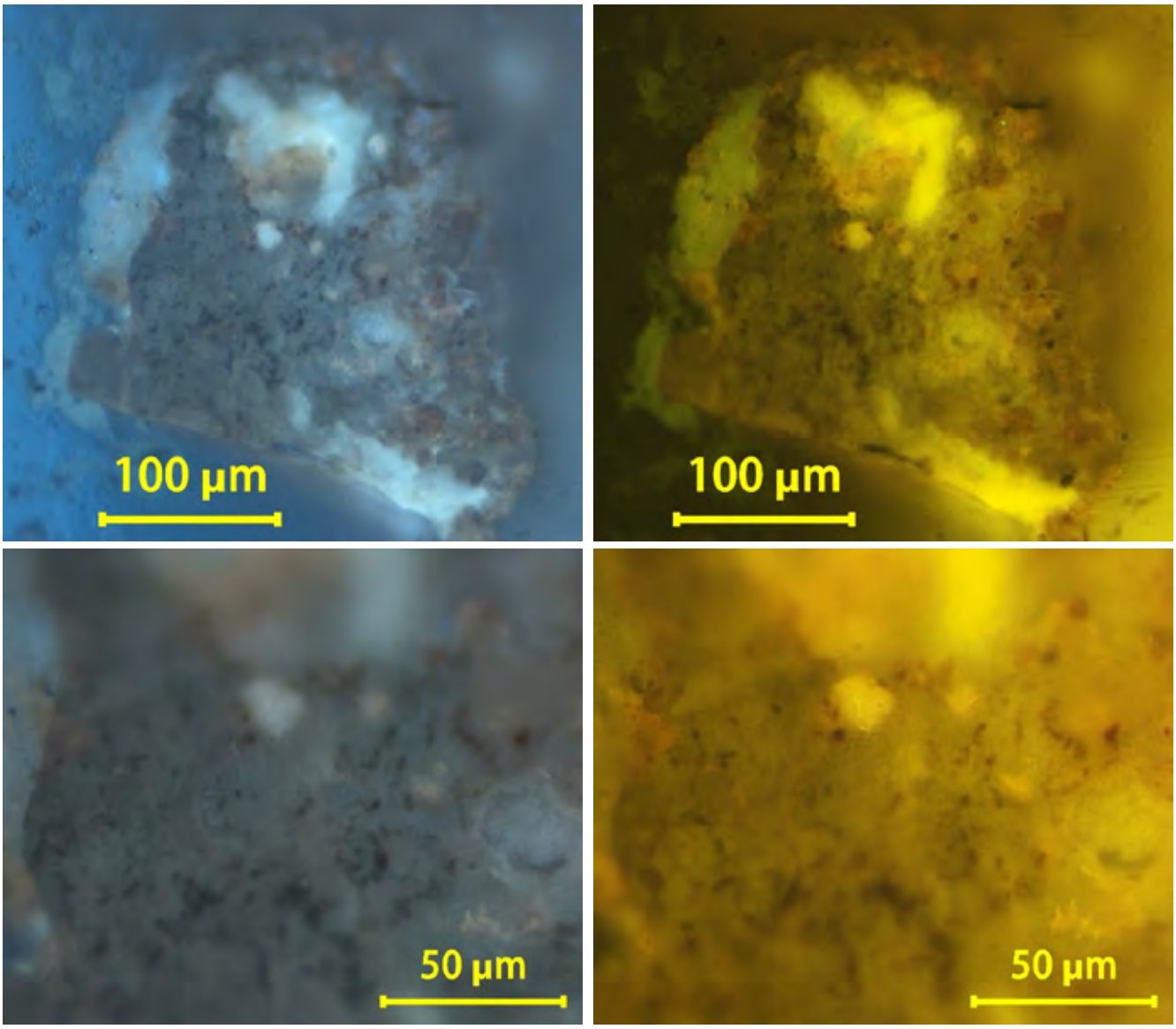

Figure 3: UV fluorescence images of the right-angle section of samples 121a. The images show a higher compression of the fibers and a higher integration of the 'oil' infiltration.

Scanning Electron Microscopy

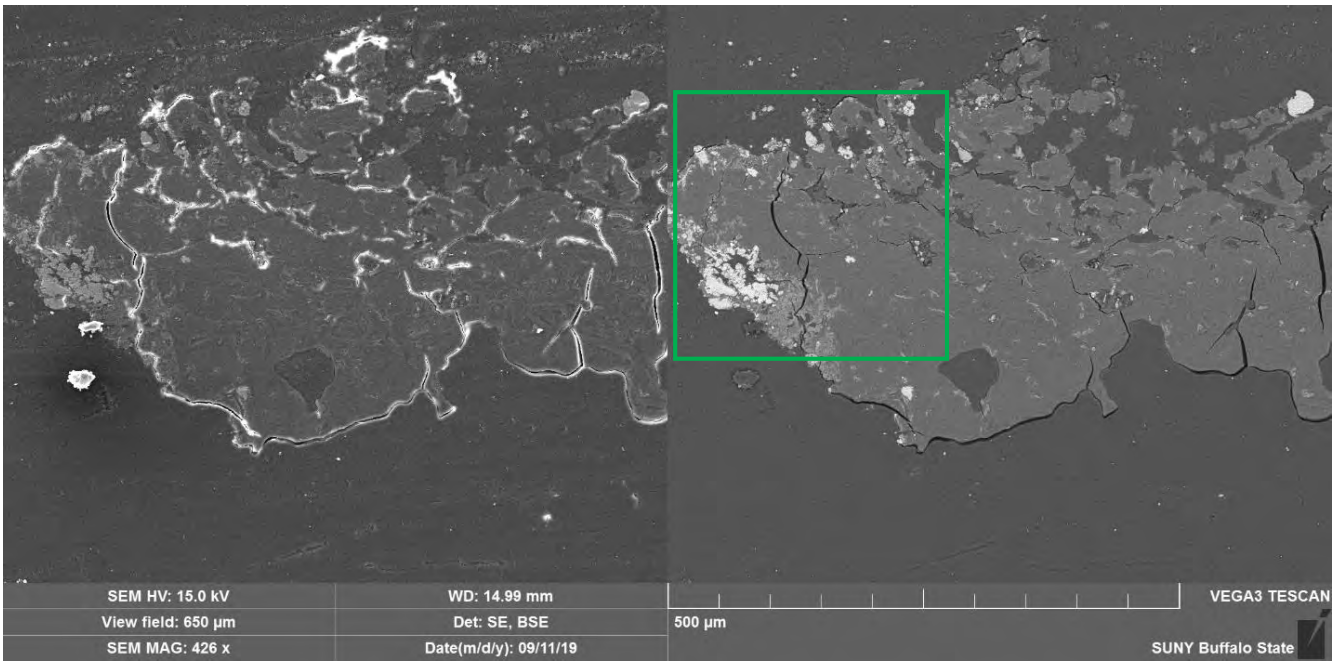

Figure 4: SEM images (SEI on the left and BSI on the right) of samples 121a. The BSI shows variation in atomic number by increasing grey scale. Within the leather itself, higher Z elements are distributed randomly, while at the edges smaller mineral formation (accretions) are present. The green box represents the region that was investigated in more detail (both mapping and isolated spectra).

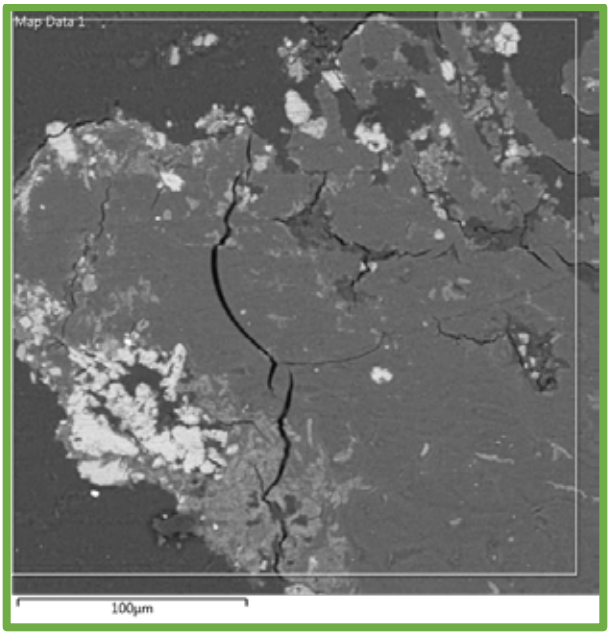

Figure 5: SEM BSI of the region that was mapped for element distribution.

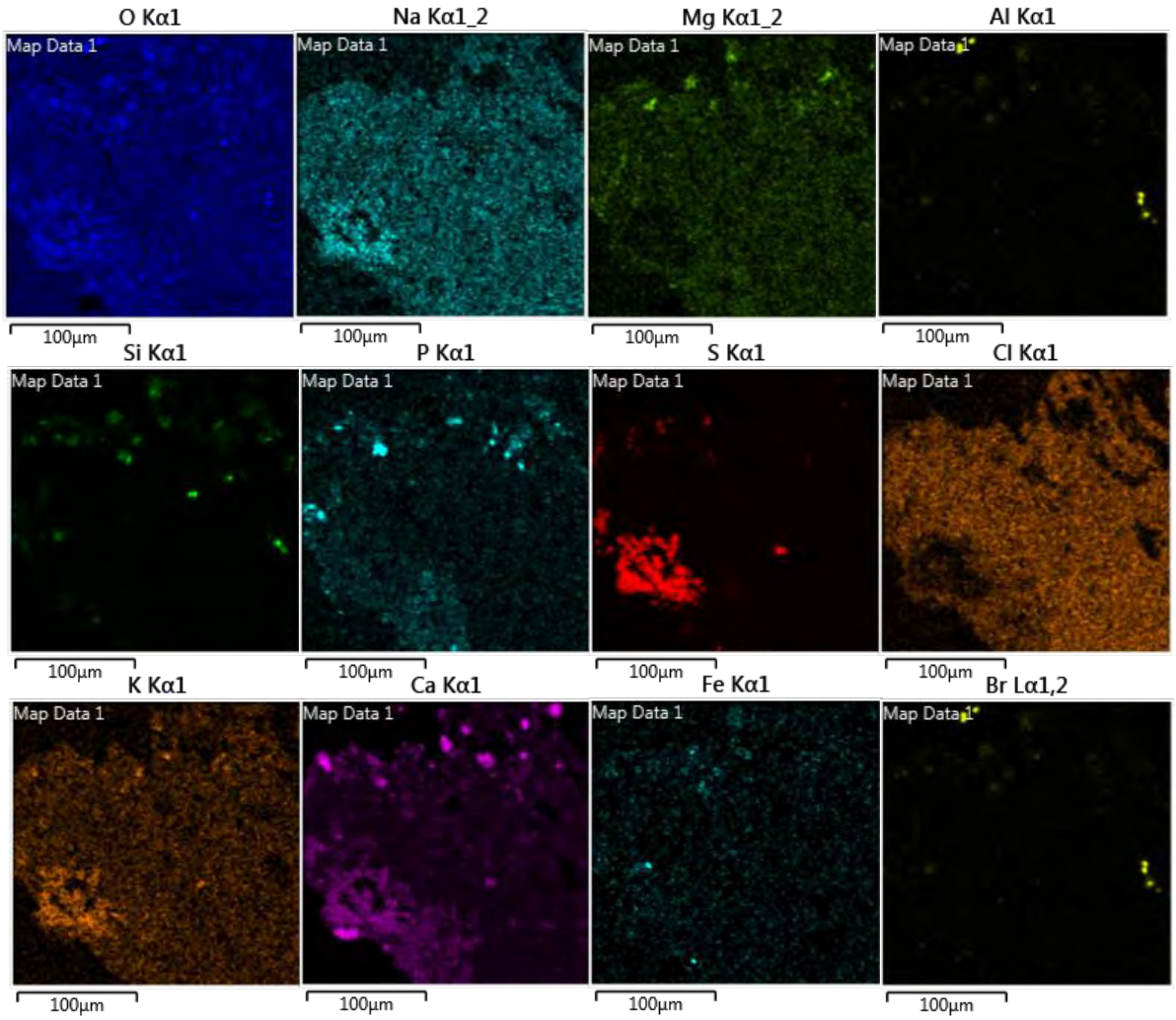

Figure 6: Elemental distribution map from Figure 5 showing a wide distribution of Ca and the relationship of elements to each other. (Al and Br overlap one another and are difficult to differentiate.)

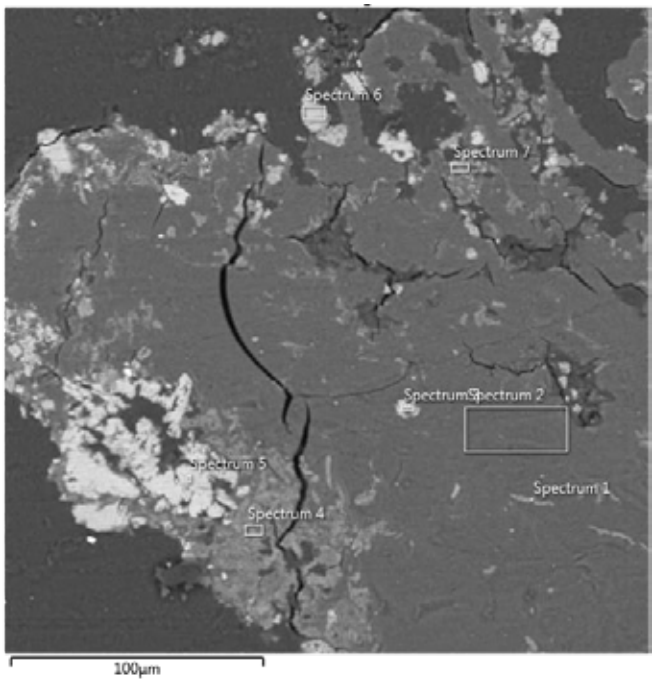

Figure 7: SEM BSI image showing the location for isolated spot and small area analysis.

Elements /Spot	O	Na	Mg	Al	Si	P	S	Cl	K	Ca	Ti	Fe	Br	Most likely mineral of discernibility
1	53.97	1.95	1.35		0.12		0.47	8.49	2.09	31.41			0.2	
2	61.53	4.87	3.19	0.74			0.94	11.4	3.74	13.65				
3	45.98	3.04					22.5	0.51	3.31	24.63				Gypsum
4	57.3	2.85	2.63			2.16	1.37	4.76	2.24	26.7				Calcium phosphate, Calcite
5	43.71	2.43					24.1		3.71	26.07				Gypsum
6	52.47		0.94	0.88	2.03		0.16	0.23	0.45	42.2		0.65		Calcite
7	48.61	2.11	3.57	3.71	9.65	4.11	1.19	3.6	3.6	17.82		2.01		Apatite, Silicate, (Na, Mg, K) salt

Table 1: Normalized elemental composition for the locations noted in Figure 7. Region 2 shows the parchment has a high Ca concentration and has some salts present (K, Na, or Mg salts). Spectra 3 and 5 are Gypsum with some K replacement for Ca $(K,Ca)SO_4 \cdot 2H_2O$. Spectrum 6 is Calcite $CaCO_3$.

Sample 121b

Optical Microscopy

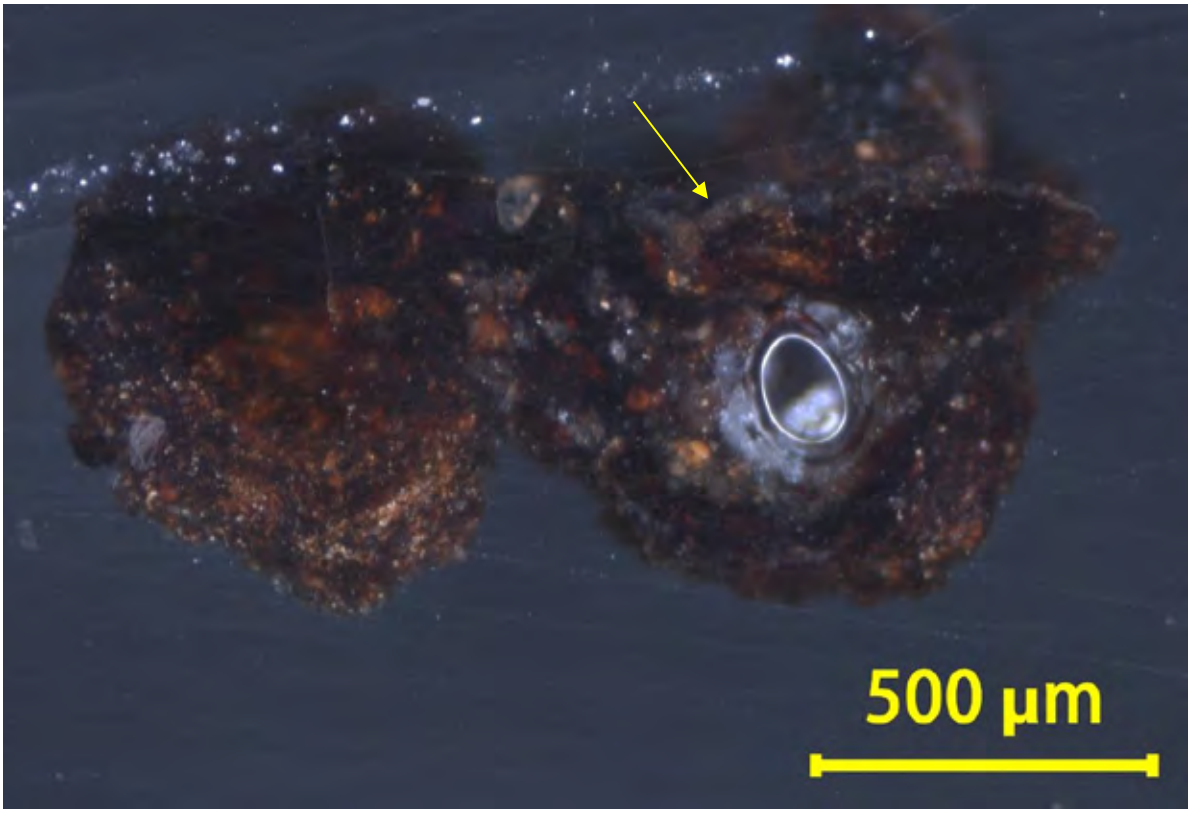

Figure 8: Darkfield image of samples 121b showing more extensive mineralization (haziness marked with arrow) and some darkening discoloration of the sample as a whole. (The sample is hard to characterize using brightfield or darkfield illumination.)

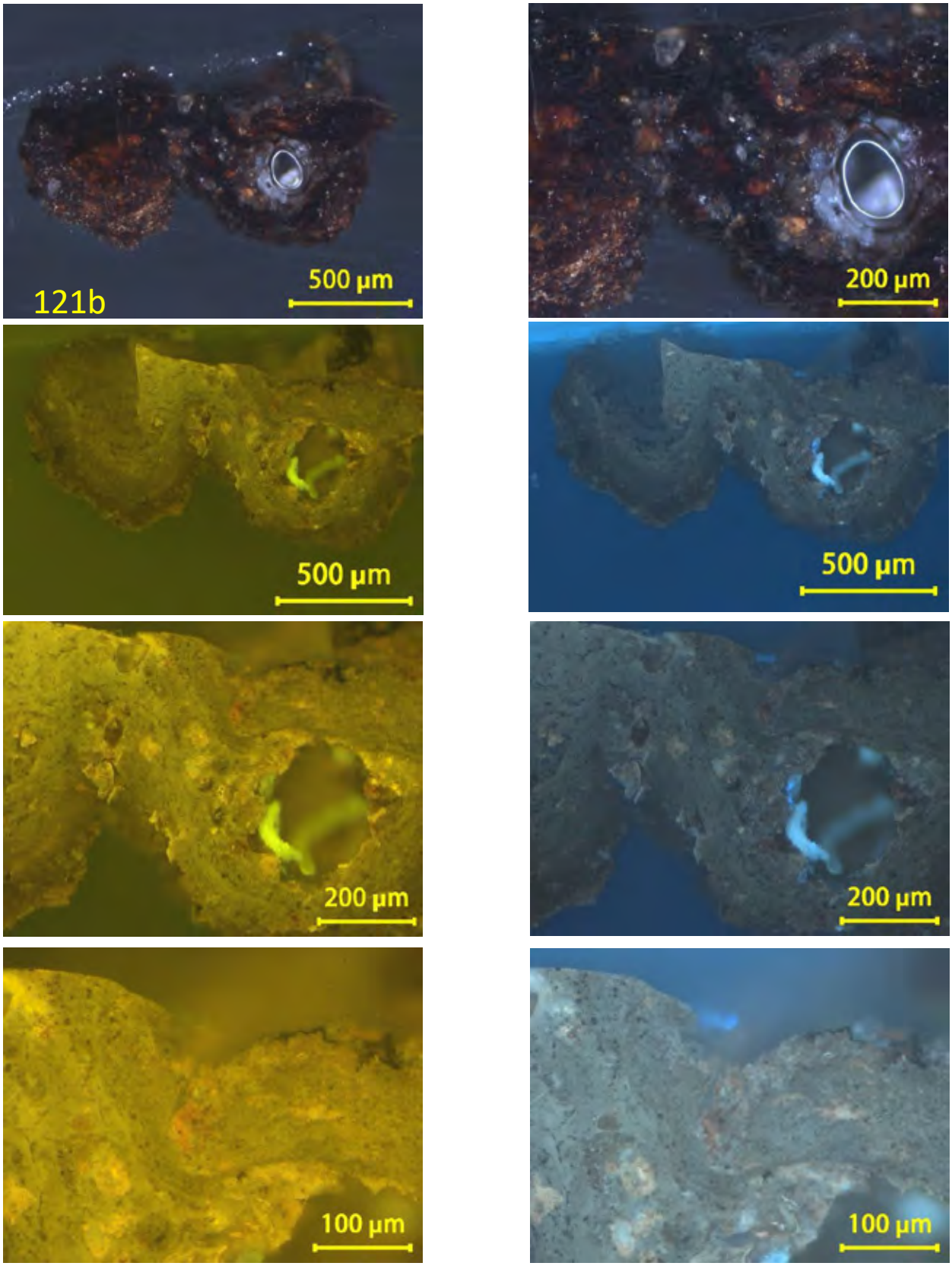

Figure 9: Images of sample 121b showing darkfield images at the top. The images below are taken under UV irradiation using DAPI illumination on the right and FITC illumination on the left. The images show a more compact fibrous structure and more embedded mineralization.

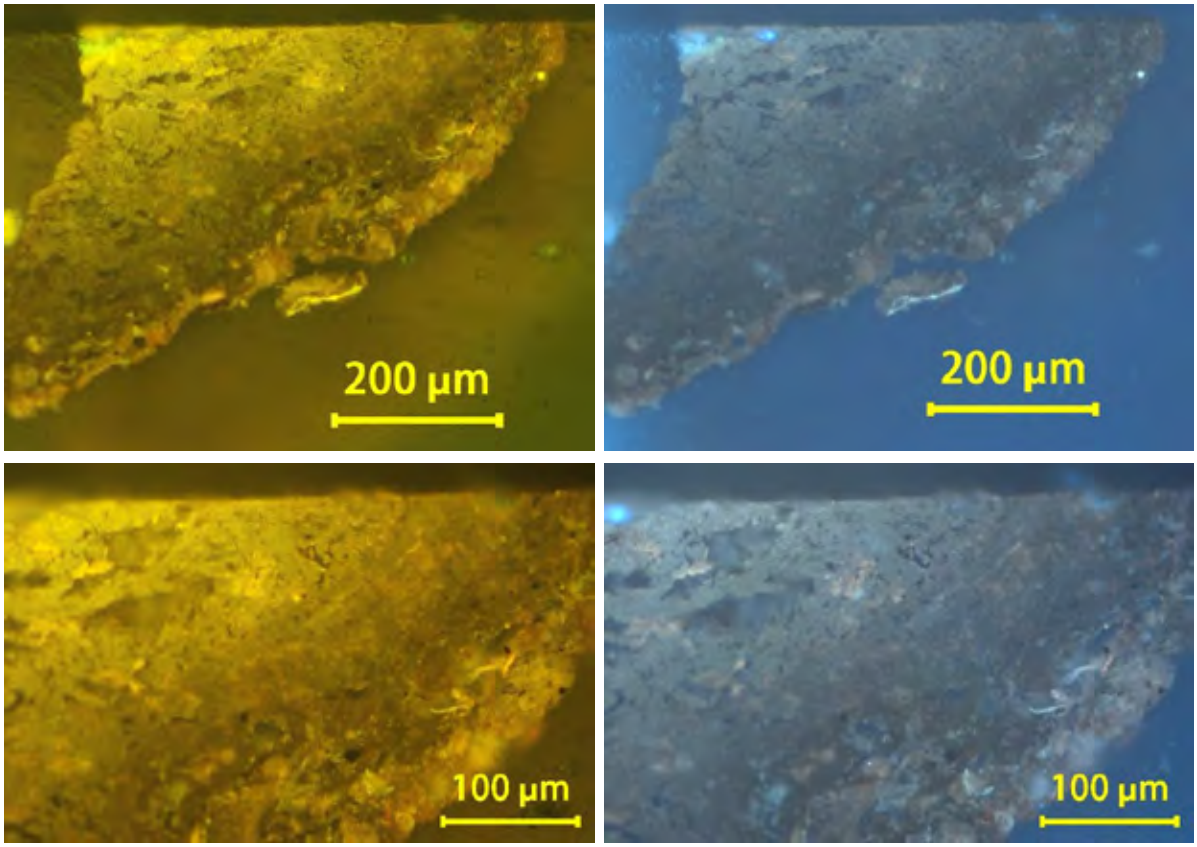

Figure 10: UV fluorescence images of the right-angle section of samples 121b. The images show the fibers compressing near the bottom with some embedded mineralization.

Scanning Electron Microscopy

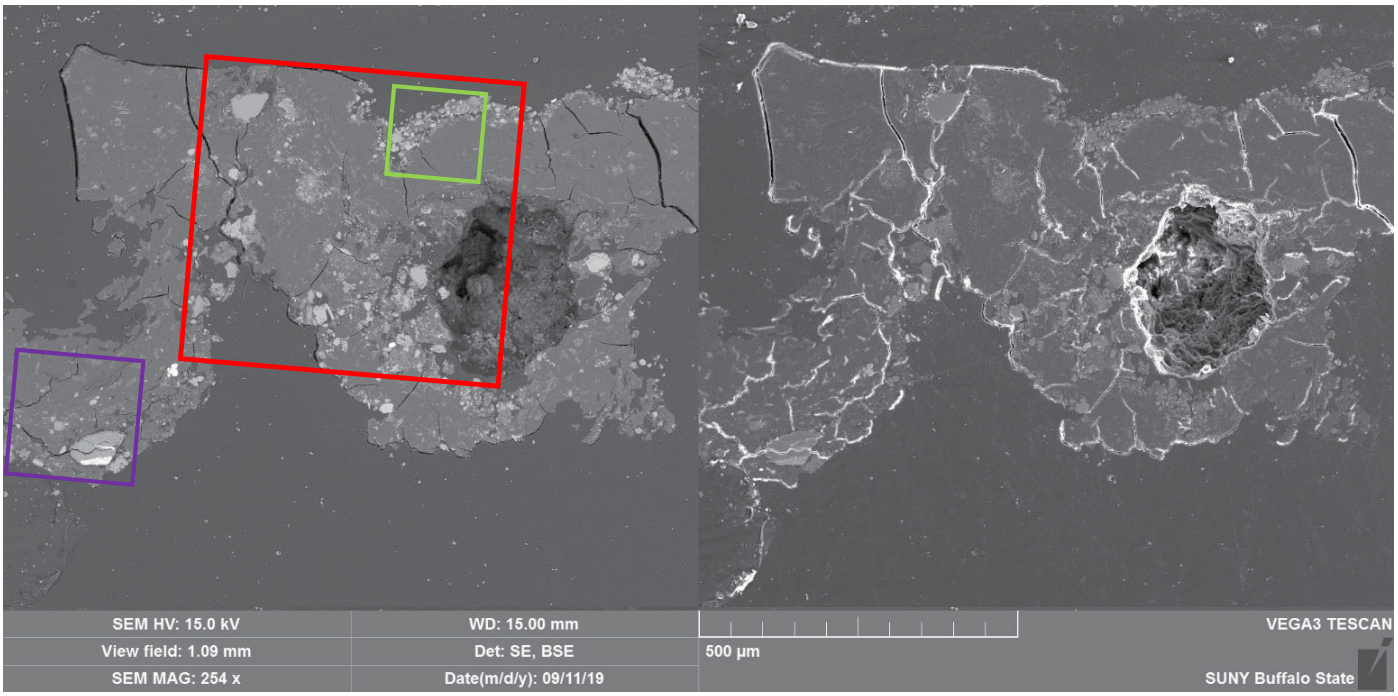

Figure 11: SEM images (SEI on the right and BSI on the left) of samples 121b. The BSI shows variation in atomic number by increasing grey scale. Within the leather itself, higher Z elements are distributed randomly and there is a higher range of embedded and surface mineralization (accretions) as compared to sample 121a. The red, purple, and green boxes represent regions that were investigated in more detail (both mapping and isolated spectra).

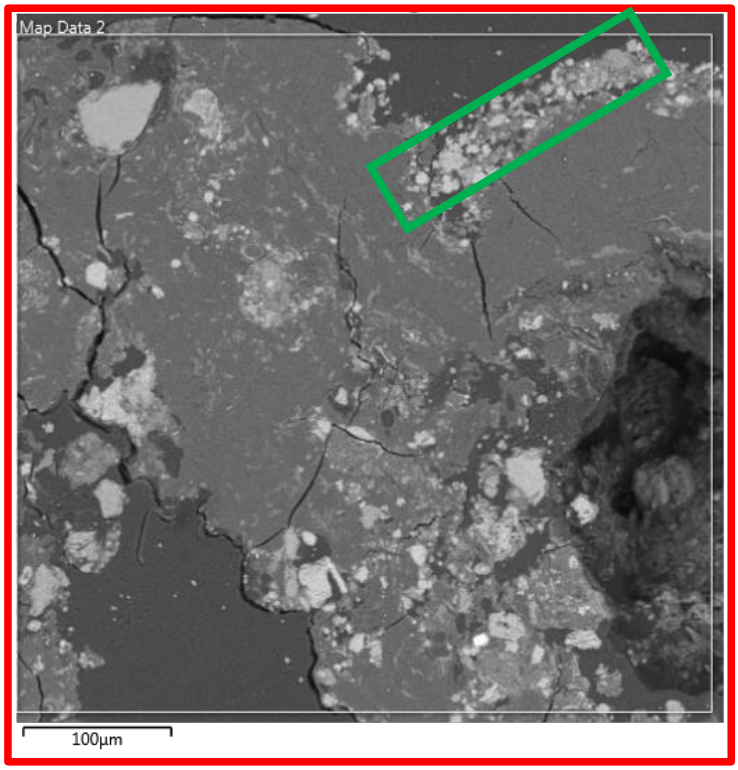

Figure 12: SEM BSI of a region mapped for elemental distribution. The Green box represents the region analyzed by reflectance FTIR.

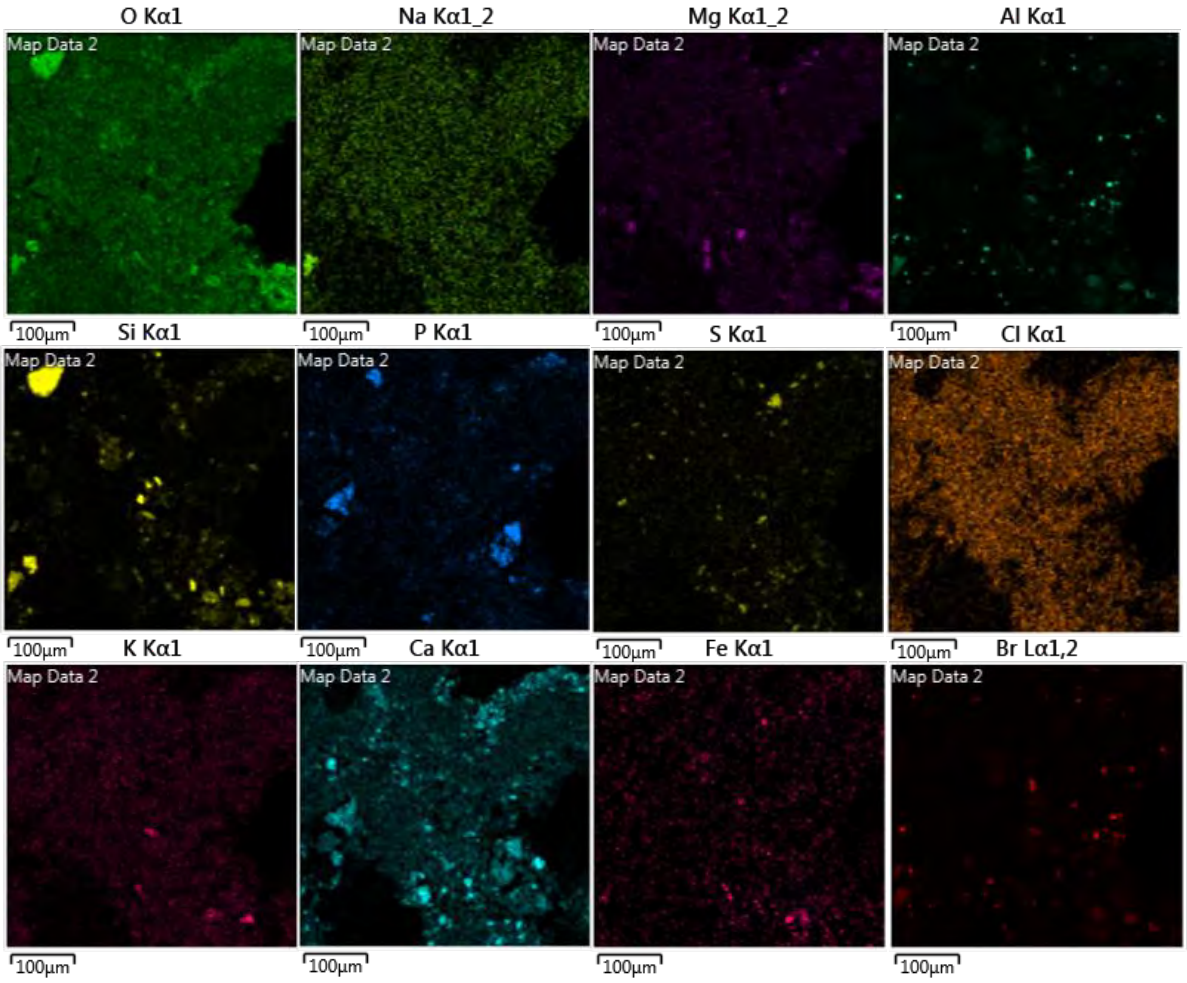

Figure 13: SEM elemental distribution maps (from figure 12) show highly mineralized sample with extensive Ca deposits, and silicates. Other elemental relationships can be seen. (Al and Br overlap one another and are difficult to differentiate.)

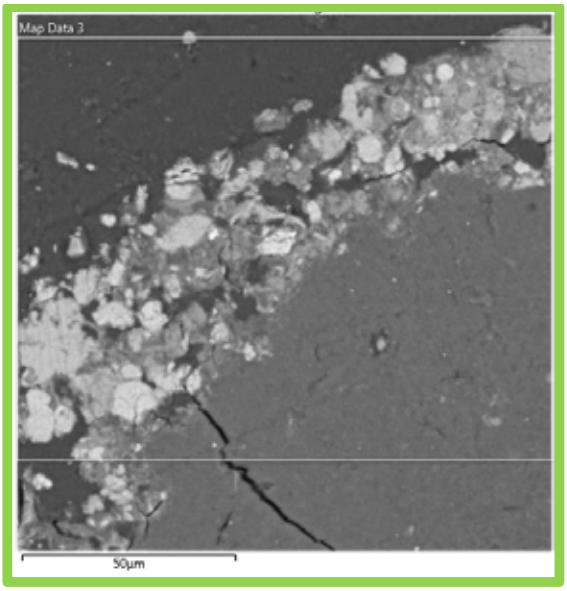

Figure 14: SEM BSI of a region mapped for elemental distribution.

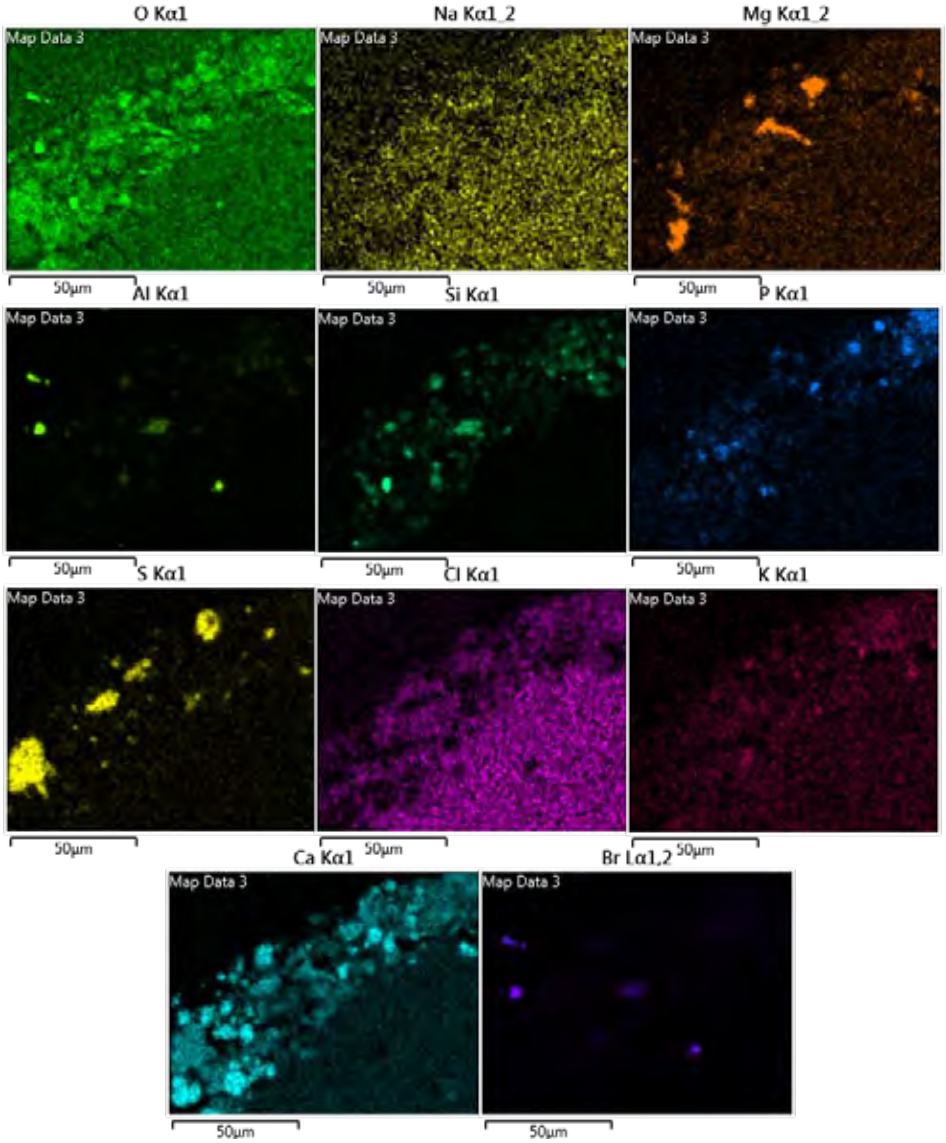

Figure 15: SEM elemental distribution maps (from Figure 14) of surface mineralization show highly mineralized sample with extensive Ca deposits and silicates. Other elemental relationships can be seen. (Al and Br overlap one another and are difficult to differentiate.)

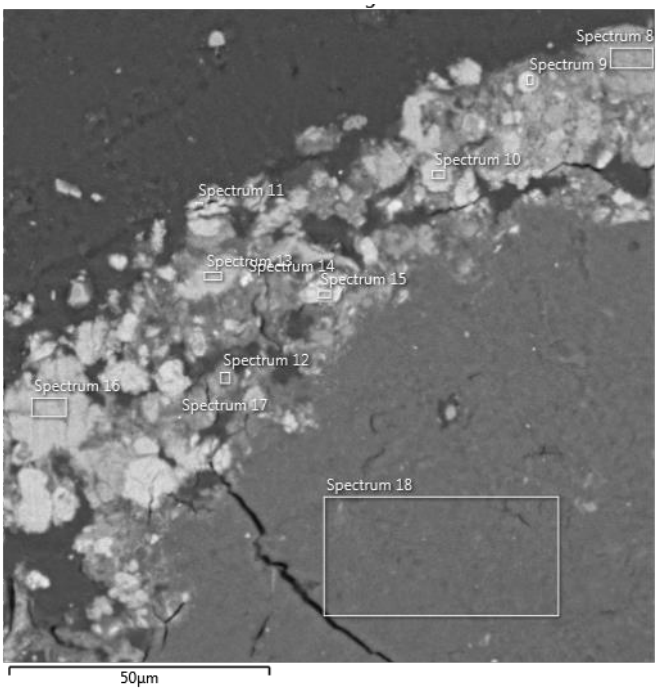

Figure 16: SEM BSI image showing the location for isolated spot and small area analysis.

Elements/ Spot	O	Na	Mg	Al	Si	P	S	Cl	K	Ca	Ti	Fe	Most likely mineral of discernibility
8	49.61	2.09	2.44	0.31	1.18	10.5	1.08	3.15	2.14	26.92		0.58	Apatite, Hydroxyapatite, Ardealite
9	47.38	1	0.63	2.42	0.39	14.1	1.04	1.79	0.72	30.55			Apatite, Hydroxyapatite, Ardealite
10	52.51	0.27	0.44					0.17	0.24	46.38			Calcite
11	59.69	0.3	0.27		0.17			0.3	0.19	39.1			
12	61.31	2.02	0.76	0.23	0.56	0.79	0.39	3.16	1.85	28.93			
13	52.3	0.33	0.27	0.21	0.59	0.42	20		0.45	25.41			Gypsum
14	45.08	0.67	3.32	6.07	16.77	0.52	3.34	2.03	4.05	5.46	0.57	12.1	Clay
15	41.67			14.8	19.32					17.36		6.86	Omphacite
16	54.69	0.21					20.4			24.69			Gypsum
17	47.88	1.47	3.09	0.33	2.61	1.68	0.66	5.89	2	34.4			
18	60.02	4.88	3.98	0.24		0.42	0.85	11	3.62	14.96			

Table 2: Normalized elemental composition for the locations noted in Figure 16. Region 18 shows the parchment has a high Ca concentration and has salts present (K, Na, or Mg salts). Spectra 8 and 9 are most likely a calcium phosphate like Apatite ($Ca_{10}(PO_4)_6(OH)_2$) or Ardealite $Ca_2(PO_3OH)(SO_4)\cdot 4H_2O$. Spectrum 13 is Gypsum $CaSO_4\cdot 2H_2O$. Spectrum 10 is Calcite $CaCO_3$. Spectrum 14 is likely an alumino silicate clay.

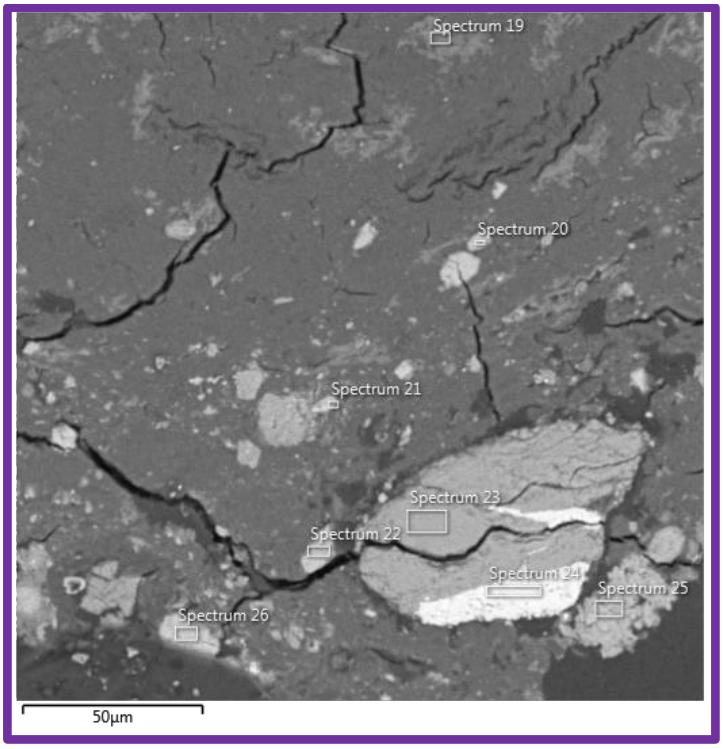

Figure 17: SEM BSI image showing the location for isolated spot and small area analysis.

Elements/ Spot	O	Na	Mg	Al	Si	P	S	Cl	K	Ca	Ti	Fe	Most likely mineral of discernibility
19	63.76	2.31	1.32		0.21		0.4	5.26	2.08	24.66			
20	52.73	0.26	0.34		0.36			0.23	0.28	45.81			Calcite
21	56.68	0.58	0.45	0.77	1.91	0.16		0.74	1.08	37.63			
22	53.47	0.56	0.55	0.51	1.02		0.14	0.91	0.61	42.23			
23	50.58				49.42								Quartz
24	39.11			1.08	1.53			0.21	0.23	0.57	45.7	11.6	Rutiled Quartz
25	53.88	0.51	0.28		18.61			0.66	0.88	25.17			Calcium Silicate
26	54.95	0.43		0.12				0.27	0.25	43.97			Calcite

Table 3: Normalized elemental composition for the locations noted in Figure 17. Spectrum 23 is quartz SiO_2. Spectra 20, 22, and 26 are Calcite $CaCO_3$. Spectrum 25 is likely related to a rutilated quartz that has needles of Rutile embedded in quartz.

Reflected FTIR

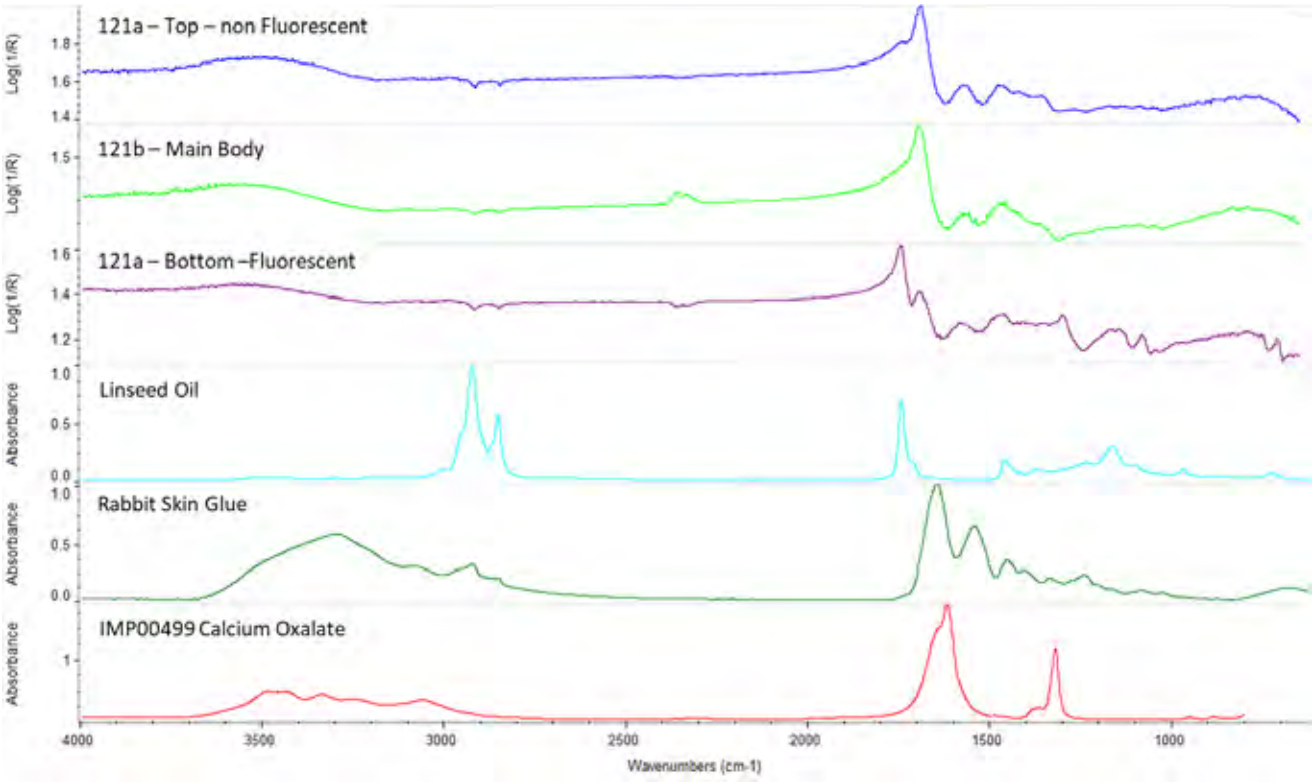

Figure 18: Comparative FTIR spectra showing the reflected data from 121a (both the upper and lower – oiled sides) and 121b. The data shows a protein (rabbit skin glue) is a good match for the leather. In addition, some calcium oxalate can be seen and linseed oil was used to identify the oiled base of sample 121a.

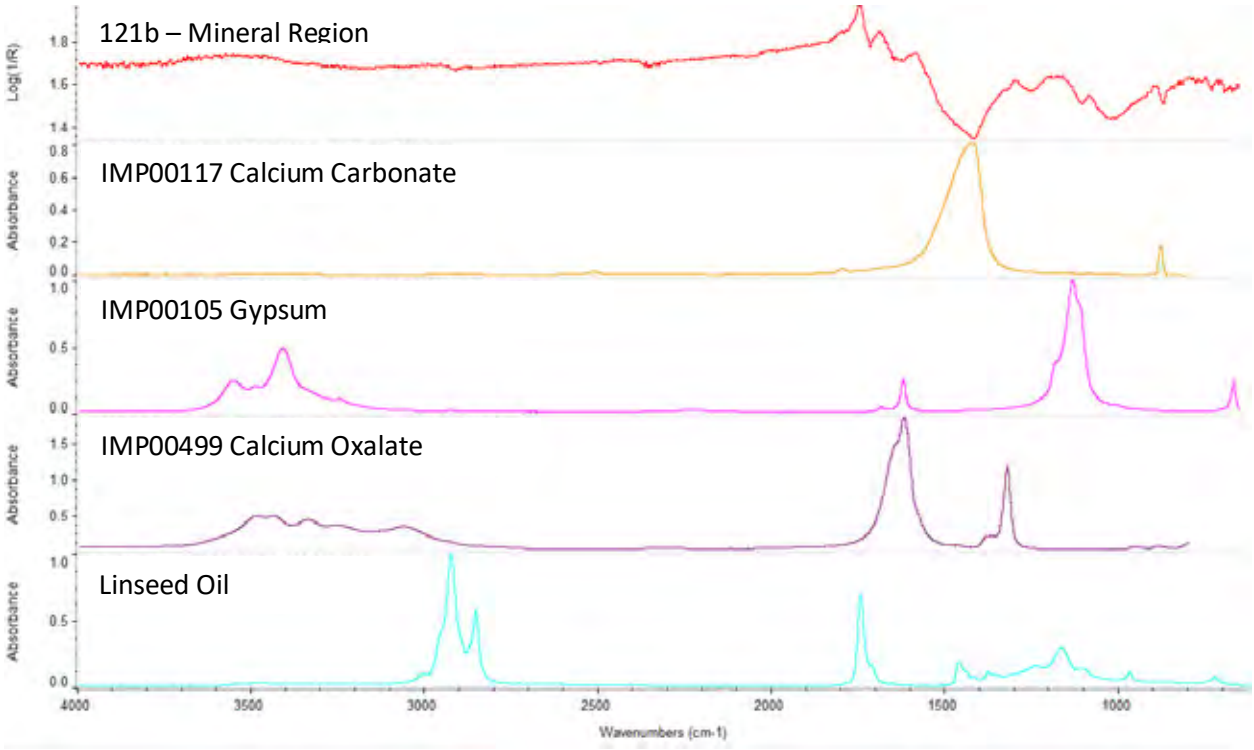

Figure 19: Comparative FTIR spectra showing the reflected data from 121b (enriched mineralization zone) seen in Figure 14. The data shows a good match for calcite, gypsum, calcium oxalate, and a trace of oil. Clay also provides a good potential match as.

Summary

Optical microscopy, scanning electron microscopy and reflected FTIR were performed on two fragments of sample SCR000121. The results show that the sample has some oil infiltration that is likely aiding in the darkening of the fragment as a whole. The fibers associated with the animal skin are visible in the section, best viewed under UV irradiation. They tend to form two main structures, one compacted and gelatinized together, and the other free flowing fibers. SEM mapping show the range of elements within the samples and on the surface/or embedded in the samples as well as their relationship to one another. The range of minerals found are based on calcium rich formations in oxide, sulphide, and oxalate forms. In addition, clay minerals, silicates, and a range of salts are present.

Microchemical Test Summary

Methodology:

Iron (II) sulfate test to determine between vegetable tanned or non-tanned skin

Microchemical testing was performed on four Museum of the Bible Dead Sea scroll fragments to determine the presence or absence of tannins, and thus whether the substrates are vegetable tanned or non-tanned animal skin. The goal of the test was to distinguish between parchment that was surface tanned, like the majority of authentic DSS, and leather that was tanned all the way through its thickness. For this reason, the test was performed in areas where the grain layer was missing with the understanding that if the substrates were surface-tanned parchment we would get a positive result on the outer surface but a negative result in areas of delamination. In the test, ferric ions react through oxidation with the phenolic compounds present in vegetable tanned leathers to produce a black or darkly colored compound. The microchemical tests were performed on at least two sample areas on each fragment, including grain and delaminated areas, in addition to a positive and negative control. A drop of 2.0% (w/v) solution of 1.0g ferrous sulfate in deionized water was applied using a micropipette to the surface of the fragment. A droplet of deionized water was similarly applied next to the sample area as a control for each test, as degraded leather can darken from contact with moisture. Color change typically occurs within minutes but can take up to several hours to develop. The test can be inconclusive, especially if the leather has been exposed to iron containing materials in its environment, but is a viable test when the phenolic compounds present may fall below detection limits of other instrumental methods, especially in mixture with other materials.

Molecular analysis – microchemical tests

Visual inspection indicated that the substrates of the studied fragments are leather, which would mean that the skins would have been treated with vegetable tannins (plant polyphenols). Tannins bind to the collagen proteins in the outer layers of skin, improving their resistance to water and bacterial degradation. However, tannins have not always been identified in period Jewish texts, nor were they identified in preliminary molecular analysis of the studied scroll fragments. As it is possible that tanning agents may be present in the studied fragments but in amounts too small to detect by infrared spectroscopy, microchemical testing was performed on four Museum of the Bible Dead Sea scroll fragments to help determine the presence or absence of tannins in the substrate materials.[1]The presence of tannin alone cannot lead to a conclusion that the material is a leather, but if detected can support a likely identification. In the test, ferric ions react through oxidation with the phenolic compounds present in vegetable tanned leathers to produce a black or darkly colored compound. Of the four fragments tested (MOTB.SCR.000121, MOTB.SCR.000124, SIG.SCR.004742 and SCR.004769), only MOTB.SCR.000124 (Genesis) gave an unambiguous, positive test result (see **Figure 2** on page 209).

The unexpected negative result of the other three fragments (MOTB.SCR.000121, SIG.SCR.004742 and SCR.004769) may be due to one or several factors. The advanced state of degradation of these fragments from age, exposure, and applied materials may affect the reactivity of phenol compounds in the substrate(s). Additionally, if the fragments were exposed to any iron containing materials in their environment, there may be no phenolic compounds available to react with the ferrous sulfate test solution.[2] All three of these fragments are darker in color and more embrittled than MOTB.SCR.000124, so it is plausible that the latter was in a better state of preservation and was a better candidate for the spot test. On this fragment, test locations included delaminated areas of the fragment to determine whether tannins are present throughout the skin matrix or had been applied only superficially. It is worth noting that despite applied glue coating or saturating several fragments, especially SIG.SCR.004742, the test drops of iron sulfate solution

and water "control" applied to the surface were fully absorbed by the substrate. Further confirmation regarding the presence of tannins in the studied fragments could be explored with additional molecular analysis such as pyrolysis gas chromatography-mass spectrometry (py-GC-MS), although a larger sample is required for this technique.

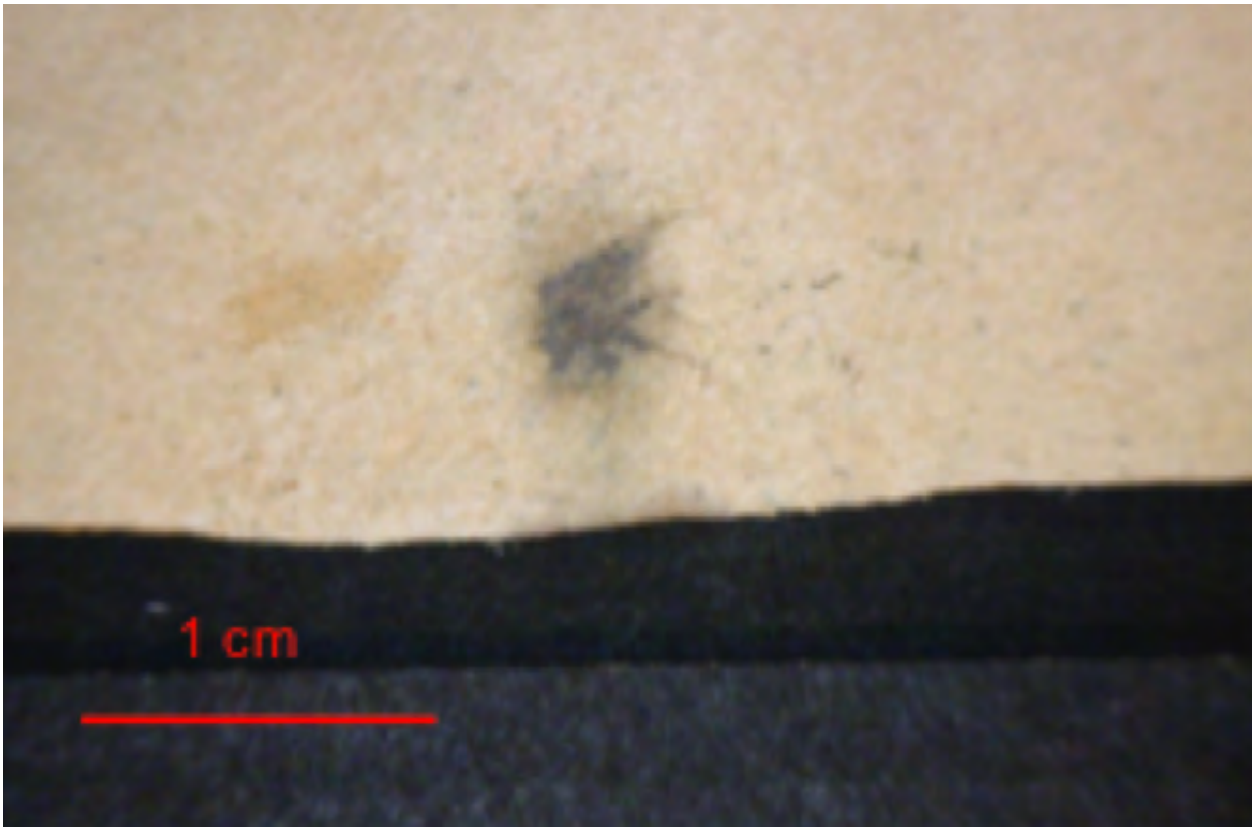

Figure 1. Modern sample of vegetable tanned leather from a known source, with positive test result for tannins visible as a gray spot at center. The ferrous sulfate is applied as a very pale yellow solution, and ferric ions react through oxidation with the phenolic compounds present in vegetable tanned leathers to produce a black or darkly colored compound. The slightly dark area to the left of the test area is a drop of water, applied as a control.

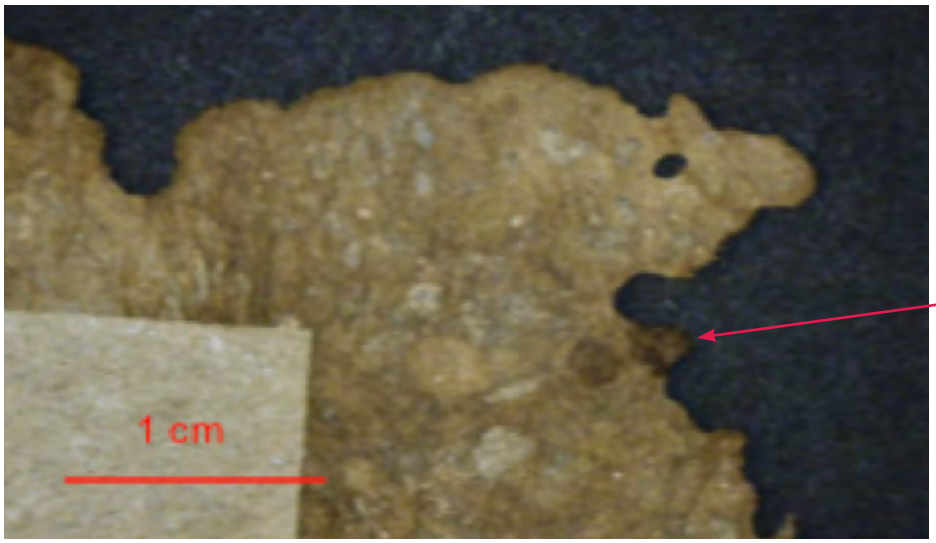

Figure 2. Detail, MOTB.SCR.000124 (Genesis), reverse of fragment. The mounting tissue adhered to the verso is visible in the bottom left corner. One of four test areas is visible right of center. The drop of water, applied as a control, is visible to the left of the test area at the outer edge of the fragment. Degraded leather can darken significantly from contact with moisture, but the test area is still visibly darker in appearance after drying.

[1]Bicchieri, M., et al. "Non-Destructive Spectroscopic Characterization of Parchment Documents." Vibrational Spectroscopy 55, no. 2 (2011): 267-72.; Falcão, L., and M. E. M. Araújo. "Tannins Characterisation in New and Historic Vegetable Tanned Leathers Fibers by Spot Tests." Journal of Cultural Heritage 12, no. 2 (2011): 149-56.

[2] van Driel-Murray, C. 2002. "Practical Evaluation of a Field Test for the Identification of Ancient Vegetable Tanned Leathers". Journal of Archaeological Science. 29 (1): 17-21.

Advisory Team Bios

Thomas Kupiec

Thomas Kupiec, PhD is the independent forensic scientific and technical advisor to this Project. He is the CEO of ARL Bio Pharma and DNA Solutions, and the Managing Member of The Kupiec Group LLC. Dr. Kupiec's forensic and pharmaceutical background includes chemical and scientific analysis utilizing chromatographic and spectroscopic methodologies. After working many years in a local law enforcement forensic laboratory and a Federal laboratory, he transitioned to the private sector. He formed a pharmaceutical testing company that provides chemical analysis to pharmaceutical companies, hospitals, raw material suppliers, and academia. Dr. Kupiec's genetic testing laboratory provides human identification and forensic DNA testing to law enforcement, attorneys, academia, and the general public.

His dedication to revealing the truth through science spans across multiple platforms including art, pharmaceuticals, toxicology, and genetics. Dr. Kupiec provides scientific consultation and expert witness testimony in the fields of forensic and pharmaceutical sciences including litigation, patent infringement, and medication errors. He has testified in over 100 cases in state and federal courts involving both civil and criminal issues, for prosecution and defense.

Dr. Kupiec received his undergraduate degree in Chemistry and his Ph.D. in Pharmaceutical Sciences from the University of Oklahoma Health Sciences Center. He serves on the Oklahoma Center for the Advancement of Science and Technology (OCAST) Board of Directors, the National Safety Council Alcohol, Drugs and Impairment Division Board, and the Foundation Board of Trustees at the University of Central Oklahoma. He is a graduate faculty member at the OU Health Sciences Center and has held teaching appointments at several universities. He has published numerous articles and abstracts in a variety of scientific fields including forensic sciences. Additionally, he has given many lectures on quality control and quality assurance. Dr. Kupiec is often requested as a guest lecturer and a speaker at national and regional conferences.

Colette Loll

Colette Loll; Founder and Director of Art Fraud Insights, LLC and Doctoral Candidate at Georgetown University. Colette Loll was the founder and CEO of a customer loyalty technology and consulting company. After 15 years of business operations, Ms. Loll sold her company and earned an MA in the History of Decorative Arts from the Corcoran College at George Washington University. Her interest in issues related to authenticity propelled her to Italy for postgraduate studies in International Art Crime. She founded Art Fraud Insights, LLC in 2013, and since its inception has been involved in several independent projects related to the topic of fine art forgery and art forensics, including serving as lead researcher in attribution and authentication investigations, conducting forensic investigations for private collectors on suspect artworks, participating in documentary film projects, and curating several exhibitions.

Ms. Loll lectures widely on the topics of art fraud and authentication at universities, museums, and forensic institutes. She had trained Federal agents in forgery investigations for the Department of Homeland Security and serves as a subject matter expert for the FBI's Art Crime Team. She has trained international law enforcement teams on strategies to combat cultural racketeering. Ms. Loll serves as a thought leader, market consultant, and strategic advisor to several technology companies applying solutions to solve the prolific problem of art fraud and illicit trafficking. Colette's doctoral research explores the intersection of material science and social science in the authentication of ancient artifacts.

Jennifer Mass

Jennifer Mass received her Ph.D. in inorganic chemistry from Cornell University and was awarded a postdoctoral fellowship at the Sherman Fairchild Center for Objects Conservation at the Metropolitan Museum of Art. She has conducted the scientific study of works of art in museum and academic contexts for over twenty years, and taught this subject in U.S. master's degree programs in art conservation for her entire career. She formed Scientific Analysis, LLC (SAFA) in 2007 because of the growing need for the objective material assessment of objects in the art market that complements the expertise of the connoisseur and conservation assessments.

Jennifer's research interests include the degradation mechanisms of artists' pigments and developing nondestructive depth profiling methods for imaging buried paintings. Jennifer has published numerous articles on her research in the art conservation and scientific literature, including Studies in Conservation and Applied Physics A. She has co-edited three volumes – two volumes of Materials Issues in Art and Archaeology, and Handheld XRF for Art and Archaeology. Jennifer gives dozens of lectures a year on her work nationally and internationally, and has received awards for her research from the Italian Society for Nondestructive Testing and from the American Materials Research Society. Jennifer's work has received worldwide media attention, being highlighted on NPR's Science Friday and MSNBC as well as in The New York Times, The Washington Post, the BBC, the L.A. Times, London's Daily Telegraph and numerous other national and international media outlets.

Rebecca Pollak

Rebecca Pollak; SAFA Senior Research Conservator and Independent Paper Conservator. Becca received her MA and Certificate of Advanced Study in Art Conservation from Buffalo State College. After completing an Andrew W. Mellon Fellowship in Paper Conservation at the Philadelphia Museum of Art, Becca joined the scientific research department at Sotheby's as Assistant Conservation Scientist, where she specialized in technical imaging and analysis of paintings and works on art on paper. Over the past 15 years, she gained additional experience in the study and conservation of works on paper and photographs in private and institutional labs including the Art Institute of Chicago, Guggenheim Museum and the Museum of Modern Art.

Becca developed a comprehensive knowledge of artists' materials during her years as manager and technical advisor for Kremer Pigments Inc. in New York, and has led various workshops on manufacturing historical and contemporary paint materials for conservators, historians, and artists throughout the United States. She has performed materials analysis for collectors, dealers, and museums, and has published research on American watercolors, media identification and terminology for works of art on paper, and synthetic dyes used in conservation treatment.

Abigail Quandt

Abigail Quandt received a M.Sc. and Diploma in Conservation from the Winterthur/University of Delaware Art Conservation Program in 1982, with a specialization in rare book conservation. From 1982-84, with grants awarded by the Institute for Museum and Library Services and the Samuel Kress Foundation, she completed an advanced internship at Trinity College Library, Dublin and spent a brief time studying with the English bookbinder and conservator Roger Powell. Ms. Quandt began working at the Walters Art Museum as a visiting manuscripts conservator in 1984, joined the staff in 1989, and was appointed Head of Book and Paper Conservation at the Walters in 2001.

An internationally recognized expert in the conservation of illuminated manuscripts on parchment Ms. Quandt has taught workshops on parchment conservation for graduate students and practicing book and paper conservators. She was the co-compiler of a chapter on parchment for the *Paper Conservation Catalog,* published in 1994 by the American Institute for Conservation, and continues to add new content to the catalog that was reformatted as a wiki in 2017. Sought after for her extensive knowledge about the care and conservation of parchment manuscripts Ms. Quandt has participated in a number of important national and international projects over the past thirty years. In 1992 she was part of a team assembled by the Getty Conservation Institute (GCI) to consult on the conservation, storage and handling of the Dead Sea Scroll fragments at the Rockefeller Museum in Jerusalem, and from 1993-96 she was a member of the Advisory Committee for the Further Analytical Examination of the Dead Sea Scrolls, also supported by GCI. Ms. Quandt was the lead conservator for the Archimedes Palimpsest Project, which took place at the Walters Art Museum from 1999-2012 and was focused on the conservation, imaging, and transcription of the earliest surviving copy of Archimedes treatises. Concurrently, she supervised the treatment and rebinding of the Syriac Galen Palimpsest for a similar multi-spectral imaging and transcription project also based at the Walters. More recently, Ms. Quandt has acted as a consultant on the Vienna Genesis Conservation and Research Project, which was supported by the Austrian Science Fund from 2016-19. This project involved the analysis, treatment, and rehousing of a very rare and fragile sixth-century Greek illuminated manuscript on purple parchment known as the Vienna Genesis, one of a handful of its type to survive. Ms. Quandt conducts research on a variety of topics relating to parchment manuscripts and has a particular interest in manuscript forgeries, sparked by her work on the Archimedes Palimpsest, which was altered by a dealer in the 1940's with seven forged Byzantine miniatures painted over both layers of text. In 2009-10 she participated in the investigation, along with a chemist and a textual scholar, of a small illuminated copy of the Gospel of Mark, known as the Archaic Mark, which was found by an intensive process of examination and scientific analysis to be an early twentieth-century forgery.

Aaron Shugar

Aaron Shugar PhD; Andrew W. Mellon Professor of Conservation Science in the Art Conservation Department, SUNY – Buffalo State. Adjunct Professor in the Anthropology Departments of both the University of Toronto and the University of Buffalo, SUNY. Adjunct Professor in the Chemistry Department, SUNY - Buffalo State.

Aaron received his PhD in Archaeometallurgy from the Institute of Archaeology, University College London and received a NERC funded postdoctoral fellowship investigating Late Bronze Age glass manufacturing in Egypt. Aaron served as Co-Director of the Archaeometallurgy Laboratory at Lehigh University, PA and was a visiting scientist at the Smithsonian Center for Materials Research and Education. He has conducted scientific analysis on archaeology material as well as works of art in museums and academic settings for over 17 years and taught in archeological, materials science, and art conservation programs over that time.

Aaron's research interests include the analysis of inorganic materials, archaeometallurgy of the Near East and Mesoamerica, developing non-invasive instrumentation for the use of art analysis, investigating the degradation phenomena of various pigments, as well as characterizing now defunct pigments including Indian yellow and zinc orange. He has published widely on these topics in conservation and scientific journals and presented his research worldwide. He has co-edited a volume of Materials Issues in Art and Archaeology.